Meerlaagse optimalisatie voor 'Day-Ahead'-energieplanning in microgrids

Multilayer Optimisation for Day-Ahead Energy Planning in Microgrids

Christof Deckmyn

UNIVERSITEIT
GENT

Multilayer optimisation for Day-Ahead energy planning in microgrids

Meerlaagse optimalisatie voor 'Day-Ahead'-energieplanning in microgrids

Christof Deckmyn

Promoters
Prof. dr. ir. Lieven Vandevelde (UGent - EEMMeCS)
Prof. dr. ir. Jan Desmet (UGent - EEMMeCS)

Chairman
Prof. dr. ir. Daniël De Zutter (UGent)

Exam Commission
Prof. dr. ir. Guillaume Crevecoeur (UGent - EEMMeCS)
Prof. dr. ir. Emmanuel De Jaeger (UCL)
Prof. dr. ir. Chris Develder (UGent - INTEC)
Prof. dr. ir. Mohammad Moradzadeh (University of Huddersfield, Verenigd
Koninkrijk/United Kingdom)
Prof. dr. ir. Greet Van Eetvelde (UGent - EEMMeCS)
dr. ir. Tine Vandoorn (UGent - EEMMeCS)

Dankwoord

De afgelopen jaren heb ik me met veel interesse kunnen verdiepen in de wereld van microgrids, waarbij ik me afvroeg hoe lokaal beheer van de decentrale productie en de eindvraag naar energie mogelijk gemaakt kan worden. Het zijn boeiende jaren geweest, waarbij ik de liefde voor projectwerk en de voldoening van wetenschappelijk onderzoek hebt ontdekt.

Dat ik bij mijn onderzoeksthema terecht ben gekomen, heb ik te danken aan mijn promotor, Lieven Vandevelde. De afgelopen vijf jaar is hij in veel opzichten een goede promotor geweest. Lieven, op jou kon ik rekenen als een betrouwbare en onderlegde persoon, die als geen ander de samenhang en rode draad ziet in complexe situaties.
Daarnaast wil ik ook mijn copromotor, Jan Desmet, bedanken voor de heldere opmerkingen en gerichte feedback.
Ik kan jullie alleen maar mijn oprechte appreciatie uitdrukken voor de mooie samenwerking tijdens de afgelopen jaren.

Ik wil ook een bijzonder oprecht woord van dank uitspreken aan Bart Meersman en Tine Vandoorn. Het is een grote geruststelling als je weet dat je tijdens je onderzoek terug kunt vallen op onderzoekers met een uitgebreide vak expertise en een grote intellectuele bagage. Jullie kritische opmerkingen heb ik altijd kunnen appreciëren. Dankzij jullie herhaaldelijke nadruk op het belang van concrete fragmenten kon dit onderzoek een duidelijke vorm krijgen.

Enorm veel dank ben ik ook verschuldigd aan alle bureaugenoten die, elk op hun eigen manier, een bijdrage hebben geleverd. Mede door de verhuis naar Zwijnaarde is dit een indrukwekkende lijst geworden: Bart, Brecht, Dominique, Giustino, Hendrik, Jens, Jeroen, Joannes,

Louis, Mohammad, Nic, Nils, Samie, Sophie, Tine. Jullie bijdrage heeft me er van overtuigd dat vijf jaar samenwerken met verschillende collega's een enorme meerwaarde kan bieden.

Naast al die collega's wil ik ook graag mijn familie en vrienden bedanken. Voor hun steun, maar ook voor de broodnodige afleiding die ze me vaak hebben geboden: de momenten thuis, op café, of op den Agé hebben hun effect niet gemist, en zorgden ervoor dat ik op tijd en stond mijn geest kon verhelderen.

Enorm veel dank en appreciatie gaat ook uit naar mijn ouders, zonder wie dit alles er nooit was geweest. Van mijn ouders heb ik mijn arbeidsethos geërfd en daar ben ik ze zeer dankbaar voor. Mijn accuratesse en onvermoeibaar optimisme heb ik aan hen te danken. Mama, papa: bedankt voor alles.

M'n laatste woord van dank heb ik voor mijn allerliefste bewaard. Julie, dat dit doctoraat er ligt, heb ik voor een groot stuk aan jou te danken. Ik zal wellicht nooit kunnen beseffen hoe zwaar de afgelopen periode voor jou is geweest. Ik was te vaak afwezig, en als ik aanwezig was, was ik nog "afwezig". Toch bleef je in me geloven, gaf je me liefde en steun. Het is mijn grootste geluk om met deze fantastische en sterke vrouw getrouwd te mogen zijn.

Gent, voorjaar 2017
Christof Deckmyn

Table of Contents

Summary

In the search for low carbon, reliable and affordable ways to provide electricity, an increased attention is going to the microgrid, a small-scale power system that uses a combination of energy generation and storage devices to serve local customers. The most promising feature of the microgrid is its flexibility to act as a standalone source of electricity for remote communities, and to be connected to the main power system, selling and purchasing power as required. Additionally, a microgrid can be considered as a coordinated system approach for incorporating intermittent renewable sources of energy. Microgrid customers can have power from their batteries or distributed generators, they can buy it from the utility grid, or they can reduce their consumption.

When designing a new optimal planning tool for a microgrid, a major challenge (and opportunity) is to decide on what units to operate in order to meet the demand. The question is what mix will provide the performance needed at the lowest cost, or with the lowest possible emissions. Unfortunately, both objectives are often contradictory. Generally, low costs mean high emissions, and vice versa. A microgrid system operator may care more about achieving lower costs rather than lower emissions. Given the preferences, the operator needs to decide how to configure and operate the microgrid while satisfying all technical requirements, such as voltage stability and power balance.

In order to control and manage the microgrid units in real-time while fully exploiting the benefit of long-term prediction, an off-line optimisation approach imposes itself to devise the online microgrid management. In this PhD thesis, an efficient multilayer control approach is developed which obtains a day-ahead unit commitment method to provide an economically and environmentally viable unit commitment (UC) that is physically feasible in terms of voltage violations. With the multilayer control approach, the future operational states of the controllable units within the microgrid are determined ahead of time. The proposed concept follows the idea of a day-ahead coordi-

nation including the unit commitment problem (scheduling layer), an off-line power flow calculation (executive layer) and a security check with feedback control (adjustment layer). Since the complete multilayer control concept works on a day-ahead time scale, the model can be considered as an off-line optimisation approach. The power reference set points provided by the multilayer control approach can, in turn, be used for an online microgrid implementation to achieve real-time system state updates.

Chapter 1 introduces the concepts, challenges and opportunities of distributed generation, smart grids, and microgrids.

Chapter 2 exposes the main shape and the necessary elements of the microgrid multilayer control approach to reveal the structure. The different layers will be described and discussed briefly. Each layer will be further examined in this PhD thesis, chapter by chapter.

In chapter 3, a survey of the different optimisation methods for power systems is presented. Subsequently, this chapter focuses on genetic algorithms, including what genetic algorithms are, the idea behind the operation, which terminology is used and the concept of the basic algorithm. By using a multi-objective genetic algorithm, the region near an optimal Pareto front can be determined relatively fast, but it can take many function evaluations to achieve convergence. Therefore, an additional (hybrid) technique is introduced in this chapter which executes the genetic algorithm for a small number of generations to get near an optimum front. The premature front returned from the genetic algorithm is used as an initial point for the hybrid goal attainment method. The hybrid scheme starts at all the points on the Pareto front returned by the genetic algorithm. The new individuals returned by the hybrid scheme are combined with the existing population and a new, more accurate, Pareto front is obtained. The chapter ends with an example of using a goal attainment method based genetic algorithm in power system planning. This technique will be used in order to solve the microgrid power system scheduling problem which is demonstrated in the next chapters.

In chapter 4, an analytical method based on a multi-objective hybrid genetic algorithm is proposed and demonstrated for a microgrid day-ahead unit commitment problem. The model aims to schedule the power among the different microgrid units while minimising the operating costs together with the CO_2 emissions produced. The approach

is demonstrated on a test case including a variety of distributed energy resources (DER) which are likely to be found in a microgrid. A storage device is added where the charge and discharge schedule is calculated according to both objectives. The presence of a storage element, as well as the possibility of exchanging energy with the utility grid adds flexibility to the microgrid operation and besides, it increases the solution space (set of feasible solutions) of the microgrid unit commitment problem. The charge and discharge commands of the storage device are allocated according to the optimal cost and CO_2 emissions. Besides, the commands of charging and discharging are associated with the energy prices as well, and the storage element takes advantage of purchasing power from the upstream grid (slack bus generator) and selling it back according to the most favorable microgrid revenue. In addition, as part of the demand side participation strategy, a charging schedule was determined for electric vehicles (EVs). A 24-hour microgrid simulation has been performed with an interval or time span of 15 minutes considering both objectives simultaneously.

Although, the voltage constraints were not considered in chapter 4, they must be carefully controlled in order to operate a power system within acceptable voltage limits. Chapter 5 extends chapter 4 with a focus on the voltage control in microgrids. This chapter begins with a brief description of voltage control in distribution grids and the differences compared to voltage control in transmission grids. Subsequently, it will be explained why the linkage between active power and voltage becomes relevant for voltage control in microgrids. Furthermore, a voltage control approach is developed and embedded in the multilayer control structure which maintains the microgrid bus voltages within pre-specified limits. Due to the introduction of this voltage control approach, active power reference set points can be provided (for real-time microgrid scheduling) not only according to the economical and the environmental objectives, but also taking into account the voltage level at every bus in the microgrid. This chapter ends with a demonstration and evaluation of the voltage control approach.

For demonstrating the developed multilayer control strategy, chapter 6 presents case studies involving the planning of a microgrid including a variety of DER units and loads which are likely to be found in a microgrid. The proposed microgrid includes renewable energy resources, a storage unit, micro turbines, a fuel cell and electric ve-

hicles. The system should run as much as possible on its renewable technologies, and when more power is needed, it may need to use the diesel generators or batteries. Finally, the system should provide perfect reliability that is, it should never fail to meet total customer demand. Based on the results, the multilayer control strategy generates a set of optimal operating strategies that will minimise costs and emissions while satisfying all technical requirements.

Chapter 7 concludes this PhD thesis and describes some possibilities for further research.

Samenvatting

In de zoektocht naar een koolstofarme, betrouwbare en betaalbare manier om elektriciteit te voorzien, wordt veel aandacht besteed aan het concept 'microgrids', een lokaal en kleinschalig elektriciteitsnet dat gebruik maakt van een combinatie van gedistribueerde energiebronnen (DER eenheden) zoals energieopwekkingseenheden en energie-opslageenheden, om de lokale eindgebruikers te kunnen voorzien van elektriciteit. Een veelbelovende kenmerk van een microgrid is de flexibiliteit om in eilandbedrijf als autonome energiebron voor afgelegen gebieden te fungeren en om in netgekoppeld bedrijf elektriciteit te kopen en verkopen. Tijdens eilandbedrijf zorgt een microgrid voor de continuïteit van energievoorziening aan de eindgebruikers. Aanvullend biedt een microgrid een gecoördineerde aanpak voor de integratie van intermitterende hernieuwbare energiebronnen. Indien er geen of onvoldoende energieproductie is uit hernieuwbare bronnen, kunnen eindgebruikers elektrische energie halen uit energie-opslageenheden (DS eenheden) of decentrale generatoren (DG eenheden), energie kopen van het elektriciteitsnet, of de eindgebruikers kunnen hun verbruik verminderen.

Om een microgrid optimaal te kunnen beheren ligt de uitdaging bij het coördineren en plannen van de DER eenheden om zo efficiënt mogelijk het evenwicht tussen vraag en aanbod van elektrische energie te bereiken. De vraag die hier moet gesteld worden is, welke mix van DER eenheden en regelbare verbruikers moet aangestuurd worden om de nodige prestaties te leveren tegen de laagste operationele kosten, of met de laagste CO_2 uitstoot. Dit zijn tegenstrijdige doelstellingen. In het algemeen gaat een minimalisatie van operationele kosten van een energiesysteem gepaard met een verhoging van de geproduceerde emissies, en omgekeerd. Het is aan de operationele manager om te beslissen op welke manier het microgrid zal worden beheerd, terwijl aan alle technische eisen, zoals spanningsstabiliteit en vermogensbalans, wordt voldaan.

Om een microgrid te kunnen coördineren in real-time, waarbij het voordeel van een lange-termijn voorspelling (hernieuwbare energie-

productie, het profiel van de elektriciteitsbehoefte en de elektriciteits-
prijzen) ten volle wordt benut, dringt een offline energiebeheersystem
voor microgrids zich op. Het uitwerken van een meerlaags optima-
lisatiemodel voor microgrids waarbij een economische en ecologische
day-ahead energieplanning wordt gecalculeerd, dat fysiek haalbaar
is in termen van spanningsstabiliteit en vermogensbalans, vormt de
kern van dit doctoraat. Met dit optimalisatiemodel wordt een ver-
mogensverdeling berekend dat het referentievermogen voor de DER
eenheden in het microgrid bepaald. Het concept volgt het idee van
een meerlaagse optimalisatie bestaande uit: een planning laag (sche-
duling layer), een offline power flow calculatie (executive layer) en
een spanningscontrole met terugkoppeling (adjustment layer). Om-
dat dit optimalisatiemodel werkt op een day-ahead tijdschaal, kan
deze methode worden beschouwd als een offline optimalisatie. De re-
ferentievermogens kunnen worden gebruikt als input voor een online
microgrid implementatie om op die manier tot een real-time status
update te komen van de verschillende DER eenheden in het micro-
grid.

Hoofdstuk 1 leidt de concepten in en bespreekt de belangrijkste voor-
delen en uitdagingen van decentrale generatoren, slimme netten en
microgrids.

Hoofdstuk 2 introduceert het meerlaags optimalisatiemodel. De op-
bouw en de verschillende lagen worden voorgesteld en kort besproken.
Elke laag wordt later in dit proefschrift, hoofdstuk per hoofdstuk, uit-
gebreid beschreven.

In hoofdstuk 3 wordt een overzicht gegeven van de verschillende me-
thoden om elektrische netten te optimaliseren. Vervolgens richt dit
hoofdstuk zich op genetische algoritmen, waarbij dieper wordt inge-
gaan op het concept, de gebruikelijke terminologieën en de werking
van de basis-algoritme. Het bepalen van de ideale vermogensverde-
ling van de DER eenheden en regelbare verbruikers om de nodige
prestaties te leveren tegen de laagste operationele kost, of met de
laagste CO_2 uitstoot, kan worden beschouwd als een mulit-criteria
optimalisatieprobleem. Een dergelijk complex optimalisatieprobleem
heeft niet één oplossing, maar een reeks oplossingen: een Pareto op-
timale verzameling. Genetische algoritmen zijn geschikt voor het op-
lossen van multi-criteria optimalisatie problemen. Hiermee kunnen
we de zogenaamde trade-offs boven water krijgen. Inzichten in deze
trade-offs maken de keuze voor een specifieke oplossing in ieder geval

transparant. Echter, om te convergeren naar een globaal optimum hebben genetische algoritmen meerdere functie evaluaties nodig, met een toenemende rekentijd als gevolg. Daarom wordt in dit hoofdstuk een aanvullende hybride techniek geïntroduceerd dewelke het genetisch algoritme uitvoert voor een beperkt aantal generaties om een quasi regio nabij de Pareto optimale verzamling te genereren. De verzameling zal worden gebruikt als een beginpunt voor de hybride goal attainment methode. De nieuwe individuen geretourneerd door het hybride model worden gecombineerd met de bestaande populatie van het genetisch algoritme. Op die manier kan een nauwkeuriger Pareto front verkregen worden. Dit hoofdstuk eindigt met een uitgewerkt voorbeeld van een hybride genetisch algoritme toegepast op de energieplanning in distributienetwerken. Deze techniek zal verder in deze verhandeling worden gebruikt om de day-ahead energieplanning in microgrids te bepalen.

In hoofdstuk 4 wordt een mathematische formulering en implementatie gepresenteerd van een multi-criteria hybride genetisch algoritme voor de ontwikkeling van een microgrid day-ahead optimalisatiemodel. Het model heeft als doel de vermogensverdeling van de DER eenheden te bepalen waarbij de operationele kosten en de CO_2 uitstoot gelijktijdig worden geoptimaliseerd. Verder wordt in dit hoofdstuk een demonstratie gegeven op een microgrid testwerk. Een energie-opslageenheid werd toegevoegd waarbij een laad en ontlaadschema wordt berekend volgens beide doelstellingen. De aanwezigheid van een energie-opslageenheid, alsmede de mogelijkheid tot uitwisseling van energie met het elektriciteitsnet voegt flexibiliteit toe aan de werking van een microgrid. Als onderdeel van de demand response (DR) programma, werd een optimaal oplaadschema bepaald voor de elektrische voertuigen in het microgrid. Een 24-uurs microgrid simulatie werd uitgevoerd met een interval of een tijdspanne van 15 minuten, waarbij de operationele kosten en de CO_2 uitstoot gelijktijdig worden geoptimaliseerd.

Hoewel de microgrid busspanningen niet in rekening werden gebracht in het day-ahead unit commitment model, moet de spanningsstabiliteit worden gewaarborgd om een betrouwbare energievoorziening in het microgrid te kunnen garanderen. Hoofdstuk 5 wordt gepresenteerd al een aanvulling op hoofdstuk 4, met een diepere focus op de spanningsregeling in microgrids. Dit hoofdstuk begint met een korte beschrijving van de spanningsregeling in distributienetten en de verschillen met de spanningsregeling in transmissienetten. Vervolgens

zal er worden uitgelegd waarom de koppeling tussen actief vermogen
en de spanning relevant is bij microgrids. Om deze reden werd een
spanningscontrole met terugkoppeling ontwikkeld en ingebed in het
meerlaags optimalisatiemodel die de busspanningen binnen vooraf be-
paalde grenzen houdt. Door de invoering van deze spanningscontrole
kan het referentievermogen worden bepaald (als input voor een real-
time microgrid planning) niet alleen volgens de laagste operationele
kost, of de laagste CO_2 uitstoot, maar ook rekening houdend met het
spanningsniveau op elke bus in het microgrid. Dit hoofdstuk eindigt
met een demonstratie en evaluatie van de spanningscontrole met te-
rugkoppeling.

In hoofdstuk 6 werd de meerlaagse optimalisatie voor het bepalen
van een day-ahead energieplanning in microgrids gedemonstreerd.
Een microgrid werd gemodelleerd met veelvoorkomende DER eenhe-
den en een gebruikelijk lastprofiel. De opgewekte hernieuwbare ener-
gie wordt zoveel mogelijk benut. Wanneer meer vermogen nodig is,
wordt deze aangevuld met vermogen van de thermische generatoren of
energie-opslageenheden. Ten slotte moet deze meerlaagse optimalisa-
tie een perfecte betrouwbaarheid leveren, waarbij een economische en
ecologische day-ahead energieplanning wordt gecalculeerd dat fysiek
haalbaar is in termen van spanningsstabiliteit en vermogensbalans.

In hoofdstuk 7 wordt een algemeen besluit gevormd en worden enkele
mogelijkheden voor verder onderzoek aangehaald.

List of Figures

List of Tables

Nomenclature

Parameters

$A_{\mathrm{eq}_{\mathrm{EV}}}$	equality term electric vehicle
$A_{\mathrm{eq}_{\mathrm{PB}}}$	equality term power balance
A_{EV}	inequality term electric vehicle
A_{storage}	inequality term storage device
$A_{\mathrm{lb}_{k,i}}$	dynamic gain of the lower boundary of the kth microgrid unit on the ith time step
$A_{\mathrm{ub}_{k,i}}$	dynamic gain of the upper boundary of the kth microgrid unit on the ith time step
$b_{\mathrm{eq}_{\mathrm{EV}}}$	equality term electric vehicle
$b_{\mathrm{eq}_{\mathrm{PB}}}$	equality term power balance
b_{EV}	inequality term storage device
b_{storage}	inequality term storage device
$C_{\mathrm{G}}(P_{\mathrm{G}})$	fuel cost as a function of active power [€/h]
$\mathcal{C}_{\mathrm{unit}_k \, \mathrm{to} \, \mathrm{bus}_m}$	represents the contribution of unit k to the voltage deviation at bus m
$\mathcal{D}_{k \, \mathrm{to} \, m}$	distance of the microgrid unit to the location of the bus with the voltage deviation
E_{EV}	energy available in the electric vehicle [kWh]
$E_{\mathrm{EV}_{\max}}$	maximum energy level of the electric vehicle [kWh]
$E_{\mathrm{EV}_{\min}}$	minimum energy level of the electric vehicle [kWh]
$E_{\mathrm{EV}_{\mathrm{T}_{\mathrm{in}}}}$	amount of energy available in the electric vehicle on the time step it will be plugged in [kWh]

$E_{\mathrm{EV_{T_{out}}}}$ amount of energy available in the electric vehicle on the time step it will be unplugged [kWh]

$\varepsilon_{\mathrm{G}}(P_{\mathrm{G}})$ CO_2 emission as a function of active power [kg/h]

E_{storage} energy available in the storage unit [kWh]

$E_{\mathrm{pre-storage}}$ energy available in the storage unit at the end of the previous day [kWh]

$E_{\mathrm{storage_{max}}}$ maximum energy level of the storage unit [kWh]

$E_{\mathrm{storage_{min}}}$ minimum energy level of the storage unit [kWh]

$\mathcal{F}$ factor matrix

$\mathcal{F}_{\mathrm{UV}}$ factor matrix for undervoltages

$\mathcal{F}_{\mathrm{OV}}$ factor matrix for overvoltages

$P_{\mathrm{D}}^{\mathrm{a}}$ actual microgrid demand [kW]

P_{EV} active power reference set point of the electric vehicle [kW]

$P_{\mathrm{D}}^{\mathrm{fixed}}$ microgrid fixed demand [kW]

$P_{\mathrm{D}}^{\mathrm{flexible}}$ microgrid flexible demand [kW]

P_{G} active power reference set point of the microgrid unit [kW]

P_{gen} vector containing active power reference set points of the microgrid units for 1 time step

P_{RES} active power reference set point of the renewable energy source [kW]

DAP_{sell} the day-ahead selling price [€/kW]

DAP_{buy} day-ahead buying price [€/kW]

P_{storage} active power reference set point of the storage unit [kW]

$P_{\mathrm{D}}^{\mathrm{total}}$ total microgrid demand [kW]

P_{UC} matrix containing active power reference set points within the complete scheduling time horizon

$P_{\mathrm{G_{min}}}$ minimum active power rate of the microgrid generation [kW]

$P_{\mathrm{G_{max}}}$ maximum active power rate of the microgrid generation [kW]

T_{in} time step the electric vehicle will be plugged

T_{out}	in time step the electric vehicle will be unplugged
T_{s}	time span of the time step [min]
N	number of time steps
N_{var}	number of variables
N_{gen}	number of microgrid units who are participating in the unit commitment strategy
$\mathcal{N}$	network matrix

Abbreviations

ACE	answers to the carbon economy
B2B	business to business
BP	business park
CHP	combined heat and power
CPP	critical-peak pricing
DAM	day-ahead market
DER	distributed energy resource
DG	distributed generation
DR	demand response
DS	distributed storage
DS	demand side management
DSO	distribution network operator
EV	electric vehicle
EMS	energy management system
ERDF	European Regional Development Fund
FC	fuel cell
GA	genetic algorithm
GHG	greenhouse gas
ICT	information and communication technology
LC	local controller
LP	linear programming
LB	lower bound
LV	low voltage
MCC	microgrid central controller
MIP	mixed integer programming
MO	market operator
MT	micro turbine
OECD	Organisation for Economic Cooperation and Development

PCC   point of common coupling

RES   renewable energy sources
RTP   real-time pricing

SQP   sequential quadratic programming
SOC   state of charge

TSO   transmission system operator
TOU   time of use

UB   upper bound
UC   unit commitment

VBD   voltage-based droop

1

Introduction

There is no longer a discussion on whether climate change is a fact, because the amount of evidence is monumental. Literally, thousands of studies done over decades by thousands of scientists in hundreds of institutions working across numerous disciplines. As some would expect, there have been uncertainties and disagreements. But the evidence, fairly interpreted, now points incontrovertibly to the conclusion that we are causing our planet to warm. Extreme weather conditions around the world, including floods and severe droughts are part of the planetary emergency in which we all live. A major cause of global warming and the associated rising sea level is the continued increase in greenhouse gas (GHG) emissions. While the fossil-fuelled energy sector is the largest contributor to the worldwide carbon dioxide (CO_2) emissions [1], it is ironically one of the industries which is most vulnerable to climate change [2]. The energy sector, which is both victim and villain, needs an infrastructure more resilient to the threats of climate change, while it reduces CO_2 emissions caused by energy generation. Various energy saving measures and the use of energy from renewable sources are helpful ways to reduce carbon dioxide emissions.

1.1   Distributed generation

The electrical grid is expected to evolve to a new grid paradigm empowered by the critical need to decarbonise the energy supply, the uncertainty of the prices of fossil fuels and concerns related to the security of energy supply. The focus is changing from large fossil fuel based electrical generators to cleaner technologies. As a result, distributed generation (DG) becomes part of the modern energy structure. This type of electricity generation generally has a low power density and is geographically dispersed. It is often based on renewable energy sources (RES) including photovoltaic panels and wind turbines, but other technologies such as in combined heat and power (CHP) units, micro turbines and fuell cells are gaining popularity.

1.1.1   Drivers and benefits

The global renewable electricity capacity is expected to grow by 42% by 2021. This forecast is 13% more optimistic as compared to the same report presented in 2015 [3]. The drivers for the increase of distributed generation are numerous and vary from country to country, yet several common main drivers exist [4, 5]:

1. Environmental drivers:

   - Limiting CO_2 emissions
   - Avoidance of the construction of new transmission circuits and large generating plants

2. Commercial drivers:

   - General uncertainty in electricity markets favours small-scale energy generation
   - Distributed generation is a cost-effective way to deliver electric power when small loads are needed close to the end-user

3. National/regulatory drivers:

   - Diversification of energy sources to enhance energy security
   - Support for competition policy

The implementation of DG units in the distribution system has many benefits, including reduced transmission and distribution costs, reduced emissions, and enhanced reliability [6]. Distributed generation located close to the end-user can reduce energy losses, allow utilities to postpone upgrades to substations, distribution and transmission facilities, and provide black-start capability. Some types of DG, including fuel cells, micro turbines, and internal combustion engines can gain increased efficiency by taking advantage of waste heat. Since DG units can be built more quickly and since they are more easily to move, less existing infrastructure and less upfront capital investment is needed compared to large central generators.

Although the widespread use of DG in the distribution system has many benefits, it poses various challenges to the power industry. Many of the assumed benefits of DG are dependent on the planning and operation of these units within the main grid. Therefore, major efforts are required in the development and integration of distributed energy systems, leading to a reinvention of the power system.

1.2   Reinventing the grid

The classical main grid was built in the past century during a period of fast urbanisation and infrastructure developments, when energy had a relatively low cost. The development of these classical power systems was dependent on economic, political and geographic factors, and therefore, each utility can be considered as a unique entity [7,8]. However, despite their differences, the basic topology of the classical electrical power system has remained unchanged. As depicted in Fig. 1.1, a power system is structured as a hierarchical system in which central power plants (generation) are at the top in order to transport and distribute the electrical energy to the consumers, which are on the bottom of the chain.

This classical system was designed as a one-way system where the source had no real-time information of the service parameters at the terminals. As a result, the classical grid was over-dimensioned in order to cover the peak demand across its aggregated load, and operates inefficiently since this peak demand occurs infrequently.

While minor upgrading has been done to meet the growing demand for energy, the electrical grid of today still operates the way it did almost 100 years ago. The electrical power flows over the grid from central power plants to consumers, and reliability is ensured by preserving surplus capacity [9]. As a result, the classical power sys-
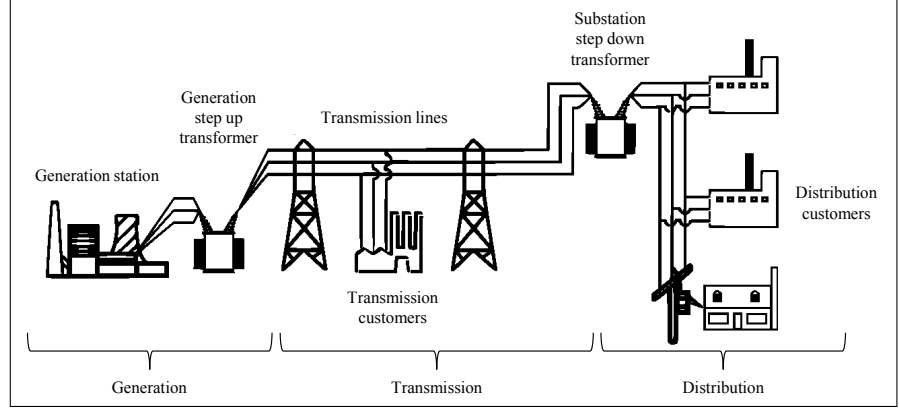
Figure 1.1: Traditional grid layout

tem became an incompetent and environmentally extravagant system which is a number one emitter of greenhouse gases and consumer of fossil fuels [7].

1.2.1 Barriers and challenges

Our aging power grid is not well suited to distributed electricity production, and to the increasing electrical demand as a result of the continued economic growth. Two major issues arise and pose limits on the further integration of DG in distribution networks.
First, distribution networks are not actively managed, i.e., they are conceived as passive facilities of the transmission network in which the control and stability is achieved. Many DG units are operated in a passive manner, where the output is dependent on the availability of the energy source (e.g., solar irradiation and wind) and the user settings (e.g., heat demand in CHP units). The state of the electrical power system generally has no influence on the power output of these units (apart from shutting down the DG unit in extreme conditions). On the one hand, the fit-and-forget strategy of deploying DG in the distribution network displaces the energy production. On the other hand, the flexibility and capacity in order to provide a reliable power supply at all times will not be provided by these DG units. Furthermore, the stochastic behaviour of generation and consumption leads to less predictable power flows in the distribution networks. Hence, despite the low installed capacity of many DG units, the huge number of these units has a significant impact on power system planning,

operation and protection.

Secondly, the continuing increase of DG is being limited because distribution systems are not designed for the subsequent bidirectional power flows and the changed voltage profiles in the distribution feeders induced by DG. The connection of a DG unit to the distribution network may result in a voltage rise at its terminals. Besides, the power system becomes overwhelmed with congestion problems, and capacity management as known and treated in the higher level transmission network, becomes a main concern in distribution networks.

It is clear these factors, together with an ageing energy infrastructure, drive the grid to its capacity limits and can result in an inefficient system, an uncoordinated integration of DG units and a decreasing system reliability [4]. Solving these issues within our current grid paradigm may have an impact on the system costs, including balancing costs and the need for backup capacity. In order to address the above challenges while mitigating these expected costs, investigations in power generation, transmission, distribution and consumption have been the focus to accelerate the transformation to an intelligent grid. Utilities have a vested interest in operating the power system in a more efficient way (i.e., smart grid), by integrating DG units in a coordinated manner (microgrids).

1.3 Smart grids

The smart grid can be defined as a part of a power system that can intelligently integrate the actions of all users connected to it (producers, consumers and prosumers), in order to efficiently deliver sustainable, economic and secure electricity supplies [8]. The perception of a smart grid is to provide a variety of possibilities including, improving the capacity of the transmission lines and distribution systems, a higher level of utilisation for renewable energy sources, the provision of a two-way interaction between consumers and providers, etc. A smart grid incorporates the features of advanced information and communication technologies (ICTs) to transmit real-time information and facilitate the instantaneous stability of supply and demand within the electrical grid. The operational information gathered by the smart grid can be used by system operators to respond to disturbances and transients due to the changes in the system. Therefore, communication and information technologies take an increasingly important role in monitoring and controlling the system [10,11].

1.3.1 Definition and characteristics

There is no single definition of a smart grid. In this thesis, the definition of the European Technology Platform [12] is used which states that:

A Smart Grid is an electricity network that can intelligently integrate the actions of all users connected to it (generators, consumers and those that do both) in order to efficiently deliver sustainable, economic and secure electricity supplies.

A smart grid can be considered as an electric system that uses information, two-way, cyber-secure communication technologies, and computational intelligence in a coordinated way across each level of the power system, from generation to consumption, in order to achieve a system that is secure, reliable, resilient, efficient, and sustainable [7, 13]. Note that the smart grid builds on the existing infrastructure and does not replace the existing power system. By implementing these smart grid technologies, the main grid becomes more observable, controllable, automated and fully integrated [14]:

- Observable: ability to view a wide range of operational indicators in real time, including where losses are occurring, the condition of equipment, and other technical information.

- Controllable: capacity to manage and optimise the power system to a greater extent than currently possible, including load control and the use of intermittent renewable generation in a controlled manner.

- Automated: the ability of the network to make certain automatic demand response decisions.

- Fully integrated: integrated and compatible with existing systems and with other new devices, e.g. smart consumer appliances.

According to de definition, the smart grid will have the following characteristics [13]:

- Self healing: automatic reconfiguration of the system to reroute supplies of energy to maintain power to all customers

- Flexible: rapid and safe interconnection of distributed generation and energy storage at any point within the system

- Predictive: use of machine learning, weather impact projections, and stochastic analysis in order to predict and anticipate on significant impacts on power system operation, planning and protection

- Interactive: allow operators and customers in the energy system to play an active role in optimal management of contingencies.

- Optimised: knowing the status of every major component in real or near real-time and having control equipment to provide optional routing paths and the capability for autonomous optimisation of power flow throughout the system.

- Secure: two-way communication capability covering the end-to-end system (the need for physical as well as cyber security of all critical assets is essential).

1.3.2 Drivers and benefits

The drivers for the deployment of a smart grid can be considered as a concrete response to one or more national or local needs, whether related to the technical improvement of the power systems or economic, social and environmental advantages. The main drivers for the smart grid deployment are listed below [4, 13]:

- Power reliability and power quality: the smart grid provides a reliable power supply with less outages, clean power, and is self healing, through the use of digital information, automated control, and autonomous systems.

- Safety and cyber security benefits: the smart grid monitors itself to detect unsafe or insecure situations that could detract from its high reliability and safe operation. Higher cyber security is built in to all systems and operations including physical plant monitoring, and privacy protection of all users and customers.

- Energy efficiency benefits: the smart grid is more efficient, providing reduced total energy use, reduced peak demand, reduced energy losses, and the ability to affect end-users to reduce electricity use instead of relying upon new generation.

- Environmental benefits: the smart grid facilitates the reduction of GHG and other pollutants by reducing generation from

inefficient energy sources, supports renewable energy sources, and enables the replacement of gasoline-powered vehicles with plug-in electric vehicles.

- Direct financial benefits: the smart grid offers direct economic benefits. Operations costs are reduced or avoided. End-users have pricing choices and access to energy information.

The ultimate smart grid vision involves the installation of new, intelligent equipment at all critical generation, transmission, distribution, and consumption points. It is clear that the smart grid is not limited to one particular technology. Several solutions are available in different combinations and for different circumstances [4]. These technologies will require a cost justification where a balance needs to be made between the cost to incorporate intelligence in the power system and the subsequent benefits. Rather than investing in an overlaying intelligence on a scale of a (large) power system, investing in small intelligent microgrids (such as business parks) can be done at a lower cost. Besides, within microgrids, intelligent features can be installed more quickly.
As a result, the trend towards smart grids starts at the distribution level. Smart grids focus on system-wide improvements with microgrids as fundamental building blocks [8]. The goals of microgrids are similar to the goals of smart grids, including minimising costs, serving the growing demand, integrating sustainable energy production and increasing the efficiency of the power system. In the next section, microgrids, which form a key to the smart grid's evolution, will be introduced.

1.4   Microgrids

Microgrids are considered as a key component of the smart grid in order to improve the power reliability and quality, to increase the system energy efficiency, and to provide the possibility of grid-independence to individual end-user sites. Microgrids are subsystems of the main grid consisting of an aggregation of (controllable) loads and DER units including dispatchable sources, renewable energy sources (RES) and distributed storage devices. They are considered as a system approach to coordinate the tremendous integration of DER units and to encounter the ensuing impacts. Microgrids are connected to the main grid via the point of common coupling (PCC)

which makes them behave like a controllable entity that can operate in both grid-connected and islanded mode [15]. Microgrids include features such as controllable production and flexible electricity demand, energy storage, commitment to energy efficiency and energy management, etc. They serve a variety of loads including residential, industrial and commercial customers as well as institutional campuses. Since microgrids aim at a local control and an optimisation of the local assets, with contribution to the higher level utility network, they can be seen as partners of the main grid rather than competitive threats [16].

1.4.1 Definition and characteristics

Although various microgrid definitions exist, in this work, the definition of the U.S. Department of Energy Microgrid Exchange Group is used, which states:

A microgrid is a group of interconnected loads and distributed energy resources within clearly defined electrical boundaries, that acts as a single controllable entity with respect to the grid. A microgrid can connect and disconnect from the grid to enable it to operate in both grid-connected or island-mode.

In Fig 1.2, a schematic diagram of a microgrid is presented as small-scale electricity network which is located downstream from the distribution substation. The microgrid includes a variety of DER units and different types of end-users of electricity and/or heat. DER units include both DG and distributed storage (DS) units with different capacities and characteristics. Microgrids can provide flexibility in matching the demand to supply, and thus, they generally include both controllable and non-controllable loads. The microgrid serves a variety of customers, e.g., residential buildings, commercial entities, and industrial parks. In order to aggregate and manage the different components, the microgrid includes a physical network which connects every unit. The connection of the microgrid to the utility network is at the low-voltage bus of the substation, through a single point of connection, the PCC [17].
The microgrid is connected to the grid and can control, based on economical and environmental decisions, the power exchange with the utility network, the costs and emissions related to the local power generation and the consumption. The high amount of penetration of DER units potentially necessitates provisions for both islanded and

grid-connected modes of operations and a smooth transition between both (i.e., islanding and synchronisation transients) to enable the best utilisation of the microgrid resources. However, it is expected to provide sufficient generation capacity, control and operational strategies are necessary in order to supply the load after being disconnected from the distribution system at the PCC and remain operational as an autonomous (islanded) entity.
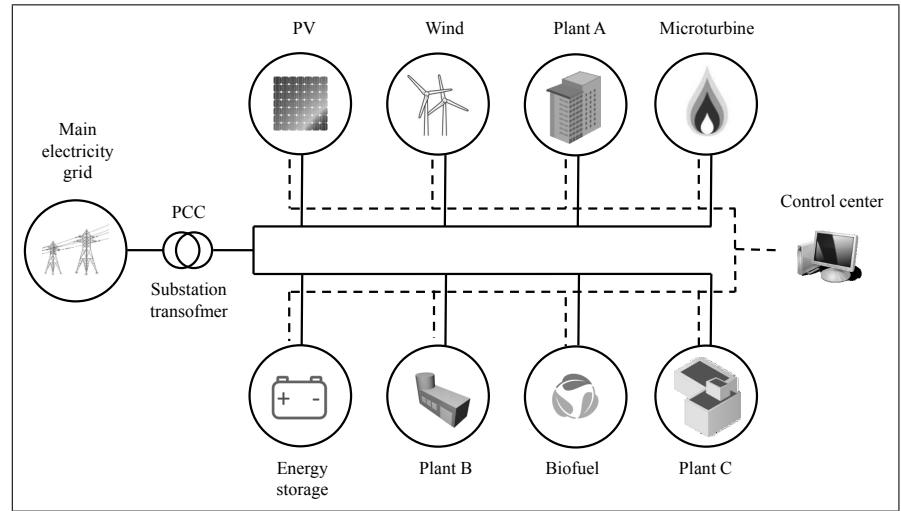
Figure 1.2: Microgrid configuration

The microgrid DER units are electronically coupled units that utilise power electronic converters to provide the coupling media with the host system. The control concepts, strategies, and characteristics of power electronic converters, as the interface media for most types of DG and DS units, are significantly different than those of the conventional rotating machines. Therefore, the control and management strategies, and the dynamic behavior of a microgrid, particularly in islanded mode, are different as compared to the conventional power system [17]. Besides the physical network, the microgrid consists of a communication network including a microgrid control center (MCC). The different control levels within a microgrid will be explained later in this thesis.

1.4.2 Drivers and benefits

DERs play a major role in the path towards the future energy landscape. These technologies, which are currently in different stages of development, drive us to a more decentralised energy world. Fuel cells, wind turbines, photovoltaics, or more traditional energy sources such as diesel generators, are being deployed at a rapid pace. Deploying DER in a widespread, efficient and cost-effective way requires advanced control strategies and can help the distribution grid in the progress towards a smarter grid. As explained in 1.2.1 , without the introduction of a coordinated approach, the continuous increase in the use of DER will reach a limit, threatening the power quality of the distribution grid.

The trend towards the enhancement of the environmical effectiveness and resilience of the main grid can be supported by smart microgrids [8]. By aggregating DERs into a microgrid, several opportunities and benefits exist for both end-users and utilities [15, 18, 19]. The technical and economical benefits offered by microgrids for the two main stakeholders are listed below:

- Microgrid customers can benefit from improvements in reliability of service and reductions in energy cost [20, 21]. A microgrid provides an improved reliability of electricity supply (locally) at places where necessary, rather than improving it in the entire system, which is more expensive. With the increasing unpredictable generation and higher consumption (peaks), reliability in distribution network becomes more challenging [22]. Unreliability in power systems can lead to economic losses. Besides, microgrids can reduce feeder losses, provide reactive power and local voltage support, remove transmission and distribution bottlenecks, increase efficiency through CHP and provide an easier large-scale integration of DG units [23, 24].
  Reductions in energy cost can come from reduced energy use, for example from increased efficiency and demand response (DR). Due to the aggregation of mixed assets into a microgrid, additional economic benefits arise by allowing the microgrid customers to participate in the electricity markets and ancillary services.

- From the grid's point of view, microgrids are regarded as a single controllable unit, enabling the microgrid to deliver the cost benefits similar to the large units. Therefore, utilities do not

have to consider each unit separately for their system management.

While not always obvious to utilities, the economics and reliability of their service can be improved by microgrids since they can be a coordinated system approach for incorporating distributed energy resources. For example, microgrids can help to meet the renewable energy obligations, and they can optimise a "troublesome" business complex or university campus, making it more economic and reliable to serve [21, 25].

It is clear that the implementation of microgrids benefits our current power system infrastructure, and by managing the energy in an efficient manner, the costs and the reliability for the end-user can also be improved [19].

1.4.3   Microgrid projects

Several microgrids and smart grids projects are being tested and demonstrated in many research projects [26–28]:

- the Linear project in Flanders, Belgium

- the Siemens Microgrid project in Flanders, Belgium

- the U.S. CERTS Microgrid Test Bed

This PhD thesis is envisioned as a microgrid research project in the framework of the European Interregional project ACE (Answers to the Carbon Economy), partly funded by the European Regional Development Fund (ERDF). The general aim of the ACE project was to set out a transition path towards a low carbon economy from a business perspective. Methods were developed on legal, economic, spatial, technical and social level to decrease greenhouse gas emissions from businesses, while increasing competitiveness in the project areas. ACE investigated how to implement low carbon principles on three levels: individual businesses, business to business (B2B) relationships and business parks (BP). Guidelines were set out to improve the energy efficiency on each of these levels and to organise collective production of green energy in an economically competitive way. Research was focussed on sustainable industrial buildings and eco-industrial business parks and was applied on the ACE pilot projects. The aim for these pilot projects was to achieve the EU 20/20/20 CO_2 reduction targets, to diversify the traditional economic structure and

to make businesses resilient to economic and climate change.

An important deliverable of the ACE project was the "Low carbon business park manual". More information of this project and its results, can be found in [29, 30].

Business parks can be considered as base units for the development of industrial economy and a breakthrough for the regional allocation of resources and environmental management. The growth of the low-carbon economy encourages industrial parks to strive for a carbon-neutral mode incorporating production, consumption, storage and resource allocation problems. As introduced before, clustering DER and energy consumers forms the guiding concept of the development of smart energy networks. Especially on industrial parks, smart energy networks become more prevalent and energy clustering can be integrated into the physical infrastructure of the area. Because industrial parks are generally interfaced to the utility network through a single PCC, these small-scale grids can be considered as microgrids. By aggregating DER into a microgrid, several opportunities and benefits exist for both end-users and utilities. However, several issues associated with planning and management must be addressed before the full benefits of the microgrid can be achieved. In this context, the main contribution of this PhD thesis is the development of a microgrid multilayer control approach which obtains a day-ahead unit commitment method to provide an economically and environmentally viable unit commitment that is physically feasible in terms of voltage violations. The outline and the addressed research questions are presented in the following section.

1.5   Research questions addressed in this PhD dissertation

In the search for low carbon, reliable and affordable ways to provide electricity, an increased attention is going to the microgrid, a small-scale power system that uses a combination of energy generation and storage devices to serve local customers. Microgrids are expected to revolutionise the existing electrical grid by allowing two-way communications to improve efficiency, reliability, economics, and sustainability of the generation and distribution of electrical power. However, several issues associated with planning and management must be addressed before the full benefits of the microgrid can be achieved.

There are a large number of economic and technical factors raised by both DER units and distribution network properties that have an impact on the operation of the microgrid. An active management of DER is needed to achieve a least-cost solution while satisfying all technical requirements. In general, this can be seen as a downsized version of the unit commitment and economic dispatch problem that is traditionally applied to large central generators. However, exceptional features of distribution networks have introduced further restrictions to this classic optimisation task. In comparison with unit commitment problem on transmission level, the microgrid scheduling task features the following major differences:

1. As a result of the climate issue, the environmental awareness becomes more important. CO2-emissions caused by combustion processes of distributed generation power plants need to be considered when developing the power system of the future. The challenge is to find an optimum which provides emission reductions while keeping costs at a reasonable level. An enviro-nomic (environmental/economic) optimisation model needs to be implemented in the energy management system of a micro-grid.

2. A complete formulation of the microgrid scheduling task includes modeling of storage dispatch, demand side management (DSM), RES control measures and spatio-temporal uncertainties (e.g., electric vehicles), while the traditional unit commitment problem faces none of them.

3. Microgrids are constructed as small-scale distribution networks, which are generally radial or weakly-meshed, and are likely subject to technical problems such as over-/under-voltage, voltage imbalances, or overloading when load/generation conditions vary.

The main contribution of this PhD thesis is the design of a multi-layer control strategy for microgrids which tackles the issues listed above. A decision making model is developed for a microgrid day-ahead scheduling, and fits in the tertiary level of the microgrid hierarchical control structure. The tertiary control is conceived to achieve global controllability of the microgrid according to different criteria and will be discussed in § 2.2.2. The model works on a day-ahead time frame and will attempt to optimise the microgrid operation, based on merits of interests, over the complete time horizon. It provides

optimal solutions by assuming that the future user and grid information are known in advance. The optimal solutions, also known as reference set points, can be provided to the underlying secondary and primary controllers.

The first issue relates to determination of the optimal mix of power generation in order to provide the performance needed at the least cost, or with the lowest possible emissions. Unfortunately, both objectives are often contradictory. In general, low costs mean high emissions, and vice versa. A microgrid system operator may care more about achieving lower costs rather than the lower emissions. Given the preferences, the operator needs to decide how to operate the microgrid. In Chapter 3, an analytical method based on a multi-objective hybrid genetic algorithm was developed in order to help the microgrid system operators in the decision making process. The method optimises both objectives simultaneously, determining the costs and emissions associated with all possible options. Based on the results, the method generates a set of optimal operating strategies that will minimise costs and emissions.

When designing a new optimal planning tool for a microgrid, a major challenge (and opportunity) is to decide the units to operate while providing the performance needed. The second issue above introduces a major modelling complexity to the microgrid unit commitment task. The unit commitment views all components of a microgrid as a whole and attempts to converge to a global optimum which delivers the best compromised result to all relevant entities. In Chapter 4, an analytical method based on a multi-objective hybrid genetic algorithm is proposed and demonstrated for a microgrid day-ahead unit commitment model. The model aims to schedule the power among the different microgrid units while minimising the operating costs together with the CO_2 emissions produced. The approach is demonstrated on a test case including a variety of DER units which are likely to be found in a microgrid. A storage device is added where the charge and discharge schedule is calculated according to both objectives. The presence of a storage element, as well as the possibility of exchanging energy with the utility grid adds flexibility to the microgrid operation and besides, it increases the solution space (set of feasible solutions) of the microgrid unit commitment problem. The charge and discharge commands of the storage device are allocated according to the lowest cost and the lowest CO_2 emissions. Besides, the commands of charging and discharging are associated to the energy prices as well, and where the storage element takes advantage of

purchasing power from the upstream grid and selling it back according to the most favourable microgrid revenue. In addition, as a part of the demand side participation strategy, a charging schedule was determined for the electric vehicles. A 24-hour microgrid simulation has been performed with an interval or time span of 15 minutes where the objectives where considered simultaneously. These reference set points, delivered by the day-ahead unit commitment, can form an input for controllers which work on a shorter time frame (such as the primary controller) around which they may vary to maintain stability.

The third issue listed above relates to the fact that microgrids are inherently more fragile as compared to transmission networks. A complex and uncoordinated integration of DG units can easily cause technical problems in a weak microgrids. Additionally, the different types and sizes of DG units makes it difficult to apply some traditional control methods adopted for transmission networks such as frequency control and voltage control. These added uncertainties must be taken into consideration when solving the scheduling problem in order to obtain reliable solutions. In Chapter 5, a voltage control approach was developed and added to the microgrid unit commitment strategy. Due to the introduction of this voltage control approach, active power reference set points can be provided (to the underlying controllers around which they may vary to maintain real-time stability) not only according to the economical and the environmental objectives, but also taking into account the voltage level at every bus in the microgrid.

In order to demonstrate this multilayer control strategy for microgrids, case studies were performed involving the planning of a microgrid including a variety of DER units and loads which are likely to be found in a microgrid. The proposed microgrid includes renewable energy resources, a battery storage unit, micro turbine generator sets, a fuel cell (FC) and electric vehicles (EVs). The system should run as much as possible on its renewable technologies, and when more power is needed, the distributed generators or batteries will be used. Finally, the system should provide perfect reliability that is, it should never fail to meet total customer demand.

2

Microgrid multilayer control structure

This chapter is written to expose the proposed structure of this PhD thesis. The main shape and the necessary elements of the microgrid multilayer control approach will be outlined to reveal the structure. Each layer will be described and discussed briefly, and later throughout this thesis, a more detailed presentation will be provided, chapter by chapter.

2.1 Introduction

As explained before, microgrids are subsystems of the electrical grid consisting of an aggregation of (controllable) loads and DER units including dispatchable sources, RES and DS devices. A coordinated control and management of the DER units is crucial within the concept of microgrids [31]. The optimal operation of individual elements in the network can provide distinct benefits to the overall microgrid performance. Therefore, efficient control and management techniques have to be developed with a proper coordination strategy among the various microgrid elements. Besides, since the architecture of microgrids can change on a regular basis, and in order to increase their potential of scalability, these control strategies should be implemented in a plug- and-play way.

The distributed structure of a microgrid comprises a network of local

controllers installed on each microgrid component. By use of these power electronic controllers, cooperative actions can be taken in order to control the microgrid [32].

The goal of this research is to develop a power system modernisation tool with the ability to optimise the microgrid. To attain this goal, an efficient multilayer control approach is developed which proposes a day-ahead unit commitment (UC) method in order to provide an optimal power generation schedule for microgrids. The objective or intention of this multilayer control concept is to provide an economically and environmentally viable unit commitment that is physically feasible in terms of voltage violations.

This chapter starts with an introduction of energy management systems (EMS) in microgrids. Subsequently, the multilayer control structure will be presented and the different levels of the hierarchy will be discussed briefly. Each level will be extensively discussed later in this dissertation.

2.2   Energy management in microgrids

In order to provide a sound operation of the microgrid, an EMS imposes itself. The purpose of a microgrid EMS is to minimise the operational cost, while delivering reliable and high quality power to the customers [17]. Due to the integration of DER units and a number of new applications, including demand response and controllable loads with spatio-temporal uncertainties (e.g., electric vehicles), the desired EMS in microgrids can be significantly different from a conventional power system. A microgrid EMS has to operate and coordinate a variety of DER units and controllable loads in order to provide high-quality, reliable, sustainable, and environmentally friendly energy in a cost-effective way [33, 34]. An EMS can be considered as a control approach which is able to optimally allocate the power output among the DG units, economically serve the load, and automatically enable the system resynchronisation response to the operating transition between grid-connected and islanded mode.

When designing and implementing a microgrid EMS, several issues should be taken into account. A microgrid runs typically in two operational modes. In grid-connected mode, the microgrid maintains the power balance by purchasing power from the main grid or selling power to the main grid in order to maximise the operational benefits. In islanded mode, the microgrid aims to keep a continuous power supply to the microgrid customers using optimal generation scheduling.

The intermittent nature of renewable sources, such as wind turbines and photovoltaic systems, leads to an output which often does not suit the load demand profile. As a result, it is difficult to provide an accurate generation schedule [35–37]. Energy storage systems allow operations with a more flexible and reliable management of energy. They can charge energy at low price hours and sell it at high price hours, which can help the microgrid to operate more efficiently and economically. Using the latter, the operation and control of the microgrid becomes more complicated and challenging.

In this section, the complete control and management structure of a microgrid will be discussed.

2.2.1 Control levels of a microgrid environment

The control levels within a microgrid environment are presented in Figure 2.1 [38, 39]. Each level has different permissions and obligations. The upper level includes the DNO and market operator (MO).
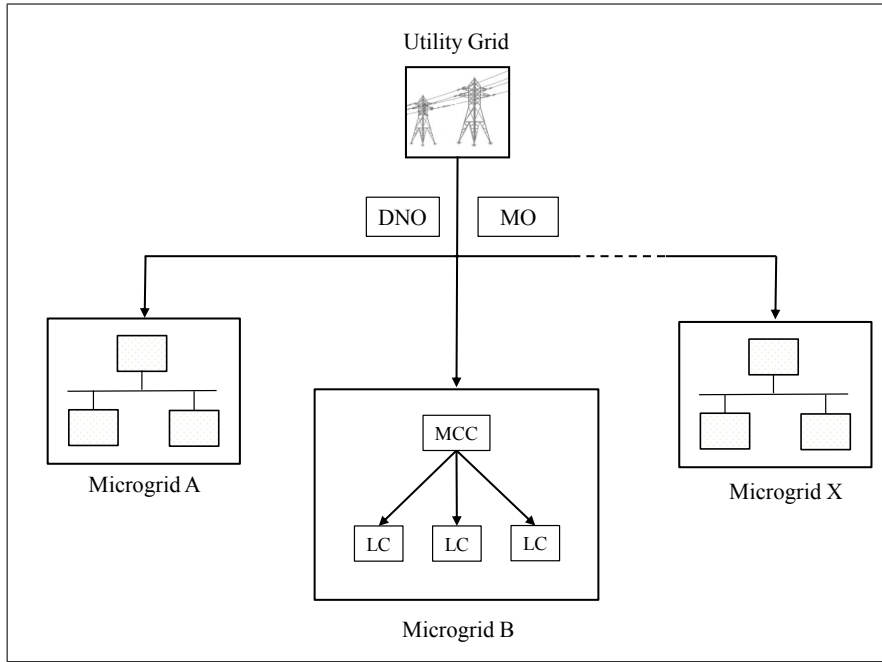
Figure 2.1: Control levels of a microgrid environment

The DNO is responsible for the electricity distribution in a MV/LV area, where more than one microgrid can exist. At the same level,

the MO is responsible for the market functions. The DNO as well as the MO belong to the utility grid and are not part of the microgrid. A microgrid central controller (MCC) can be found on the lower level. The MCC forms the link between the DNO/MO and is responsible for the coordination of the local controllers (LCs) within the microgrid. An LC has a certain level of intelligence and controls the DER units and the controllable loads within the microgrid. The control and management strategy, which is integrated in the MCC, forms the central governing body of the microgrid. The LCs associated with each DER and/or load are established within the level of the microgrid.

2.2.2 Hierarchical control architecture of a microgrid

The use of a hierarchical control architecture has been proposed for microgrids in order to manage different objectives within different time-scales [40]. Generally, a three-level hierarchy is considered including a primary, a secondary and a tertiary control level. Within each level, different control algorithms are embedded with necessary information exchange between the levels but with decoupled behaviors. Fig. 2.2 presents a schematic diagram of the control architecture of a microgrid consisting of local and centralised controllers and a communication system. A literature review of optimal control techniques applied to the energy management and control of microgrids is given in [41, 42].
The primary controller is implemented in the LCs of the microgrid units. This controller is fast and automatic, and operates without communication. The primary controller contributes to the system reliability. This controller performs the control of local power, voltage and current. It normally follows the reference set points given by upper level controllers and performs control actions over interface power converters. Because of the fast dynamics in the microgrid, which mostly lacks a significant amount of rotating inertia, the primary controller should be fast, i.e., in time scales of milliseconds. Also, for reliability reasons, communication is often avoided in the primary control, similar to conventional grid control [43]. Since this controller is based only on local measurements, the primary controller is conceived as a local control strategy. A survey of primary control strategies for microgrids is presented in [44]. An example of the primary control is the active power/grid voltage (P/V) droop concept in general and the voltage-based droop (VBD) controller [8]. In [15], a
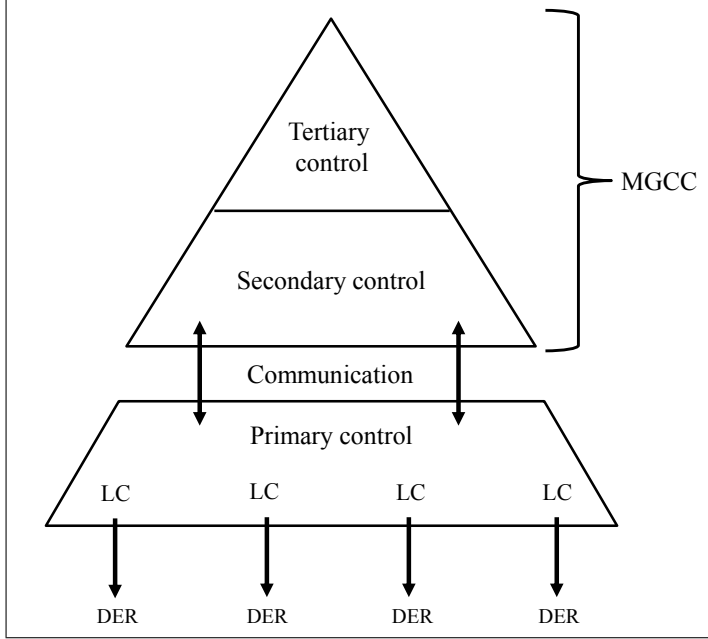
Figure 2.2: Microgrid architecture

control algorithm was developed for stabilising microgrids in islanded operation by controlling all grid assets (DG units, loads and storage elements) with a coherent control structure without inter-unit communication, i.e., a primary controller. Since the primary controller does not need ICT and remote measurements, it can facilitate the smart grid communication.

In the existing hierarchy, secondary control appears on top of primary control. In order to improve the system power quality and achieve an accurate power sharing, secondary control approaches are developed that act over the primary control loops. This controller deals with corrections of steady-state errors in frequency and voltage magnitudes produced by the primary controller and provides adjustment and compensation reference set points to the LCs, around which they may vary to maintain stability. This secondary controller operates on a longer time frame compared to the primary controller. Since it uses communication and metering assets of the smart grid, this controller fits directly in the smart grid concept.

The tertiary control is conceived for energy management according to different design criteria. The aim of the tertiary controller is to

introduce intelligence in the whole microgrid system. This controller
will attempt to optimise the microgrid operation based on merits of
interests, mostly efficiency and economics. Knowledge from both the
microgrid side as from the external grid are essential to execute the
optimisation functions. Decision making algorithms are employed to
process the gathered information and take proper actions [42].

As presented in Fig. 2.3, the time frames in which the control is
performed are increased (from the primary, secondary levels to the
tertiary level) to achieve a decoupled behaviour between the layers,
which simplifies the implementation of higher level controllers as well
as the system stability analysis [45]. In order to achieve global con-
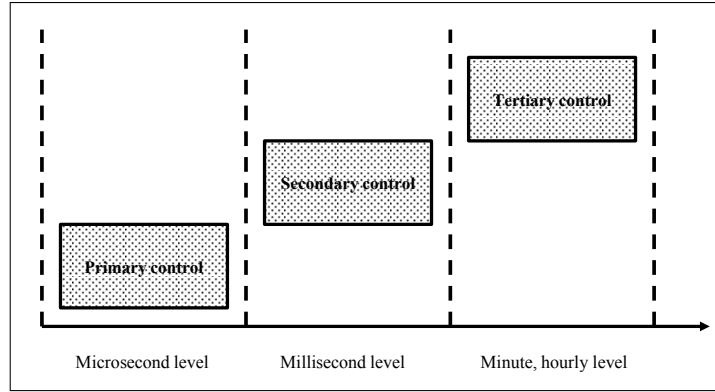
Figure 2.3: Microgrid hierarchical control time frame

trollability of the microgrid, the secondary and tertiary controllers
are often used. As depicted in Fig. 2.2, in this conventional control
structure, both the secondary and tertiary controller are included in
the MGCC. Since this MGCC is responsible for coordination of the
LCs and to manage the overall microgrid as one integrated entity, this
central controller is generally based on an EMS. The MGCC performs
an energy management analysis, and sends control commands to the
LCs.

In the next section an energy management approach for microgrids
will be discussed with the focus on optimal scheduling of the micro-
grid units.

2.2.3 Energy management architecture

Within microgids, an EMS controls the power flows by adjusting the
exchanged power with the utility grid, the dispatchable DERs, and

the controllable loads based on the present and forecast information of the market, the production by the RES, and the loads in order to meet certain operational objectives [33, 34, 46]. A diagram of the
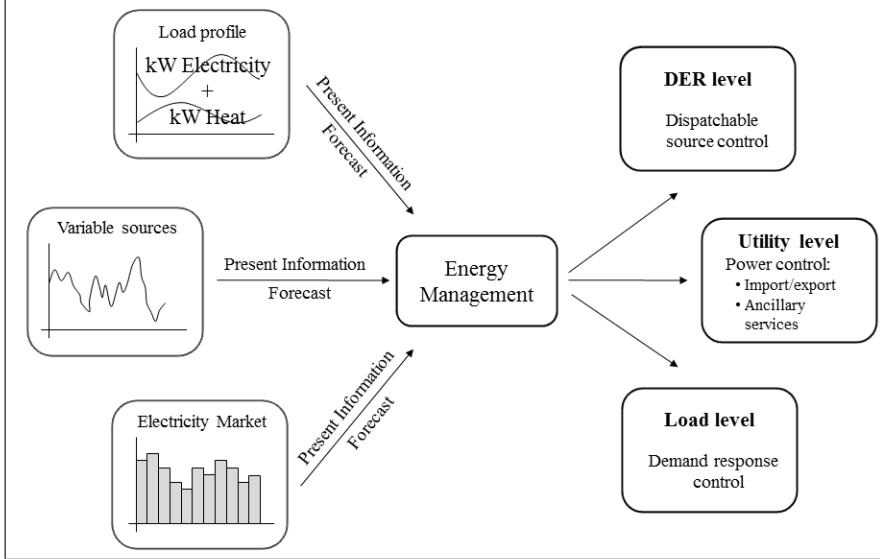
Figure 2.4: Structure of an energy management system

EMS is presented in Figure 2.4 [17]. The EMS considers present and forecast information, such as the microgrid load profile, the variable renewable sources and information of the electricity market, and operates on three levels, i.e. DER, utility and load level. The EMS has the responsibility to schedule the power among the different DER. It has to determine the set points of the DER units and controllable loads in order to obtain economic and environmental objectives while maintaining power quality. Furthermore, the EMS should ensure a convenient resynchronisation of the islanded microgrid with the utility grid. Besides, the system also provides ancillary services by participating in the energy market.

Energy management systems for microgrids are differentiated according to the time scale of their management cycle, including day-ahead scheduling and short or real-time dispatch. As presented in Fig. 2.5, the energy management problem is solved offline, on a day-ahead basis, allowing an online implementation to be achieved via real-time system state updates.

A real-time management operates in an online setting, where the complete input is not known a priori. The real-time management finds
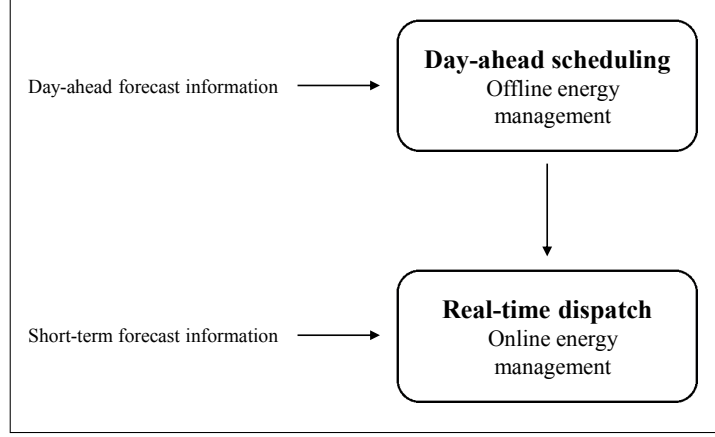
Figure 2.5: Energy management in microgrids

its usefulness in addressing the lack of accurate mathematical models and the lack of future information of electricity demand and supply in this problem. Because of the uncertainties in the demand and renewable energy forecast, the day-ahead scheduling may deviate from the real-time dispatch. Energy management based on short-term forecast will provide more accurate results on a short term. However, in order to control and manage the microgrid units in real-time while fully exploiting the benefit of long-term prediction, an offline optimisation approach imposes itself in order to devise the online microgrid management.

The focus of this PhD is on the optimal microgrid day-ahead scheduling to achieve a near perfect real-time dispatch. A decision making model is developed which fits in the tertiary level of the microgrid hierarchical control structure. The model works on a day-ahead time frame and will attempt to optimise the microgrid operation over the complete time horizon. It provides optimal solutions by assuming that the future user and grid information are known in advance.

In the following paragraph, the main shape and the necessary elements of the microgrid multilayer control approach will be outlined to reveal the structure. Each layer will be described and discussed briefly, and later in throughout thesis, a more detailed presentation will be provided, chapter by chapter.

2.3   Microgrid multilayer control

In this research, an efficient multilayer control approach is developed that proposes a day-ahead security-constrained unit commitment method to provide an economically and environmentally viable unit commitment that is physically feasible in terms of voltage violations. With the multilayer control approach, the future operational states of the controllable units within the microgrid are determined ahead of time. The multilayer control approach fits directly in the tertiary level of the microgrid hierarchical control structure, which is conceived to achieve global controllability of the microgrid according to different criteria. The power reference set points provided by the multilayer control approach can, in turn, be used as an input for the underlying secondary and primary controllers that operate on a shorter time frame, and around which they may vary to maintain stability [47].

The proposed concept follows the idea of a day-ahead coordination including the unit commitment problem (scheduling layer), an offline power flow calculation (executive layer) and a security check with feedback control (adjustment layer). Since the complete multilayer control concept works on a day-ahead time scale, the model can be considered as an offline optimisation approach. The proposed multilayer control concept is presented in Fig. 2.6. The scheduling layer calculates the power set points of the microgrid units and is based on optimisation techniques, the day-ahead energy market, the demand bids, and the availability of renewable energy sources. The executive layer performs an offline system load flow calculation in order to determine the voltages at the different buses in the network. The adjustment layer provides a dynamic gain to adjust the boundaries of the microgrid generation units according to the data coming from the executive layer. This layer is utilised to maintain the voltage within the acceptable limits. Subsequently, when closing the loop, the scheduling layer recalculates and updates the power settings of the DER units by considering the output from the adjustment layer as a feedback. This iterative process will continue until all voltage violations are eliminated and a converged optimal solution is found. The different layers of the microgrid multilayer control structure will be described briefly in the following paragraphs.
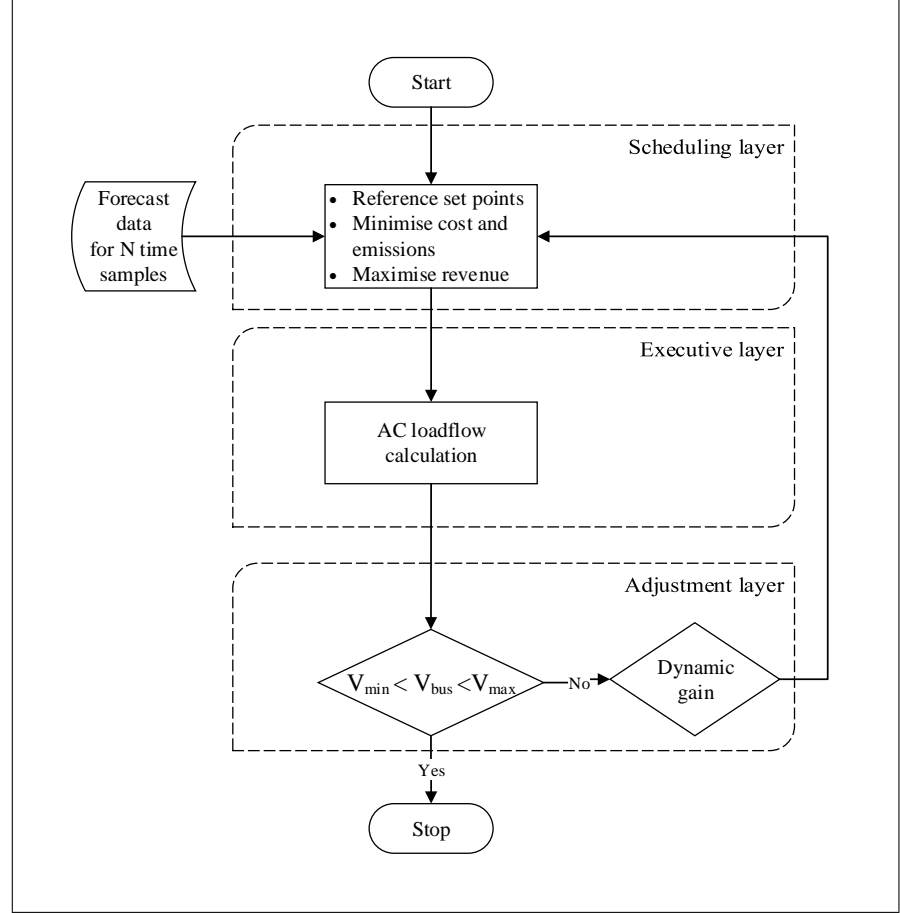
Figure 2.6: Structure of a microgrid multilayer control

2.3.1 Scheduling layer

The scheduling layer forms the highest layer in this microgrid multi-layer control concept. Within this layer, a day-ahead UC strategy is implemented which involves the simultaneous optimisation of the fuel costs and the CO_2 emissions of the local generators [48,49]. This layer starts with the initialisation of the characteristics of the DER units, the availability of the (predicted) renewable energy production, the demand bids, and the day-ahead market conditions. Subsequently, a 15 minute power generation schedule will be calculated for the next 24 hours. This short optimisation interval is chosen to adequately reflect issues described in § 4.2.1.

Given the input characteristics, the objectives and the constraints, the power set points of the different microgrid generation units are calculated (for each time step) in a way that over the complete time horizon the objectives are optimised.

The scheduling layer is presented in chapter 4 where a heuristics-based day-ahead unit commitment model for microgrids is proposed and demonstrated. The approach is demonstrated on a test case including a variety of DER units which are likely to be found in a microgrid. A 24-hour microgrid simulation has been performed with an interval or time span of 15 minutes where the objectives were considered simultaneously.

2.3.2 Executive layer

In order to determine the future operational states of the microgrid units whereby the bus voltages are maintained within acceptable limits, an offline load flow calculation should be performed to obtain the initial values of the voltage magnitudes of the different microgrid buses. Therefore, within the executive layer, an AC power flow calculation will be performed with the power reference set points calculated by the scheduling layer to obtain the values of the voltage magnitudes of the different buses in the microgrid network.

2.3.3 Adjustment layer

After the load flow calculation, the numerical values of the bus voltages are transmitted to the third layer. The adjustment layer is utilised to maintain the bus voltages and contains a security check with feedback control to the first layer. The purpose of this third layer, is to keep the bus voltages within pre-specified bounds by producing more or less power provided by the microgrid generation units. In case of a severe voltage deviation at any bus within the microgrid, a dynamic gain will be introduced. Depending on the deviation (positive or negative), and on the location of the power generation units and their respective distance from the voltage problem, an appropriate gain will be provided to adjust the boundaries of the microgrid generation units. In this way, the range (between the lower and upper bound) in which the set point can be committed will be modified. Subsequently, when closing the loop, the renewed boundaries are then fed back to the scheduling layer, which recalculates the UC solution. The updated power generation schedule will again go through the second and third layer of the control hierarchy. This iterative process

will continue until all voltage violations are eliminated and a converged optimal solution is found.

Chapter 5 focuses on the voltage control in microgrids. The performance and effectiveness of the proposed hierarchical multilayer control structure is tested and presented in this chapter. Due to the introduction of this third layer, active power reference set points can be provided (for real-time scheduling) not only according to the economical and the environmental objectives, but also taking to account the voltage level at every bus in the microgrid. Sections 2.3.1, 2.3.2 and 2.3.3 form a short version of the three layers and can be considered as a transition to the next chapters where the full context of each level will be provided.

3

Optimisation in power system planning

The electrical power system is a large and complex system that consists of an enormous number of elements that are interconnected. It includes a set of synchronous generators, transformers, transmission and distribution lines, switches, controllers, loads, etc. Within this large system, several objectives, operational actions and design decisions, each with their own priorities, require an optimisation problem to be solved. Power system optimisation problems have multiple dimensions because of their numerous variables and constraints. Many different optimisation strategies have been employed to solve power system problems.

In this chapter, a survey of different optimisation methods for power systems is presented. Subsequently, an introduction to genetic algorithms is provided. The chapter ends with an example of using a genetic algorithm in power system planning.

3.1 Introduction

The goal of an optimisation problem is to find the combination of parameters that optimise a given quantity (or multiple quantities), possibly subject to some restrictions on the allowed parameter ranges. The quantity to optimise (maximise or minimise) is also called the objective function. The parameters that may be changed in the quest

for the optimum are called the control or decision variables. The restrictions on allowed parameter values are known as constraints. Any optimisation problem can be formulated as a sequence of steps presented below:

- Choosing design variables (control and state variables)

- Defining constraints

- Defining objective function(s)

- Setting up variable limits

- Selecting an algorithm to solve the problem

- Solving the problem to obtain the optimal solution

The optimisation problem may have a single objective function or multiple objective functions. A multi-objective optimisation problem, also called multi-criteria, multi-performance, or vector optimisation problem, can be defined as the problem of finding a vector of decision variables that satisfies constraints and optimises a vector function whose elements represent the objective functions. The objective functions form a mathematical description of performance criteria that are usually in conflict with each other. Therefore, the term "optimising" means finding a solution that would give the acceptable values of all the objective functions to the decision maker. Most real-world problems involve more than one objective, making multiple conflicting objectives to be solved as multi-objective optimisation problems. In literature, several optimisation techniques have been applied to solve power system problems [48, 50–54]. In the next section the most important mathematical optimisation techniques used in power system problems are briefly discussed.

3.2   Optimisation techniques

Many optimisation algorithms are available with many methods appropriate only for a certain type of problems. It is important to recognise the characteristics of a problem to be optimised in order to identify the appropriate optimisation technique. Two elements that directly affect the success of an optimisation technique are the quantity and domain of decision variables and the objective function. The identification of these elements requires familiarity with the available

optimisation techniques and knowledge of how they interface with the system to be optimised. Optimisation problems can be classified according to the mathematical characteristics of the objective function, the constraints, and the control variables. Within each class of problems, there are different methods, varying in computational requirements, convergence properties, etc. In general, two optimisation methods can be distinguished, including conventional optimisation techniques and evolutionary optimisation techniques. Both will be discussed in § 3.2.1 and § 3.2.2.

3.2.1 Conventional optimisation techniques

Conventional optimisation techniques consist of calculus-based, enumerative, and random techniques. These techniques are based on well-established theories and work perfectly well for a case wherever applicable.

A first technique is called linear programming (LP) which is a reliable and robust technique for solving a wide range of optimisation problems characterised by linear objectives and linear constraints. Many commercially available power system optimisation packages contain linear programming algorithms for solving power system problems for both planning and operation engineers [55].

Sequential quadratic programming (SQP) can be used for solving non-linearly constrained problems. The idea is to obtain a search direction by solving a quadratic program which can be considered as a problem with a quadratic objective function and linear constraints. This approach is a generalization of Newton's method for unconstrained optimisation. This method does not guarantee to converge to a global solution of the optimisation problem and it is computationally expensive. Therefore, SQP is not often used.

Gradient-based search methods use the gradient of the objective function to find an optimal solution. Every iteration of the optimisation algorithm adjusts the values of the decision variables in order to generate a lower objective function value. Each decision variable is changed by an amount which is proportional to the reduction in the objective function value. The advantages of gradient-based techniques are that computation and set-up time are relatively low. However, because gradient-based search methods rely purely on the local values of the objective function in their search, these methods may not be able to provide an optimal solution and usually get stuck at a local optimal solution. Besides, these methods cannot be applied

with discrete variables. Gradient-based search methods are best used on systems where there is one clear optimum.

Lagrangian methods which can be considered as classical analytical methods are used to identify candidate solutions. Because of their combinatorial nature, these methods become impractical for large numbers of decision variables, and solutions are obtained numerically instead by means of suitable numerical algorithms.

Non-linear programming techniques are developed to solve optimisation problems with very high accuracy, but their execution time is very long and therefore cannot be applied to highly complex problems. Successive programming algorithms are improved linear programming techniques which can be used effectively to solve the optimisation problem. The problem is solved by successively approximating the original problem by Taylor series expansion at the current operating point and then moving in an optimal direction until the solution converges.

Mixed integer programming (MIP) is an integer programming technique used for optimising linear functions that are constrained by linear bounds. This technique is a type of integer programming in which not all of the variables to be optimised have integer values. MIP was found to have the widest application. However, when the nature of the problem to be solved is continuous and dynamic, a stochastic approximation (discussed later) is preferred.

The classic methods presented in this section have some drawbacks due to the difficulty of convergence, the long (expensive) execution time, the algorithmic complexity, and the generation of a weak number of non-dominated solutions. The existence of noise in the objective and constraint functions, as well as the presence of discontinuities in the functions, constitute further obstacles in the application of standard and established methods.

We can conclude that many inhibiting difficulties remain when these methods are applied to real-world problems, and therefore, due to these inconveniences, evolutionary algorithms are more popular.

3.2.2   Evolutionary optimisation techniques

Since power systems are dynamic, complicated and non-linear systems including considerable uncertainties, and different objectives are to be satisfied, the number of combinations of the optimisation problem becomes excessively high. Due this increased complexity of problems to be optimised in power systems, the need for advanced

programming techniques to find the approximate solutions to optimisation problems have gained more importance. These unconventional techniques include evolutionary programs such as genetic algorithms. Having a population of initial solutions increases the possibility of converging to an optimum solution, and additionally, updating the current information of the search strategy from the (previous) historical information, is a natural tendency [56]. With this ambition, research has been done to restructure the standard optimisation techniques for solving real-world problems, which have the characteristics of memory update and population-based search solutions.

Evolutionary algorithms are robust and powerful global optimisation techniques for solving large-scale problems that may have many local optima. This type of algorithms simulates the principle of evolution, and maintain a population of potential solutions through repeated application of some evolutionary operators such as mutation and crossover. They are able to improve the fitness of the individuals and they converge to the fittest individuals representing the optimum solutions. Evolutionary algorithms can avoid premature entrapment in local optima because of the stochastic search mechanism. However, they require high CPU times, and can be poor in terms of convergence performance. On the other hand, local search algorithms can converge in a few iterations but lack a global perspective. The combination of global and local search procedures can offer the advantages of both optimisation approaches. Therefore, these techniques are often hybridised with other intelligent system techniques in order to increase their performance.

Most of the real-world problems involve more than one objective, making multiple conflicting objectives to be solved as multi-objective optimisation problems. Evolutionary algorithms are suitable to solve multi-objective optimisation problems because they deal simultaneously with a set of possible solutions (the so-called population). This feature allows to find several members of the Pareto optimal set (which will be explained in § 3.2.2.1) in a single run of the algorithm, instead of having to perform a series of separate runs as in the case of classical programming techniques as presented in the previous section. Additionally, evolutionary algorithms are less susceptible to the shape or continuity of the Pareto front (e.g., they can easily deal with discontinuous or concave Pareto fronts), whereas these two issues are a real concern with the programming techniques described in § 3.2.1.

3.2.2.1 Pareto efficiency

In many engineering applications, computationally expensive multi-objective optimisation problems arise where several conflicting objectives are to be optimised simultaneously while satisfying constraints [57]. Because these optimisation problems may have a set of many Pareto optimal solutions, the decision maker is required to select the most preferred one. Pareto optimal, also called non-dominated, refers to a state where resources are allocated in the most efficient manner. It is obtained when a distribution strategy exists where none of the objective functions can be improved without degrading any of the other objective functions. Unfortunately, most of the time, this does not give a single solution, but rather a set of solutions called the Pareto optimal set. Without additional preference information (priorities), all solutions within this set are considered equally good. An example is presented in Fig. 3.1, where two quadratic functions are plotted both with a local minimum. If we want to find the value x so that both functions are minimised, the Pareto front should be found. In this case, the Pareto front lies between the minima of both functions, $(-2.52, 0.71)$ and $(0.84, 10)$ respectively. Within this Pareto front, it is clear that an improvement of one objective results in a degradation of the other objective.
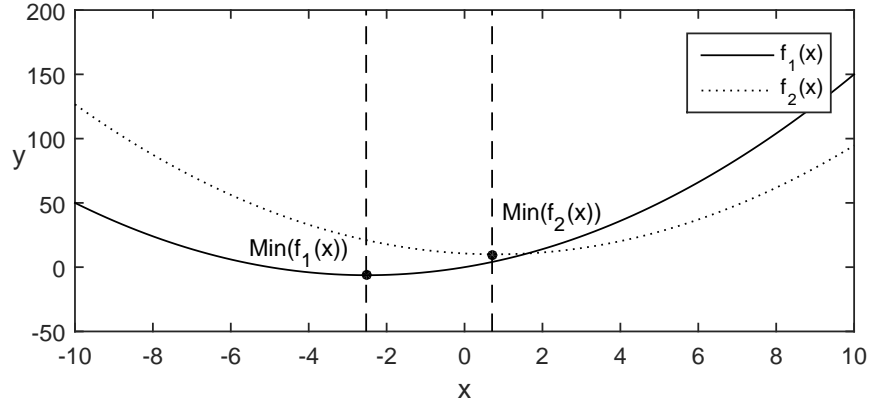
Figure 3.1: Pareto front

The advantage of evolutionary algorithms is that they have minimum requirements regarding the problem formulation. Objectives can be easily added, removed, or modified. Moreover, because evolutionary algorithms operate on a set of solution candidates, they are well suited

to generate Pareto set approximations. It has been demonstrated in various applications that evolutionary algorithms are able to tackle highly complex problems and, therefore, they can be seen as a complementary approach to traditional methods such as integer linear programming. Among the evolutionary computational algorithms, genetic algorithms are the most widely-used evolutionary computational algorithm. The next section explains what genetic algorithms are, the idea behind the operation, which terminology is used and the concept of the basic algorithm.

3.3   Genetic algorithms

During the past four decades, several heuristic algorithms have been developed. They are applicable to a wide range of real-world problems. Due to the fast development of these algorithms, it has become challenging to choose the most suitable one [58]. Genetic Algorithms (GA), Particle Swarm Optimisation (PSO), Ant Colony Optimisation (ACO), etc. are nature-inspired techniques which can find global optimal solutions. Recently, the these approaches have been hybridised with other (classical) techniques to solve this problem more efficiently [59–61].
The genetic algorithm is widely used for solving optimisation problems because it is simple and function-independent [62]. Various GA-based techniques have been used to solve the unit commitment problem. A literature survey of various genetic algorithm based techniques for the UC problems is given in [63].
In [58], 5 optimisation algorithms were compared including the genetic algorithm GA and PSO. The GA shows an overall consistently performance with all kinds of problems. The PSO has offered the highest convergence speed, though the optimality and accuracy were not as good as the GA. Based on the performance and the accuracy, the genetic algorithm was chosen in this work.
A genetic algorithm is a search algorithm based on natural selection, the process which drives biological evolution. The genetic algorithm is a stochastic search method, and is proven to be a robust problem solving technique [64,65]. The algorithm essentially replicate the way in which life uses evolution to find solutions to real-world problems. In 1975, the genetic algorithm was mathematically formulated for the first time [66]. The genetic algorithm repeatedly modifies a population of individual solutions. At each step, the genetic algorithm selects individuals randomly from the current population to be par-

ents and uses them to produce the children for the next generation. Over successive generations, the population proceeds toward an optimal solution. The outcome resulting from this simulated evolution is not discovered by a random search through the problem state space, instead it is discovered by a directed search from random positions in that space. Since random or enumerative searches can be very exhaustive for large problem dimensions, the simulated evolution of a solution using genetic algorithms can be more efficient and robust than the random search, enumerative or calculus based techniques. Additionally, the problem solving strategy of genetic algorithms uses the fitness to direct the search and, therefore, they do not require any specific knowledge of the search space, and they can operate well on noisy search spaces with jump discontinuities [67]. As each individual string within a population directs the search, the genetic algorithm searches, in parallel, numerous points on the problem state space with numerous search directions. The fact that the genetic algorithm operates on a population of individuals, rather than a single point in the search space of the problem, is an essential aspect of the algorithm. This can be compared with the benefit of dropping 1000 parachutists (population size), rather than one, on the landscape. The population serves as the reservoir of the probably valuable genetic material that the crossover operation needs to create new individuals with probably valuable new combinations of characteristics [68]. The method used by genetic algorithms to simulate nature in computer-based evolutionary systems is explained in the next paragraphs. Since genetic algorithms are inspired by evolutionary biology, some important key terms are introduced in the Appendix A of this thesis before using them in the context of genetic algorithms.

3.3.1 A genetic algorithm example

The following example is intended to illustrate the process of the genetic algorithm. Consider a population of 4 strings, each with 5 bits. The objective function is presented as $f(x) = 2x$. The aim is to optimise (in this case maximise) the objective function over the domain $0 \leq x \leq 31$. The population (4 strings) is presented in Table 3.1, generated at random before the execution of the genetic algorithm. The corresponding fitness values and percentages are derived from the objective function $f(x)$.

In the fourth column, the values of $f_i / \sum f_i$ represents the probability that a string can be selected. In this example, bit string 11000

i	String x_i	Fitness $f_i = f(x_i) = 2 \cdot x_i$	$f_i / \sum f_i$	Expected count $f_i / \overline{f}$	Actual count
1	11000	48	0.381	1.524	2
2	00101	10	0.079	0.317	0
3	10110	44	0.349	1.397	1
4	01100	24	0.191	0.762	1
Sum		126	1.000	4.000	4
Avg		31.5	0.250	1.000	1
Max		48	0.381	1.524	2

Table 3.1: A genetic algorithm example

has a 38.1% chance of selection, 00101 has an 7.9% chance, and so on. The actual count column provides the results of the selections by the algorithm. As expected, these values are similar to those in the expected count column.

Once the selection process is completed, the genetic algorithm randomly pairs the newly selected members and looks at each pair individually. For each pair (e.g. $A = 11000$ and $B = 10110$), the algorithm decides whether or not to perform crossover. If it does not, then both strings in the pair are placed into the population with possible mutations (explained later on). If it does, then a random crossover point is selected and crossover proceeds as follows: $A = 11|000$ and $B = 10|110$ are crossed and become $A' = 11110$ and $B' = 10000$.

Subsequently, the children A' and B' are placed in the population with possible mutations. The genetic algorithm calls the mutation operator on the new bit strings very rarely (usually on the order of ≤ 0.01 probability), generating a random number for each bit and flipping this particular bit only if the random number is less than or equal to the mutation probability. Once selections, crossovers, and mutations of the current generation are complete, the new strings are placed in a new population representing the next generation, as shown in Table 3.2.

In this example (of one generation), the average fitness increased by approximately 30% and maximum fitness increased by 25%. This simple process would continue for several generations until a stopping criterion is met. The stopping condition (criteria) was not considered in this example since we looked at only one iteration of the genetic

After reporoduction	Mate	Crossover	After crossover	Fitness $f_i = f(x_i) = 2 \cdot x_i$
11|000	x_3	2	11110	60
1|1000	x_4	1	11100	56
10|110	x_1	2	10000	32
0|1100	x_2	1	01000	16
Sum				164
Avg				41
Max				60

Table 3.2: A genetic algorithm example

algorithm. Repeating this procedure will continue until the function is maximized within the limits of x.

3.4   Multi-objective optimisation

Decision-making problems usually involve conflicting interests. For example, industrial development versus agriculture or budget min-imisation versus comfort maximisation. These problems are mathe-matically formulated based on objective functions. In this section, an example of a multi-objective optimisation using a genetic algorithm is presented.

3.4.1   Genetic algorithm

The multi-objective genetic algorithm which is used in this work is a controlled elitist genetic algorithm, a variant of the non-dominated sorting genetic algorithm II (NSGA-II) [69, 70]. The NSGA-II is pro-posed and demonstrated in [71]. An elitist genetic algorithm always favours individuals with better fitness value (rank). Since it is very important to maintain the diversity of population for convergence to an optimal Pareto front, a controlled elitist genetic algorithm is used, which favours individuals that can help increase the diversity of the population even if they have a lower fitness value. This is done by controlling the elite members of the population as the algorithm progresses. Two options "Pareto fraction" and "distance function" are used to control the elitism. The Pareto fraction option limits the number of individuals on the Pareto front (elite members) and the

distance function helps to maintain diversity on a front by favouring individuals that are relatively far away on the front. In this work, the Pareto fraction was set to 0.35, i.e., the genetic algorithm will try to limit the number of individuals in the current population that are on the Pareto front to 35 percent of the population size. Besides, the distance measure function, was set to "distance crowding" which takes an optional argument to calculate the distance either in function space (phenotype) or design space (genotype). If "genotype" is chosen, then the diversity on a Pareto front is based on the design space. In case of "phenotype", the diversity is based on the function space. Here, we choose "phenotype" for our distance function.

For the example presented in this section, the genetic algorithm is applied to obtain a Pareto front for two objectives. Real-valued functions are used which consist of two objectives, including cost and emissions as a function of x (the produced electrical energy by a unit). Both objective functions are contradictory, and can be presented by quadratic functions. Each objective function includes three decision variables and are mathematically formulated below and graphically presented in Fig. 3.2.

- Objective 1: cost function (€/h)

$$
\begin{aligned}
y_1 = {} & 100 \cdot 10^{-5.5} + 50 \cdot 10^{-5.5} \cdot x_1 + 20 \cdot 10^{-5.5} \cdot x_1^2 \\
& +140 \cdot 10^{-5.5} + 40 \cdot 10^{-5.5} \cdot x_2 + 100 \cdot 10^{-5.5} \cdot x_2^2 \\
& +20 \cdot 10^{-5.5} + 20 \cdot 10^{-5.5} \cdot x_3 + 10 \cdot 10^{-5.5} \cdot x_3^2
\end{aligned}
\tag{3.1}
$$

- Objective 2: emission function (kg/h)

$$
\begin{aligned}
y_2 = {} & 4.09 \cdot 10^{-3} - 5.55 \cdot 10^{-3} \cdot x_1 + 6.49 \cdot 10^{-3} \cdot x_1^2 \\
& +2.54 \cdot 10^{-3} - 6.05 \cdot 10^{-3} \cdot x_2 + 5.64 \cdot 10^{-3} \cdot x_2^2 \\
& +5.33 \cdot 10^{-3} - 3.55 \cdot 10^{-3} \cdot x_3 + 3.38 \cdot 10^{-3} \cdot x_3^2
\end{aligned}
\tag{3.2}
$$

In this example, bound constraints were imposed on the decision variables: $0 \leq x_1 \leq 160$, $0 \leq x_2 \leq 240$ and $0 \leq x_3 \leq 260$. Additionally, an equality constraint was set, whereby the sum of each variable has to be equal to 240.6.

The results obtained are visualised on a Pareto curve in Fig. 3.3 including all possible 'optimal solutions' (Pareto front).

As introduced before, genotypes are represented as the population in the computation space. Phenotypes are the population in the actual
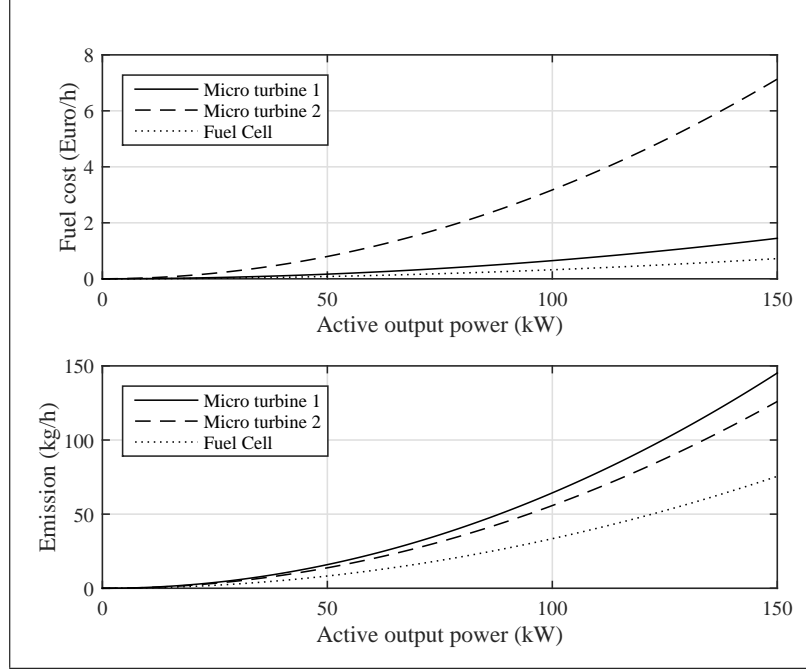
Figure 3.2: Quadratic objective functions

real-world solution space in which solutions are represented in a way they are represented in real-world situations. All possible optimal (phenotype) solutions form a curve between the two objectives. The extremes on the curve should be considered as the best solutions that perform in the field of one of the two objectives. Their values are presented in Fig. 3.3

In this work, priority is given to the extreme solution with the lowest CO_2 emission. The values of the calculated variables on the extreme of objective 1 (cost) are:

- $x_1 = 74.4357$

- $x_2 = 15.0528$

- $x_3 = 151.1104$

The bound constraints are satisfied and the sum of the variables equals 240.6. The total cost is 2.09€ and the total emission is 91.16kg. Note that variable x_3 (Fuel cell) has the greatest share because of the lowest cost produced per output power (kW). The
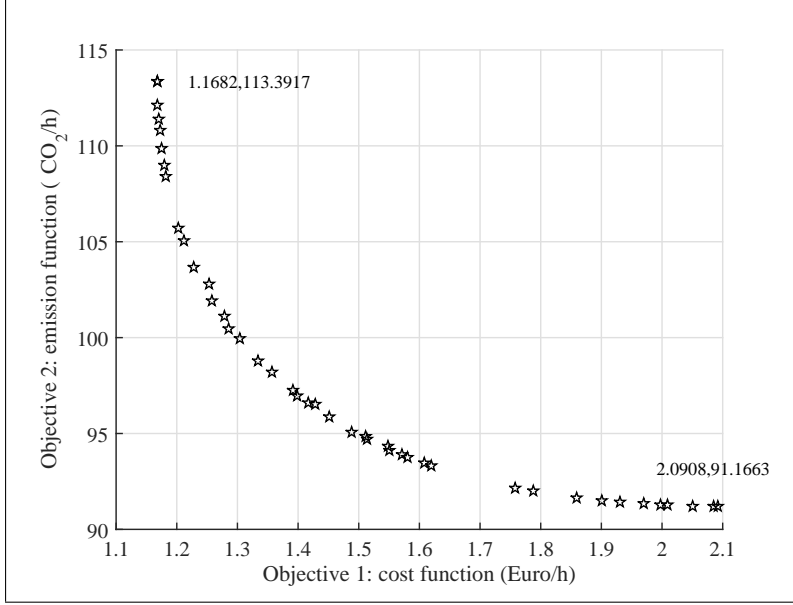
Figure 3.3: Pareto optimal solutions

smallest share goes to x_2 (Micro turbine 2) which has to highest cost curve per output power (kW).

The values of the calculated variables on the extreme of objective 2 (emission) are:

- $x_1 = 58.9482$

- $x_2 = 65.1676$

- $x_3 = 116.4831$

Again, the bound and equality constraints are satisfied. The total cost is 1.16€ and the total emission is 113.39kg. In this extreme situation, the greatest share is covered by the fuel cell which has the lowest emission rate. On the other hand, the smallest share is now covered by micro turbine 1 which has the highest emission rate. The Pareto front can be used to assist decision makers to make a satisfactory decision taking into account the balance among several conflicting objectives.

In this work, the solution with the lowest emissions is chosen.

3.4.2   Hybrid goal attainment based genetic algorithm

As explained in section 3.2.2, evolutionary algorithms can avoid pre-
mature entrapment in local optima because of their stochastic search
mechanism. However, they require high CPU times, and can be poor
in terms of convergence performance. On the other hand, local search
algorithms can converge in a few iterations but lack a global perspec-
tive. The combination of global and local search procedures can offer
the advantages of both optimisation methods.

In this section, a hybrid scheme is introduced to find an optimal
Pareto front for our multi-objective problem. A goal attainment
method based genetic algorithm was used to determine the global
optimum.

Using the multi-objective genetic algorithm, the region near an op-
timal Pareto front can be determined relatively fast, but it can take
many function evaluations to achieve convergence [72]. An additional
(hybrid) technique is introduced that performs the genetic algorithm
for a small number of generations to get near an optimum front. Sub-
sequently, the solution returned from the genetic algorithm is used as
an initial point for a second optimisation solver which is faster and
more efficient for a local search.

In this work, the goal attainment method is used as the hybrid solver
together with the genetic algorithm. This hybrid technique solves
the goal attainment problem, which is a formulation for minimising
a multi-objective optimisation problem. The hybrid solver starts at
all the points on the Pareto front returned by the genetic algorithm.
The new individuals returned by the hybrid solver are combined with
the existing population and a new Pareto front is obtained.

The genetic algorithm estimates the pseudo weights (which are a
required input for goal attainment method) for each point on the
Pareto front and runs the hybrid solver starting from each point on
the Pareto front. Since the hybrid solver needs 'a goal' (vector speci-
fying the goal for each objective), the genetic algorithm provides this
input as the extreme points from the (near optimum) Pareto front.
Using this hybrid scheme results in the satisfaction of both objec-
tives wherein the results can be calculated more accurately and with
a better convergence performance, especially for problems with many
variables.

In order to demonstrate the effectiveness of the hybrid goal attain-
ment function, a minimisation of a multi-objective optimisation prob-
lem using the genetic algorithm will be performed with and without
the hybrid function. The objective functions to be minimised are

presented below:

- Objective 1: cost function

$$y_1 = \sum_{i=1}^{N} \sum_{j=1}^{N_{\text{gen}}} a_j(i) + b_j(i) \cdot x(j + (i - 1) \cdot N_{\text{gen}})+$$
$$c_j(i) \cdot x^2(j + (i - 1) \cdot N_{\text{gen}}) \qquad (3.3)$$

- Objective 2: emission function

$$y_2 = \sum_{i=1}^{N} \sum_{j=1}^{N_{\text{gen}}} d_j(i) + e_j(i) \cdot x(j + (i - 1) \cdot N_{\text{gen}})+$$
$$f_j(i) \cdot P_{\text{G}}^2(j + (i - 1) \cdot N_{\text{gen}}) \qquad (3.4)$$

N and N_{gen} are the time steps and the number of power generation units respectively. In this example, N was set to 25 and N_{gen} was set to 3, which results in a number of decision variables (N_{var}) of 75. The cost coefficients of the jth power generation unit are presented by a_j, b_j and c_j. The emission coefficients of the jth unit are presented by d_j, e_j and f_j. The decision variables are constrained by a continuous range: $0 \leq x(1 + (i - 1) \leq 160$, $0 \leq x(2 + (i - 1) \leq 240$ and $0 \leq x(3 + (i - 1) \leq 260$. For each time step ($N$) an equality constrained is added and are presented by a row vector (A_{eq}):

$$A_{\text{eq}} = [240.60 \; 249.48 \; 254.82 \; 261.52 \; 268.23 \; 274.94 \; 281.6471$$
$$288.35 \; 295.05 \; 301.76 \; 308.47 \; 315.17 \; 321.88 \; 328.58$$
$$342.00 \; 342.00 \; 301.76 \; 288.35 \; 281.64 \; 274.94 \; 234.70 \qquad (3.5)$$
$$221.29 \; 221.29 \; 167.64 \; 140.82]$$

In the first case, we perform the genetic algorithm without hybrid function. The average distance measure of the solutions on the Pareto front was $1.1806 \cdot 10^{-4}$. The spread measure of the Pareto front was 0.0889. A plot of the Pareto front is presented in Fig. 3.4.
As explained in § 3.2.2.1, Pareto optimal, also called non-dominated solution, refers to a state where resources are allocated in the most efficient manner. It is obtained when a distribution strategy exists where none of the objective functions can be improved without degrading any of the other objective values. Unfortunately, most of
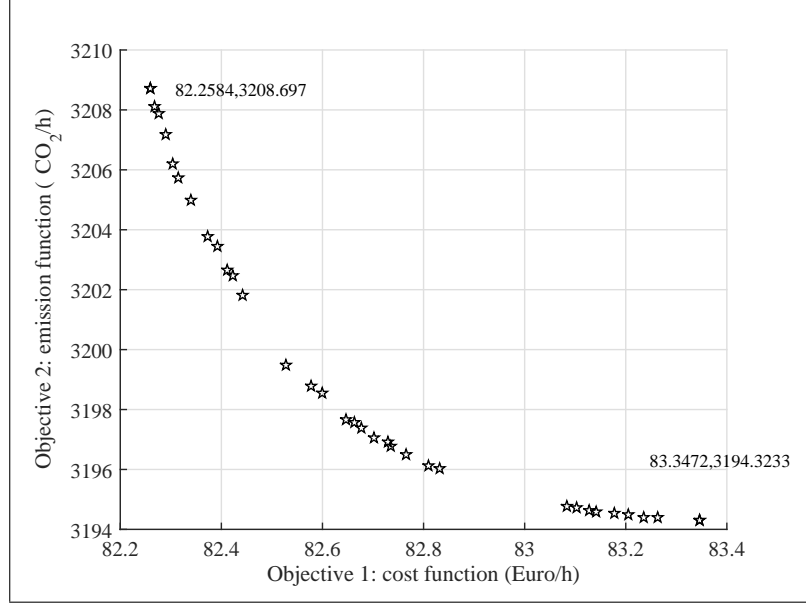
Figure 3.4: Pareto front without hybrid function

time, this does not give a single solution, but rather a set of solutions called the Pareto optimal set. Without additional preference information (priorities), all solutions within this set are considered equally good. The decision maker is required to select the most preferred one from the Pareto optimal front. As mentioned before, in this example, both objectives were considered simultaneously, and priority is given to the extreme solution (within the Pareto front) with the lowest CO_2 emission. In this extreme, extracted from the Pareto front, the total cost is 83.34€ and the total emission is total emission 3194.32kg. Note that, giving priority to the solution (within the same Pareto front) with the lowest cost will lead to a lower total cost (82.25€), but a higher total emission (3208.69kg).

In the second case we use the goal attainment method as the hybrid function. The average distance measure of the solutions on the Pareto front was 0.0283. The spread measure of the Pareto front was 0.546. The Pareto front is presented in Fig. 3.5.

On the extreme of objective function 2 (from Pareto front), the total cost is 69.89€ while the total emission is 3015.72kg.

Since both Pareto fronts are quite similar, a comparison can be made based on the spread and the average distance measures. The average
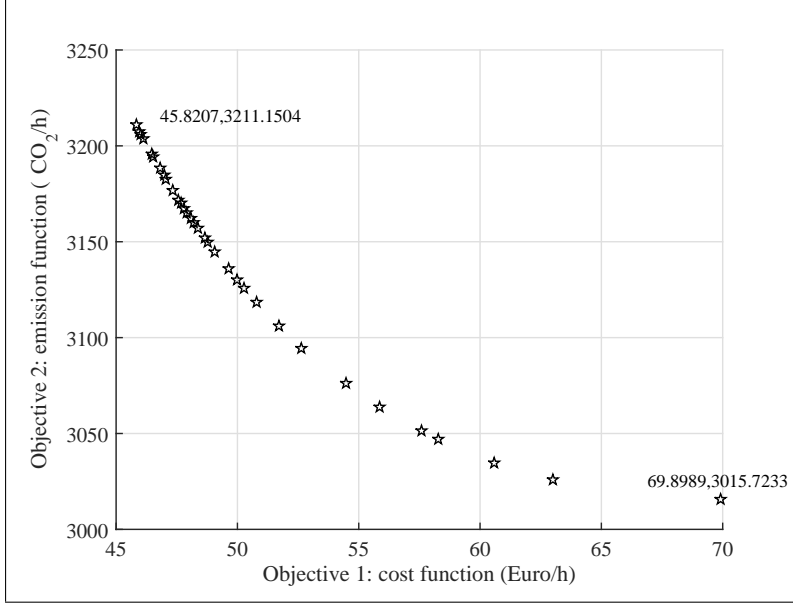
Figure 3.5: Pareto front with hybrid function

distance of the solutions on the Pareto front can be improved with the hybrid function. The spread is a measure of the change in two fronts and that may be higher when hybrid function is used which indicates that the front has changed considerably from that obtained by using the genetic algorithm without hybrid function.

Using the hybrid function will result in more accurate Pareto front. This can also be confirmed by the lower total cost and emission in the second case as compared to the solution without hybrid function.

3.4.3 Global optimum

It is clear that the combination of a global and a local search procedure can offer the advantages of both optimisation methods. In order to determine whether an optimisation algorithm has converged to global optimum, a tuning of the algorithm parameters was performed. Multiple runs or random restarts with different stopping criteria can enhance the solution, and achieve a global or near global optimal solution.

In this work the algorithm finds the minimum of both objectives or fitness functions. The algorithm stops if the average relative change in the best fitness function value over the generations is less than or

equal to the function tolerance. If the fitness value changes over a number of runs of the algorithm (a run comprises of certain number of iterations as per stopping criteria), the global optima is not found yet. Here, a small function tolerance of 10^{-4} was chosen which increases the accuracy of the solution. A smaller function tolerance does not provide more accurate results and besides, it increases the calculation time. Increasing the function tolerance leads to inaccurate results.

3.5   Conclusions

In this chapter, a hybrid scheme is introduced which finds an optimal Pareto front for the multi-objective problem. A goal attainment based genetic algorithm is presented to determine the global optimum. Using the multi-objective genetic algorithm, the region near an optimal Pareto front can be determined relatively fast, but it can take many function evaluations to achieve convergence. An additional (hybrid) technique is introduced which performs the genetic algorithm for a small number of generations to get near an optimum front. The solution returned from the genetic algorithm is used as an initial point for the hybrid goal attainment method. The hybrid solver starts at all the points on the Pareto front returned by the genetic algorithm. The new individuals returned by the hybrid solver are combined with the existing population and a new Pareto front is obtained. The results have proven that the combination of these two methods offer a more accurate Pareto front. This technique will be used in order to solve the microgrid power system scheduling problem which is demonstrated in the next chapters.

4

Microgrid power system scheduling

4.1 Introduction

According to U.S. Energy Information Administration released International Energy Outlook [73], the world energy demand is projected to increase with 48% between 2010 and 2040. The largest share of this growth will come from non-OECD (Organisation for Economic Cooperation and Development) countries, where demand is strongly driven by economic growth. The industrial sector continues to account for the largest share of the energy use and is expected to increase to more than half of the global delivered energy in 2040. Demand or energy use changes daily and seasonally, where the pattern varies widely by sector. The manufacturing industry uses more on weekdays than on saturdays and sundays. Heating and cooling systems are turned on and off seasonally. The rate of the residential electricity use is higher during the morning and evening than between midnight and early in the morning. Utilities are facing load shape patterns which can be divided into a base load, an intermediate load and a peak load. The largest amount of electricity is needed during peak times, but on the other hand, a base load is needed throughout the year.

The production of electrical energy to meet the energy use depends on the combination of available energy resources. Fossil-fuelled energy resources continue to supply nearly 78% of the world's energy

usage in 2040, where natural gas will become a major source [73]. As a result, the economic growth in developing nations, fuelled by a continued reliance on fossil fuels, has a negative impact on the carbon footprint and the environment. However, nuclear energy and renewable energy are the world's fastest growing energy sources [73]. Efforts that have been made in the pursuit of the low-carbon economy have led to a huge boom in the use of intermittent RES. DG and storage will become part of the modern energy structure. Unfortunately, conventional energy grids are not designed for the subsequent bidirectional power flows. Moreover, the aging electrical distribution networks are not actively managed, i.e., they are conceived as passive facilities of the transmission network in which the control and stability is achieved. The growth in decentralised unpredictable electricity production and the ever-increasing electricity consumption can lead to grid congestion problems. As these techniques grow in popularity, so do the challenges. Ensuring a reliable and sustainable electricity supply is driving the need for technology improvements in power networks. The implementation of 'intelligence' into the main grid forms an essential part of this innovation.

Within the concept of smart grids, energy users are able to use electrical energy they produce themselves. Furthermore, they can adjust their supply at demand peak times and decrease power production when required. This flexibility is a straightforward way to leverage grid controllability in order to make better use of the existing system and to meet the growing demand with the existing the infrastructure. In the next sections, a microgrid scheduling tool is presented which outlines the complex task of unit commitment and demand response.

4.2 Power system scheduling

The energy deregulation and concerns over human impact on climate change created a context in which the revival of distributed generation became possible [74]. The conventional power system faces a paradigm change where the centralised electricity generation evolves to a more distributed and localised way of generating electricity. Decentralised power generation is changing the way the distribution networks need to be operated. The planning and operation of distribution networks is challenged by the increased integration of DER. DNOs are committed to integrate these sources into their distribution networks without jeopardising the existing quality of service. Besides, the fit-and-forget approach of integrating distributed DG units is no longer suitable to future power distribution. As explained in chapter 3, distribution grids require computational and algorithmic improvements in order to meet real-time operational requirements.

As a result, distribution grids are forced to become more intelligent in which the smart grid will play a critical role. Future smart grid systems are expected to be flexible. Their scheduling algorithms will play a key role for an efficient integration and coordination of the different resources in the network. For the implementation of the smart grid model, unit commitment and demand response are crucial for the daily operation of the network.

4.2.1 Unit commitment

The general objective of the UC problem is to determine which units should be kept online and which should be kept offline in order to minimise the total operating cost while satisfying the different constraints. Different types of thermal generating units exist and they all have different production costs, generating capacities, ramp up and shut down rates, and other characteristics. Since fuel expenses represent a large part of the overall generation cost, it is not economically efficient to keep every generating unit continuously online when demand is low. Utility companies may benefit from the determination of the optimal mix of different generation units operating at the lowest fuel cost.

Unit commitment can be defined as a scheduling of generation units to be in service over a time horizon in order to achieve optimisation objectives subject to the device and operating constraints. UC is a complex scheduling task which is one of the most challenging problems in power system optimisation [75]. It has to deal with both

discrete and continuous variables, each with different characteristics, and with multiple linear and quadratic objective functions and constraints. The problem of UC within power systems dates back to the early 1940's. As explained in chapter 3, different optimisation techniques have been applied to solve the UC problem, ranging from simple heuristic methods to complicated algorithmic methods [76–78]. The methods applied vary from utility to utility, depending on their mix of generating units and on the operating constraints as well as the selected objectives.

In order to provide high-quality electric power to the microgrid customers in a secured and economic way, a UC strategy is considered to be a complex but reliable option [79]. Similarly, for smart microgrids, the UC problem can be formulated as the determination of the optimal up and down schedule of the microgrid DER units, and controllable loads over a time horizon while minimising the overall cost of the electricity production and satisfying the overall forecast demand. The outcome indicates which microgrid unit need to be in service during the scheduling period taking into account the load requirements and the constraints of the generating units.

Classical unit commitment methods typically assume a one-hour time resolution or interval [80–83]. Compared to the classical power system, the UC problem is different for smart distribution networks. Due to the combination of conventional and renewable sources (e.g., because of the individual characteristics of RES, different power generation levels, and grid characteristics), unit commitment becomes more crucial and more complicated in the management of a microgrid. As a result, shorter optimisation intervals might be required to adequately reflect this uncertainty [84]. Day-ahead scheduling no longer has to fit only with slow and easily predictable changes in load, but also with more abrupt changes in power production. Besides, markets for energy-related commodities work on shorter time frames [85]. Therefore, hourly scheduling protocols are no longer just and reasonable [86]. For this reason, the UC strategy developed in this work is based on 15-minute intervals. Note that in this work, the data points within these intervals are considered as 15-minute averaged values. Data points on a shorter time fame (e.g., real-time renewable energy production or power consumption) are not considered in this work.

4.2.2   Demand response

Demand response (DR) programs provide an opportunity for electricity users to participate in the grid operation in response to time-based rates or other forms of financial incentives. These programs are introduced by power system operators as an option for balancing supply and demand. They can be considered as a method to motivate changes in electricity use by end-users (households or businesses) when the power system reliability is jeopardised [87]. Methods of engaging customers in demand response efforts can be categorised as: [88]:

1. Implicit DR (also called price-based DR) provides customers time-varying rates which reflect the value and cost of electricity in different time periods such as day-ahead-pricing (DAP), critical-peak pricing (CPP) and time-of-use (TOU) tariffs. With price-based DR, consumers can decide to shift their electricity consumption away from times of high prices and thereby reduce their energy bill.

2. Explicit DR (also called incentive-based or volume-based DR) provides a specific reward to electricity consumers who change their consumption upon request by the power system operator, triggered either by a grid reliability problem or high electricity prices. These DR actions are sold upfront on electricity markets, sometimes directly for large industrial consumers or through demand response service providers.

One of the goals of this research is to develop a grid modernisation tool to utilise demand response with the ability to dynamically optimise the grid. To attain this goal, both types of DR programs were investigated, added to the UC model and presented in the next paragraphs.

4.3   Mathematical formulation

In this section, the mathematical formulation of the day-ahead unit commitment model for microgrids, developed in this work [49], is presented. The aim is to schedule the power among the different microgrid generation units and controllable loads while minimising the operating costs together with the CO_2 emissions produced. A flexible load is introduced which can be charged within its limits and when it is connected to the microgrid. As a part of the demand side participation strategy, a charging schedule should be determined for the different microgrid storage devices in order to further reduce the costs and emissions. Furthermore, a congestion control signal is added whereby the power exchange between microgrid and utility network can be controlled (on request of the DNO) which causes a smooth transition to a virtual islanded operating condition.

4.3.1   Objective function

The objective of the optimisation problem is to find the optimal set of power set points of the microgrid units to be scheduled while minimising the operating costs together with the CO_2 emissions produced. The microgrid units include the thermal generation units, the utility grid, storage devices and controllable loads. The general objective function is presented below:

$$\text{Min}(C_\text{G}(P_\text{G}), \varepsilon_\text{G}(P_\text{G})) \tag{4.1}$$

where $C_\text{G}(P_\text{G})$ and $\varepsilon_\text{G}(P_\text{G})$ are the operating costs and the CO_2 emissions of the microgrid power generation units respectively. Both should be minimised over the variable P_G, which represents the active power output of the corresponding generator units. The values of P_G can be considered as the set points, optimised according to both objectives, and are presented in the vector P_gen:

$$P_\text{gen} = \begin{bmatrix} P_{\text{G}_1} & \cdots & P_{\text{G}_j} & \cdots & P_{\text{G}_{N_\text{gen}}} \end{bmatrix}^\text{T} \tag{4.2}$$

where N_gen is the number of generators within the microgrid, including thermal generation units, the utility grid, storage devices and controllable loads. In this vector, the real power output (kW) of the jth generation unit is presented. The values of P_{G_j} are positive if the units are committed to inject or deliver active power to the microgrid bus. In case of charging a storage unit or scheduling a

controllable load as a part of the demand side participation strategy, active power is taken from the bus and the values of P_{G_j} are negative. Furthermore, it is important to highlight that the different types of microgrid units (including the thermal generation units, the utility grid and storage devices) have a certain position within the row vector P_{gen} which is important for the composition of the different matrices explained further in this chapter.

Since unit commitment is a preliminary calculation of active power reference set points over a given time period, the set points listed in vector P_{gen} need to be calculated for the number of time steps (N) in which the time horizon (e.g., day-ahead) is divided. As introduced in § 4.2.1, the UC strategy developed in this work is based on 15-minute intervals. Therefore, in this work, P_{UC} is built up as an $(N \cdot N_{\mathrm{gen}})$-by-1 matrix. Every row within P_{UC} (thus, for every time step within the complete time horizon) contains the vector P_{gen}. As a result, P_{UC} contains the calculated active power outputs within the scheduling time horizon and represents the solution of the UC problem.

$$P_{\mathrm{UC}} = \begin{bmatrix} P_{\mathrm{gen}_1} & \cdots & P_{\mathrm{gen}_i} & \cdots & P_{\mathrm{gen}_N} \end{bmatrix}^{\mathrm{T}} \qquad (4.3)$$

where P_{gen_i} is the vector described in (4.2) for the ith time step.

4.3.2 Power production cost

For many decades, traditional central power plants have been committed following minimum fuel cost criteria without considering the emissions produced. The component that dominates the operating cost, especially for thermal generating units, is the power production cost of the committed units. The greatest share of this cost is related to the cost of fuel input per hour. Maintenance contributes only to a small extent. Fuel-based thermal generators where fuel is oil, coal and gas (e.g., internal combustion engines (ICEs), micro turbines or gen sets, and fuel cells) have a fuel cost function. To evaluate the fuel cost of each generator, a mathematical model, which describes the fuel cost as a function of the power generation, is used. The accuracy of this model has a considerable influence on the accuracy of the minimisation strategy. The most prevalent fuel cost model, is the quadratic model which describes the fuel cost as a quadratic function of the generator's active power output [89]. Accordingly, the quadratic operating cost function, in €/h, of these generating units

within the scheduling time horizon can be presented as follows:

$$C_{\mathrm{G}}(P_{\mathrm{G}}) = \sum_{i=1}^{N} \sum_{j=1}^{N_{\mathrm{gen}}} a_j(i) + b_j(i) \cdot P_{\mathrm{G}}(j + (i-1) \cdot N_{\mathrm{gen}}) +$$

$$c_j(i) \cdot P_{\mathrm{G}}^2(j + (i-1) \cdot N_{\mathrm{gen}}) \qquad (4.4)$$

where a_j, b_j and c_j are the fuel cost coefficients of the jth generation unit. a_j is a constant term which represents the cost of operating the generator without power output, b_j is a linear term that varies directly with the level of power generation, and c_j is the term that accounts directly for efficiency changes over the range of the power output of the generator [90, 91]. In this work, a time horizon of 24 hours (day-ahead) will be discussed where the fuel cost is expected to be constant during the complete scheduling time horizon. Therefore, the cost coefficients of the thermal generation units are not time-dependent.

4.3.3   Time-dependent production cost

In grid-connected mode, the utility grid will participate as a dispatchable unit in the commitment strategy and is then co-integrated in the vector given in (4.2). The fuel cost function of the utility grid can be presented as a piecewise linear function and is dependent on the market price, and therefore time-dependent. The market price can be divided into a buying and selling price. The buying price (cost) represents the day-ahead market price and is proportional to the power delivered by the utility grid to the microgrid. This factor has a role in the minimisation of the microgrid operating cost.

The day-ahead unit commitment model considers a predicted microgrid power demand as well as the buying and selling price. In this work, a variable day-ahead price (DAP) is used, taken from the Belpex Day-Ahead Market (DAM) 2014 historical data [92].

As explained in § 4.3.1, the values of P_{G_j} are positive if the microgrid units are committed to inject or deliver active power to the microgrid bus. When the microgrid units are committed to consume, active power is taken from the bus and the values of P_{G_j} are negative. As a result, when the utility grid is committed to deliver power to the microgrid, its value P_{G_j} is positive. The selling price represents the market value or the price for which the power produced by the DER can be sold to the utility grid. This factor plays a role in the maximisation of the microgrid revenue or further minimising the microgrid

cost. When the microgrid generation units are committed to deliver power to the main grid, or when the main grid 'extracts' power from the microgrid, the corresponding value P_{G_j} is negative. The coefficients of the piecewise linear function of the utility grid are presented below:

$$b_j(i) = \text{DAP}_{\text{sell}_j}(i) \quad \text{if} \quad P_{G_j}(j + (i-1)) \leq 0$$
$$b_j(i) = \text{DAP}_{\text{buy}_j}(i) \quad \text{if} \quad P_{G_j}(j + (i-1)) > 0 \tag{4.5}$$

A plot of the cost function of the utility grid is presented in Fig. 4.1. The slope of DAP_{sell} and DAP_{buy} can be seen as a snapshot of the market condition at a certain moment and varies in time. In this work, the bid-ask spread, which is the difference between the bid price (which is the selling price from the microgrid's view) and the ask price (which is the buying price from the microgrid's view) is dependent on different factors which are mentioned in [93]. In this work, the buying price is assumed to be 20% higher than the selling price.
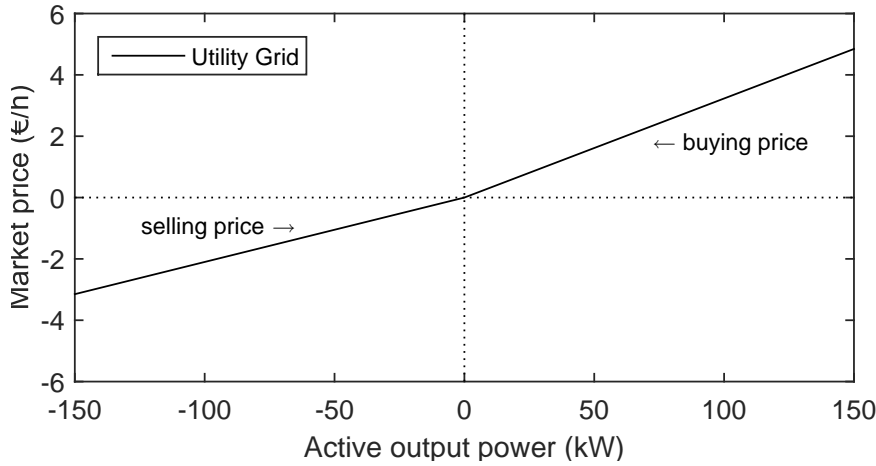
Figure 4.1: Cost function utility grid

4.3.4 Emissions

As described above, the objective is to find an optimal UC at minimum operating cost subject to the power system constraints. Nowadays, as a result of the climate issue, the environmental public awareness becomes more important. Greenhouse gas (GHG) emissions,

caused by the combustion processes of fuel-based distributed generators (reciprocating internal combustion engine, micro-turbine, Stirling engine, etc.), have to be considered when improving or developing future power systems [94]. Utilities are forced to modify their design and operational strategies in order to reduce pollution and atmospheric emissions of the thermal power plants. Additional to the objectives that minimise the total operating cost, environmental objectives such as minimising the greenhouse gas emissions have to be considered. The form of the emission function model depends on the type of pollutants. In general, GHG emissions, especially CO_2, of fuel-burning generators are directly related to the consumed amount of fuel, and therefore can be expressed based on the quadratic fuel consumption curves [94]. Hence, the amount of CO_2 emission in kg/h can be expressed as a quadratic function of the generator's active power output.

$$
\varepsilon_{\mathrm{G}}(P_{\mathrm{G}}) = \sum_{i=1}^{N} \sum_{j=1}^{N_{\mathrm{gen}}} d_j(i) + e_j(i) \cdot P_{\mathrm{G}}(j + (i-1) \cdot N_{\mathrm{gen}}) +
$$
$$
f_j(i) \cdot P_{\mathrm{G}}^2(j + (i-1) \cdot N_{\mathrm{gen}}) \qquad (4.6)
$$

where d_j, e_j and f_j are the emission coefficients. The emission rate of thermal generation units can be significant in case of poor maintenance or engine wear. In this work, a time horizon of 24 hours (day-ahead) will be discussed where the emission coefficients of the microgrid thermal generation units are expected to be constant during the complete scheduling time horizon. Therefore, the emission coefficients of the thermal generation units are not time-dependent. The utility emission rate is linear with the output power and is dependent on the used resource mix which includes mainly coal, gas, nuclear and renewables. Therefore, the coefficients d and f are set to zero and e represents the linear emission coefficient of the utility grid. The emission rate of the utility grid is time-dependent and can change from month to month. In this work, a time horizon of 24 hours (day-ahead) will be discussed where the emission rate of the utility grid is considered as constant. When power is delivered to the utility grid, the emissions of the utility grid are set to zero. This is due to the fact that the power (delivered to the utility grid) is produced by microgrid generation units that already have an emission rate included.
The cost and emission coefficients of the storage units and the con-

trollable loads are set to zero, since they are already included in the coefficients of the thermal generation units which are producing the energy to charge the storage unit and to cover the controllable power consumption.

Note that, revenues from carbon emissions trading or a carbon tax are not included in this work.

4.3.5 Demand side participation

As introduced before, a demand side participation strategy is added to the UC model that can increase the system security and further reduce the cost and emissions. By integrating the time-varying electricity cost of the utility grid in the general cost function (4.4), an implicit (price-based) DR program can be provided to the controllable microgrid loads. In this work, storage units, which can be seen as controllable loads, are provided with a charging schedule in order to further reduce the costs and emissions. Besides, an electric vehicle is added which can also be considered as a flexible load. This type of load can only store energy (acting as a load) and differs in this way from a traditional storage unit that can also discharge (acting as a production unit). Electric vehicles which discharge power to the grid are not considered in this work.

In addition, an explicit (or incentive-based) DR program is added which can be considered as an ancillary service arrangement for congestion management. In order to deploy the DER units in a widespread and efficient way, microgrids can be a coordinated system approach for incorporating these sources. On request of the DNO (e.g., when the system is overloaded, or when there is too much production by RES), the microgrid can be requested to operate in virtual islanded condition. Therefore, a congestion control signal (predicted by the DNO) is implemented whereby the power exchange between microgrid and utility network can be controlled (by effective microgrid unit scheduling) which causes a smooth transition to a virtual islanded operating condition. Both DR programs will be explained further in this chapter.

4.3.6 Constraints

The conditions can be completed by constraints including physical relations in load flows and system performance requirements. In the next sections the system constraints and the unit constraints will be discussed in detail.

4.3.6.1   System constraints

A first constraint is that the sum of all power generating unit within the microgrid (including the thermal generation units, the utility grid and storage devices) must equal the actual consumption within the microgrid, as expressed below:

$$\sum_{j=1}^{N_{\text{gen}}} P_{\text{G}_j} = P_{\text{D}}^{\text{a}} \tag{4.7}$$

where P_{D}^{a} represents the actual demand. Note that the UC strategy developed in this work operates on a day-ahead time frame with a 15-minute interval. However, because of the uncertainties in the demand and renewable energy forecast, the day-ahead scheduling may deviate from the real-time dispatch. Therefore, the instantaneous dispatch and real time market supplements the day-ahead unit commitment and helps secure the necessary balance between supply and demand in the power system. The operation of the real-time control is outside the scope of this work and will not be further discussed in this dissertation.

Since RES, such as PV and wind, produce power at zero running cost and zero emissions, their output power can be treated as a negative load. Therefore, the (forecast) power generated by renewables P_{RES} is subtracted from the total demand $P_{\text{D}}^{\text{total}}$ in order to obtain the actual demand P_{D}^{a}:

$$P_{\text{D}}^{\text{a}} = P_{\text{D}}^{\text{total}} - P_{\text{RES}} \tag{4.8}$$

The total demand includes a fixed part ($P_{\text{D}}^{\text{fixed}}$) which is non-controllable and a flexible part ($P_{\text{D}}^{\text{flexible}}$) which plays a role in the demand side participation strategy:

$$P_{\text{D}}^{\text{total}} = P_{\text{D}}^{\text{fixed}} + P_{\text{D}}^{\text{flexible}} \tag{4.9}$$

As introduced in § 4.2.1, the UC strategy developed in this work is based on 15 minute intervals where the data points within these intervals are considered as 15-min averaged values. Data points on a very short time resolution (e.g. real-time renewable energy production or power consumption) are not considered in this work.

4.3.6.2 Unit constraints

Besides the system constraints, the power generating units within the network have constraints as well. The power reference set point of each microgrid unit is bounded by the upper bound and by the lower bound. These boundaries, in which the microgrid units can be committed, are expressed by $P_{\mathrm{G_{min}}}$ and $P_{\mathrm{G_{max}}}$ respectively.

$$P_{\mathrm{G_{min}}} < P_{\mathrm{G}} < P_{\mathrm{G_{max}}} \tag{4.10}$$

The index to the variable name P_{storage} (within the matrix P_{gen}) is given as an indication to the reference set point of the storage unit. Since P_{storage} is a power reference set point (kW) and E_{storage} (kWh) represents the (dis)charged energy over a period with N time steps, P_{storage} is multiplied by the time span (T_{s}) of the time step as presented below:

$$E_{\mathrm{storage}} = E_{\mathrm{pre-storage}} - \sum_{i=1}^{N} P_{\mathrm{storage}(i)} \cdot T_{\mathrm{s}} \cdot \eta \tag{4.11}$$

where $E_{\mathrm{pre-storage}}$ is the energy stored in the storage unit at the end of the previous day. The (dis)charge efficiency is presented by η. As introduced in § 4.2.1, in this work, the UC strategy operates on a day-ahead time frame with a 15-minute interval. Therefore, the state of the storage unit will be considered on a time base of 15 minutes.
In order to manage the storage device, additional constraints were added. At any time, E_{storage} or the energy level of the storage unit is non-negative and has a defined range with a minimum and a maximum:

$$\mathrm{DOD_{max}} < \mathrm{E_{storage}} < \mathrm{E_{storage_{max}}} \tag{4.12}$$

where $\mathrm{DOD_{max}}$ represents the maximum depth of discharge. In case the storage unit is charging and acting as a load, P_{storage} has a negative value. For the charging operation, the set point P_{storage} committed within a time step is constrained by:

$$P_{\mathrm{storage}} \cdot T_{\mathrm{s}} \cdot \eta \leq E_{\mathrm{storage_{max}}} - E_{\mathrm{storage}} \tag{4.13}$$

When the storage unit is discharging, active power will be injected in the microgrid bus and P_{storage} has a positive value. For discharging, the set point P_{storage} during the time span T_{s} of a time step is constrained by:

$$P_{\text{storage}} \cdot T_{\text{s}} \cdot \eta \leq E_{\text{storage}} - E_{\text{storage}_{\text{min}}} \tag{4.14}$$

Note that E_{storage} should not be confused with $P_{\text{storage}} \cdot T_{\text{s}} \cdot \eta$. E_{storage} represents the sum of the (dis)charged electrical energy over a period of $N \cdot T_{\text{s}}$, also called the energy level or the state of charge (SOC). While $P_{\text{storage}} \cdot T_{\text{s}} \cdot \eta$ indicates how much energy the storage unit (dis)charges at a given time step T_{s}. The (dis)charge efficiencies will be further explained in 4.26, 4.29 and 4.33. Furthermore, the rate of the storage unit (for charging and discharging) is constrained and already included in (4.10) where $P_{\text{G}_{\text{min}}}$ is the maximum rate for discharging and $P_{\text{G}_{\text{max}}}$ for charging.

In addition, a flexible load with the characteristics of an electric vehicle is implemented and can only store energy (only acting as a load). The process of discharging power from the EV into the (micro)grid is not considered in this work. The index to the variable name P_{EV} is given as an indication (within the matrix P_{gen}) to the reference set point of the electric vehicle (EV). The flexible load can only be committed when it is connected to the microgrid (between T_{in} and T_{out}):

$$E_{\text{EV}} = E_{\text{EV}_{\text{T}_{\text{in}}}} - \sum_{i=T_{\text{in}}}^{T_{\text{out}}} P_{\text{EV}(i)} \cdot T_{\text{s}} \cdot \eta \tag{4.15}$$

where E_{EV} represents the energy level of the EV. $E_{\text{EV}_{\text{T}_{\text{in}}}}$ is the energy stored in the EV at the time step when the electric vehicle is plugged in. Similar to the storage device, E_{EV} has a defined range with a minimum and a maximum:

$$E_{\text{EV}_{\text{min}}} < E_{\text{EV}} < E_{\text{EV}_{\text{max}}} \tag{4.16}$$

An extra constraint is added where the EV should be charged with a certain amount of energy on the time step it will be unplugged ($E_{\text{EV}_{\text{T}_{\text{out}}}}$) and can be represented as a percentage of $E_{\text{EV}_{\text{max}}}$:

$$E_{\text{EV}_{\text{T}_{\text{out}}}} = E_{\text{EV}_{\text{max}}} \cdot n\% \tag{4.17}$$

When the EV is committed to charge and acting as a load, P_{EV} has a negative value. For charging, the set point P_{EV} during the time span of a time step T_{s} is constrained by:

$$P_{\text{EV}} \cdot T_{\text{s}} \cdot \eta \leq E_{\text{EV}_{\text{max}}} - E_{\text{EV}} \tag{4.18}$$

The active power rate of the EV unit is non-negative and has a defined range with a minimum and a maximum (4.10).

4.4 Mathematical implementation

In this section, the different constraints of the optimisation problem are presented and it is explained we explain how they are implemented into the day-ahead unit commitment model.

4.4.1 Equality constraints

As explained in § 4.3.6.1 and § 4.3.6.2, several equality and inequality constraints are to be satisfied when solving the unit commitment problem.
The active power balance (4.7) is considered as a first equality constraint and is presented below:

$$A_{\text{eq}_{\text{PB}}} \cdot P_{\text{UC}} = b_{\text{eq}_{\text{PB}}} \tag{4.19}$$

where the index $_{\text{pb}}$ stands for power balance. P_{UC} should be calculated as a set of reference set points of the microgrid units to be scheduled. As explained in 4.3, these reference set points are real power outputs representing the outcome of the UC problem, and are presented by an $(N \cdot N_{\text{gen}})$-by-1 matrix.
The matrix $b_{\text{eq}_{\text{PB}}}$ includes the actual microgrid demand $(P_{\text{D}}^{\text{a}})$ for each time step (N) and is presented as an N-by-1 matrix.

$$b_{\text{eq}_{\text{PB}}} = \begin{bmatrix} P_{\text{D}_1}^{\text{a}} & \cdots & P_{\text{D}_{\text{N}}}^{\text{a}} \end{bmatrix}^{\text{T}} \tag{4.20}$$

Taking into account the dimensions of P_{UC} and $b_{\text{eq}_{\text{PB}}}$, $A_{\text{eq}_{\text{PB}}}$ is built up as a diagonal block matrix as presented below:

$$A_{\text{eq}_{\text{PB}}} = \begin{bmatrix} A_{\text{eq}_{\text{PB}_{1,1}}} & 0 & 0 & 0 \\ 0 & A_{\text{eq}_{\text{PB}_{2,2}}} & 0 & 0 \\ 0 & 0 & \ddots & 0 \\ 0 & 0 & 0 & A_{\text{eq}_{\text{PB}_{n,n}}} \end{bmatrix} \tag{4.21}$$

The input matrices in the diagonal direction $(A_{\text{eq}_{\text{PB}_{1,1}}}, ..., A_{\text{eq}_{\text{PB}_{n,n}}})$ do not have to be square, nor they have to be of equal size. Here, the diagonal entries are row matrices of the form 1-by-N_{gen} (same dimension of P_{gen}) where the input entries are assigned with the value 1 or 0. These values can be seen as labels which are assigned to the corresponding units within vector P_{gen}, and determine whether or not these units participate in the UC strategy. Mark 1 means that the unit is participating in the commitment strategy. Units that are

not participating are indicated with mark 0. For each time step it can be defined whether or not a unit participates in the UC. For example, an EV is only participating in the UC strategy when it is plugged in (1) and can not be committed when it is unplugged (0). The position of the input entries within these row matrices corresponds to the position of the unit within P_{gen}. Besides, the off-diagonal entries are row matrices as well and have the same form, but their input entries are all set to 0. As a result, the newly created matrix $A_{\text{eq}_{\text{PB}}}$ can be represented as an N-by-$(N \cdot N_{\text{gen}})$:

$$A_{\text{eq}_{\text{PB}}} = \begin{bmatrix} \mathbf{111...1} & 000...0 & 000...0 & ... \\ 000...0 & \mathbf{111...1} & 000...0 & ... \\ 000...0 & 000...0 & \mathbf{111...1} & ... \\ ... & ... & ... & ... \end{bmatrix} \qquad (4.22)$$

Note that every time step comes with an additional row and a plurality of N_{gen} columns. According to the equation of the equality constraint (4.19), the multiplication of $A_{\text{eq}_{\text{PB}}}$ and P_{UC} has to be equal to $b_{\text{eq}_{\text{PB}}}$. As a result, for each time step, the sum of the reference set points calculated by the optimisation model has to be equal to the actual load.

As introduced in § 4.3.5, an electric vehicle is added which can be considered as a flexible load. This type of load can only store energy (acting as a load) and differs in this way from a traditional storage unit which can also discharge (acting as a production unit). Electric vehicles with the ability to discharge power to the grid are not considered in this work. As mentioned in (4.17), $E_{\text{EV}_{\text{T}_{\text{out}}}}$ is considered as the second equality constraint. An EV participates in the UC strategy when it is plugged (between T_{in} and T_{out}). At time step T_{out}, the EV may be required to be charged with a certain (pre-specified) amount of energy ($E_{\text{EV}_{\text{T}_{\text{out}}}}$). This equality constraint is presented below:

$$A_{\text{eq}_{\text{EV}}} \cdot P_{\text{EV}} = b_{\text{eq}_{\text{EV}}} \qquad (4.23)$$

$E_{\text{EV}_{\text{T}_{\text{out}}}}$ represents the energy level, the EV should contain at T_{out} and is integrated in $b_{\text{eq}_{\text{EV}}}$.

$$b_{\text{eq}_{\text{EV}}} = \begin{bmatrix} E_{\text{EV}_{\text{T}_{\text{out}}}} \end{bmatrix} \qquad (4.24)$$

Since the EV is the only unit which is included in this second equality constraint, P_{EV} should be calculated as a set of power reference set

points of the EV.

$A_{\text{eq}_{\text{EV}}}$ is generated as an 1-by-N row matrix:

$$A_{\text{eq}_{\text{EV}}} = \begin{bmatrix} A_{\text{eq}_{\text{EV}_1}} & \cdots & A_{\text{eq}_{\text{EV}_n}} \end{bmatrix} \qquad (4.25)$$

where the input matrices $(A_{\text{eq}_{\text{EV}_1}}, ..., A_{\text{eq}_{\text{EV}_n}})$ are row matrices of the form 1-by-N_{gen} (same dimension as P_{gen}).

$$A_{\text{eq}_{\text{EV}}} = [000...0 \quad \overbrace{\mathbf{000...0(-T_s \cdot \eta)} \cdots \mathbf{000...0(-T_s \cdot \eta)}}^{T_{\text{in}} \text{ to } T_{\text{out}}} \quad 000...0] \qquad (4.26)$$

The input entries of these row matrices are directly related to the type of the microgrid unit and their position within the vector P_{gen}. Between $N = T_{\text{in}}$ and $N = T_{\text{out}}$, the input entry on the corresponding location of the EV within the row matrix is assigned with $(-T_s \cdot \eta)$, where η represents the charging efficiency of the EV. This position is chosen arbitrarily in order to explain how the constraints are implemented in the matrix. The values on the position of the non-EV units within the row matrices are set to 0. As explained before, the EV can only charge (and not discharge or deliver power to the microgrid), so the set point(s) P_{EV} will be negative. Note that T_s has been made negative in order to become a positive value when multiplied by a negative P_{EV}. The positive value is needed in order to satisfy equation (4.23) where $b_{\text{eq}_{\text{EV}}}$ has a positive value. The input entries outside T_{in} and T_{out} are assigned with 0.

When the EV is committed to charge and acting as a load, P_{EV} has a negative value. $-P_{\text{EV}} \cdot -T_s \cdot \eta$ indicates how much energy the EV charges at a given time step T_s. According to (4.23), at time step T_{out}, the EV should contain a certain predefined energy level $E_{\text{EV}_{T_{\text{out}}}}$.

4.4.2 Inequality constraints

As explained in § 4.3.6.2, the amount of energy that can be charged and discharged by the distributed storage unit within the scheduling time horizon is implemented as a first inequality constraint. The form of the inequality constraint is given by:

$$A_{\text{storage}} \cdot P_{\text{storage}} \leq b_{\text{storage}} \qquad (4.27)$$

where P_{storage} should be calculated as a set of reference set points of the microgrid storage unit(s). As presented in (4.13), for the charging operation, $P_{\text{storage}} \cdot T_s \cdot \eta$ is restricted by $E_{\text{storage}_{\text{max}}} - E_{\text{storage}}$. On the other hand, for discharging (4.14), $P_{\text{storage}} \cdot T_s \cdot \eta$ is restricted

by $E_{\text{storage}} - E_{\text{storage}_{\min}}$. As explained before, E_{storage} represents the cumulative sum of the (dis)charged electrical energy over a period of $N \cdot T_{\text{s}}$, known as the state of charge (SOC). In order to ensure that for each time step the (dis)charged energy of all former time steps is implemented as an equality constraint, A_{storage} is built as a lower triangular matrix of the form N-by-N.

$$A_{\text{storage}} = \begin{bmatrix} A_{\text{storage}_{1,1}} & 0 & 0 & 0 \\ A_{\text{storage}_{2,1}} & A_{\text{storage}_{2,2}} & 0 & 0 \\ \vdots & \vdots & \ddots & 0 \\ A_{\text{storage}_{n,1}} & A_{\text{storage}_{n,2}} & \cdots & A_{\text{storage}_{n,n}} \end{bmatrix} \quad (4.28)$$

The input entries, located on and below the main diagonal $(A_{\text{storage}_{1,1}}, ..., A_{\text{storage}_{n,n}})$, are row matrices of the form 1-by-N_{gen}. Subsequently, the input values of these row matrices are directly related to the type of the microgrid unit and their position within the vector P_{gen}. Here, the input entry on the corresponding location of the storage unit within the row matrix is assigned with $(T_{\text{s}} \cdot \eta)$. As explained before, the charging and discharging efficiencies are included and presented by η. The values on the position of the non-storage units within the row matrices are set to 0. The entries above the main diagonal are row matrices of the same form and their values are set to 0.

In order to include the charging and discharging operation of the storage unit into one matrix, A_{storage} is duplicated one below the other, where the upper sub-matrix represents the charging operation and the lower sub-matrix represents the discharging operation of the storage unit. As a result, the newly created matrix A_{storage} can be represented as an $(2 \cdot N)$-by-$(N \cdot N_{\text{gen}})$ matrix:

$$A_{\text{storage}} = \begin{bmatrix} \begin{bmatrix} (-T_{\text{s}} \cdot \eta)\mathbf{0}...\mathbf{0} & 0...0 & 0...0 & \cdots \\ (-T_{\text{s}} \cdot \eta)\mathbf{0}...\mathbf{0} & (-T_{\text{s}} \cdot \eta)\mathbf{0}...\mathbf{0} & 0...0 & \cdots \\ (-T_{\text{s}} \cdot \eta)\mathbf{0}...\mathbf{0} & (-T_{\text{s}} \cdot \eta)\mathbf{0}...\mathbf{0} & (-T_{\text{s}} \cdot \eta)\mathbf{0}...\mathbf{0} & \cdots \\ \cdots & \cdots & \cdots & \cdots \end{bmatrix} \\ \begin{bmatrix} (+T_{\text{s}} \cdot \eta)\mathbf{0}...\mathbf{0} & 0...0 & 0...0 & \cdots \\ (+T_{\text{s}} \cdot \eta)\mathbf{0}...\mathbf{0} & (+T_{\text{s}} \cdot \eta)\mathbf{0}...\mathbf{0} & 0...0 & \cdots \\ (+T_{\text{s}} \cdot \eta)\mathbf{0}...\mathbf{0} & (+T_{\text{s}} \cdot \eta)\mathbf{0}...\mathbf{0} & (+T_{\text{s}} \cdot \eta)\mathbf{0}...\mathbf{0} & \cdots \\ \cdots & \cdots & \cdots & \cdots \end{bmatrix} \end{bmatrix} \quad (4.29)$$

As presented within both sub-matrices, the storage unit has the first position in the row matrices (of the form 1-by-N_{gen}) on and below

the main diagonals, and their entries are assigned with $(T_\text{s} \cdot \eta)$. This position is chosen arbitrarily in order to explain how the constraints are implemented in the matrix. A negative T_s (which is then multiplied by a negative P_storage) charges the battery. Vice versa, a positive T_s (which is then multiplied by a positive P_storage) discharges the battery. Building up these sub-matrices within A_storage as lower triangular matrices (which is then multiplied by $\pm P_\text{storage}$) ensures that for every time step (N) the energy level of the previous step is taken into account and added to the next step. In this way, E_storage is included as well.

According to the equation of the inequality constraint 4.27, the multiplication of A_storage and P_storage has to be less than or equal to b_storage. Since E_storage forms the outcome of $A_\text{storage} \cdot P_\text{UC}$, the charging operation at every time step within the scheduling time horizon will be restricted by $E_{\text{storage}_\text{max}} - E_\text{storage}$, and the discharging operation will be restricted by $E_{\text{storage}_\text{min}} - E_\text{storage}$. Both the charging and discharging restrictions are included in b_storage, which can be presented as an $(2 \cdot N)$-by-1 column matrix as presented below:

$$b_\text{storage} = \begin{bmatrix} (E_{\text{storage}_\text{max}} - E_\text{storage})_1 \\ \vdots \\ (E_{\text{storage}_\text{max}} - E_\text{storage})_N \\ \\ (E_\text{storage} - E_{\text{storage}_\text{min}})_1 \\ \vdots \\ (E_\text{storage} - E_{\text{storage}_\text{min}})_N \end{bmatrix} \qquad (4.30)$$

The amount of energy which can be charged by the EV between T_in and T_out is implemented as a second inequality constraint as well. Similar to (4.27), the form of the equality constraint of the EV is presented below:

$$A_\text{EV} \cdot P_\text{EV} \leq b_\text{EV} \qquad (4.31)$$

where P_EV should be calculated as a set of reference set points of the microgrid EV. As presented in (4.18), the charging operation of the EV is constrained by $E_{\text{EV}_\text{max}} - E_\text{EV}$. E_EV represents the cumulative sum of the charged electrical energy over a period of $N \cdot T_\text{s}$, also called energy level or the SOC of the EV.

Similar to the storage unit (4.28), A_EV is built up as a lower triangular matrix of the form N-by-N, in order to include E_EV of the EV. As a

result, for each time step the charged energy of all former time steps (cumulative sum) is implemented as an equality constraint.

$$A_{\mathrm{EV}} = \begin{bmatrix} A_{\mathrm{EV}_{1,1}} & 0 & 0 & 0 \\ A_{\mathrm{EV}_{2,1}} & A_{\mathrm{EV}_{2,2}} & 0 & 0 \\ \vdots & \vdots & \ddots & 0 \\ A_{\mathrm{EV}_{n,1}} & A_{\mathrm{EV}_{n,2}} & \ldots & A_{\mathrm{EV}_{n,n}} \end{bmatrix} \tag{4.32}$$

The input entries, located on and below the main diagonal $(A_{\mathrm{EV}_{1,1}}, ..., A_{\mathrm{EV}_{n,n}})$, are row matrices of the form 1-by-N_{gen}. The input values of these row matrices are directly related to the type of the microgrid unit and their position within the vector P_{gen}. Since the EV can only store energy (acting as a load), the entries on this position are assigned with $(-T_{\mathrm{s}} \cdot \eta)$. Again, T_{s} has been made negative in order to become a positive value when multiplied by a negative P_{EV}. The positive value is needed in order to satisfy equation (4.31) where b_{EV} has a positive value. The values on the position of the non-EV units within the row matrices are set to 0. The entries above the main diagonal are row matrices of the same form and their values are set to 0. As a result, the newly created matrix A_{EV} can be represented as an (N)-by-$(N \cdot N_{\mathrm{gen}})$ matrix:

$$A_{\mathrm{EV}} = \begin{bmatrix} \mathbf{0}...\mathbf{0}(-\boldsymbol{T}_{\mathbf{s}} \cdot \boldsymbol{\eta}) & 0...0 & 0...0 & \ldots \\ \mathbf{0}...\mathbf{0}(-\boldsymbol{T}_{\mathbf{s}} \cdot \boldsymbol{\eta}) & \mathbf{0}...\mathbf{0}(-\boldsymbol{T}_{\mathbf{s}} \cdot \boldsymbol{\eta}) & 0...0 & \ldots \\ \mathbf{0}...\mathbf{0}(-\boldsymbol{T}_{\mathbf{s}} \cdot \boldsymbol{\eta}) & \mathbf{0}...\mathbf{0}(-\boldsymbol{T}_{\mathbf{s}} \cdot \boldsymbol{\eta}) & \mathbf{0}...\mathbf{0}(-\boldsymbol{T}_{\mathbf{s}} \cdot \boldsymbol{\eta}) & \ldots \\ \ldots & \ldots & \ldots & \ldots \end{bmatrix} \tag{4.33}$$

In the matrix presented above, the EV has the last position in the row matrices (of the form 1-by-N_{gen}) on and below the main diagonal. Again, this position is chosen arbitrarily in order to explain how this constraint is implemented in the matrix. Because the EV can only store energy (charging operation) this matrix differs from the matrix presented in (4.29), where the upper sub-matrix represents the charging operation and the lower sub-matrix represents the discharging operation of the storage unit.

According to the equation of the inequality constraint 4.31, the multiplication of A_{EV} and P_{EV} has to be less than or equal to b_{EV}. Since E_{EV} forms the outcome of $A_{\mathrm{EV}} \cdot P_{\mathrm{UC}}$, the charging operation at every time step within the scheduling time horizon will be restricted by $E_{\mathrm{EV}_{\max}} - E_{\mathrm{EV}}$. The charging restriction is included in b_{EV}, which can be presented as an N-by-1 column matrix and is presented below:

$$b_{\text{EV}} = \begin{bmatrix} (E_{\text{storage}_{\max}} - E_{\text{EV}})_1 \\ \vdots \\ (E_{\text{storage}_{\max}} - E_{\text{EV}})_N \end{bmatrix} \tag{4.34}$$

4.4.3 Bound constraints

The third restrictions are the bound constraints on the power reference set points of each microgrid generation unit. These boundaries, in which the microgrid units can be committed, are characterised by the lower (LB) and upper (UB) bounds and have the form LB<P$_\text{G}$<UB as formulated in (4.10). They are presented as an $N \cdot N_{\text{gen}}$-by-1 matrix:

$$\left[(P_{\text{G}_j \min(i)} \cdots P_{\text{G}_{N_{\text{gen}}} \min(i)}) \cdots (P_{\text{G}_j \min N} \cdots P_{\text{G}_{N_{\text{gen}}} \min N}) \right] \tag{4.35}$$

and

$$\left[(P_{\text{G}_j \max(i)} \cdots P_{\text{G}_{N_{\text{gen}}} \max(i)}) \cdots (P_{\text{G}_j \max N} \cdots P_{\text{G}_{N_{\text{gen}}} \max N}) \right] \tag{4.36}$$

4.4.4 Overview constraints

Table 4.1 represents an overview of the different constraints of the optimisation problem:

Equality constraints	Inquality constraints	Bound constraints
Power Balance (4.7), (4.19)	(dis)charged energy by P_{storage} (4.13), (4.14), (4.27)	On reference set points P$_\text{G}$ (4.10), (4.35), (4.36)
EV should contain $E_{\text{EV}_{\text{T}_{\text{out}}}}$ at T_{out} (4.17), (4.23)	Charged energy by EV between T_{in} and T_{out} (4.18), (4.31)	

Table 4.1: Overview of constraints

4.5 Demonstration and validation

In this section, the proposed day-ahead unit commitment model is investigated on a microgrid test network in order to verify the effectiveness and to validate the performance. The demonstration tackles four specific issues:

1. The simultaneous minimisation of the operating costs together with the produced CO2 emissions;

2. The implementation of a demand side participation strategy;

3. The implementation of a congestion control signal whereby the microgrid anticipates to grid congestion by effective microgrid unit scheduling, and whereby the power exchange between microgrid and utility network can be controlled which causes a smooth transition to a virtual islanded operating condition;

4. The complete day-ahead time horizon is divided in 96 time steps (each with 15 min averaged values), which increases the complexity but is necessary for the studied problem.

4.5.1 Microgrid test set up

The microgrid test set up includes 11 low voltage (LV) buses connected downstream from a distribution transformer. Furthermore, the studied system includes renewable energy resources, a storage unit, two micro turbines, and a fuel cell. In this work, a solid oxide fuel cell (SOFC) is considered, where natural gas is used as fuel input [95]. As a result, this fuel cell has an emission rate and will be described in the next paragraph. Additional, in this work commercialised micro turbines are used with power ranges that may vary from 30 to 400 kW [96–98].

Serving the microgrid load (Load 1 + Load 2 + Load 3 + Controllable Load), active power can be produced either by the thermal generation units, the utility grid, the storage device, or the renewable energy resources.
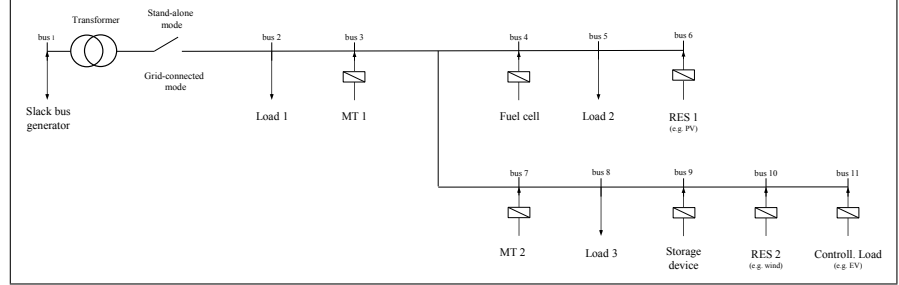
Figure 4.2: Microgrid test set up

Storage elements can be used to cope with the microgrid's technical, economical and environmental challenges. The presence of a storage element, as well as the possibility of exchanging energy with the utility grid adds flexibility to the microgrid operation and besides, it increases the solution space (set of feasible solutions) of the microgrid unit commitment problem. In this work, a storage element is used and participates in the commitment strategy where the charge and discharge commands are allocated according to the lowest cost and the lowest CO_2 emissions. The commands of charging and discharging are associated to the energy prices, where the storage element takes advantage of purchasing power from the upstream grid (utility grid) and selling it back according to the most favorable microgrid revenue. Equations (4.10)-(4.15) are general representations and can be used for any storage element. The storage model used in this work is modelled and simulated according to a general model with a certain minimum and maximum (dis)charge rate, a certain minimum and maximum storage capacity, a cumulative (dis)charged electrical energy constraint (E_{storage}) which represents the SOC, and a constraint on how much energy the storage unit (dis)charges ($P_{\text{storage}} \cdot T_{\text{s}}$) at a given time step T_{s}. In this work, no specific type of storage element is considered and thus a more general representation is applied.

The day-ahead unit commitment model considers a predicted microgrid power demand as well as a renewable energy profile. The actual demand profile (P_{D}^{a}) is presented Fig. 4.3:
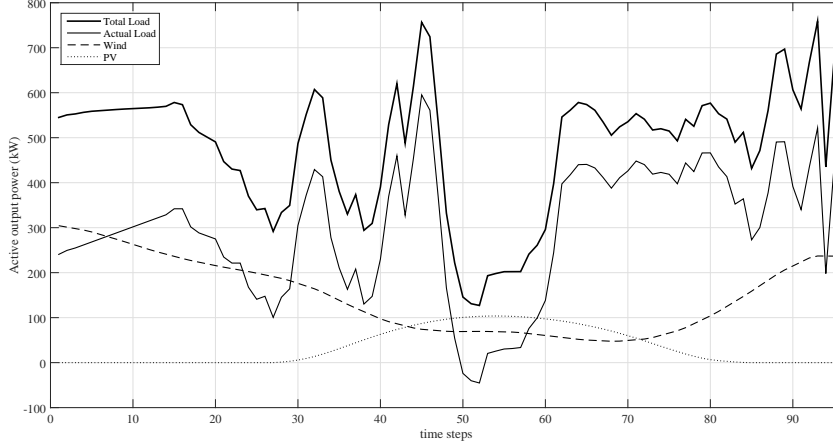
Figure 4.3: Microgrid actual demand

Besides, a variable pricing scheme is used, taken from the Belpex spot market 2014 historical data [92] and is plotted in Fig. 4.4.
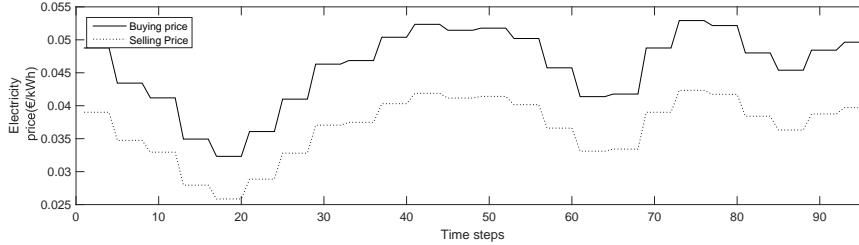
Figure 4.4: Market conditions

4.5.2 Parameter setting

The microgrid unit commitment model presented in this chapter considers a day-ahead (24 hours) time frame with 96 (N) snapshots or time steps each with a time span (T_s) of 15 minutes. For the demonstration, 5 controllable power generation units were considered, including two micro turbines, a fuel cell [95], a storage device and the utility grid. Furthermore, a controllable load including 4 electric vehicles is added to the microgrid set up. The cost and emission coefficients of three different thermal generation units are listed in Table 4.2, and are graphically presented in Fig. 4.5. Note that the

cost curve of the utility grid is not displayed in the upper graph of the figure since this cost varies in time.

$C_{\mathrm{G}}(P_{\mathrm{G}})$	a	b	c
Micro Turbine 1	$100 \cdot 10^{-5.5}$	$50 \cdot 10^{-5.5}$	$20 \cdot 10^{-5.5}$
Micro Turbine 2	$140 \cdot 10^{-5.5}$	$40 \cdot 10^{-5.5}$	$100 \cdot 10^{-5.5}$
Fuel Cell	$20 \cdot 10^{-5.5}$	$20 \cdot 10^{-5.5}$	$10 \cdot 10^{-5.5}$
$\varepsilon_{\mathrm{G}}(P_{\mathrm{G}})$	d	e	f
Micro Turbine 1	$4.09 \cdot 10^{-3}$	$-5.55 \cdot 10^{-3}$	$6.49 \cdot 10^{-3}$
Micro Turbine 2	$2.54 \cdot 10^{-3}$	$-6.05 \cdot 10^{-3}$	$5.64 \cdot 10^{-3}$
Fuel Cell	$5.33 \cdot 10^{-3}$	$-3.55 \cdot 10^{-3}$	$3.38 \cdot 10^{-3}$

Table 4.2: Fuel cost and emission coefficients
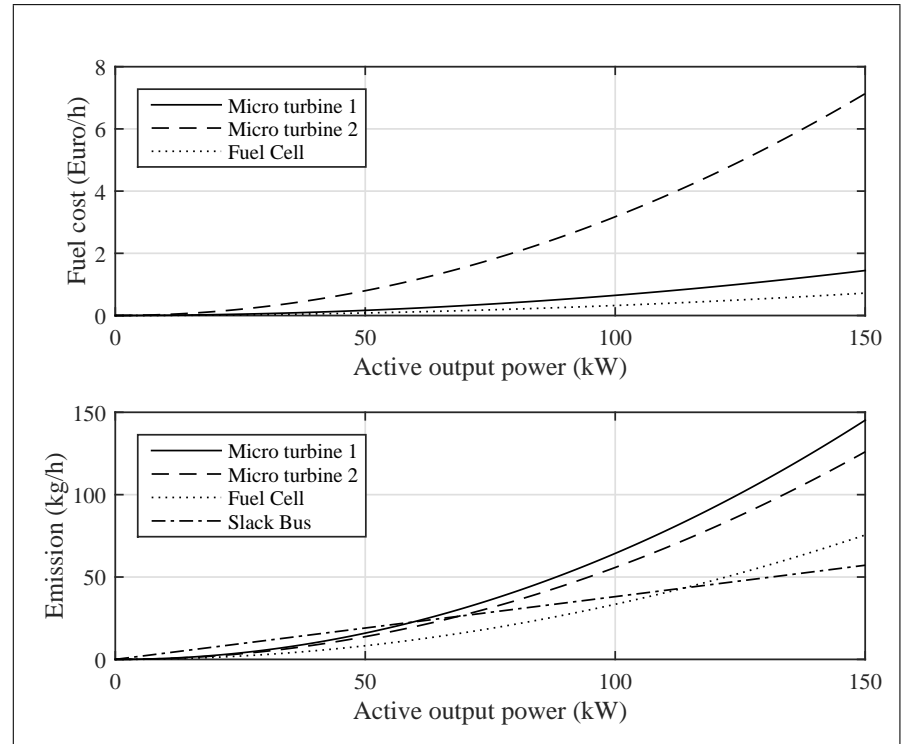
Figure 4.5: Fuel and emission curves thermal generation units

A CO_2 emission intensity of $381 \cdot 10^{-3}$kg/kWh [99] is considered for the power supply of the utility grid and is included in the lower graph of Fig. 4.5. Since a time horizon of 24 hours is considered in this model, the emission rate of the utility grid is regarded as a constant. As explained in section 4.3.4, the cost and emission coefficients of the storage unit and the controllable loads are set to zero. Additionally, the capacities of the microgrid generation units are listed in Table 4.3. For the storage unit, $E_{\min}$ is set to 0 kWh, $E_{\max}$ is set to 40 kWh, and $E_{\text{EV}_{\max}}$ of each EV is set to 80 kWh. The charging rate of each EV is limited between -19.2kW and -7.2kW, which results in a total (4 EVs) minimum and maximum charging rate of -28.8kW and -76.8kW respectively.

	MT 1	MT 2	Fuel Cell	Storage
$P_{\text{G}_{\max}}$ (kW)	160	240	260	± 50

Table 4.3: Microgrid generator capacities

The problem to be optimised includes multiple conflicting objective functions. In this work, a (hybrid) goal attainment method based genetic algorithm is applied to determine the global optimum. As explained in § 3.3, genetic algorithms are based on the process of natural selection which means they take the fundamental properties of natural selection and apply them to the problem to be solved. The genetic algorithm repeatedly modifies a population of individual solutions. At each step, the genetic algorithm selects individuals at random from the current population to be parents and uses them to produce the children for the next generation. Over successive generations, the population proceeds toward an optimal solution. The outline and the operators of the genetic algorithm are described in appendix A.1.2. Using the multi-objective genetic algorithm, the region near an optimal Pareto front can be determined relatively fast, but it can take many function evaluations to achieve convergence. Therefore, the goal attainment method is used as the hybrid solver together with a controlled elitist genetic algorithm. This hybrid technique solves the goal attainment problem, which is a formulation for minimising a multi-objective optimisation problem. The hybrid method runs the genetic algorithm for a small number of generations to get near an optimum front. Subsequently, the solution (Pareto front) returned by the genetic algorithm is used as an initial point for the

hybrid goal attainment method which is faster and more efficient for a local search. The new individuals returned by the hybrid solver are combined with the existing population and a new Pareto front is obtained. Using this hybrid scheme results in the satisfaction of both objectives wherein the results can be calculated more accurately and more quickly.

Since we have multiple conflicting objective functions, the outcome will not give a single solution, but rather a set of solutions (Pareto optimal set). Without additional preference information (priorities), all solutions within this set are considered equally good. In this work, priority is given to the solution (extreme) with the lowest produced CO_2, rather than considering the full range of solutions. A detailed description and example of this hybrid method is presented in § 3.4.2. The model starts by initialising the different input characteristics, parameters and settings, including N, N_{gen}, $C_G(P_G)$, $\varepsilon_G(P_G)$, P_D^a, $P_{G_{min}}$, $P_{G_{max}}$, $E_{storage_{min}}$, $E_{storage_{max}}$, $E_{EV_{min}}$, $E_{EV_{max}}$, $E_{EV_{T_{out}}}$ and $E_{EV_{T_{in}}}$. Since the behaviour of the algorithm and the accuracy of the result is dependent on the solver options and settings, it is important to determine the parameters properly. The population size used to seed the genetic algorithm is set to 100 (candidate solutions). With a large population size, the genetic algorithm searches the solution space more thoroughly, thereby reducing the chance that the algorithm returns a local minimum that is not a global minimum. However, a large population size also causes the algorithm to run more slowly [70]. This value was chosen since a larger population size does not provide more accurate results. The iterations or generations are set to ($N_{var} \cdot 200$). N_{var} is the number of decision variables which is equal to $N_{gen} \cdot N$. The algorithm finds the minimum of both objective or fitness functions. Here, a small function tolerance of 10^{-4} is set, which increases the accuracy of the calculated optimal value. The initial population, used to seed the genetic algorithm, is set to a 100-by-N_{gen} matrix whereby each entry is assigned with the value 0.

4.5.3   Procedure of method validation

The model aims to schedule the power among the different microgrid units while minimising the operating costs together with the produced CO_2 emissions. Given the input characteristics, the objectives, the (in)equality constraints, and the algorithm options, the model automatically builds up the matrices as presented in § 4.4, and

the set points of the UC problem are calculated for the complete time horizon in one execution run. These reference set points are calculated in a way that over the complete time horizon the objectives are optimised. For the validation of the day-ahead UC model, a 24-hour microgrid operation was simulated for 2 different cases:

1. In the first case, the studied system can be considered as the test set-up presented in Figure 4.2 where the controllable loads (EVs) are neglected and are not participating in the UC strategy. In this case, the UC model does not provide a DR program.

2. In the second case, the EVs were added, as presented in Figure 4.2 , and a DR program was included in the UC model. Based on the time-varying electricity cost of the utility grid in the general cost function (4.4), an implicit (or price-based) DR program is provided to the controllable EVs. In this case, as a part of the demand side participation strategy, a charging schedule is determined for the EVs. Besides, an explicit (also called incentive-based) DR program in the form of a congestion control signal (that originates from the DNO) is added. The microgrid anticipates to grid congestion by effective microgrid unit scheduling, and whereby the power exchange between microgrid and utility network can be controlled which causes a smooth transition to a virtual islanded operating condition.

Both cases are simulated according to three commitment strategies, including environomic UC (cost + CO_2), environmental UC (only CO_2) and economic UC (only cost). The complete day-ahead time horizon includes 96 time steps (each with 15 minute averaged values), which makes the UC problem more complicated. Considering the complete time horizon as a set of 'pieces' (15 min interval) creates a more general and piecewise steady-state situation. Therefore, the dynamics and transitional phenomena on a very short time period between the time steps do not fit in the scope of this work and are not considered.

4.5.4 Case 1: unit commitment without demand response

4.5.4.1 Environomic optimisation

In this case, the first simulation is done where the model involves the optimisation of the fuel costs and the CO_2 emissions of the local generators. As explained before, the algorithm provides the Pareto front

as the set of choices that are Pareto optimal. All solutions in this Pareto front are equally optimal. In this case, priority is given to the (extreme) solution with the least produced CO_2, rather than considering the full range of every solution or the (extreme) solution with the least produced fuel cost. The results of the simulation are presented in Fig. 4.6. The active power is scheduled among the different microgrid units while minimising the operating costs together with the CO_2 emissions produced. In what follows, the different results will be discussed per microgrid DER unit.

Thermal generators:
It is clear that the fuel cell has the largest share (among the thermal generators) in the commitment schedule. The contribution of micro turbine 1 is slightly higher than micro turbine 2. The commitment among the thermal units can be explained by the fact that the fuel cell has the lowest cost and the lowest emission rate, and has therefore the largest share in the commitment schedule. A closer look to Fig. 4.5 confirms this distribution. Both, micro turbine 1 and micro turbine 2 are committed in the range of 50kW. A closer look to the fuel and emission curves on Fig. 4.5 confirms that in this range, both micro turbines have a similar emission intensity, but micro turbine 2 has a slightly larger fuel cost as compared to micro turbine 1. This explains why micro turbine 1 delivers more output power, over the complete time horizon, as compared to micro turbine 2.

Utility grid:
The contribution of the utility grid depends on the variable market price (buying and selling) and the emissions, which are considered as constant (within this time horizon). Fig. 4.4 shows that the buying price is low during time steps 12-20. During these time steps, it is more profitable to use the utility grid instead of using the microgrid units. Between time step 35-40, the buying price becomes high and therefore, the utility grid is scheduled near to zero. On Fig. 4.6, it is clear that the output power of the utility grid rises above the fuel cell when the market price is low. When the market price becomes high, the utility grid is scheduled close to 0kW. Between time steps 30-35, 40-50 and 60-96, the microgrid total demand becomes excessively high, making it more favourable in terms of cost and emission optimisation to extract energy from the utility grid, rather than increasing the power set points of the microgrid thermal generation units. During time steps 48-57, the energy demand becomes negative due to the overproduction of the RES. Even then, the thermal generation units

are not committed to zero. This can be explained by the high selling price of the utility grid. During this period, the microgrid is selling energy (produced by the thermal generators and RES) to the main grid in order to gain revenue and further reduce the overall microgrid costs.

Storage device:
The storage device is provided with a charging schedule in order to contribute to the optimisation of both objectives. When the energy demand is low, at time steps 25-30 and 37-40, the storage device is committed to charge. During these periods, it is more profitable to charge the storage device, rather than producing extra energy by the thermal generation during periods of high energy demand in order to charge the storage unit. During time steps 50-52, the energy demand becomes negative (due to the surplus of renewable energy production), and the storage device will be charged with the maximum rate (-50kW). During periods of high energy demand (time steps 30-35 and 40-50), the storage device will be discharged in order to reduce the need of extra power produced by the thermal generation units or the utility grid. As a result, the thermal generation units and the utility grid should not be committed in their excessively high output power range, which limits extra fuel costs and emissions.
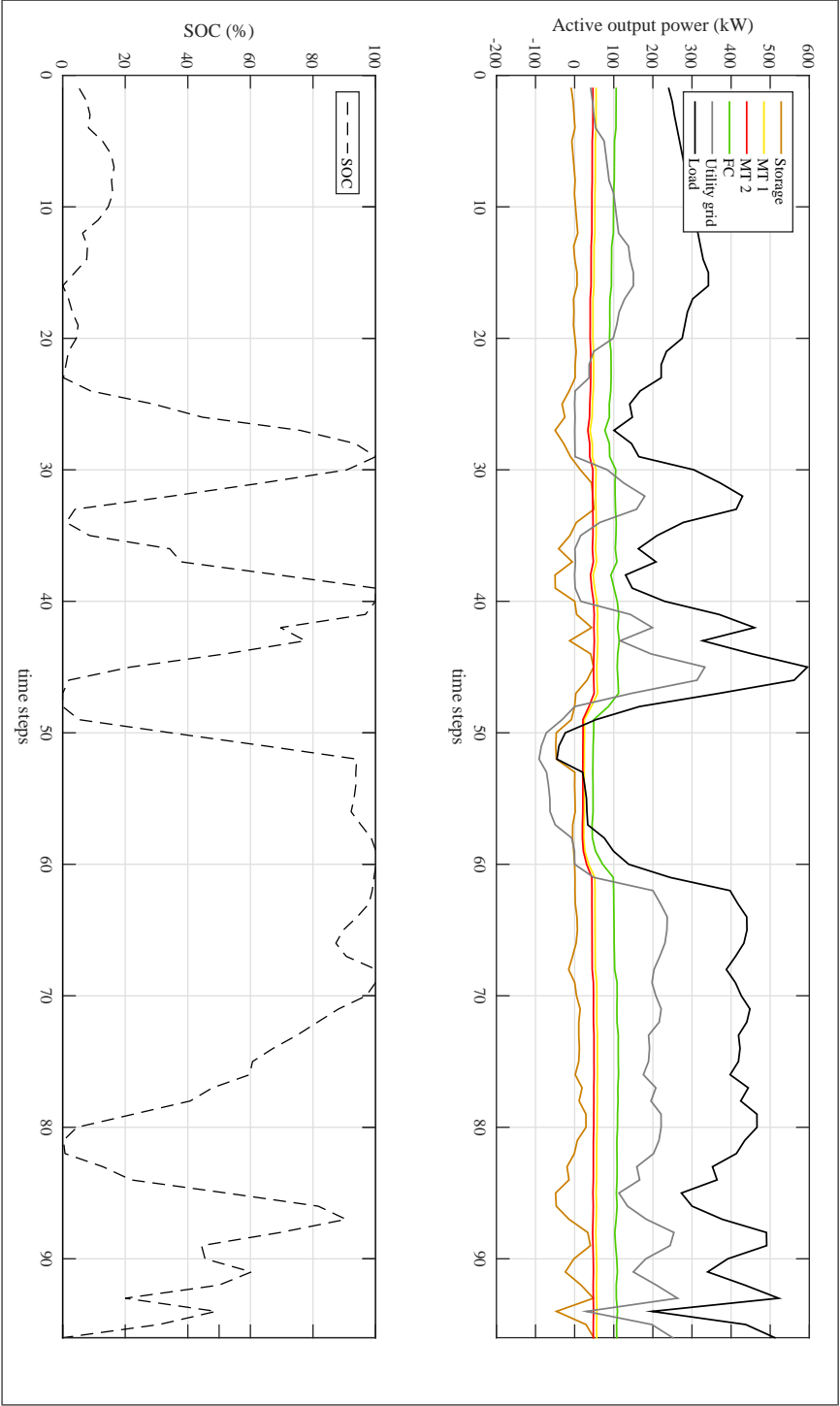
Figure 4.6: Environomic optimisation

4.5.4.2 Environmental optimisation

Within this first case, a second optimisation is performed which involves the optimisation of the CO_2 emissions of the local generators without considering the fuel costs. The results of the simulation are plotted in Fig. 4.7 and are discussed below.

Thermal generators:
The reference set points of the thermal generators in the microgrid are scheduled relatively constantly over the complete time horizon. The fuel cell has a larger contribution as compared to the micro turbines. This can be explained on the basis of the lower graph in Fig. 4.5, in which both micro turbines have a higher emission rate than the fuel cell. Note that the contribution of micro turbine 2 is slightly higher than micro turbine 1, which is just the opposite as in the case for an environomic optimisation. This can be explained by the fact that the fuel costs are not taken into account, and micro turbine 2 has a lower emission rate as compared to micro turbine 1. Besides, during time steps 48-57, the thermal generation units are committed close to zero, which differs from the environomic optimisation. In this case, it is not profitable (in terms of emission reduction) to produce energy with the thermal generators in order to sell it back to the grid.

Utility grid:
Over the complete time horizon, the majority of the microgrid actual demand is covered by the utility grid. This can be explained by the lower emission rate of the utility grid, which is due to the used resource mix which includes carbon neutral nuclear power generation. Since it is not profitable (in terms of emission reduction) to produce energy with the thermal generators in order to sell it back to the grid, the utility grid is committed close to zero during periods of low demand and high selling prices (time steps 48-57).

Storage device:
Within the environmental optimisation strategy, the storage device is provided with a charging schedule the minimise the CO_2 emissions. During periods of low energy demand (time steps 24-30, 35-40 and 50-30), the storage device will be charged by the thermal generation units. Again, it is more profitable to charge the storage device during periods of low energy demand, rather than producing extra energy by the thermal generation (with additional emissions) during periods of high energy demand in order to charge the storage unit. The storage

device will be discharged during periods of high energy demand (time steps 30-35 and 40-50). This prevents the commitment of the thermal generation units in their high output power range and reduces additional emissions. The charging and discharging operation can be verified by the SOC, as presented on the lower graph of Fig. 4.7.

The environmental optimisation results in an a reduction of 11.11% in CO_2 emissions and an increase of 47.18% in microgrid operating costs. We can conclude that a purely emission optimisation results in a reduction of produced CO_2 emissions but an increase of total fuel costs.
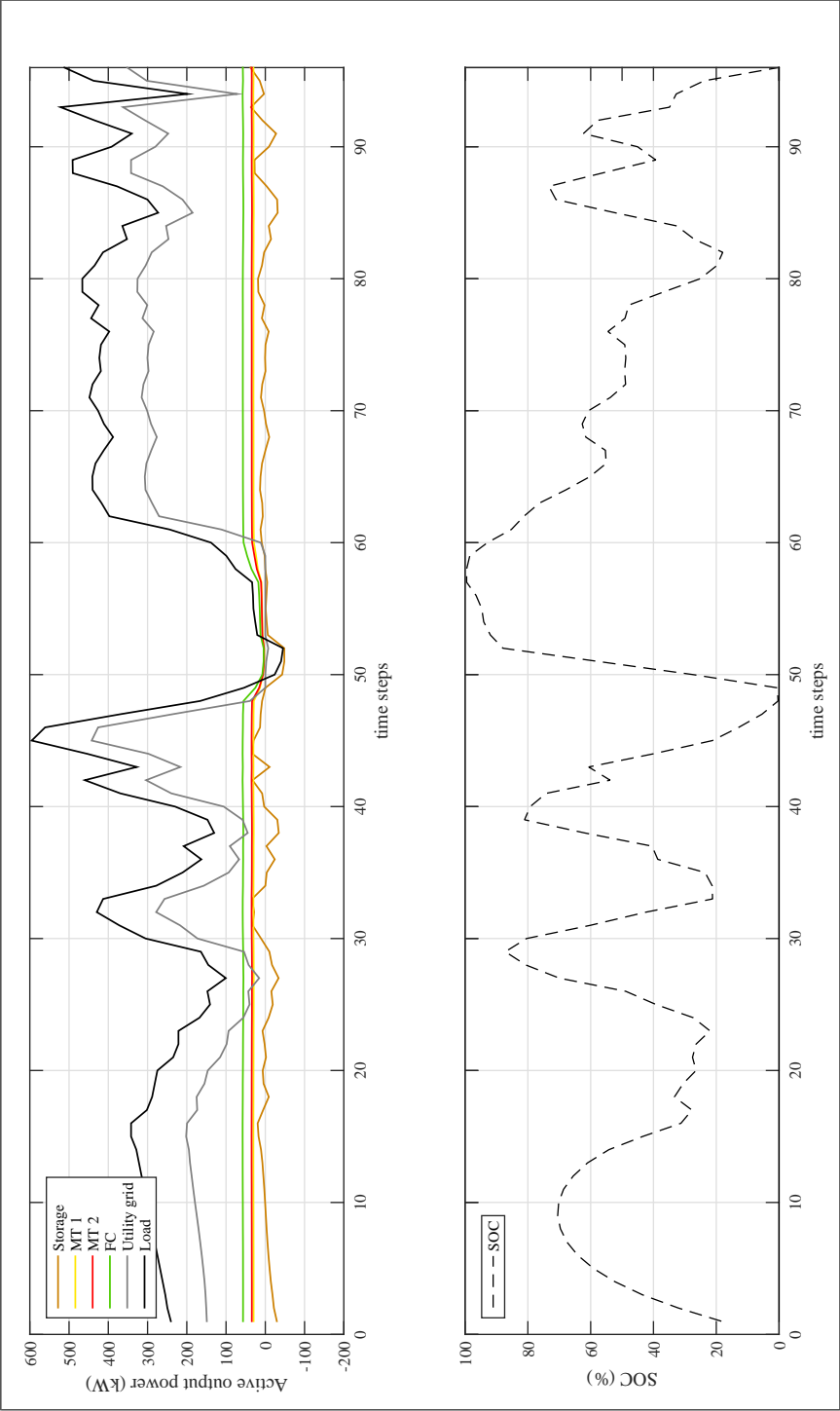
Figure 4.7: Environmental optimisation

4.5.4.3   Economic optimisation

Within this first case, a third optimisation is performed where the microgrid generation units are committed following the lowest cost without considering the produced emissions. The results of the simulation are plotted in Fig. 4.8 and are discusses below.

Thermal generators:
It is clear that the thermal generating units are producing more energy than the actual demand. The greatest contribution comes from the fuel cell, followed by micro turbine 1. Both units are producing energy at lowest cost in order to cover de actual demand, and to sell energy to the main grid. This maximises the microgrid revenue and further reduces the overall operating cost. Micro turbine 2 has a high fuel cost rate and is therefore less committed.

Utility grid:
During a large part of the time horizon, the utility grid is scheduled with a negative power output. Since this optimisation strategy aims to minimise the total operating cost over the complete time horizon, the microgrid is committed to export energy and sell it to the main grid in order to gain revenue and to reduce the operating costs. During periods of high peak demand (time steps 45-47) the utility grid is committed to deliver energy to the microgrid. During these time steps, it becomes more profitable (in terms of economic optimisation) to use the utility grid instead of producing more energy using micro turbine 2 (still less profitable than the fuel cell and micro turbine 1). Between time step 51 and 52, the microgrid exports 500kW (utility grid is set to -500kW). This can be explained by the combination of the very low energy demand (due to the surplus of the energy produced by the RES) and the high selling price (see Fig. 4.4).

Storage device:
In this case, the contribution of the storage device is rather small. During periods of low energy demand, the storage device will be charged by the thermal generation units. Besides, the storage device will be discharged during periods of high energy demand.
Purely economic unit commitment without congestion management results in a reduction of 88.11% in microgrid operating costs and an increase of 141.69% in CO_2 emissions compared to environomic unit commitment without congestion management.
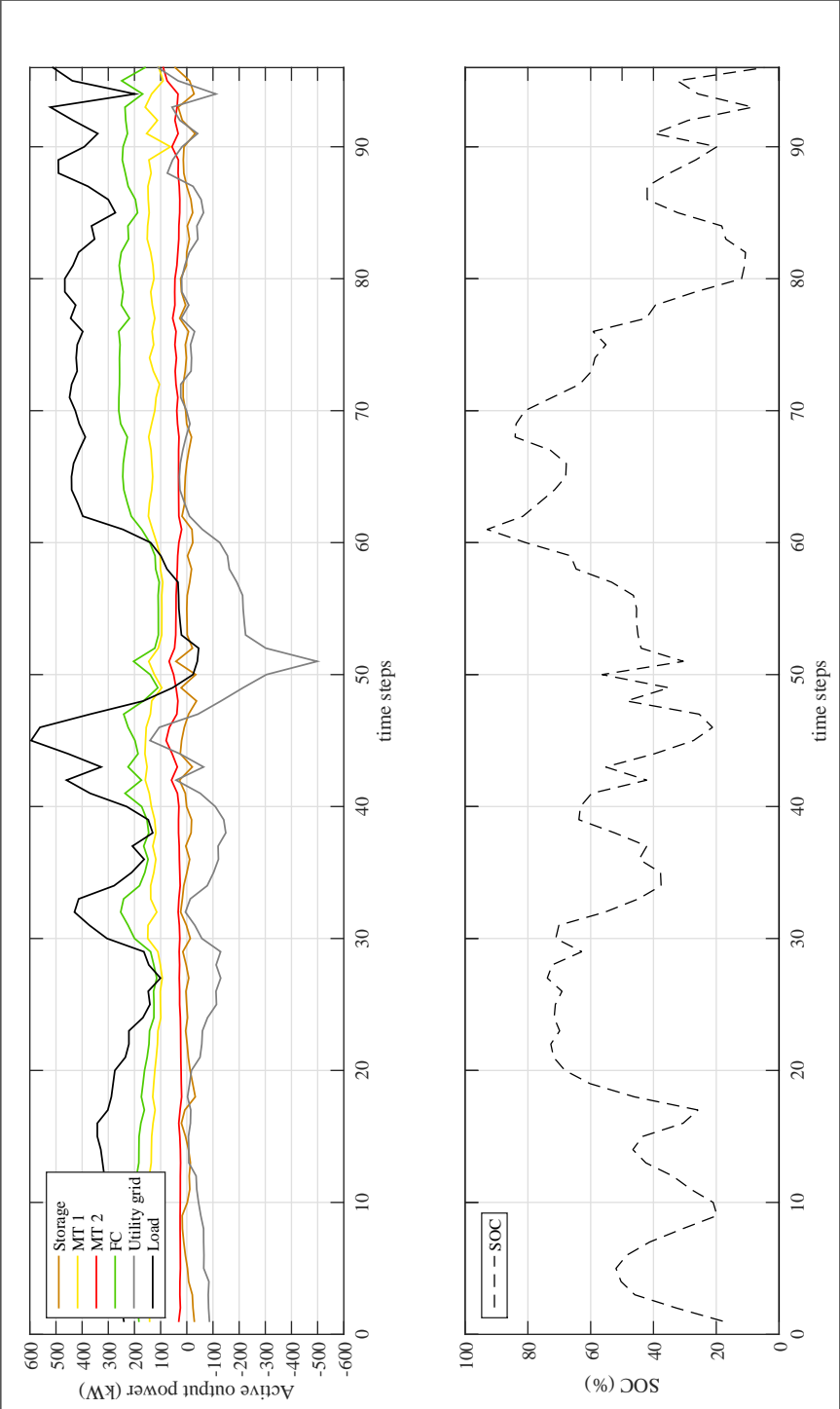
Figure 4.8: Economic optimisation

4.5.4.4 Overview of the results

Table 4.4 represents an overview of the different optimisation results:

	Total cost	Total emission
Environomic optimisation	reference	reference
Environmental optimisation	47.18% ↗	11.1% ↘
Economic optimisation deviation	88.11% ↘	141.69% ↗

Table 4.4: Overview optimisation results

4.5.5 Case 2: unit commitment with demand response

In the second case, the EVs are added, and a DR program is included in the UC model. As a part of the demand side participation strategy, an implicit DR (or price-based) program is provided through the EVs.

4.5.5.1 Environomic optimisation

Simulation without DNO congestion signal:
In a first simulation, the active power is scheduled among the different microgrid units while minimising the operating costs together with the produced CO_2 emissions. The results of the simulation are presented in Fig. 4.9 and are discussed below.

Thermal generators:
It is clear that the contribution of micro turbine 1 is slightly higher than micro turbine 2, but much lower than the contribution of the fuel cell. This can be explained by the fact that the fuel cell has the lowest cost and the lowest emission rate, and has therefore the largest share in the commitment schedule. This conclusion can be supported on the basis of the lower graph in Fig. 4.5.

Utility grid:
The contribution of the utility grid is dependent on the variable market price (buying and selling) and the emissions, which are considered as constant (within this time horizon). During time steps 12-20, the actual demand increases, and at the same time (as we can see on Fig. 4.4), the buying price is low. Therefore, it is more profitable to use

the utility grid instead of using the microgrid units. Increasing the output power of the thermal units would lead to increased emissions and increased costs. Between time steps 25-30, the buying price increases and the actual demand decreases. Therefore, the utility grid is scheduled close to zero. Both can be verified on Fig. 4.9, where the output power of the utility grid rises above the fuel cell when the market price is low, and is scheduled close to 0kW, when the market price becomes high. Between time steps 30-35, 40-50 and 60-96, the microgrid total demand becomes excessively high, making it more favourable in terms of cost and emission optimisation to extract energy from the utility grid, rather than increasing the power set points of the microgrid thermal generation units. Between time steps 50-55, due to to overproduction of the RES (negative actual demand), the microgrid exports energy to the main grid and the utility grid is committed in a negative output power range.

Storage device and electric vehicles:
During periods of low energy demand (e.g., time steps 25-30, 35-40 and 50-60), the storage unit is committed to charge (by the fuel cell and micro turbines). During time steps 50-55, when the energy demand becomes low and even negative, the storage device is committed to charge at the maximum rate of -50kW. On the other hand, at high peak demand (time step 30-35 and 40-50), the storage unit will be discharged, which reduces the usage of grid power, and as a result reduces the total cost and emission of the microgrid operation. The charging and discharging operation of the storage device can be verified by the SOC, as presented on the lower graph of Fig. 4.9.
The EVs were plugged in between 09:00 and 17:00 (time step 36-68). Between time step 50 and 57, the energy demand becomes very low (even negative) due to the high (over)production of the RES. During these time steps the EVs will be scheduled at their maximum charging rate ($4 * -19.2kW = -76.8$kW) and as a result, their SOC_{EV} has the steepest curve. As mentioned in 4.17 and 4.23, an equality constraint is imposed on the EVs. At time step 68, the EVs are expected to be fully charged. This can be verified on Fig. 4.9, where the SOC_{EV} equals 320kWh ($4 * 80$kWh) and remains constant since the Evs can be unplugged at any time and do not participate in the UC strategy any more.

Simulation with DNO congestion signal:
A second simulation is done where an explicit (also called incentive-based) DR program in the form of a congestion control signal (that

originates from the DSO) was added. The microgrid anticipates to grid congestion by effective microgrid unit scheduling which causes a smooth transition to a virtual islanded operating condition. The results are shown in Fig. 4.10 and are discussed below.

Congestion signal:
Between 11:00 a.m. and 14:30 p.m. (time step 44-58), and between 18:00 p.m. and 19:30 p.m. (time step 72-78), a congestion signal is introduced by the DSO. These time steps are chosen arbitrarily in order to present the influence on the commitment strategy. During this signal, the utility grid is committed to zero and no energy is exchanged between the microgrid and the main grid. As a result, a transition to islanded mode was simulated.

Thermal generators:
Because of the lack of the utility grid, the buying and selling price are neglected during these periods. The maximum power which can be delivered depends on the upper bounds of the controllable thermal generators and the stored energy. During the islanded operation mode, the fuel cell has the greatest contribution in the unit commitment. This can be explained by the fact that the fuel cell has the lowest fuel cost and lowest emission rate. Note that in Fig. 4.10, micro turbine 2 has a slightly larger share in the UC than micro turbine 1, compared to Fig. 4.9. This can be explained by the fact that due to the DSO signal, the actual demand (over the complete time horizon) should be covered by more output power coming from the generation units (MT 1, MT2, FC, and Storage) and less coming from the utility grid, which is committed to 0kW for 21 time steps. This makes it more favourable in terms of cost and emission optimisation to extract more power from micro turbine 2 than from micro turbine 1. This can be supported by the fact that, within this environomic optimisation, priority is given to the (extreme) solution with the least produced CO_2, and micro turbine 2 has a lower emission rate in the range of higher power output (see Fig. 4.5).

Storage device and electric vehicles:
When the energy demand becomes very low, the storage device will be charged. At high peak demand (time step 30-35 and 40-50) the storage unit will be discharged which reduces the usage of grid power, and as a result reduces the total cost and emission of the microgrid operation. The EVs were plugged in between 09:00 and 17:00 (time step 36-68). At 17:00 p.m, the EVs are fully charged. During time

steps 48-57, the actual energy demand becomes negative due to the high (over)production of the RES. Since this event happens when the microgrid operates in islanded mode, the energy surplus of the RES cannot be exported to the main grid (is committed to zero). As a result, the storage device and the EVs are charged at their maximum rate in order to store the overproduction coming from the RES.
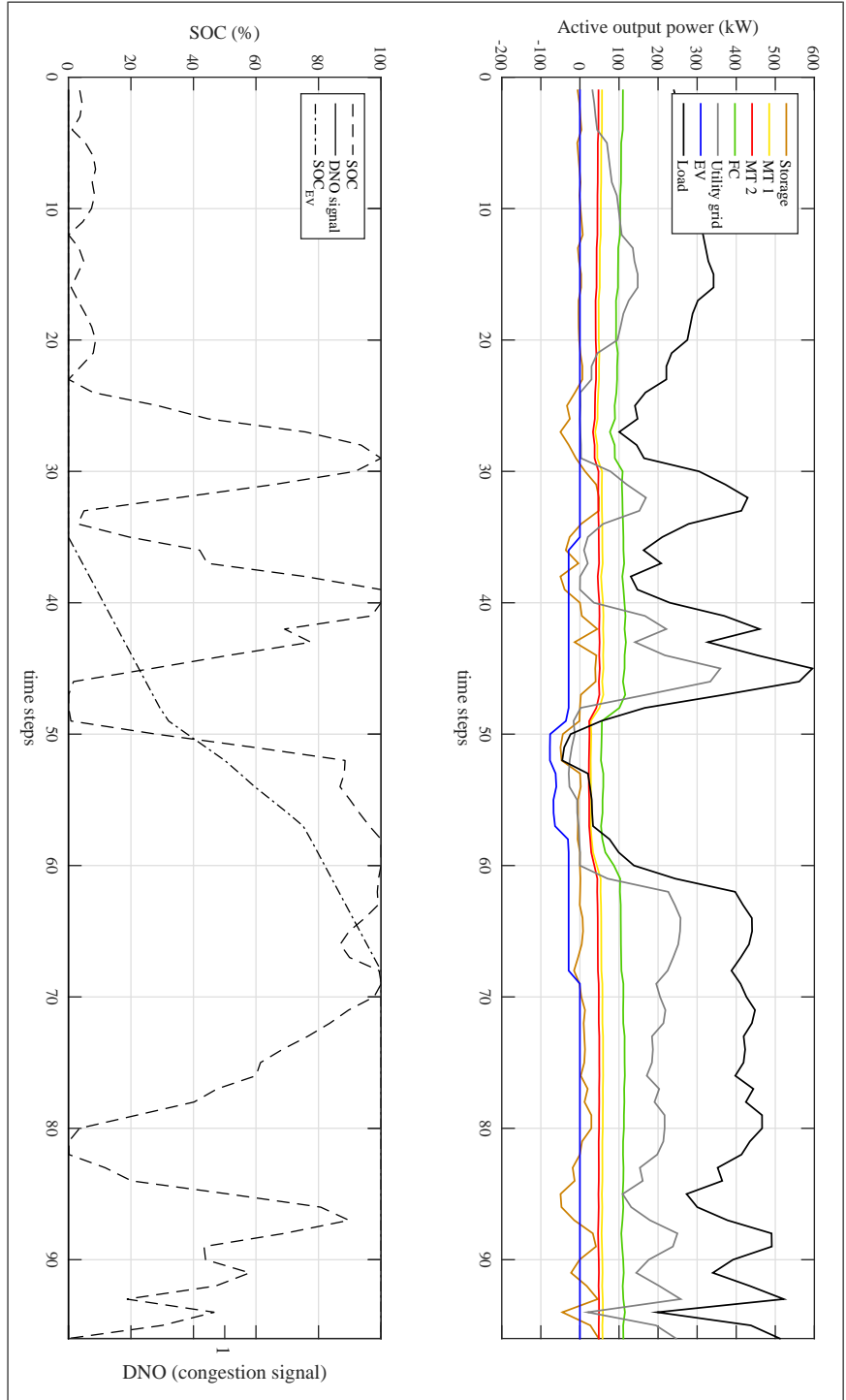
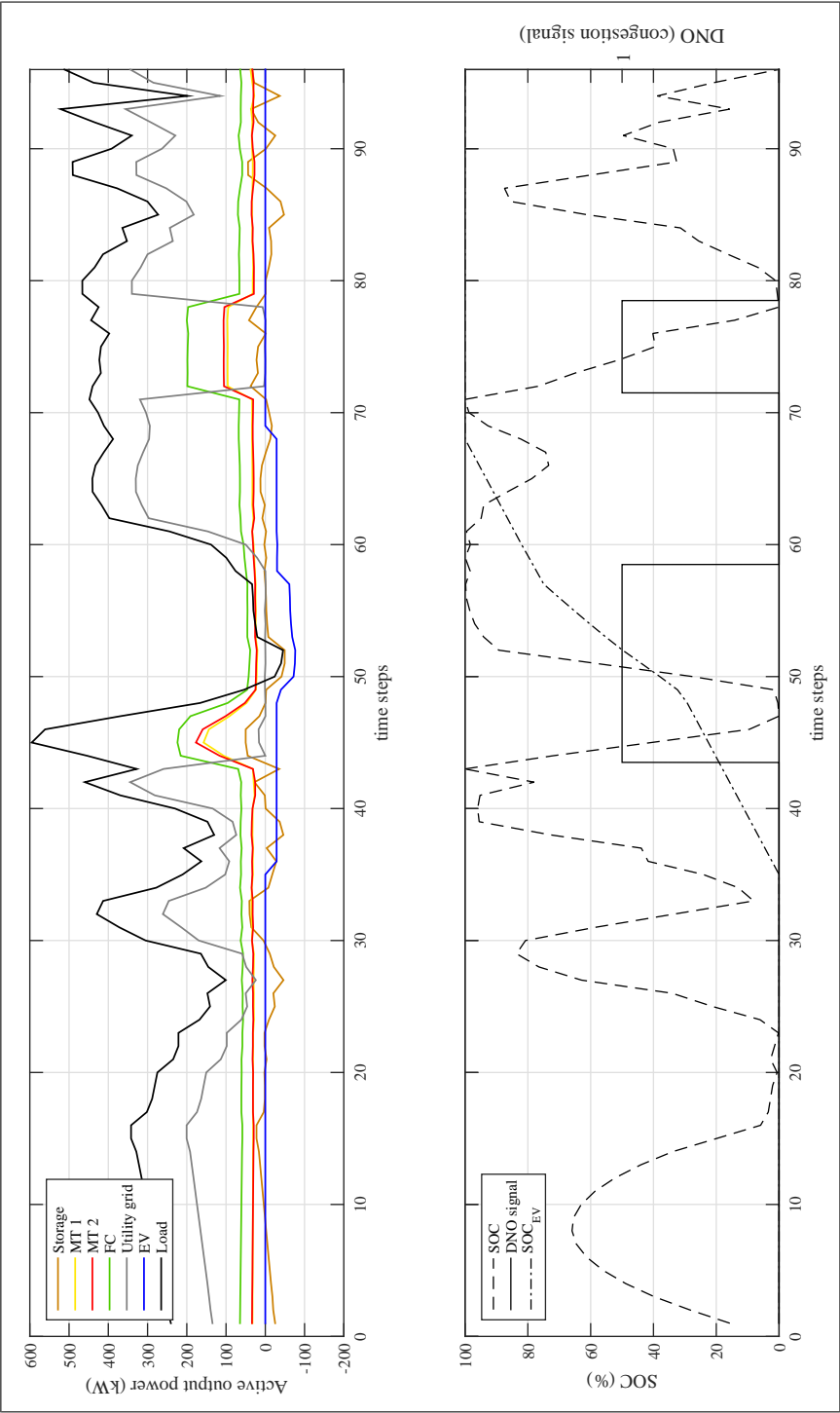**Figure 4.9:** Environomic optimisation

Figure 4.10: Environomic optimisation + congestion management

4.5.5.2   Environmental optimisation

Simulation without DNO congestion signal:
Within case 2, a second optimisation is performed which involves the optimisation of the CO_2 emissions of the local generators without considering the fuel costs. The results of the simulation are plotted in Fig. 4.11 and are discussed below.

Thermal generators:
The reference set points of the thermal generators in the microgrid are kept relatively constant, whereby the fuel cell has the largest contribution as compared to the micro turbines. This can be verified on the basis of the lower graph in Fig. 4.5, in which both micro turbines have a higher emission rate. Note that the contribution of micro turbine 2 is slightly higher than micro turbine 1, which is just the opposite as in the case of an environomic optimisation. This can be explained by the fact that micro turbine 2 has a lower emission rate as compared to micro turbine 1.

Utility grid:
During the complete time horizon, the majority of the microgrid actual demand is covered by the utility grid. This can be explained by the lower emission rate of the utility grid, which is due to the used resource mix which includes carbon neutral nuclear power generation. Note that the intersection where it becomes more profitable (in terms of emissions) to use the utility grid above both micro turbines lies around to 60kW. This is confirmed on both, Fig. 4.9 (time steps 25-30) and the lower graph on Fig. 4.5.

Storage device and electric vehicles:
The storage unit is committed to charge during off peak energy demand (time steps 25-30, 35-40 and 48-57) and to discharge during peak demand (e.g. 30-35 and 40-50). This conclusion can be supported by the SOC which is depicted on the lower graph on Fig. 4.9. The EVs were plugged in between 09:00 a.m. and 17:00 p.m. (time step 36-68). Between time steps 36-48 and 57-68, the EVs are charged at their minimum rate ($4*-7.2kW = -28.8$kW). Between time step 48 and 57, the energy demand becomes very low (even negative) due to the high production of the RES. During this period, the EVs will be scheduled at their maximum rate ($4*-19.2kW = -76.8$kW) and their SOC_{EV} has the steepest curve (between time steps 48-57).
The environmental optimisation without congestion management results in a reduction 11.46% in CO_2 emissions and an increase of

45.85% in microgrid operating costs. It is clear that pure emission optimisation results in a reduction of produced CO_2 emissions but an increase of total fuel costs.
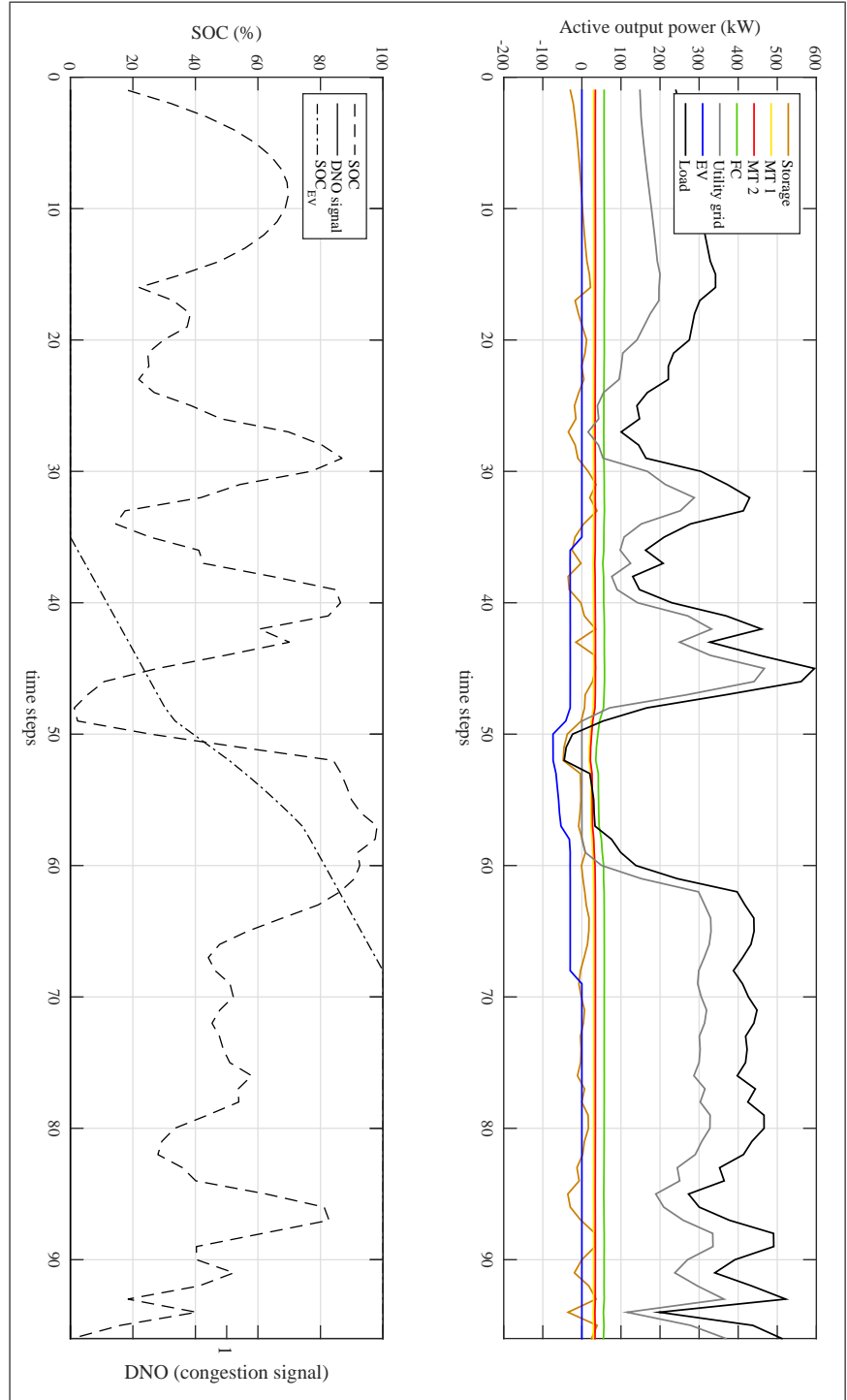
Figure 4.11: Environmental optimisation

Simulation with DNO congestion signal:
A second simulation is done by including the congestion management approach. A DNO imposes a congestion signal between 11:00 and 14:30, and between 18:00 and 19:30. The UC model anticipates to the grid congestion signal and causes a transition to islanded mode. The results are presented in Fig. 4.12.

Congestion signal:
Between time step 44-58, and between time step 72-78, a congestion signal is introduced by the DSO. These time steps are chosen arbitrarily in order to investigate the impact on the commitment strategy. During this signal, a transition to islanded mode was simulated. Fig. 4.12 shows that the utility grid is committed to zero kW and no energy is exchanged between the microgrid and the main grid.

Thermal generators:
In the islanded operation mode, the fuel cell has the greatest contribution in the unit commitment. During the complete time horizon, the output power of both micro turbines is scheduled to 50kW. This can be explained by the fact that in this case, only the produced emissions are considered. The CO_2 emissions of both micro turbines are equal in the output power range of 50kW. This can be verified on the lower graph on Fig. 4.5. When the actual demand becomes excessively high (e.g., time step 45-50), micro turbine 2 produces more power, since micro turbine 1 is limited to it's upper limit of 160kW.

Storage device and electric vehicles:
During time step 72-78 (in islanded mode), the storage unit will be discharged, which reduces the need to schedule the thermal generation units in their high emission range. Therefore, the total cost and emission of the microgrid operation can be reduced. The EVs were plugged in between 09:00 and 17:00 (time step 36-68). At 17:00, the EVs are fully charged (see lower graph on Fig. 4.12). During the event of islanded mode, the actual energy demand becomes negative due to the high (over)production of the RES (time steps 48-57). As a result, the storage device and the EVs are charged at their maximum rate in order to store the overproduction coming from the RES.
The environmental optimisation with congestion management results an increase of 1.77% in microgrid operating costs as compared to the environomic optimisation with congestion management. The total emissions in both cases is quite similar which can be verified on Fig. 4.10 and Fig. 4.12, where the difference in set points is rather small.
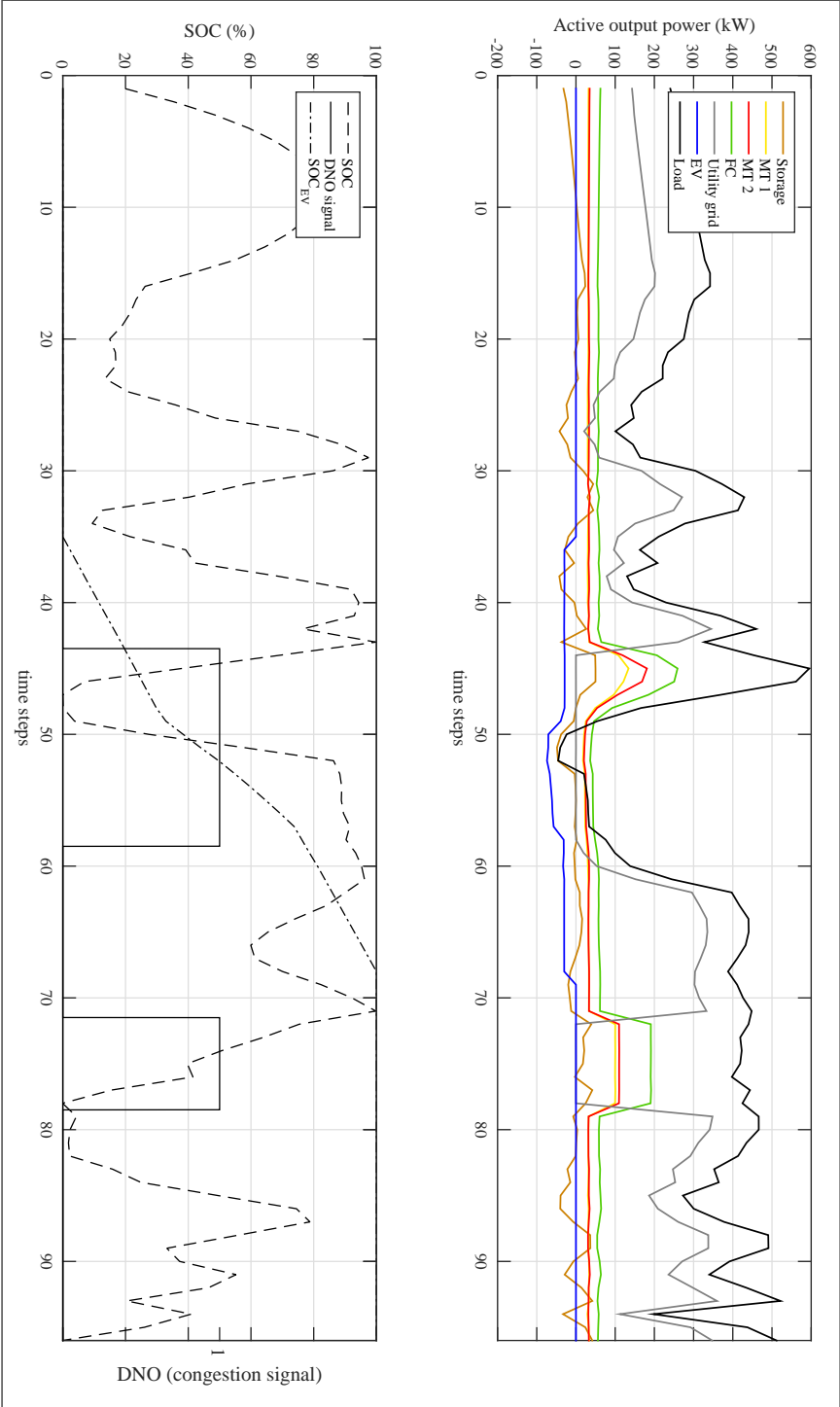
Figure 4.12: Environmental optimisation + congestion management

4.5.5.3   Economic optimisation

Simulation without DNO congestion signal:
A third optimisation is performed where the microgrid generation
units are committed following the lowest cost without considering
the produced emissions. The results of the simulation are plotted in
Fig. 4.13.

Thermal generators:
Clearly, the thermal generating units are producing more energy than
the actual demand. The greatest contribution comes from the fuel
cell, followed by micro turbine 1. Since the objective of this opti-
misation method is to minimise the total operating cost (over the
complete time horizon), both units are producing energy at a rela-
tively low cost in order to cover de actual demand, and to sell energy
to the main grid. This maximises the microgrid revenue and further
reduces the overall operating cost. Micro turbine 2 has a high fuel
cost rate and is therefore less committed.

Utility grid:
During a large part of the time horizon, the microgrid exports en-
ergy to the main grid. Therefore, the utility grid is scheduled with a
negative power output. The microgrid sells energy to the main grid
in order to gain revenue and to reduce the operating costs. Dur-
ing periods of high peak demand (time steps 45-47) the utility grid
is committed to deliver energy to the microgrid. During these time
steps, it becomes more profitable (in terms of economic optimisa-
tion) to use the utility grid instead of producing more energy using
micro turbine 2. Between time step 47 and 52, the microgrid exports
217kW (utility grid is set to -217kW). This can be explained by the
combination of the very low energy demand (due to the surplus of
the energy produced by the RES) and the high selling price (see Fig.
4.4).

Storage device and electric vehicles:
In this case, the contribution of the storage device is rather small.
During periods of low energy demand, the storage device will be
charged by the thermal generation units. Besides, the storage device
will be discharged during periods of high energy demand. During
time steps 36-47, the charging rate of the EVs changes between its
limits which can be explained by the varying actual demand in this
period. During peak moments, the EVs will charge at lowest rate and

vice versa. During time steps 48-57, the actual demand becomes low (even negative) and the EVs are charged at maximum power rate. Purely economic unit commitment without congestion management results in a reduction of 86.2% in microgrid operating costs and an increase of 138.12% in CO_2 emissions as compared to environomic unit commitment without congestion management.

Simulation without DNO congestion signal:
A final simulation was done, where a DSO congestion signal is added to the economic UC strategy. The results are presented in Fig. 4.14.

Congestion signal:
A congestion signal was imposed during time steps 44-58, and time steps 72-78. The UC model anticipates to the grid congestion signal and causes a transition of the microgrid to islanded mode. Again, these time steps are chosen arbitrarily in order to impose the influence on the commitment strategy. Fig. 4.14 shows that the utility grid is committed to zero kW and no energy is exchanged between the microgrid and the main grid. During these periods, the microgrid operates in islanded mode.

Thermal generators:
In the islanded operation mode, the fuel cell has the greatest contribution in the unit commitment. During the complete time horizon, the output power of micro turbine 1 is slightly less than the fuel cell. This can be explained by the fact that in this case, only the fuel costs are considered which are quite equal in the output for both thermal generation units. This can be verified on the lower graph on Fig. 4.5. When the actual demand becomes excessively high (e.g. time step 45-50), micro turbine 2 is scheduled in a high output power range, since the fuel cell and micro turbine 1 are producing at their maximum power rate of 160kW and 260kW respectively.

Storage device and electric vehicles:
When the energy demand becomes very low, the storage device will be charged. At high peak demand (e.g. time step 30-35) the storage unit will be discharged which reduces the usage of grid power, and as a result reduces the total cost and emission of the microgrid operation. The EVs were plugged in between 09:00 a.m. and 17:00 p.m. (time step 36-68). At 17:00 p.m, the EVs are fully charged. During time steps 45-50, the microgrid actual demand becomes excessively high, making it more profitable to discharge the storage unit instead

of scheduling the thermal generation units in their higher output power ranges. During time steps 48-57, the actual energy demand becomes negative due to the high (over)production of the RES. Since this event happens when the microgrid operates in islanded mode, the energy surplus of the RES cannot be exported to the main grid (is committed to zero). As a result, the storage device and the EVs are charged at their maximum rate in order to store the overproduction coming from the RES.

Purely economic unit commitment with congestion management results in a reduction of 39.57% in microgrid operating costs and an increase of 37.67% in CO_2 emissions as compared to environomic unit commitment with congestion management.
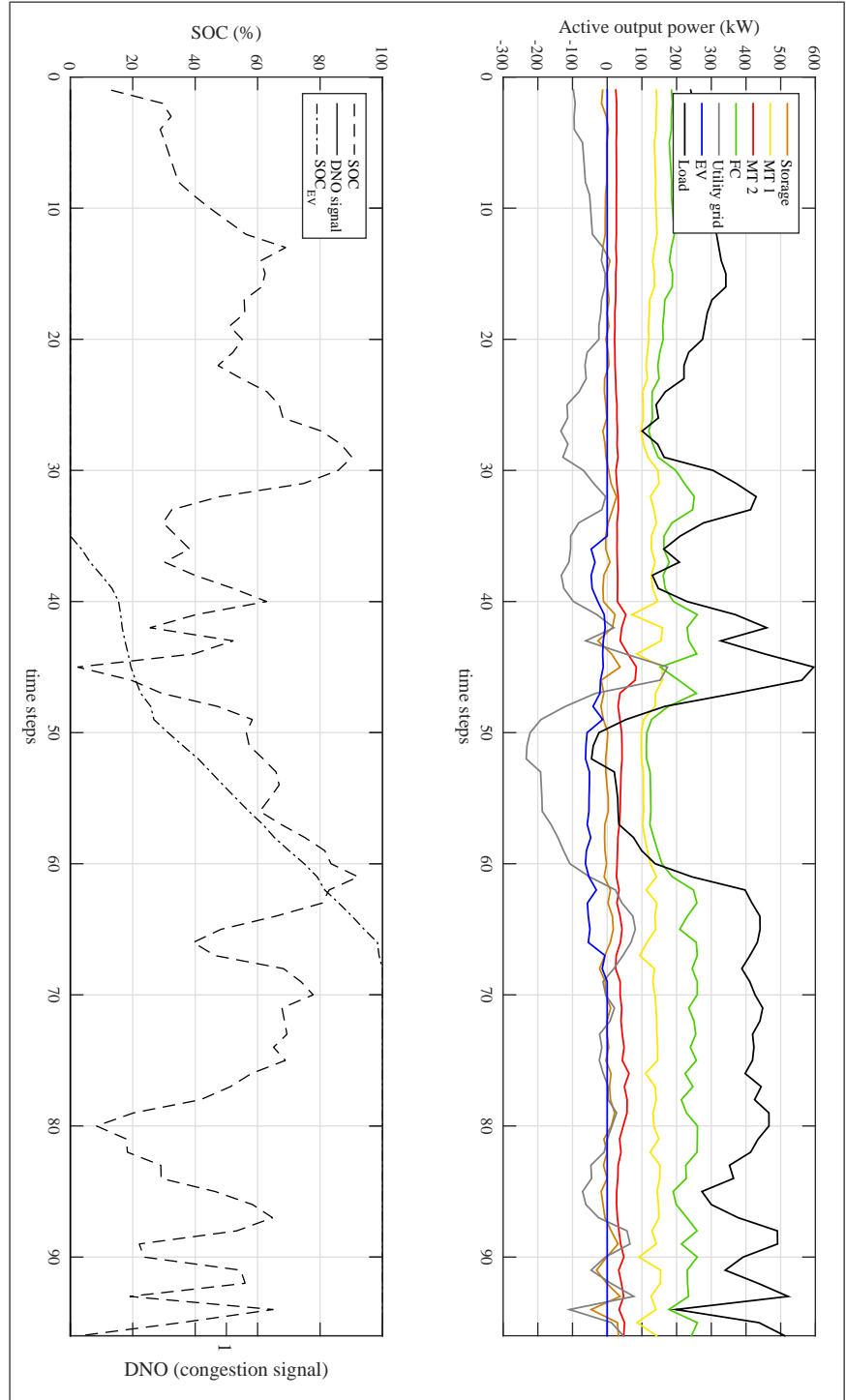
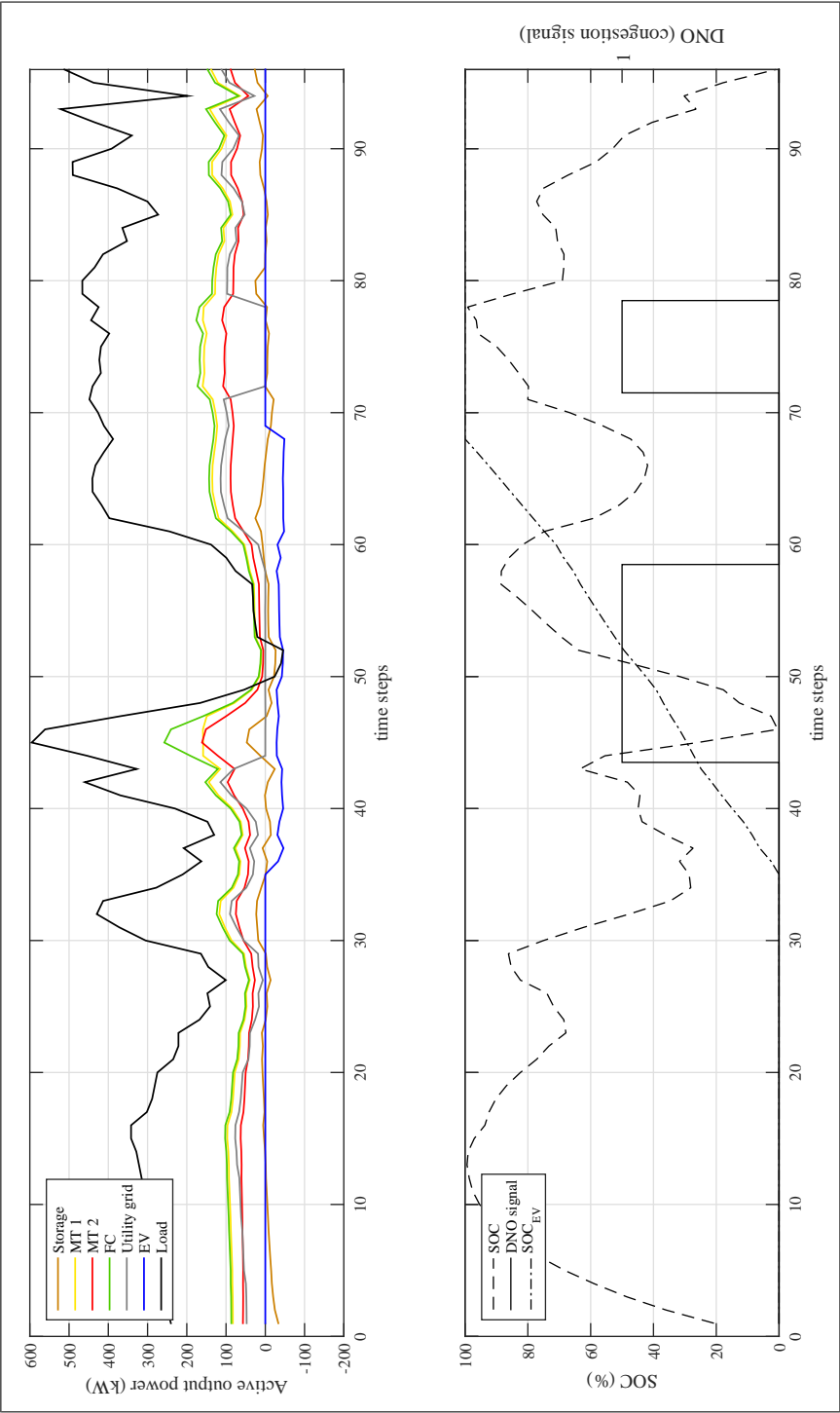**Figure 4.13:** Economic optimisation

Figure 4.14: Economic optimisation + congestion management

4.5.5.4   Overview of the results

Table 4.5 represents an overview of the different optimisation results without congestion signal.

	Total cost	Total emission
Environomic optimisation	reference	reference
Environmental optimisation	45.85% ↗	11.46% ↘
Economic optimisation deviation	86.2% ↘	138.12% ↗

Table 4.5: Overview optimisation results without congestion signal

Table 4.5 represents an overview of the different optimisation results with congestion signal.

	Total cost	Total emission
Environomic optimisation	reference	reference
Environmental optimisation	1.77% ↗	0.25% ↘
Economic optimisation deviation	39.57% ↘	37.67% ↗

Table 4.6: Overview optimisation results with congestion signal

4.6   Conclusions

In this chapter, an analytical method based on a multi-objective hybrid genetic algorithm is proposed and demonstrated for a microgrid day-ahead unit commitment model. The model aims to schedule the power among the different microgrid units while minimising the operating costs together with the CO_2 emissions produced. The approach is demonstrated on a test case including a variety of DER units which are likely to be found in a microgrid. A storage device is added where the charge and discharge schedule is calculated according to both objectives. The presence of a storage element, as well as the possibility of exchanging energy with the utility grid adds flexibility to the microgrid operation and besides, it increases the solution space (set of feasible solutions) of the microgrid unit commitment problem. The charge and discharge commands of the storage device are allocated according to the lowest cost and the lowest CO_2 emissions. Besides, the commands of charging and discharging are associated with the energy prices as well, and where the storage element takes advantage of purchasing power from the upstream utility grid and selling it back according to the most favourable microgrid revenue. In addition, as a part of the demand side participation strategy, a charging schedule is determined for the electric vehicles. A 24-hour microgrid simulation has been performed with an interval or time span of 15 minutes where the objectives are considered simultaneously. Considering the complete time horizon as a set of 'pieces' (15 min interval) creates a more general and piecewise steady-state situation. Therefore, the dynamics and transitional phenomena on a very short time period between the time steps do not fit in the scope of this work. Simulations are done according to the three UC strategies, including environomic optimisation (fuel cost $+$ CO_2 emissions), environmental optimisation (CO_2 emissions) and economic optimisation (fuel cost). In a second case, an additional simulation is done (for every optimisation strategy) including a congestion control signal where the microgrid anticipates to the grid congestion by effective microgrid unit scheduling, and whereby the power exchange between microgrid and utility network can be controlled which causes a smooth transition to a virtual islanded operating condition. Finally, the overall study has clearly demonstrated the effectiveness and the performance of a robust day-ahead unit commitment model which tackles the four issues listed in § 4.5, and has been published in [49]. Including a forecasting error on the production of renewable energy can be an

area for further research.

5

Voltage control in microgrids

5.1 Introduction

As introduced in Chapter 2, the multilayer control concept, which is
presented in Fig. 2.6, is decoupled into three sub-problems, including
a UC problem (scheduling layer), a load flow calculation (executive
layer) and a security check with feedback control (adjustment layer).
The model can be considered as an offline optimisation approach
which can provide an input for a real-time microgrid application.
Note that the real-time application is not considered in this work.

In Chapter 4, the scheduling layer, including unit commitment and
demand response was developed and presented. Based on the day-
ahead energy market, the demand bids, and the availability of re-
newable energy sources, the microgrid units are scheduled in order to
achieve optimisation objectives subject to the device and operating
constraints. A 24-hour microgrid simulation has been performed di-
vided in 96 time steps (each with 15 min averaged values). Although
the voltage constraints were not considered, they must be carefully
controlled in order to operate a power system within acceptable volt-
age limits. Chapter 5 emerges as an extension to Chapter 4, with a
deeper focus on the voltage level at every bus in the microgrid.

In order to determine the future operational states of the microgrid
units whereby the bus voltages are maintained within acceptable lim-

its, an offline load flow calculation should be performed to obtain the values of the voltage magnitudes of the different microgrid buses. Therefore, within the executive layer, an AC power flow calculation will be performed with the power reference set points calculated by the scheduling layer to obtain the values of the voltage magnitudes of the different buses in the microgrid network.

After the load flow calculation, the numerical values of the bus voltages are transmitted to the third layer. The adjustment layer, which is the scope of this chapter, is utilised to maintain the bus voltages and contains a security check with feedback control to the first layer. In this chapter, first, the power flow equations in conventional networks and microgrids are considered. Subsequently, an explanation is provided to why the linkage between active power and voltage becomes relevant for voltage control in microgrids. Furthermore, a voltage control approach which is embedded in the multilayer control structure and maintains the microgrid bus voltages within pre-specified limits will be demonstrated and evaluated.

5.2   Power flow analysis

Power flow analysis, often referred to load flow analysis, is the backbone of steady-state power systems analysis. Multiple power system applications ranging from scheduling to operation require the solution of power flow equations. The power flow problem can be considered as the calculation of complex bus voltages and line flows in an electrical network.

The simple system of Fig. 5.1, consisting of a power source, a line and a load is considered to derive the power flow equations. The voltage at the power source is considered as $\underline{V}_i = V_i$, the load voltage as $\underline{V}_l = V_l e^{j\delta}$, and the current flowing through the line as $\underline{I} = I e^{j\phi}$.
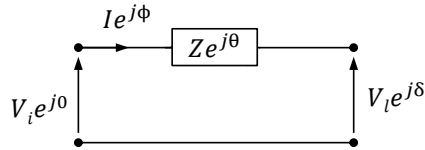
Figure 5.1: Power flow through a line

The line impedance is characterised with a resistance (R) and reactance (X). The shunt capacitance of the line is neglected since Fig. 5.1 represents an equivalent of a short line. The angles θ, ϕ and δ are

the phase angles of the impedance, the current and and load voltage with the inverter voltage as reference. This is graphically represented in the phasor digram below:
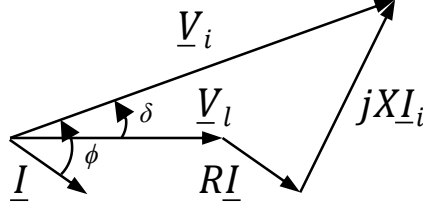
Figure 5.2: Phasor diagram

The power injected by the inverter into the line is described as follows:

$$
\begin{aligned}
\underline{S} = P + jQ &= \underline{V}\underline{I}^* \\
&= \underline{V}_i \left(\frac{\underline{V}_i - \underline{V}_l}{\underline{Z}} \right)^* \\
&= \frac{V_i^2}{Z} e^{j\theta} - \frac{V_i V_l}{Z} e^{j(\theta - \delta)}
\end{aligned} \tag{5.1}
$$

Using Euler's formula, the total apparent power can rewritten in:

$$
\begin{aligned}
S &= \frac{V_i^2}{Z} \cdot (\cos\theta + j \cdot sin\theta) - \frac{V_i \cdot V_l}{Z} \cdot [\cos(\theta - \delta) - j \cdot \sin(\theta - \delta)] \\
&= \frac{V_i^2}{Z} \cdot \cos\theta - \frac{V_i \cdot V_l}{Z} \cdot \cos(\theta - \delta) \\
&\quad + j \cdot \left[\frac{V_i^2}{Z} \cdot \sin\theta - \frac{V_i \cdot V_l}{Z} \cdot \sin(\theta - \delta) \right]
\end{aligned} \tag{5.2}
$$

Collecting the real and imaginary parts, the active and reactive power are given by:

$$
\begin{aligned}
P &= \frac{V_i^2}{Z} \cdot (\cos\theta) - \frac{V_i \cdot V_l}{Z} \cdot \cos(\theta - \delta) \\
&= \frac{R}{Z^2} \cdot (V_i^2 - V_i \cdot V_l \cdot \cos\delta) - \frac{X}{Z^2} \cdot V_i \cdot V_l \cdot \sin\delta
\end{aligned} \tag{5.3}
$$

$$Q = \frac{V_i^2}{Z} \cdot (\sin\theta) - \frac{V_i \cdot V_l}{Z} \cdot \sin(\theta - \delta)$$
$$= \frac{X}{Z^2} \cdot (V_i^2 - V_i \cdot V_l \cdot \cos\delta) + \frac{R}{Z^2} \cdot V_i \cdot V_l \cdot \sin\delta \tag{5.4}$$

where the Simpson goniometric rules are used to expand $\cos(\theta - \delta)$ and $\sin(\theta - \delta)$:

$$\cos(\theta + \delta) = \cos\theta \cdot \cos\delta - \sin\theta \cdot \sin\delta \tag{5.5}$$

$$\sin(\theta + \delta) = \cos\theta \cdot \cos\delta + \sin\theta \cdot \sin\delta \tag{5.6}$$

and $\underline{Z} = Ze^{j\theta} = R + j \cdot X$, thus $Z = \sqrt{R^2 + X^2}$, and where $\cos\theta = \frac{R}{Z}$ and $\sin\theta = \frac{X}{Z}$ is applied.

A general assumption is that the phase angle variations are limited in the network, hence, $\cos\delta \approx 1$ and $\sin\delta \approx \delta$ [47]. Therefore, the equations (5.3) and (5.4) can be rewritten as:

$$P \cong \frac{R}{Z^2} \cdot (V_i^2 - V_i \cdot V_l) - \frac{X}{Z^2} \cdot V_i \cdot V_l \cdot \delta \tag{5.7}$$

$$Q \cong \frac{X}{Z^2} \cdot (V_i^2 - V_i \cdot V_l) + \frac{R}{Z^2} \cdot V_i \cdot V_l \cdot \delta \tag{5.8}$$

In the next paragraph, the power flow equations are examined for inductive and resistive networks.

5.3 Decoupled active and reactive power control

Microgrids are receiving a growing interest as they can provide a coordinated approach for the integration of DER units [100]. When developing a unit commitment strategy while considering the voltages at every bus within the microgrid, the differences in network characteristics, as compared to conventional networks, need to be considered carefully.

5.3.1 Conventional networks

The concept of voltage and frequency control was obtained from the active and reactive power equations. In conventional networks, e.g., high-voltage transmission lines, the network reactance is much higher than the network resistance $(X > R)$, and therefore, the resistance R can be neglected $(R = 0)$. Taking into account this simplification, equations (5.7) and (5.8) can be rewritten in:

$$
\begin{aligned}
P &\cong -\frac{X}{Z^2} \cdot V_i \cdot V_l \cdot \sin \delta \\
&\cong \frac{V_i \cdot V_l}{X} \cdot \sin \delta
\end{aligned}
\tag{5.9}
$$

$$
\begin{aligned}
Q &\cong \frac{X}{Z^2} \cdot V_i \cdot (V_i - V_l) \\
&\cong \frac{V_i(V_i - V_l)}{X}
\end{aligned}
\tag{5.10}
$$

For inductive networks $(X > R)$, a decoupling of P and Q is achieved, where P is predominantly dependent on the phase difference over the line, while Q is determined mainly by the voltage difference over the line. This leads to the well-known P/f and Q/V linkage in transmission networks [47, 101–103]. This dependency is the opposite of that in resistive networks and will be explained in the next paragraph.

5.3.2 Microgrids

Microgrids have different characteristics in comparison with traditional networks and are often based on mainly resistive low-voltage distribution network lines. Typical R/X values vary between 2 and 8 [104]. The highly resistive character $(R > X)$, reduces equation (5.7) and (5.8) to:

$$
\begin{aligned}
P &\cong \frac{R}{Z^2} \cdot V_i \cdot (V_i - V_l) \\
&\cong \frac{V_i}{R} \cdot (V_i - V_l)
\end{aligned}
\tag{5.11}
$$

$$
\begin{aligned}
Q &\cong \frac{R}{Z^2} \cdot V_i \cdot V_l \cdot \sin \delta \\
&\cong \frac{V_i \cdot V_l}{R} \cdot \sin \delta
\end{aligned}
\tag{5.12}
$$

As a result, a decoupling of P and Q is achieved in microgrids with resistive characteristics. Q is predominantly dependent on the phase difference over the line (which is dynamically dependent on the frequency), while P is determined mainly by the voltage difference over the line. In the transition from the conventional power grid to a smart microgrid, the conventional control principles of frequency and voltage should be reconsidered for the use in low-voltage microgrids. For resistive power lines ($X \ll R$), the voltage can be controlled with active power [47, 103]. Therefore, P/V control strategies are increasingly being considered in low-voltage microgrids because of the natural linkage between P and V [32, 105].

5.4 Voltage control strategy

The variability in loads and in renewable energy resource outputs necessitates the development and implementation of voltage control strategies in microgrids [106]. Since the voltage at the different nodes in the low-voltage network is less affected by the reactive power, the voltage control method presented in this chapter is done by influencing the active power set points.

The scheduling layer, which is explained in Chapter 4, calculates the power set points at different DER units and is based on the day-ahead energy market, the demand bids, and the renewable energy production forecast. In order to determine the future operational states of the microgrid units, whereby the bus voltages are maintained within acceptable limits, an offline load flow calculation should be performed in order to obtain the values of the voltage magnitudes of the different microgrid buses. Therefore, within the executive layer (presented in Fig. 2.6), an AC power flow calculation will be performed with the power reference set points calculated by the scheduling layer in order to obtain the values of the voltage magnitudes of the different buses in the microgrid network. This executive layer performs an AC power flow calculation for the complete time horizon (96 time steps). After the load flow calculation, the numerical values of the bus voltages are transmitted to the third layer. The adjustment layer is utilised to control the bus voltages and contains a security check with feedback control to the first layer. The purpose of this third layer, is to keep the voltage within a pre-specified tolerance band by producing more or less power provided by the microgrid generation units.

In case of a severe voltage deviation at any bus within the microgrid, a dynamic gain will be introduced. Depending on the deviation (pos-

itive or negative), and on the location of the power generation units and their respective distance from the voltage problem, an appropriate gain will be provided to adjust the boundaries (see equation (4.10) in Chapter 4) of the microgrid generation units. In this way, the range (between the lower and upper bound) in which the set point can be committed will be modified. Subsequently, when closing the loop, the renewed boundaries are then fed back to the scheduling layer, which recalculates the UC solution. The updated power generation schedule will again go through the second and third layer of the control hierarchy. This iterative process will continue until all voltage violations are eliminated and a converged optimal solution is found.

Due to the introduction of this third layer, active power reference set points can be provided (for real-time scheduling) not only according to the economical and the environmental objectives, but also taking into account the voltage level at every bus in the microgrid.

As introduced in § 2.3, the control approach developed in this work fits directly in the tertiary level (of the microgrid hierarchical control structure) which is conceived to introduce intelligence in the whole system. The power reference set points provided by the multilayer control approach can be used as an input for the upper secondary or primary controller (for real-time dispatch) which operate on a shorter time frame and which are responsible for local control and are dealing errors in frequency and voltage magnitudes.

In the next section, the voltage control method will be presented in more detail and will be verified with an example.

5.4.1   Embedded voltage control approach

In this subsection, the dynamic voltage control approach, which is embedded in the adjustment layer, will be explained. The process of the control strategy by using a dynamic gain which influences the boundaries of the microgrid generation units can be presented with the flowchart depicted in Fig. 5.3. As a first step, the numerical values of the bus voltages transmitted by the executive layer will be evaluated. If one of the bus voltages exceeds the permissible limits, the voltage control approach will be activated in order to adjust the boundaries of the microgrid generation units. Depending on the deviation (under- or overvoltage), a 'factor' and a 'network' matrix will be introduced in order to generate the dynamic gain that modifies the boundaries of the microgrid generation units. The definition and

construction of both matrices will be explained in the next section. In case of an undervoltage, the lower boundaries of the microgrid power generating units will be increased by the dynamic gain in order to increase the reference set points and to reduce the voltage deviation. In case of an overvoltage, the upper limit will be decreased and as a result the reference set points will be reduced. The output power of RES can only be adjusted by curtailment (by adjusting their upper boundaries).

With this third layer and feedback loop, active power reference set points can be provided (for real-time scheduling) according to the economical and the environmental objectives, taking into account the microgrid bus voltages. In the following subsection, the voltage control method will be explained in more details.

5.4.2 Mathematical model

Distribution networks are typically constructed in a loopy or meshed configuration. However, for practical engineering concerns, the majority of distribution grids are constructed as radial networks. These networks consist of a topology which is structured like a tree and rooted at the secondary of a substation transformer which may have a tap-changer based low-voltage regulator. This radial topology distinguishes distribution networks from transmission networks which have multiple loops energised all the time to guarantee continuous delivery of power to every bus. The microgrid considered in this work has a radial network topology. The structure of a radial distribution network has important features which motivates the development of our control strategy.

The dynamic gain, which influences the boundaries and, as a result, the reference set points of the power generation units, will be explained by introducing a network matrix ($\mathcal{N}$) and a factor matrix ($\mathcal{F}$). The network matrix contains the structure of the microgrid network. The factor matrix indicates on which bus a voltage deviation occurs. Both matrices are discussed below.

5.4.2.1 Network matrix

The network matrix is represented as an N_{unit}-by-N_{bus} matrix and contains the contribution of the microgrid units (connected to the appropriate bus) to mitigate the voltage deviation at a certain bus. N_{unit} can be considered as the number of units within the microgrid,
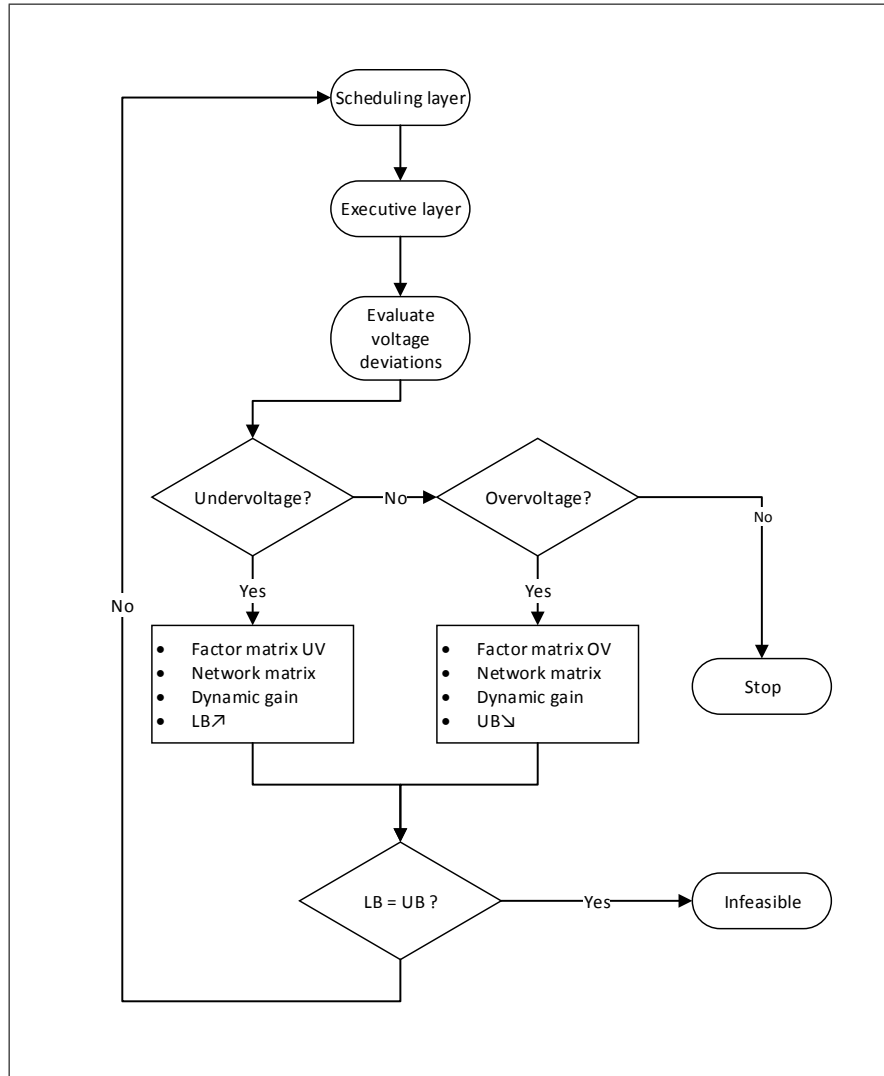
Figure 5.3: Flowchart of security check with feedback voltage control approach

such as loads, controllable loads and DER units including dispatchable sources, RES and distributed storage devices.

$$\mathcal{N}_{N_{\mathrm{unit}},N_{\mathrm{bus}}} = \begin{bmatrix} \mathcal{C}_{\mathrm{unit}_1\,\mathrm{to\,bus}_1} & \cdots & \mathcal{C}_{\mathrm{unit}_1\,\mathrm{to\,bus}_{N_{\mathrm{bus}}}} \\ \mathcal{C}_{\mathrm{unit}_2\,\mathrm{to\,bus}_1} & \cdots & \mathcal{C}_{\mathrm{unit}_2\,\mathrm{to\,bus}_{N_{\mathrm{bus}}}} \\ \vdots & \vdots & \vdots \\ \mathcal{C}_{\mathrm{unit}_{N_{\mathrm{unit}}}\,\mathrm{to\,bus}_1} & \cdots & \mathcal{C}_{\mathrm{unit}_{N_{\mathrm{unit}}}\,\mathrm{to\,bus}_{N_{\mathrm{bus}}}} \end{bmatrix} \tag{5.13}$$

where $\mathcal{C}_{\mathrm{unit}_k\,\mathrm{to\,bus}_m}$ represents the contribution of unit k to the voltage deviation at bus m. This contribution is represented by a positive value which depends on the distance $(\mathcal{D}_{k\,\mathrm{to}\,m})$ of the microgrid unit to the location of the bus with the voltage deviation, and is dimensionless:

$$\mathcal{C}_{\mathrm{unit}_k\,\mathrm{to\,bus}_m} = 1 + \frac{1}{\mathcal{D}} \tag{5.14}$$

where $\mathcal{D}$ is a dimensionless quantity:

$$\mathcal{D} = \frac{\mathrm{L}_{k\,\mathrm{to}\,m}}{\mathrm{L}_{\mathrm{max}}} \tag{5.15}$$

with,

$$\mathrm{L}_{\mathrm{max}} = \max_{k,m}(\mathrm{L}_{k\,\mathrm{to}\,m}) \tag{5.16}$$

$\mathrm{L}_{k\,\mathrm{to}\,m}$ is the line length, which reflects the line impedance from unit k to bus m. The closer the unit is located to the voltage deviation, the greater its contribution to the voltage deviation. In case of a voltage deviation at the location of the microgrid unit, the contribution of the unit itself will be set to '1'. This is because the voltage deviation caused in such a case, is due to, and can be reduced by the unit itself. At the same time the contribution of the other units will be set to '0'.

Note that the network matrix $(\mathcal{N})$ is built up by including every unit within the microgrid (as well the non-controllable loads which are not participating in the UC). Therefore, within $\mathcal{N}$, the number of microgrid units (N_{unit} with index k) is used and not N_{gen}, which includes only the microgrid units who are participating the UC.

Since in this work, only controllable loads and DER units (including dispatchable sources, RES and distributed storage devices) are assumed to contribute to voltage deviations, the contribution of the non-controllable loads was set to '0' within $\mathcal{N}$.

5.4.2.2 Factor matrix

Secondly, two factor matrices are introduced which indicate on which bus a voltage deviation occurs. Both of them, a factor matrix for undervoltages ($\mathcal{F}_{\mathrm{UV}}$) and a factor matrix for overvoltages ($\mathcal{F}_{\mathrm{OV}}$) will be used. They can be presented as an N_{bus}-by-N matrix (N time steps).

$$\mathcal{F}_{\mathrm{UV}} = \begin{bmatrix} \mathcal{F}_{\mathrm{UV}_{1,1}} & \cdots & \mathcal{F}_{\mathrm{UV}_{1,\mathrm{N}}} \\ \mathcal{F}_{\mathrm{UV}_{2,1}} & \cdots & \mathcal{F}_{\mathrm{UV}_{2,\mathrm{N}}} \\ \vdots & \vdots & \vdots \\ \mathcal{F}_{\mathrm{UV}_{N_{\mathrm{bus}},1}} & \cdots & \mathcal{F}_{\mathrm{UV}_{N_{\mathrm{bus}},\mathrm{N}}} \end{bmatrix} \tag{5.17}$$

$$\mathcal{F}_{\mathrm{OV}} = \begin{bmatrix} \mathcal{F}_{\mathrm{OV}_{1,1}} & \cdots & \mathcal{F}_{\mathrm{OV}_{1,\mathrm{N}}} \\ \mathcal{F}_{\mathrm{OV}_{2,1}} & \cdots & \mathcal{F}_{\mathrm{OV}_{2,\mathrm{N}}} \\ \vdots & \vdots & \vdots \\ \mathcal{F}_{\mathrm{OV}_{N_{\mathrm{bus}},1}} & \cdots & \mathcal{F}_{\mathrm{OV}_{N_{\mathrm{bus}},\mathrm{N}}} \end{bmatrix} \tag{5.18}$$

The input input entries $\mathcal{F}_{\mathrm{UV}_{m,i}}$ and $\mathcal{F}_{\mathrm{OV}_{m,i}}$ are:

$$\mathcal{F}_{\mathrm{UV}_{m,i}} = f_{\mathrm{UV}} \cdot \Delta v_{\mathrm{m}}(\%) \tag{5.19}$$

$$\mathcal{F}_{\mathrm{OV}_{m,i}} = f_{\mathrm{OV}} \cdot \Delta v_{\mathrm{m}}(\%) \tag{5.20}$$

where the factors f_{UV} and f_{OV} are represented as dimensionless binaries which indicate an under- or overvoltage. In case of an undervoltage deviation ($V_{\mathrm{bus}} < V_{\mathrm{min}}$), factor f_{UV} will be set to '1' and f_{OV} will be set to '0'. In case of an overvoltage ($V_{\mathrm{bus}} > V_{\mathrm{max}}$), f_{UV} will be set to '0' and f_{UV} will be set to '1'. In case no voltage deviation occurs, both values are set to '0' as presented in the table below.

	f_{UV}	f_{OV}
undervoltage	1	0
overvoltage	0	1
no voltage deviation	0	0

Table 5.1: Voltage deviation factors

Subsequently, as presented in (5.19) and (5.20), the factor values are multiplied by the relative deviation with respect to V_{N} of the corresponding bus ($\Delta v_{\mathrm{m}}(\%) = \frac{V_{bus}-V_{nom}}{V_{nom}} * 100$). This will make the dynamic gain dependent on the voltage deviation of the corresponding bus. Note that the complete day-ahead time horizon, on which the UC strategy in this work operates, includes 96 time steps, each with 15-min averaged values. Hence, V_{nom} is considered as an averaged value of 230V.

5.4.2.3 Dynamic gain

In order to build up the dynamic gain which enables the microgrid units to contribute proportionally to the voltage deviation and with the distance to the location (of the voltage deviation), the network matrix ($\mathcal{N}$) and the factor matrix ($\mathcal{F}$) are multiplied. As a result, the dynamic gain for the lower and upper boundaries are constructed as N_{bus}-by-N matrices and are given by:

$$\mathcal{N} \cdot \mathcal{F}_{\mathrm{UV}} = \begin{bmatrix} A_{\mathrm{lb}_{1,1}} & \cdots & A_{\mathrm{lb}_{1,\mathrm{N}}} \\ A_{\mathrm{lb}_{2,1}} & \cdots & A_{\mathrm{lb}_{2,\mathrm{N}}} \\ \vdots & \vdots & \vdots \\ A_{\mathrm{lb}_{\mathrm{N}_{\mathrm{bus}},1}} & \cdots & A_{\mathrm{lb}_{\mathrm{N}_{\mathrm{bus}},\mathrm{N}}} \end{bmatrix} \tag{5.21}$$

$$\mathcal{N} \cdot \mathcal{F}_{\mathrm{OV}} = \begin{bmatrix} A_{\mathrm{ub}_{1,1}} & \cdots & A_{\mathrm{ub}_{1,\mathrm{N}}} \\ A_{\mathrm{ub}_{2,1}} & \cdots & A_{\mathrm{ub}_{2,\mathrm{N}}} \\ \vdots & \vdots & \vdots \\ A_{\mathrm{ub}_{\mathrm{N}_{\mathrm{bus}},1}} & \cdots & A_{\mathrm{ub}_{\mathrm{N}_{\mathrm{bus}},\mathrm{N}}} \end{bmatrix} \tag{5.22}$$

where, $A_{\mathrm{lb}_{k,i}}$ and $A_{\mathrm{ub}_{k,i}}$ represent the gain of the lower and upper boundaries of the kth microgrid unit on the ith time step. Note that a dynamic gain is provided for every unit within the microgrid since this is a result of the multiplication with the network matrix ($\mathcal{N}$). However, non-controllable loads are not participating in the UC strategy, and therefore, they cannot be controlled by a certain gain. This was included by providing a contribution value of '0' to the units which are not participating in the UC strategy as explained in 5.4.2.1. As a result, the dynamic gain of these units will be zero.

Depending on the deviation (positive or negative), and on the location of the power generation units and their respective distance from the voltage problem, an appropriate gain will be provided to

adjust the boundaries of the microgrid units which are participating in the voltage control strategy. When an undervoltage occurs, the lower bound of the microgrid units should be increased. In case of an overvoltage, the upper bounds of the microgrid units should be decreased. The relationship between the dynamic gain and the boundaries is presented in the equations below:

$$P_{G_{\min_{k,i}}} = P_{G_{\min_{k,i}}} - P_{\text{range}} \cdot A_{\text{lb}_{k,i}} \tag{5.23}$$

$$P_{G_{\max_{k,i}}} = P_{G_{\max_{k,i}}} - P_{\text{range}} \cdot A_{\text{ub}_{k,i}} \tag{5.24}$$

where P_{range} represents the range between the lower and upper bound. Note that the dynamic gain is proportional to the range, and besides, depends on the type of microgrid unit. By using (5.23) and (5.24), the range (between the lower and upper bound) in which the set point can be committed will be modified. In case of an undervoltage, A_{lb} is negative which results in an increase of $P_{G_{\min}}$. In case of an over voltage A_{ub} is positive and results in a decrease of $P_{G_{\max}}$.

5.4.3 Example

By means of an example, the operation of this voltage control approach will be presented in this section. The microgrid presented in Fig. 5.4, operates in islanded mode and consists of 4 buses, including 2 non-controllable loads and 2 micro turbines. In this example, the length between each bus (L) is assumed to be equal. The islanded operation example is chosen arbitrarily, although the principle of the voltage control approach is similar to the grid-connected operation where the utility grid participates in the multilayer control concept.
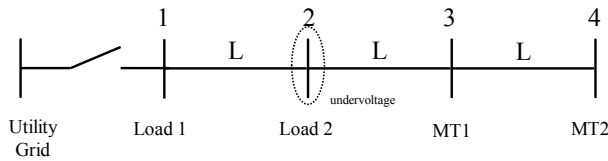
Figure 5.4: Example Voltage Control Application

Assume that an undervoltage occurs at bus 2 on which load 2 is connected. In case of an undervoltage, the lower bounds of both

micro turbines should be increased by the dynamic gain. According to the description of the network and factor matrix, the dynamic gain of the lower and upper bounds is built up and presented in 5.25 and 5.26.

$$
\overbrace{\begin{bmatrix} A_{\text{lb1}} \\ A_{\text{lb2}} \\ A_{\text{lb3}} \\ A_{\text{lb4}} \end{bmatrix}}^{\text{dynamic gain}} = \overbrace{\begin{bmatrix} 0 & 0 & 0 & 0 \\ 0 & 0 & 0 & 0 \\ 1 + \frac{1}{\mathcal{D}_{3\,\text{to}\,1}} & 1 + \frac{1}{\mathcal{D}_{3\,\text{to}\,2}} & 1 & 0 \\ 1 + \frac{1}{\mathcal{D}_{4\,\text{to}\,1}} & 1 + \frac{1}{\mathcal{D}_{4\,\text{to}\,2}} & 0 & 1 \end{bmatrix}}^{\mathcal{N}} \cdot \overbrace{\begin{bmatrix} 0\,.\,\Delta v_1 \\ 1\,.\,\Delta v_2 \\ 0\,.\,\Delta v_3 \\ 0\,.\,\Delta v_4 \end{bmatrix}}^{\mathcal{F}_{\text{UV}}}
$$
$$
= \begin{bmatrix} 0 \\ 0 \\ (1 + \frac{1}{\mathcal{D}_{3\,\text{to}\,2}})\,.\,\Delta v_3 \\ (1 + \frac{1}{\mathcal{D}_{4\,\text{to}\,2}})\,.\,\Delta v_4 \end{bmatrix} \tag{5.25}
$$

$$
\overbrace{\begin{bmatrix} A_{\text{ub1}} \\ A_{\text{ub2}} \\ A_{\text{ub3}} \\ A_{\text{ub4}} \end{bmatrix}}^{\text{dynamic gain}} = \overbrace{\begin{bmatrix} 0 & 0 & 0 & 0 \\ 0 & 0 & 0 & 0 \\ 1 + \frac{1}{\mathcal{D}_{3\,\text{to}\,1}} & 1 + \frac{1}{\mathcal{D}_{3\,\text{to}\,2}} & 1 & 0 \\ 1 + \frac{1}{\mathcal{D}_{4\,\text{to}\,1}} & 1 + \frac{1}{\mathcal{D}_{4\,\text{to}\,2}} & 0 & 1 \end{bmatrix}}^{\mathcal{N}} \cdot \overbrace{\begin{bmatrix} 0\,.\,\Delta v_1 \\ 0\,.\,\Delta v_2 \\ 0\,.\,\Delta v_3 \\ 0\,.\,\Delta v_4 \end{bmatrix}}^{\mathcal{F}_{\text{OV}}}
$$
$$
= \begin{bmatrix} 0 \\ 0 \\ 0 \\ 0 \end{bmatrix} \tag{5.26}
$$

As explained before, the network matrix ($\mathcal{N}$) is constructed as an N_{unit}-by-N_{bus} matrix and contains the contribution of the microgrid units (connected to the appropriate bus). As a result, $\mathcal{N}$ is built up as a 4-by-4 matrix. $\mathcal{C}_{\text{unit}_k\,\text{to}\,\text{bus}_m}$ represents the contribution of unit k to the voltage deviation at bus m. In this example, both loads are non-controllable, and therefore, they do not participate in the UC strategy. As a result, they do not contribute to the mitigation of voltage deviations in the network and therefore, their contribution, which is entered on row 1 and row 2 of $\mathcal{N}$, is set to '0'. On row 3 and 4 of the network matrix, the contribution of each micro turbine to the corresponding bus is provided. As introduced in (5.14), this contribution is represented by a positive value which depends on the distance ($\mathcal{D}_{k\,\text{to}\,m}$) of the microgrid unit to the location of the bus with the voltage deviation, and is dimensionless. The contribution of a unit to the voltage deviation at its own location, is set to '1'. This can be verified on location $(3,3)$ and $(4,4)$ within the network matrix. This is because the voltage deviation caused in such a case, is due to, and can be reduced by the unit itself. At the same time

the contribution of the other units is set to '0'. This can be verified on location $(3, 4)$ and $(4, 3)$ within the network matrix.

The factor matrices ($\mathcal{F}_{\mathrm{UV}}$ and $\mathcal{F}_{\mathrm{OV}}$) are constructed as an N_{bus}-by-N matrix and indicate on which bus the voltage deviation occurs. In this example, only 1 time step is considered and therefore both factor matrices are built up as an N_{bus}-by-1 column vector. As explained in (5.19) and (5.20), the input entries of both matrices are factors (f_{UV} and f_{OV}) which are multiplied by the voltage deviation of the corresponding bus ($\Delta v_{\mathrm{m}}(\%)$). The percentage voltage deviations of the different buses are presented as Δv_1 to Δv_4. In this example, an undervoltage occurs at bus 2, and as a result, the factor f_{UV} on position $(2, 1)$ within $\mathcal{F}_{\mathrm{UV}}$ is set to '1'. In $\mathcal{F}_{\mathrm{OV}}$, every value of f_{OV} was set to '0' since there is no overvoltage in this example. Note that, although both matrices are built up, only $\mathcal{F}_{\mathrm{UV}}$ is relevant for this case.

It is clear that the contribution of micro turbine 1 in order to mitigate to the voltage deviation at bus 2 to, the voltage deviation at bus 2 is greater that the contribution delivered by micro turbine 2. This can be explained by the fact that the distance ($\mathcal{D}_{3\,\mathrm{to}\,2}$) is shorter as compared to ($\mathcal{D}_{4\,\mathrm{to}\,2}$). The closer the unit is located to the voltage deviation, the greater its contribution to the voltage deviation.

Subsequently, the renewed boundaries are fed back to the first layer, which performs a new optimisation and redistributes the reference set points of the thermal generation units. This process continues until the microgrid bus voltages are within acceptable limits. In case when the upper bounds equal the lower bounds, and the voltage deviation is still not maintained between the limits, there is no feasible solution possible for the algorithm. This is also illustrated in the flowchart in Fig. 5.3. Hence, a message dialog box was created, which displays a warning message "Could not find a feasible solution". This event can happen when the system is overloaded. Solutions to circumvent this problem (such as active load curtailment) can be a direction for future research. Note that in order to apply this voltage control approach, we assume that the initial topology of the network is known.

5.5 Demonstration and validation

The ability of a power system to maintain acceptable voltages at all buses in the network can be considered as a critical performance factor [107, 108]. The EN50160 is a European standard that defines voltage characteristics of the electricity supplied by public distribu-

tion systems. According to this standard, the DSO is considered to keep the voltage between -10% (207.0 V) and +10% (253.0 V) of the nominal distribution voltage (V_N = 230 V) [109]. In pure voltage optimisation, the aim is to maintain the system voltage magnitudes as close as possible to a nominal voltage. The proposed new multilayer control concept, developed in this work, provides an economically and environmentally viable UC that is feasible in terms of voltage violations. Due to the introduction of this third layer (in which the voltage control is embedded), active power reference set points can be provided (for real-time scheduling) not only according to the economical and the environmental objectives, but also taking to account the voltage level at every bus in the microgrid. The voltage control approach aims to maintain acceptable bus voltages by providing a dynamic gain to the corresponding power generation units in order to adjust their boundaries, and as a result, the range in which they can be committed. In fact, the strategy will from the economical and environmental optimal set points given by the first layer in order to maintain the voltage at every bus. This can be strengthened by the fact that security of supply has an overriding priority. On the other hand, a too small tolerance band can increase the deviation from the economical and environmental optimal set points.

In this section, a demonstration is given in order to validate the performance and effectiveness of the proposed hierarchical multilayer control structure. As introduced before, the voltage control approach is embedded in the multilayer control structure and maintains the microgrid bus voltages within pre-specified limits. Additional to the issues tackled by the scheduling layer (§ 4.5), presented in Chapter 4, this demonstration provides an:

1. Executive layer: an AC power flow calculation is performed with the power reference set points as calculated by the scheduling layer in order to obtain the values of the voltage magnitudes of the different buses in the microgrid network. Subsequently, the numerical values of the bus voltages are transmitted to the adjustment layer.

2. Adjustment layer including the provision of a dynamic gain: in case of a voltage deviation, an appropriate gain will be provided to the microgrid units (depending on their location in the microgrid and their respective distance from the voltage problem) to adjust their boundaries, and as a result, the range in which they can be committed.

3. Feedback control to the executive layer: the renewed boundaries are fed back to the scheduling layer, which recalculates the UC solution. The updated power generation schedule will again go through the second and third layer of the control hierarchy. This iterative process will continue until all voltage violations are eliminated and a converged optimal solution is found.

5.5.1 Microgrid test model

The proposed hierarchical multilayer control structure is tested on the same microgrid test network as used in chapter 4, in order to verify the effectiveness and to validate the performance. The microgrid model used for the simulations is depicted in Fig. 5.6 and includes 11 low voltage (LV) buses connected downstream from a distribution transformer. Furthermore, the studied system includes renewable energy resources, a storage unit, two micro turbines, a fuel cell and a controllable load including 4 electric vehicles. Serving the microgrid load (Load 1 + Load 2 + Load 3 + Controllable Load), active power can be produced either by the thermal generation units, the utility grid, the storage device, or the renewable energy resources. The profile of the different microgrid loads, and the renewable energy production over the complete time horizon are depicted in Fig. 5.5.
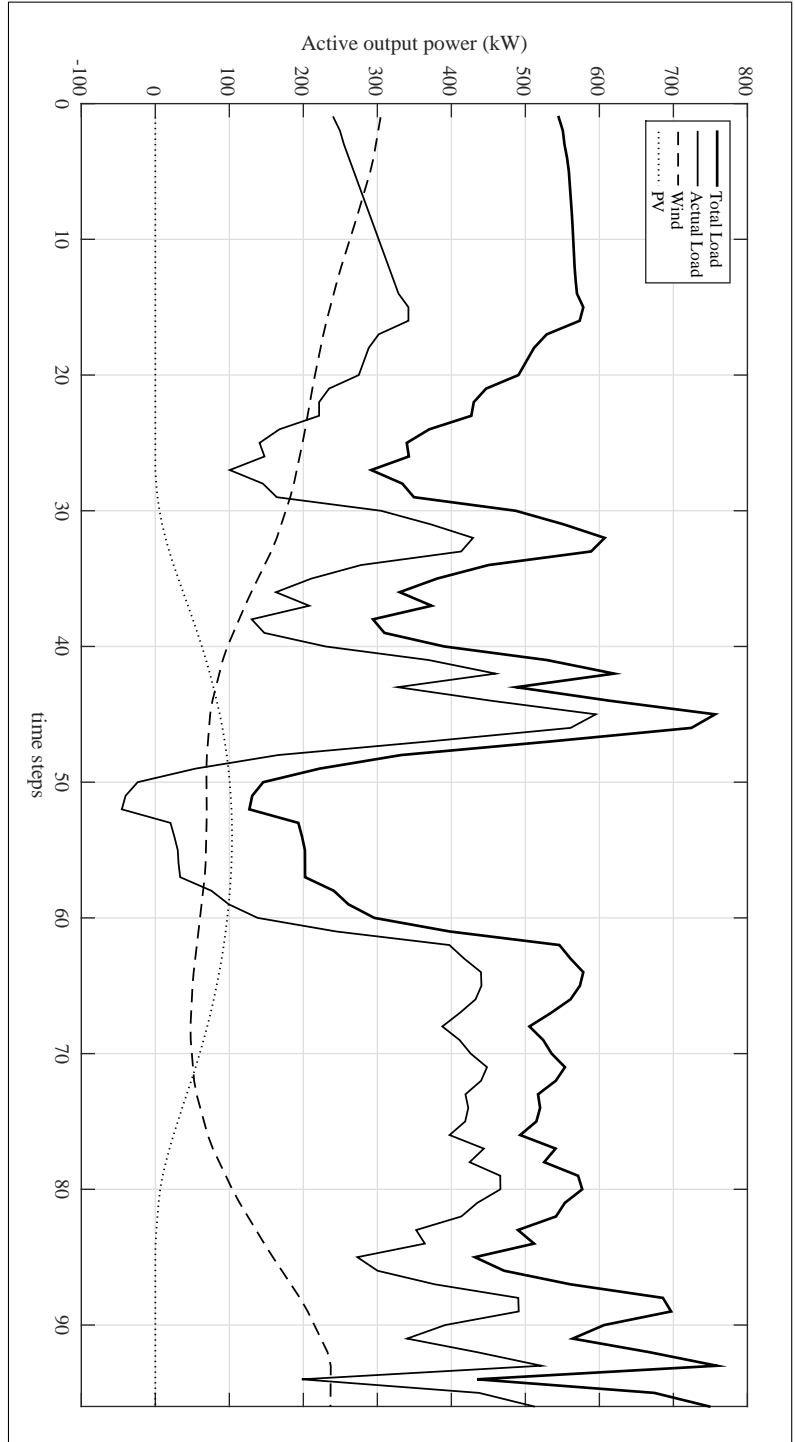
Figure 5.5: Microgrid load profile and RES production

The cost and emission coefficients of the thermal generation units are listed in Table 5.2. A CO_2 emission intensity of $381 \cdot 10^{-3}$kg/kWh [99] is considered for the power supply of the utility grid. The cost coefficient of the utility grid is related to a variable pricing scheme which is presented in Fig. 4.4. The capacities of the microgrid generation units are listed in Table 5.3. For the storage unit, E_{min} was set to 0 kWh, E_{max} was set to 40 kWh, and $E_{EV_{max}}$ of each EV was set to 80 kWh. The charging rate of each EV is limited between -19.2kW and -7.2kW, which results in a total (4 EVs) minimum and maximum charging rate of -28.8kW and -76.8kW respectively. The length (L) between the buses are assumed to be 50m with an R/X value of 5. These values are chosen arbitrarily in order to present the operation of the model. In Chapter 6, a case study will be provided with different line parameters.

| $C_{\mathbf{G}}(P_{\mathbf{G}})$	a	b	c
Micro Turbine 1	$100 \cdot 10^{-5.5}$	$50 \cdot 10^{-5.5}$	$20 \cdot 10^{-5.5}$
Micro Turbine 2	$140 \cdot 10^{-5.5}$	$40 \cdot 10^{-5.5}$	$100 \cdot 10^{-5.5}$
Fuel Cell	$20 \cdot 10^{-5.5}$	$20 \cdot 10^{-5.5}$	$10 \cdot 10^{-5.5}$
$\varepsilon_{\mathbf{G}}(P_{\mathbf{G}})$	d	e	f
Micro Turbine 1	$4.09 \cdot 10^{-3}$	$-5.55 \cdot 10^{-3}$	$6.49 \cdot 10^{-3}$
Micro Turbine 2	$2.54 \cdot 10^{-3}$	$-6.05 \cdot 10^{-3}$	$5.64 \cdot 10^{-3}$
Fuel Cell	$5.33 \cdot 10^{-3}$	$-3.55 \cdot 10^{-3}$	$3.38 \cdot 10^{-3}$

Table 5.2: Fuel cost and emission coefficients

	MT 1	**MT 2**	**Fuel Cell**	**Storage**
$P_{\mathbf{G_{max}}}$ **(kW)**	160	240	260	± 50

Table 5.3: Microgrid generator capacities

5.5.2 Power system simulation

Power system simulation involves modelling power generation equipment and performing generator control. The microgrid presented in Fig. 5.6 is modelled as a 50-Hz AC system using Matlab Simscape
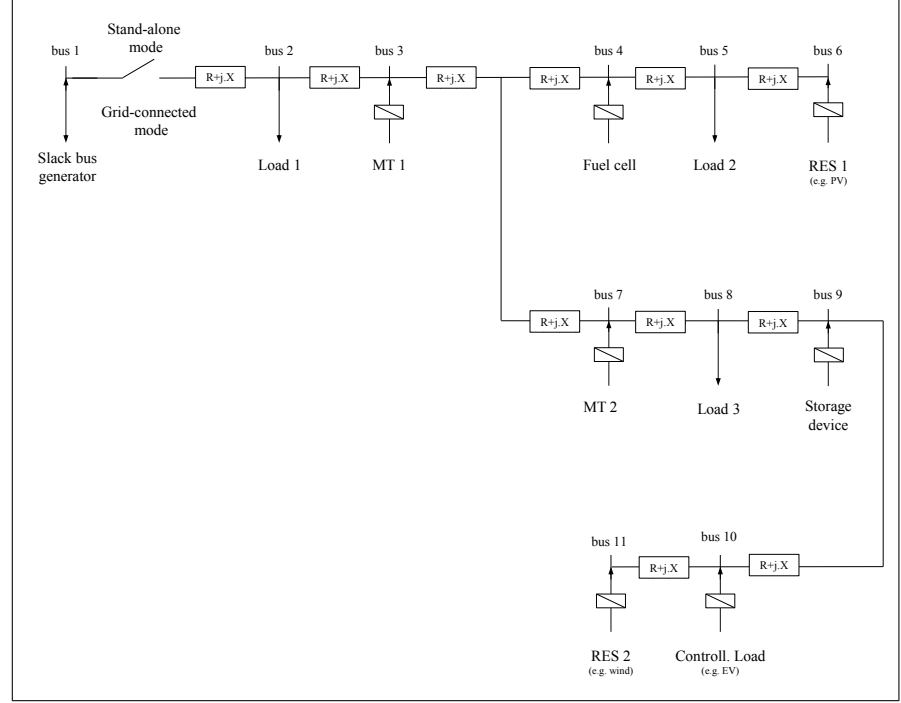
Figure 5.6: Microgrid test set up

Power Systems$^{\text{TM}}$ which provides component libraries and analysis tools for modelling and simulations of electrical power systems. The Matlab-based microgrid model is simulated by computing the states at successive time steps over a specified time span. The process of computing the states of a model in this manner is known as solving the model. Since the model uses only Simscape Power Systems component blocks, the appropriate moderately stiff solver type 'ode23tb', using the default variable-step, is chosen. The simulation start at 0.0s and ends at 0.06s. After 0.06s, the states computed by the solver are accurate and ready to use (numerical values of the bus voltages) within the adjustment layer. Note that this simulation time does not take the same time measured on a clock. The amount of time it takes to run a simulation depends on different factors including the complexity of the model, the step sizes, and the computer speed.

In the following case study, a day-ahead microgrid was simulated with and without voltage control approach. Additionally, events of voltage deviations within the complete time horizon will be discussed

and it will be explained how they are tackled by the voltage control approach.

5.5.3 Day-ahead unit commitment with voltage control

In this section, a demonstration is given where the voltage control approach is embedded in the multilayer control structure and maintains the microgrid bus voltages within pre-specified limits. In purely voltage optimisation, the aim is to maintain the system voltage magnitudes as close as possible to a nominal voltage. Working on the allowed limit of $\pm$ 10% does not guarantee the quality of the energy to be supplied to the users because disturbances will prevent meeting the standard for voltage. Therefore, in this work, the tolerance band of the voltage control approach is set to 5%.

5.5.3.1 Scheduling layer

Based on the day-ahead energy market, the demand bids, and the availability of renewable energy sources, the scheduling layer provides a 15 minute power generation schedule for the next 24 hours. Similar to § 4.5.5.1, in this simulation, the active power is scheduled among the different microgrid units while minimising the operating costs together with the produced CO_2 emissions. The reference set points are presented in Fig. 5.7. Since the focus of this chapter is on the adjustment layer including the voltage control strategy, these reference set points will be discussed briefly.

The total microgrid load (P_D^{total}) is presented by the thick black line. The actual load (P_D^a) (excluding the power produced by the renewable sources) is presented by the thin black line. Since renewable energy sources are participating in the voltage control strategy, e.g. by curtailment when an overvoltage occurs, P_D^a can be modified by the voltage control strategy (see 4.8).

The fuel cell has the greatest contribution in the unit commitment followed by micro turbine 1. This can be explained by the fact that the fuel cell has the lowest fuel cost and lowest emission rate.

The contribution of the utility grid is dependent on the variable market price (buying and selling) and the emissions, which are considered as constant (within this time horizon). During time steps 12-20, the actual demand increases, and at the same time (as presented on Fig. 4.4), the buying price is low. Therefore, it is more profitable to use the utility grid instead of using the microgrid units. Between time step 25-30, the buying price increases and the actual demand

decreases. Therefore, the utility grid is scheduled close to zero. Between time steps 30-35, 40-50 and 60-96, the microgrid total demand becomes excessively high, making it more favourable in terms of cost and emission optimisation to extract energy from the utility grid, rather than increasing the power set points of the microgrid thermal generation units. Between time steps 50-55, due to to overproduction of the RES (negative actual demand), the microgrid exports energy to the main grid and the utility grid is committed in a negative output power range.

The storage unit is committed to charge (by the fuel cell and micro turbines) during periods of low energy demand (e.g. time steps 25-30, 35-40 and 50-60). When the energy demand becomes low and even negative (time steps 50-55), the storage device is committed to charge at the maximum rate of -50kW. On the other hand, at high peak demand (time step 30-35 and 40-50), the storage unit will be discharged which reduces the usage of grid power, and as a result reduces the total cost and emission of the microgrid operation. The EVs were plugged in between 09:00 and 17:00 (time step 36-68). Between time step 50 and 57, the energy demand becomes very low (even negative) due to the high (over)production of the RES. During these time steps the EVs will be scheduled at their maximum charging rate ($4 * -19.2\text{kW} = -76.8\text{kW}$) and as a result, their state of charge (SOC_{EV}) has the steepest curve. At time step 68, the EVs are expected to be fully charged. This can be verified on the lower graph in Fig. 5.7, where the SOC_{EV} equals 320kWh ($4 \cdot 80\text{kWh}$) and remains constant.
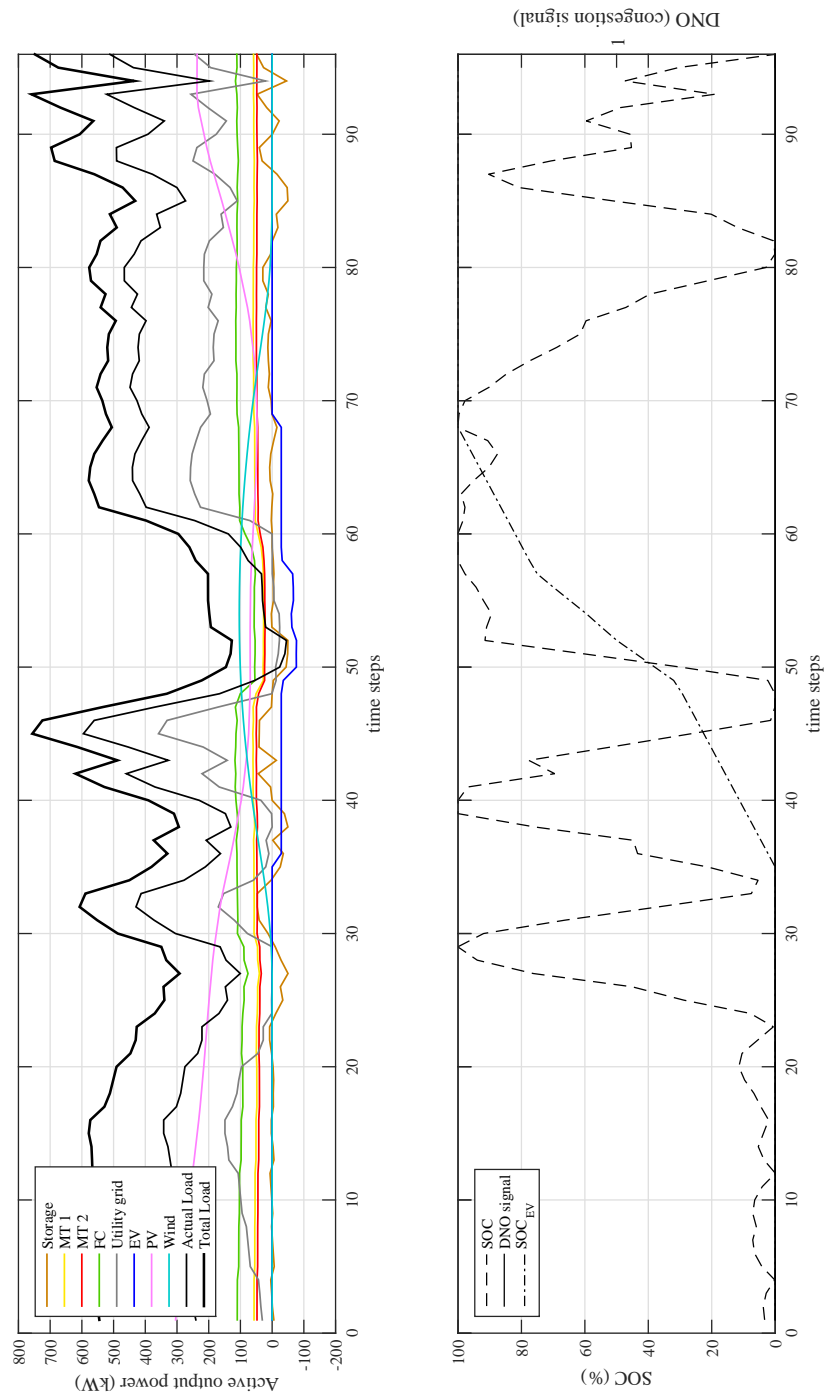
Figure 5.7: Set points UC without voltage control

5.5.3.2 Executive layer

In order to determine the future operational states of the microgrid units whereby the bus voltages are maintained within acceptable limits, an offline power flow calculation should be performed in order to obtain the values of the voltage magnitudes of the different microgrid buses. Within the executive layer (presented in Fig. 2.6), an AC power flow calculation is performed with the power reference set points calculated by the scheduling layer. As introduced in § 5.5.2, using Simscape Power Systems, the microgrid model (as presented in 5.5.1) is simulated in order to obtain the numerical values of the bus voltages. This executive layer performs an AC power flow calculation using the reference set points of each time step within the complete time horizon (96 time steps).

The bus voltages are presented in Fig. 5.8. During the complete time horizon, the voltage at bus 5 and bus 8, on which load 2 and load 3 are connected, are the lowest. Especially, during periods of high energy demand and low RES production, the voltage drops below -5% (with a base unit quantity $V_N = 230$ V). It is clear that during time steps 40-50 an undervoltage occur at bus 5 and bus 6, to which load 2 is connected. This can be explained by the fact that during this period (time step 45), the energy demand becomes excessively high and causes and undervoltage. The same happens between time steps 60 and 70.

As a result, we can conclude that power scheduling without considering the bus voltages can result in voltage violations. In the following section, the adjustment layer is presented, which is utilised to maintain the bus voltages and contains a security check with feedback control to the first layer.
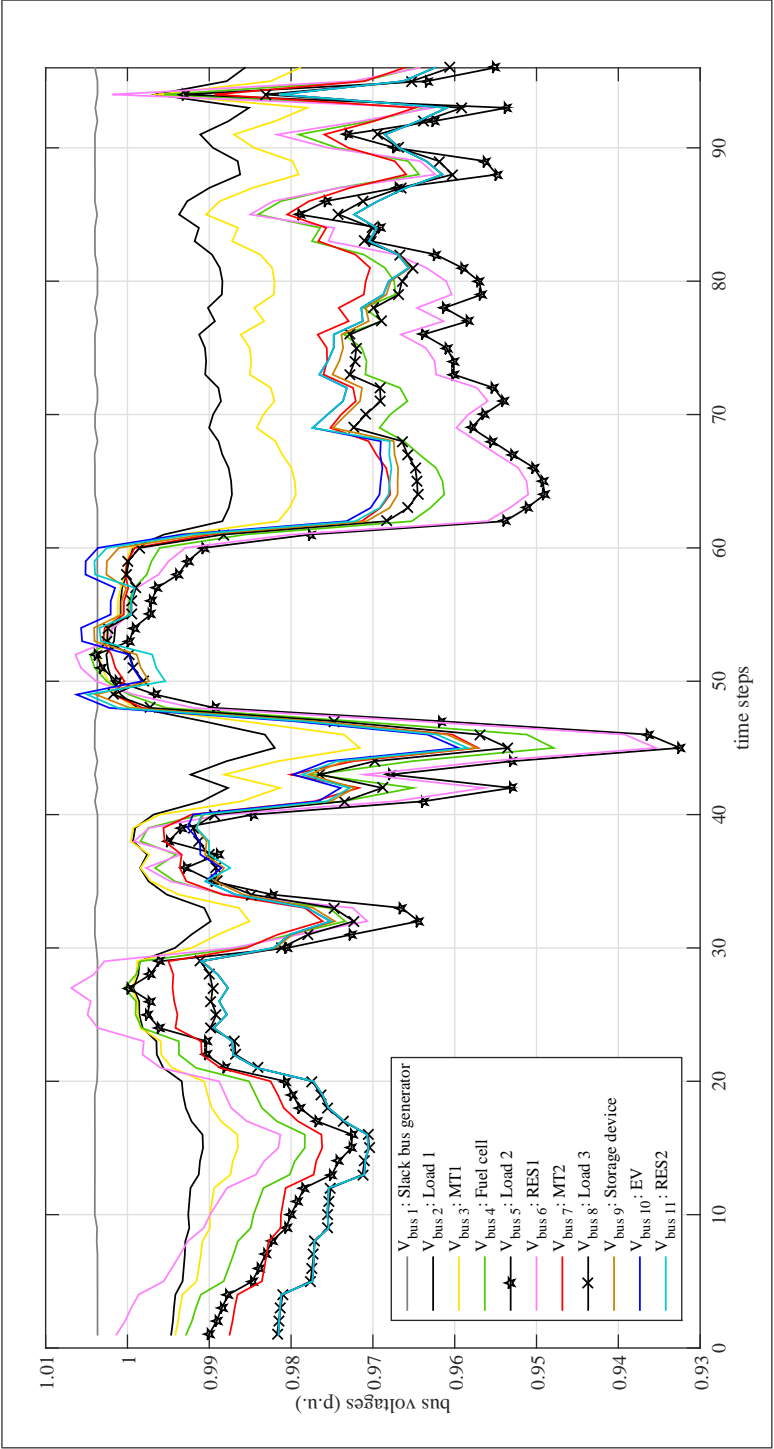
Figure 5.8: Busvoltages without voltage control
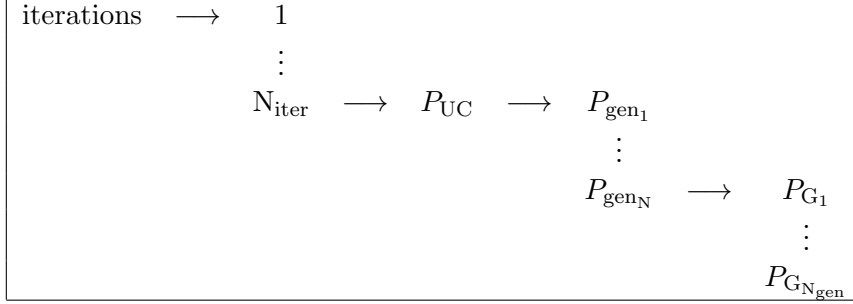
5.5.3.3   Adjustment layer

The adjustment layer, which is the scope of this chapter, includes a control strategy to maintain the voltage in the network. The purpose of this third layer is to keep the voltages within a pre-specified tolerance band by adjusting the boundaries of the microgrid units. Depending on the voltage deviation, the location of the microgrid units in the network and their distance from to voltage deviation, an appropriate dynamic gain will be provided in order to adjust the boundaries of the microgrid units in which they can be committed. Subsequently, when closing the loop, the renewed boundaries are then fed back to the scheduling layer, which performs a new optimisation and redistributes the adjusted reference set points among the microgrid units. The updated power generation schedule will again go through the second and third layer of the control hierarchy. This iterative process will continue until all voltage violations are eliminated and a converged optimal solution is found.

Due to the introduction of this third layer, the active power reference set points will be provided not only according to the economical and the environmental objectives, but also taking into account the voltage level at every bus in the microgrid. In fact, a deviation will be made in the economical and environmental optimal set points given by the first layer in order to maintain the voltage at every bus. In this work, the tolerance band of the voltage control approach is set to 5%.

Based on the voltage deviation ($\Delta v_{\mathrm{m}}(\%)$), it can take several iterations until the bus voltages are controlled within the tolerance band. Within every iteration, a loop through each layer of the control hierarchy will be performed. As a result, each iteration comes with an updated set of reference set points for whenever step N of the complete time horizon. This iteration structure (while-loop) is presented in Fig. 5.9.

For every set of reference set points $(P_{\mathrm{G}_1} \cdots P_{\mathrm{G}_{\mathrm{N}_{\mathrm{gen}}}})$ per iteration, an updated set of bus voltages will be provided. In order to clarify the operation of the voltage control strategy and its dynamic gain, we will focus on the iterations within the hierarchical multilayer control approach for each voltage deviation.

The sequence of power references and the corresponding bus voltages are presented in Fig. 5.7 and 5.8. Within the complete time horizon, two events with a voltage deviation (greater than 5%) occur. One between time step 40-50 and one between time step 60-70. As a result, the voltage control approach will be activated and it will take several

$$\text{iterations} \quad \longrightarrow \quad 1$$
$$\vdots$$
$$\text{N}_{\text{iter}} \quad \longrightarrow \quad P_{\text{UC}} \quad \longrightarrow \quad P_{\text{gen}_1}$$
$$\vdots$$
$$P_{\text{gen}_N} \quad \longrightarrow \quad P_{\text{G}_1}$$
$$\vdots$$
$$P_{\text{G}_{\text{N}_{\text{gen}}}}$$

Figure 5.9: Iteration structure of the hierarchical multilayer control

iterations until the bus voltages (at every bus within the complete time horizon) are controlled within the tolerance band.

The first event of a voltage deviation (greater that 5%) occurs between time step 40 and 50 and a detailed plot of the power reference set points and the corresponding bus voltages during this period are presented in Fig. 5.10.
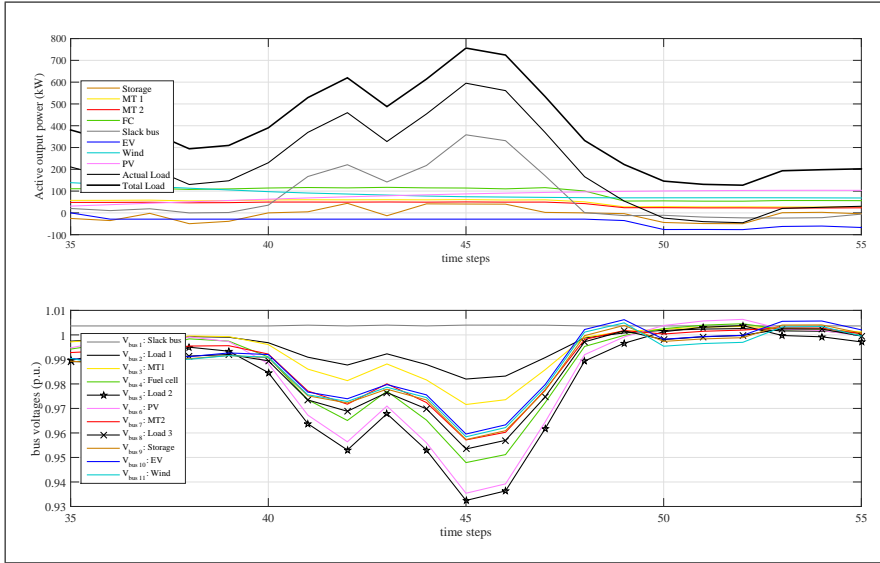
Figure 5.10: Set points and bus voltages between time steps 35-55

On time step 45, Load 1 consumes 226.9 kW, Load 2 consumes 378.17 and Load 3 consumes 151.27 kW. During this time step, the voltage at bus 5 and bus 6 drops below 5% and as a result the voltage control

approach will be activated. The largest deviation is on bus 5, to which Load 2 is connected, which can be verified on Fig. 5.10. The voltage control approach aims to reduce this deviation by providing a dynamic gain to the corresponding power generation units in order to adjust their boundaries, and as a result, their range in which they can be committed. The lower boundaries will be increased by the dynamic gain in order to increase the reference set points and to reduce the voltage deviation. This process will continue until the microgrid bus voltages are within acceptable limits. The range and the reference set points of the microgrid units throughout the iterations are presented in Fig 5.11.
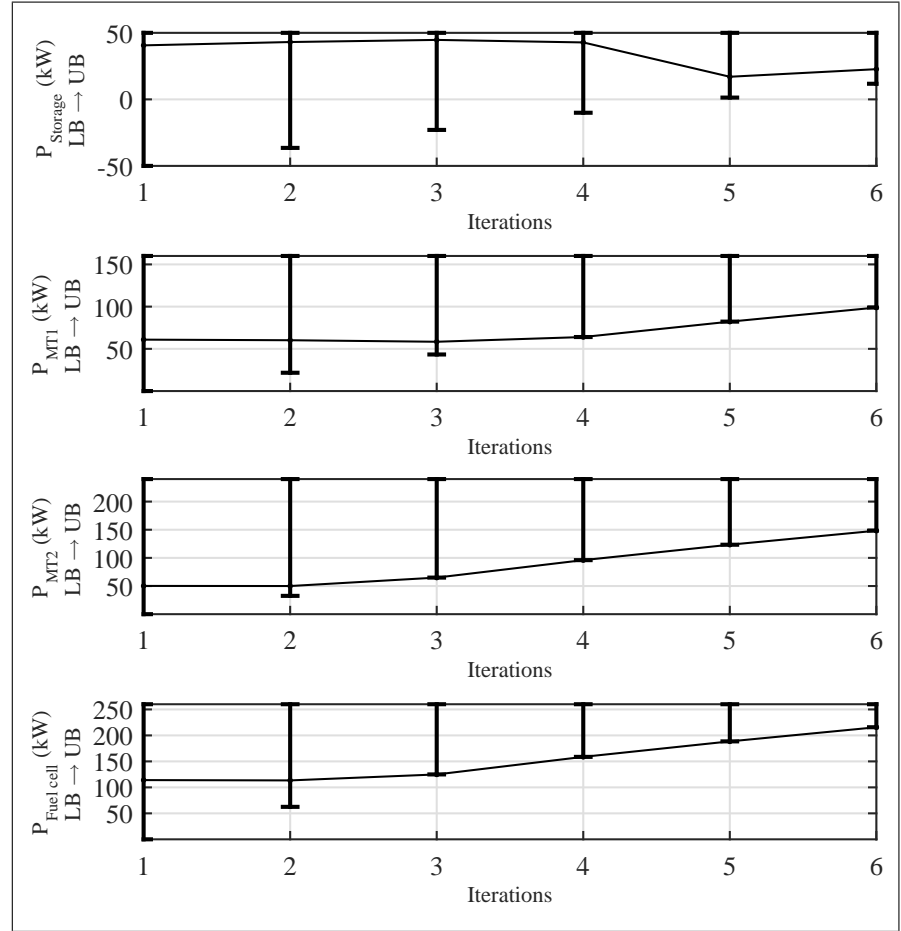
Figure 5.11: Set points and boundaries on time step 45

It is clear that the lower bounds of the microgrid units are increasing in order to increase the reference set points and to reduce the voltage deviation at bus 5. The lower boundary of the fuel cell has the steepest increase since is closest to the voltage deviation (bus 4, bus 5 and bus 6). The relative increase (according to their range) of the lower bounds of micro turbine 1 and 2 are quite similar (between iteration 1 and 6) since their distance to location of the voltage deviation is equal. Note that the lower boundary of the storage unit is modified in order to charge less during an undervoltage. The reference set points and the boundaries of the EVs are not presented since they are not plugged in (on time step 45) and do not participate in the UC and voltage control strategy at that moment. The redistribution of the reference set points among the different microgrid units together with the bus voltages, between iteration 1 and 6, are presented in Fig. 5.12.
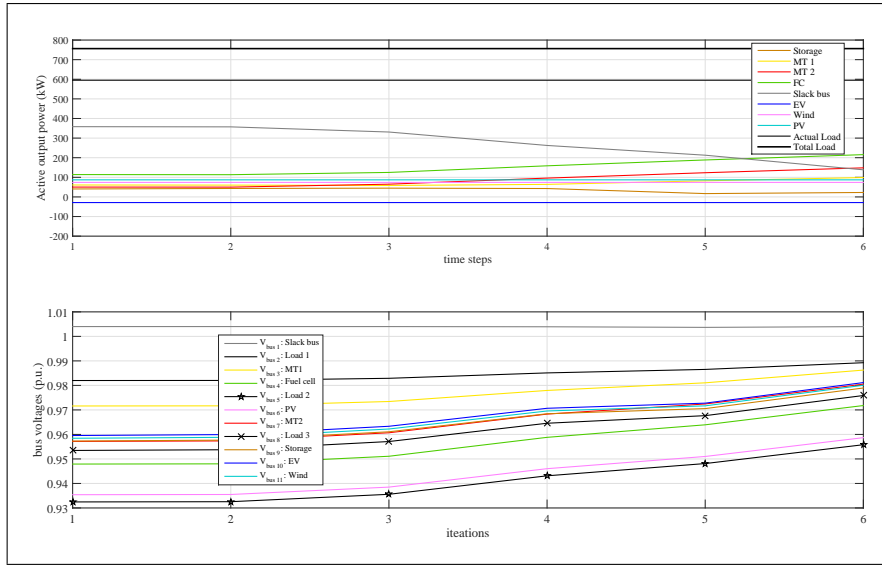
Figure 5.12: Set points and bus voltages on time step 45

It is clear that during these iterations the model increases the lower bounds of the microgrid units in order to increase their set points and as a result to increase the voltage at bus 5. After 6 iterations the undervoltage at bus 6 is reduced within the 5% tolerance band. A second event of a voltage deviation (greater that 5%) occurs between time step 60 and 70. This can be explained by the fact that during this period, the energy demand becomes excessively high and

causes an undervoltage in the network. A closer look of the power reference set-points and the corresponding bus voltages during this period is presented in Fig. 5.13.

Figure 5.13: Set points and bus voltages between time steps 60-80

On time step 64, Load 1 consumes 173.48 kW, Load 2 consumes 289.13 kW and Load 3 consumes 115.65 kW. During this time step, an second undervoltage occur at bus 5 and 6 due to the high power demand of Load 2 which can be verified on Fig. 5.13. During this time step, the EVs are plugged in and are participating in the UC and the voltage control strategy. During the same iterations the voltage control approach kicks in, as well on time step 64, and aims to reduce this deviation by providing a dynamic gain to the corresponding power generation units in order to adjust their boundaries, and as a result, the range in which they can be committed. The lower boundaries will be increased by the dynamic gain in order to increase the reference set points and to reduce the voltage deviation. The range and the reference set points of the microgrid units are presented in Fig 5.14.

The lower bounds of the microgrid units are increased in order to increase the reference set points and to increase the voltage at bus 5. Note that the increase of the lower bounds is less, since the voltage deviation is less as compared to time step 45. The lower boundary of the fuel cell has the steepest increase since this unit has the closest
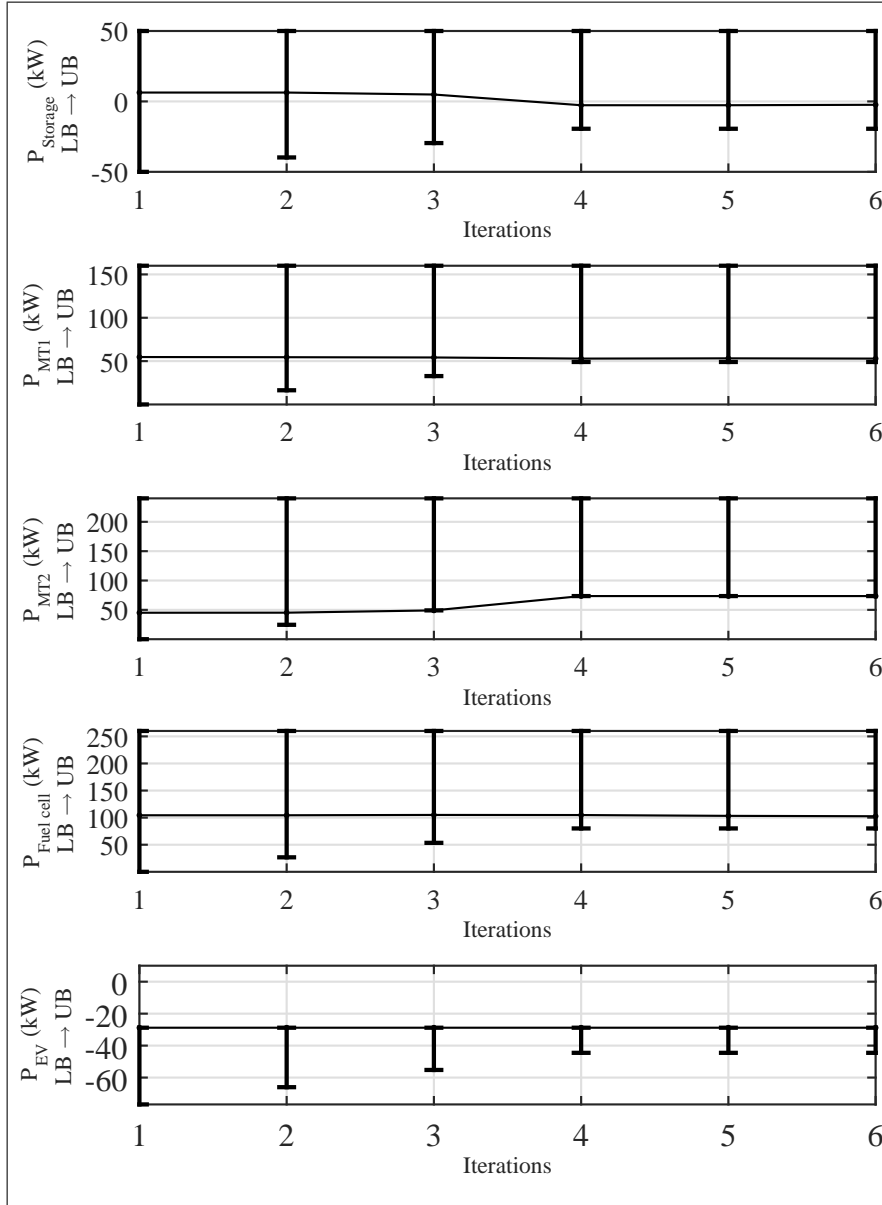
Figure 5.14: Set points and boundaries on time step 64

location to the voltage deviation (load 2). Again, the increase of
the lower bounds of micro turbine 1 and 2 are quite similar since
their distance to bus 5 is equal. Note that the lower boundaries of

the storage unit and the EVs are modified in order to charge less when an undervoltage occur. After 6 iterations the undervoltage at bus 6 (on time step 64) is reduced within the 5% tolerance band. The redistribution of the reference set points among the different microgrid units together with the bus voltages are presented in Fig. 5.15.
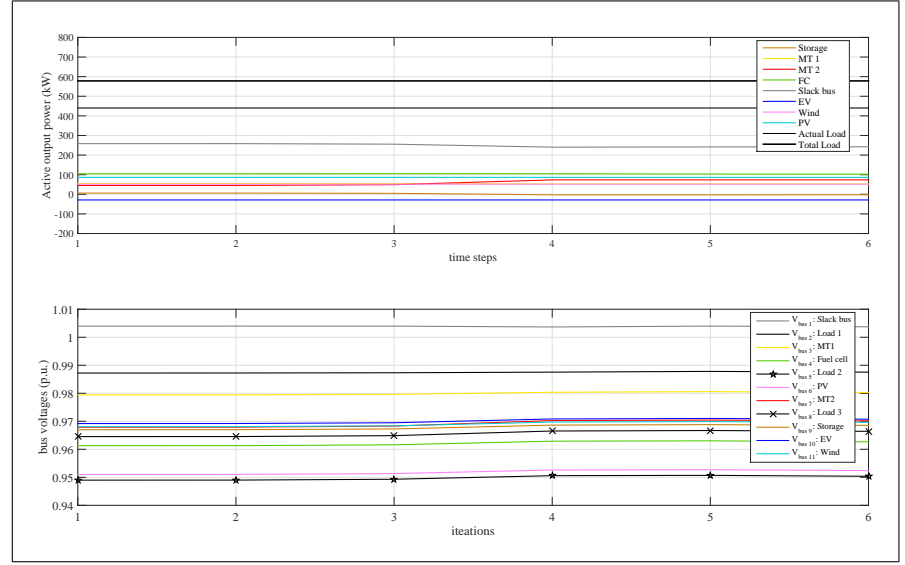
Figure 5.15: Set points and boundaries on time step 64

The converged sequence of power references and the corresponding bus voltages are presented in Fig. 5.16 and Fig. 5.17. During the complete time horizon, the voltages at every bus in the microgrid are reduced within the 5% tolerance band. As compared to the sequence of power reference set points without voltage control (Fig. 5.7), the use of the utility grid is reduced during periods of voltage deviations (time step 45 and 64). This can be explained by the fact that during these time steps, the voltage deviations are eliminated (or compensated) by the local thermal generation units, which reduces the use of the utility grid. The total cost is slightly decreased with 0.0025% and the total CO_2 emission is slightly increased with 0.0063%. The difference in total cost and total emission is very less. This can be explained by the fact that the redistribution of the power reference set points among the different microgrid units is dependent on the voltage deviations and their location in the network. As a result, the

total cost and total emission for simulations including the voltage control strategy is dependent on the voltage deviation.
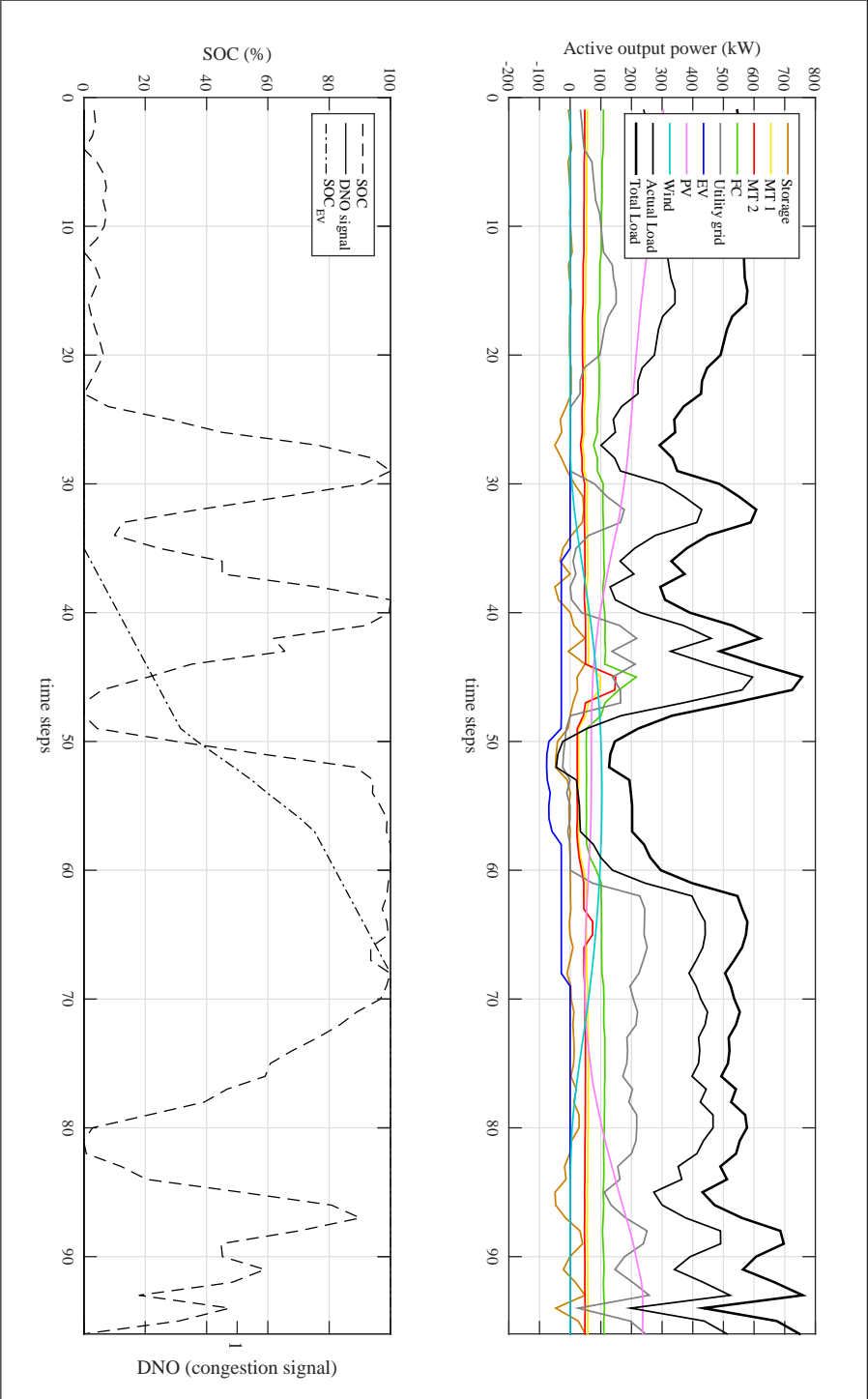
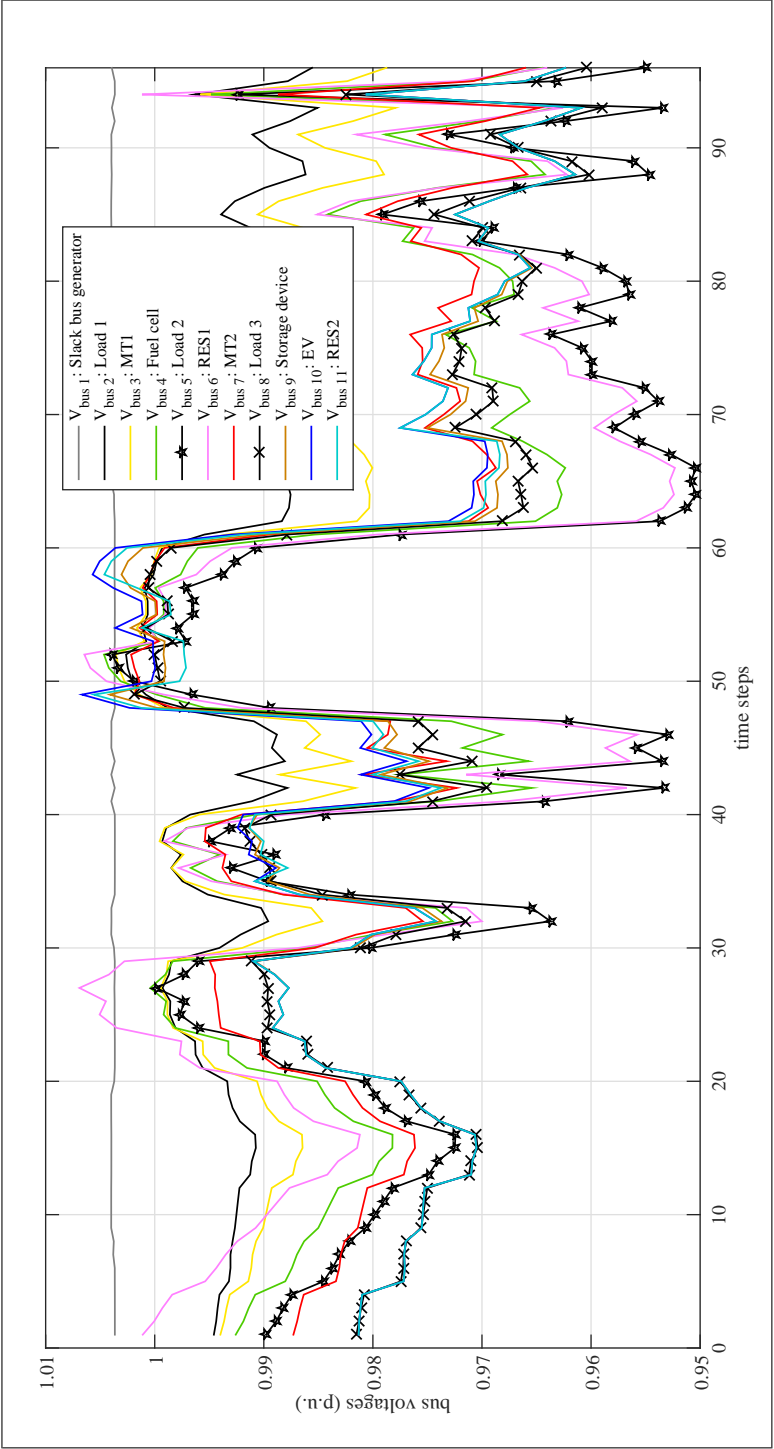**Figure 5.16:** Set points UC with voltage control

Figure 5.17: Busvoltages with voltage control

Overvoltages can occur at the low-voltage level of microgrids, caused by the high penetration of RES. Events of overvoltages will be discussed in Chapter 6 where a microgrid case study will be discussed with and without congestion signal (introduced by the DSO) and while mitigating both under- and overvoltages.

5.6   Conclusions

Additional to the issues tackled by the scheduling layer (§ 4.5), presented in Chapter 4, a voltage control approach is embedded in the multilayer control structure and maintains the microgrid bus voltages within pre-specified limits. The adjustment layer, which is the scope of this chapter, includes a control strategy to maintain the voltage in the network. The purpose of this third layer is to keep the voltage within a pre-specified tolerance band by adjusting the power provided by the microgrid distributed energy resources (DER). Depending on the voltage deviation, the location of the DER units in the network and their distance from the voltage deviation, an appropriate dynamic gain will be provided to the relevant DER units. The renewed settings are then fed back to the first layer, which performs a new optimisation and redistributes the adjusted reference set points among the DER units. The performance and effectiveness of the proposed hierarchical multilayer control structure were tested and presented in this chapter. It is clear that due to the introduction of this third layer, active power reference set points can be provided (for real-time scheduling) not only according to the economical and the environmental objectives, but also taking to account the voltage level at every bus in the microgrid. This work is published in [110].

6

Applications of the multilayer control structure

6.1 Introduction

In this chapter, the multilayer control structure for microgrids is demonstrated. The objective of this multilayer control concept is to provide an economically and environmentally viable UC that is feasible in terms of voltage violations. The microgrid model used in this application has different line parameters than those used in the previous chapters. This chapter concludes with a brief examination of the sensitivity of the model to variations in the microgrid load and line parameters.

6.2 Applications

The proposed hierarchical multilayer control structure is applied on two microgrid cases in order to verify the effectiveness and to validate the performance. The microgrid model used for both cases is depicted in Fig. 6.1 and includes 11 low voltage (LV) buses connected downstream from a distribution transformer. Furthermore, the studied system includes renewable energy resources, a storage unit, two micro turbines, a fuel cell and a controllable load including 4 electric

vehicles. Serving the microgrid load (Load 1 + Load 2 + Load 3 + Controllable Load), active power can be produced either by the thermal generation units, the slack bus generator, the storage device, or the renewable energy resources.
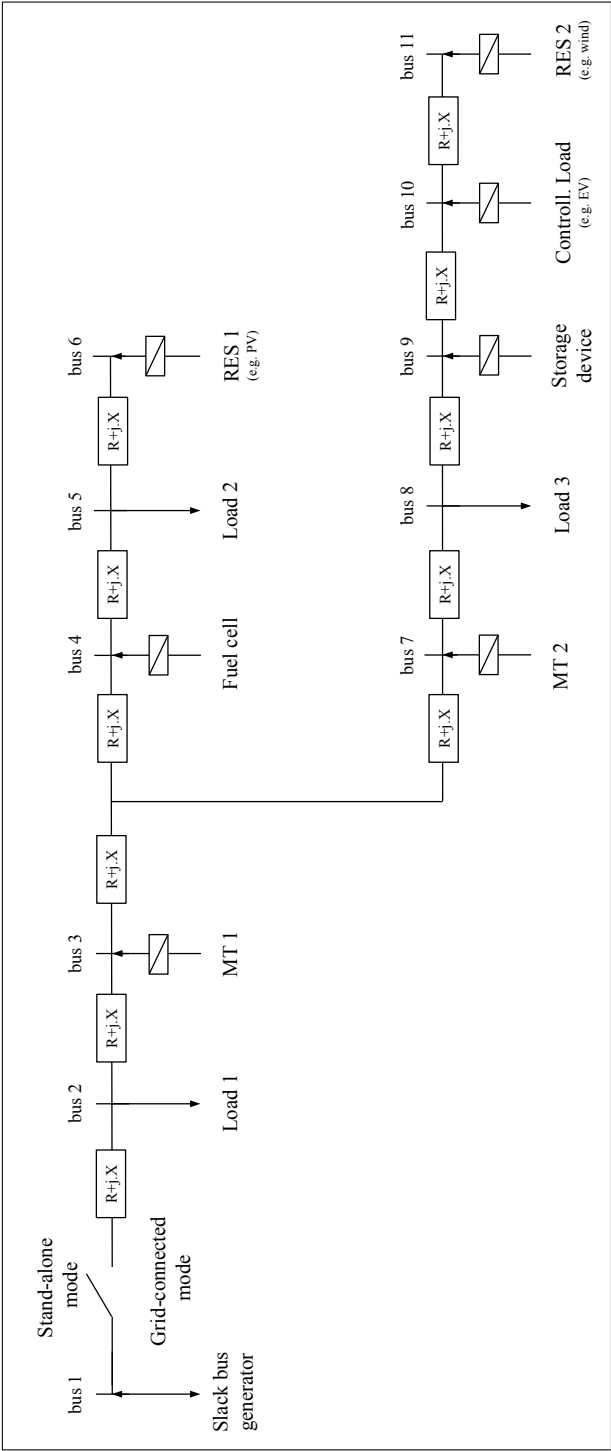
Figure 6.1: Microgrid test set up

The cost and emission coefficients of the thermal generation units are listed in Table 6.1. A CO_2 emission intensity of $381 \cdot 10^{-3}$kg/kWh [99] is considered for the power supply of the slack bus generator. The cost coefficient of the slack bus generator is related to a variable pricing scheme which is presented in Fig. 6.2. The capacities of the microgrid generation units are listed in Table 6.2. For the storage unit, $E_{\min}$ was set to 0 kWh, $E_{\max}$ was set to 40 kWh, and $E_{\mathrm{EV_{max}}}$ of each EV was set to 80 kWh. The charging rate of each EV is limited between -19.2kW and -7.2kW, which results in a total (4 EVs) minimum and maximum charging rate of -28.8kW and -76.8kW respectively.

$C_{\mathrm{G}}(P_{\mathrm{G}})$	a	b	c
Micro Turbine 1	$100 \cdot 10^{-5.5}$	$50 \cdot 10^{-5.5}$	$20 \cdot 10^{-5.5}$
Micro Turbine 2	$140 \cdot 10^{-5.5}$	$40 \cdot 10^{-5.5}$	$100 \cdot 10^{-5.5}$
Fuel Cell	$20 \cdot 10^{-5.5}$	$20 \cdot 10^{-5.5}$	$10 \cdot 10^{-5.5}$
$\varepsilon_{\mathrm{G}}(P_{\mathrm{G}})$	d	e	f
Micro Turbine 1	$4.09 \cdot 10^{-3}$	$-5.55 \cdot 10^{-3}$	$6.49 \cdot 10^{-3}$
Micro Turbine 2	$2.54 \cdot 10^{-3}$	$-6.05 \cdot 10^{-3}$	$5.64 \cdot 10^{-3}$
Fuel Cell	$5.33 \cdot 10^{-3}$	$-3.55 \cdot 10^{-3}$	$3.38 \cdot 10^{-3}$

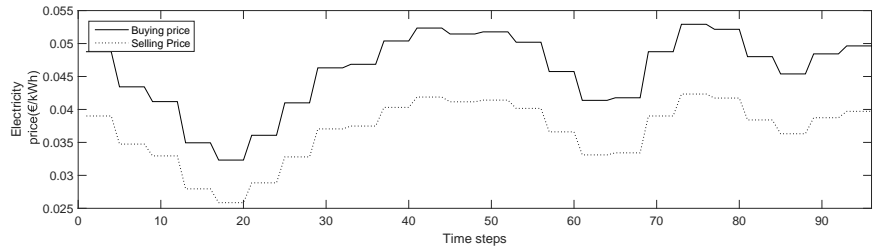**Table 6.1:** Fuel cost and emission coefficients

Figure 6.2: Market conditions

6.2.1 Case 1

In the first case study, a day-ahead microgrid is simulated with and without voltage control approach. Additionally, events of under and overvoltages will be discussed and it will be explained how they are

	MT 1	MT 2	Fuel Cell	Storage
$P_{\mathbf{G_{max}}}$ (kW)	160	240	260	± 50

Table 6.2: Microgrid generator capacities

tackled by the voltage control approach. The profiles of the different microgrid loads, and the renewable energy production during the complete time horizon (24 hour, 96 time steps of 15 minutes) are depicted in Fig. 6.3.
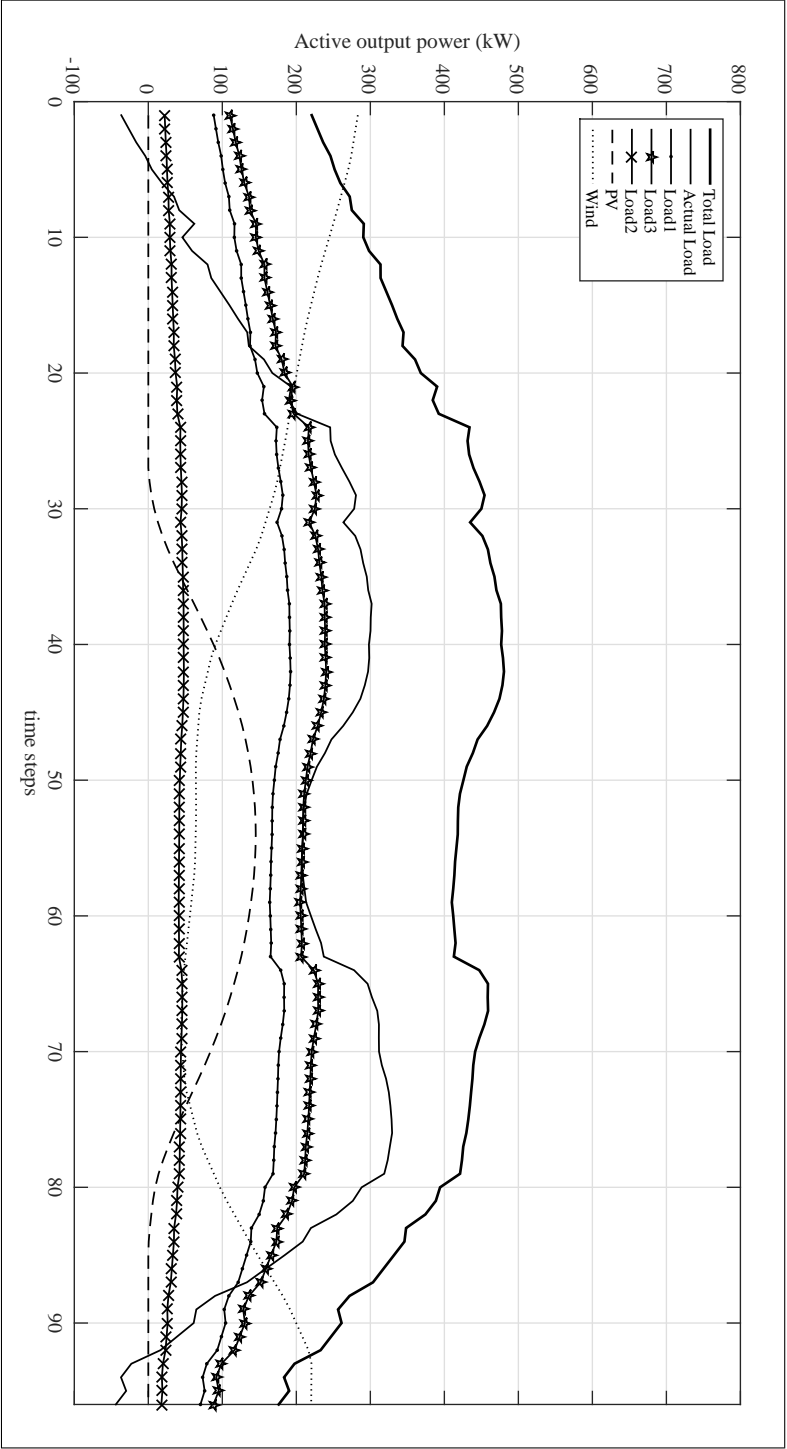
Figure 6.3: Microgrid load profile and RES production

The length (L) between the buses are assumed to be 200m with an R/X value of 7.7 ($R = 0.0642\Omega$/km and $X = 0.0083\Omega$/km).

6.2.1.1 Scheduling layer

Based on the day-ahead energy market, the demand bids, and the availability of renewable energy sources, a 15 minute power generation schedule for the next 24 hours is calculated by the scheduling layer. The active power is scheduled among the different microgrid units while minimising the operating costs together with the produced CO_2 emissions. The reference set points are presented in Fig. 6.4. The total microgrid load (P_D^{total}) is presented by the thick black line. The actual load (P_D^{a}) (excluding the power produced by the renewable sources) is presented by the thin black line. Between 11:00 and 14:30 (time step 44-58), and between 18:00 and 19:30 (time step 72-78), a congestion signal is introduced by the DSO. During this signal, the slack bus generator is committed to zero and no energy is exchanged between the microgrid and the main grid. As a result, a transition to virtual islanded mode is scheduled. Because of the lack of the slack bus generator, the buying and selling price are neglected during these periods. The maximum power which can be delivered depends on the upper bounds of the controllable thermal generators and the stored energy. During the islanded operation mode, the fuel cell has the greatest contribution in the unit commitment. This can be explained by the fact that the fuel cell has the lowest fuel cost and lowest emission rate.

When the power produced by the wind turbine becomes high (time steps 1-6 and 90-96), the storage device will be charged. During periods of virtual virtual islanded operation, the storage unit will be discharged which reduces additional output power from the thermal generation units, and as a result reduces the total cost and emission of the microgrid operation. The EVs were plugged in between 09:00 and 17:00 (time step 36-68). At 17:00, the EVs are fully charged. During virtual islanded mode, the EVs are charged at their maximum rate in order to reduce additional output power from the thermal generation units.
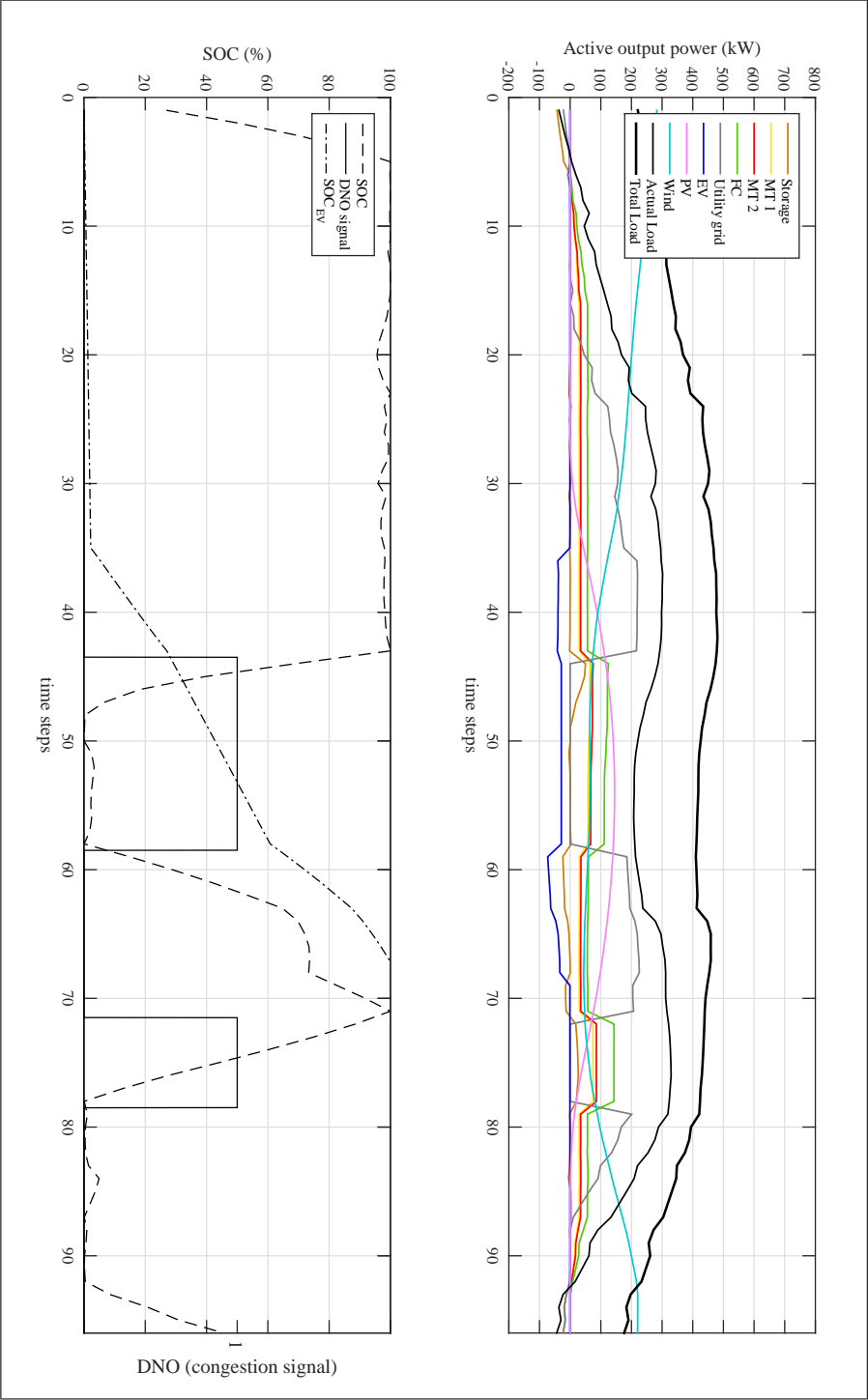
Figure 6.4: Set points UC without voltage control

6.2.1.2 Executive layer

Within the executive layer, an AC power flow calculation is performed with the power reference set points calculated by the scheduling layer. The bus voltages are presented in Fig. 6.5. During the complete time horizon, the voltage at bus 5 and bus 6, to which load 2 and RES1 are connected, are the lowest. Especially, during periods of high energy demand, the voltage drops below 5%. It is clear that during time steps 70-84 an undervoltage occur at bus 5 and bus 6, to which load 2 is connected. This can be explained by the fact that during this period (time step 79), the energy demand becomes excessively high and causes and undervoltage. The same happens between time steps 22 and 42.

During periods of low microgrid demand (time steps 1-6 and 90-96) and while the power produced by the wind turbine becomes very high, an overvoltage occurs at bus 11 to which RES2 is connected.

We can conclude that power scheduling without considering the bus voltages can result in voltage violations. In the following section, the adjustment layer is presented, which is utilised to maintain the bus voltages and contains a security check with feedback control to the first layer.
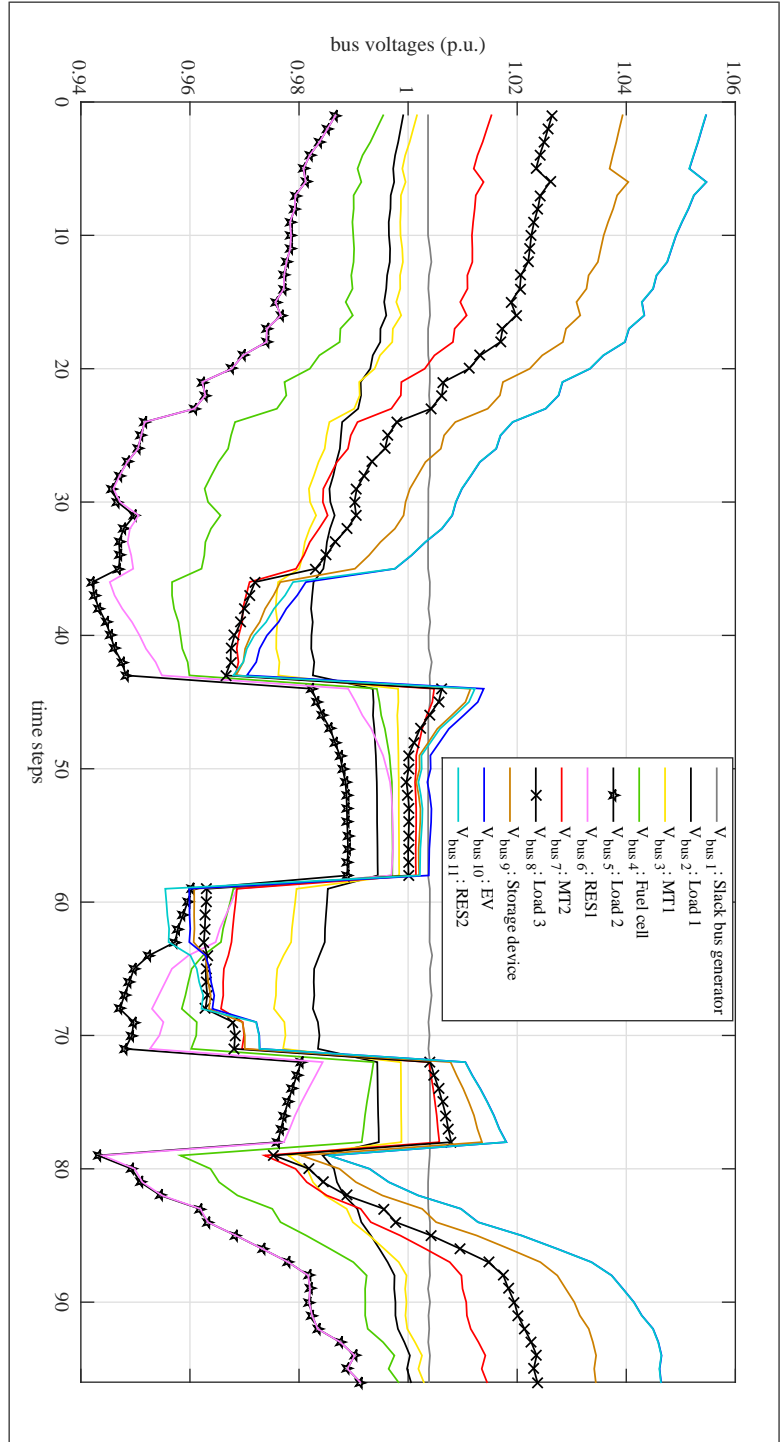
**Figure 6.5:** Busvoltages without voltage control

6.2.1.3 Adjustment layer

The adjustment layer, which is the scope of this chapter, includes a control strategy to maintain the voltage in the network. The purpose of this third layer is to keep the voltage within a pre-specified tolerance band by adjusting the boundaries of the microgrid units. Due to the introduction of this third layer, the active power reference set points will be provided not only according to the economical and the environmental objectives, but also taking into account the voltage level at every bus in the microgrid. In fact, a deviation will be made from the economical and environmental optimal set points given by the first layer in order to maintain the voltage at every bus. In this work, the tolerance band of the voltage control approach is set to 5%. Based on the voltage deviation ($\Delta v_\mathrm{m}(\%)$), it can take several iterations until the bus voltages are controlled within the tolerance band. Within every iteration, a loop through each layer of the control hierarchy will be performed. As a result, each iteration comes with an updated set of reference set points for each time step N of the complete time horizon. Additionally, for every set of reference set points per iteration, an updated set of bus voltages will be provided. In order to clarify the operation of the voltage control strategy and its dynamic gain, we will focus on the iterations within the hierarchical multilayer control approach each time for a certain time step a voltage deviation occurs.

The sequence of power references and the corresponding bus voltages are presented in presented in Fig. 6.4 and Fig. 6.5. Two events with a voltage deviation (greater than 5%) will be discussed in this case. One between time step 1-15 and one between time step 70-84.

The first event of a voltage deviation (greater than 5%) occurs between time step 1 and 15 and a detailed plot of the power reference set points and the corresponding bus voltages during this period is presented in Fig. 6.6.

On time step 5, Load 1 consumes 100.68 kW, Load 2 consumes 91.38 and Load 3 consumes 94.40 kW. During this time step, RES2 (Wind) produces 270.17 kW. As a result, the voltage bus 11 rises above 5% (which can be verified on Fig. 6.6) and as a result, the voltage control approach will be activated. The voltage control approach aims to reduce this deviation by providing a dynamic gain to the corresponding power generation units in order to adjust their boundaries, and as a result, their range in which they can be committed. In this particular case, the upper bound of RES2 will be decreased by the dynamic gain in order to decrease the reference set points and to
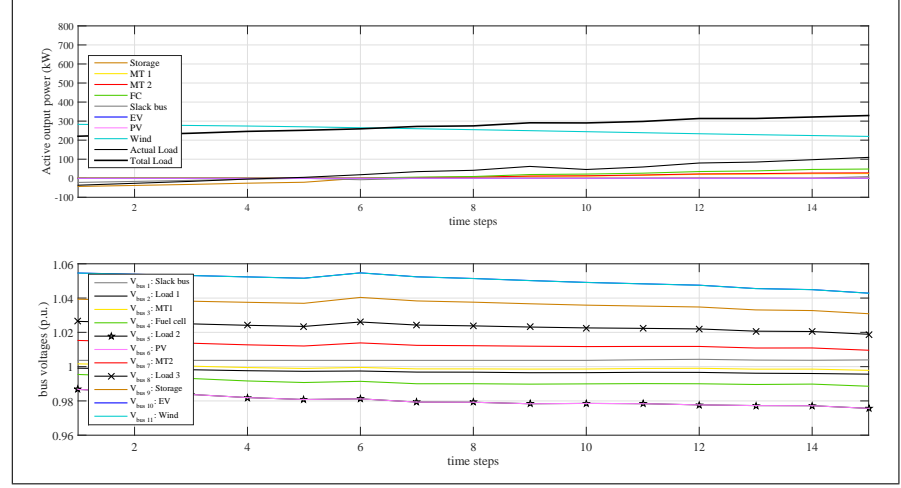
Figure 6.6: Set points and bus voltages between time steps 1-15

reduce the voltage deviation. This process continues until the microgrid bus voltages are within acceptable limits. The reference set points of RES2 throughout the iterations are presented in Fig 6.7.
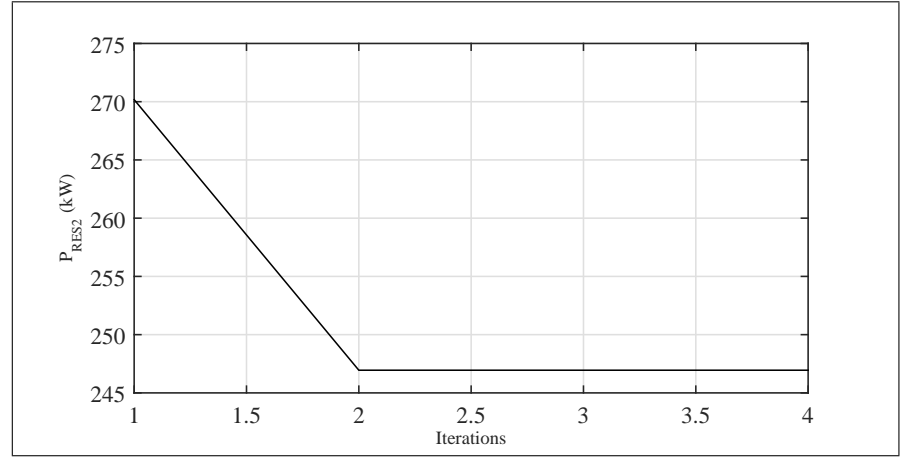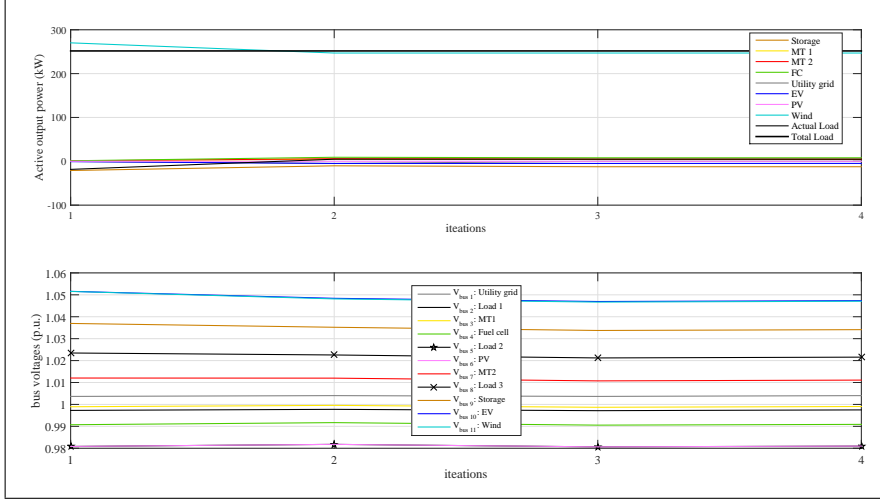

Figure 6.7: Set points and boundaries on time step 5

It is clear that the upper bound of RES2 is decreasing in order to decrease the reference set points and to reduce the voltage deviation at bus 11. The redistribution of the reference set points among the different microgrid units together with the bus voltages, between

iteration 1 and 4, are presented in Fig. 6.8.

Figure 6.8: Set points and bus voltages on time step 5

Note that the reference set points of the other generation units are increasing in order to cover the reduced wind power and to maintain the power balance. After 2 iterations the overvoltage at bus 11 is reduced within the 5% tolerance band. Note that the process continues for 4 iterations. This is because the application eliminates a second voltage deviation within the same (4) iterations. This will be explained in the second case.

A second event of a voltage deviation (greater that 5%) occurs between time step 70 and 84. This can be explained by the fact that during this period, the energy demand becomes excessively high and causes and undervoltage in the network. A closer look of the power reference set points and the corresponding bus voltages during this period is presented in Fig. 6.9.

On time step 79, Load 1 consumes 168.47 kW, Load 2 consumes 210.59 kW and Load 3 consumes 42.11 kW. During this time step, an undervoltage occurs at bus 5 and 6 due to the high power demand of Load 2 which can be verified on Fig. 6.9. During the same iterations, the voltage control approach kicks in at this time step, and aims to reduce this deviation by providing a dynamic gain to the corresponding power generation units in order to adjust their boundaries, and as a result, the range in which they can be committed. The lower boundaries will be increased by the dynamic gain in order
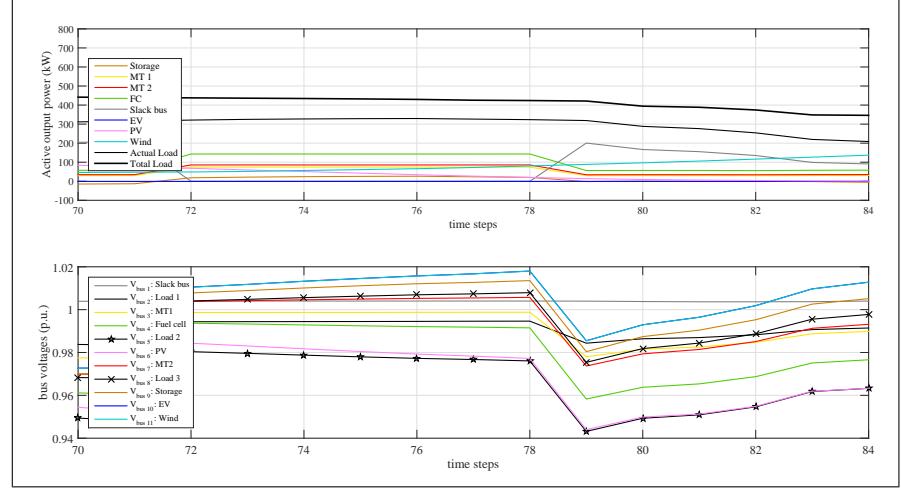
Figure 6.9: Set points and bus voltages between time steps 70-84

to increase the reference set points and to reduce the voltage deviation. The range and the reference set points of the microgrid units are presented in Fig 6.10.
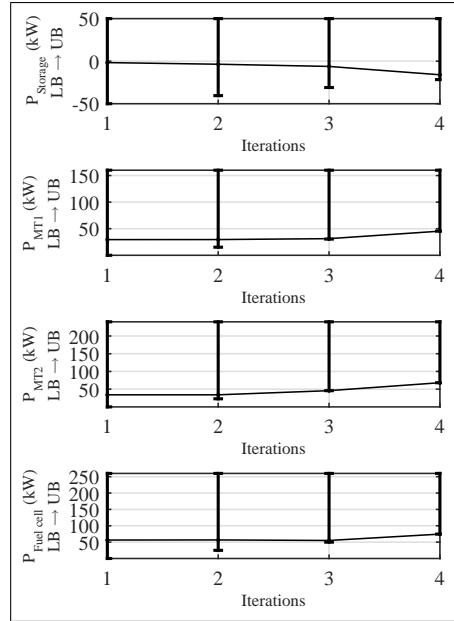
Figure 6.10: Set points and boundaries on time step 79

The lower bounds of the microgrid units are increasing in order to increase the reference set points and to increase the voltage at bus 5. The lower boundary of the fuel cell has the steepest increase since this unit has the closest location to the voltage deviation (load 2). The increase of the lower bounds of micro turbine 1 and 2 are quite similar since their distance to bus 5 is equal. Note that the boundaries of the EVs are not presented since they do not participate in the UC at time step 79 (already unplugged). After 4 iterations the undervoltage at bus 5 and 6 (on time step 79) is reduced within the 5% tolerance band. The redistribution of the reference set points among the different microgrid units together with the bus voltages are presented in Fig. 6.11.
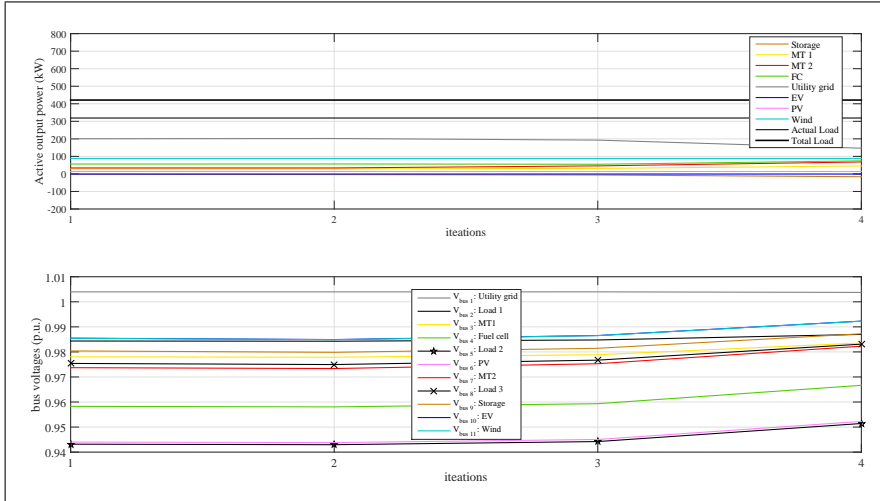
Figure 6.11: Set points and boundaries on time step 79

The converged sequence of power references and the corresponding bus voltages are presented in Fig. 6.12 and Fig. 6.13. During the complete time horizon, the voltages at every bus in the microgrid are reduced within the 5% tolerance band. The total cost is slightly decreased by 8.02% and the total CO_2 emission is slightly increased by 2.3%. This can be explained by the fact that the use of the slack bus generator is reduced in order to reduce the undervoltages over the complete time horizon. In order to compensate for this reduction, the thermal generators (especially the micro turbines) were committed in a higher output range, and with a higher emission rate. The difference

in total cost and total emission lower. This can be explained by the
fact that the redistribution of the power reference set points among
the different microgrid units is dependent on the voltage deviations
and their location in the network. As a result, the total cost and
total emission for simulations including the voltage control strategy
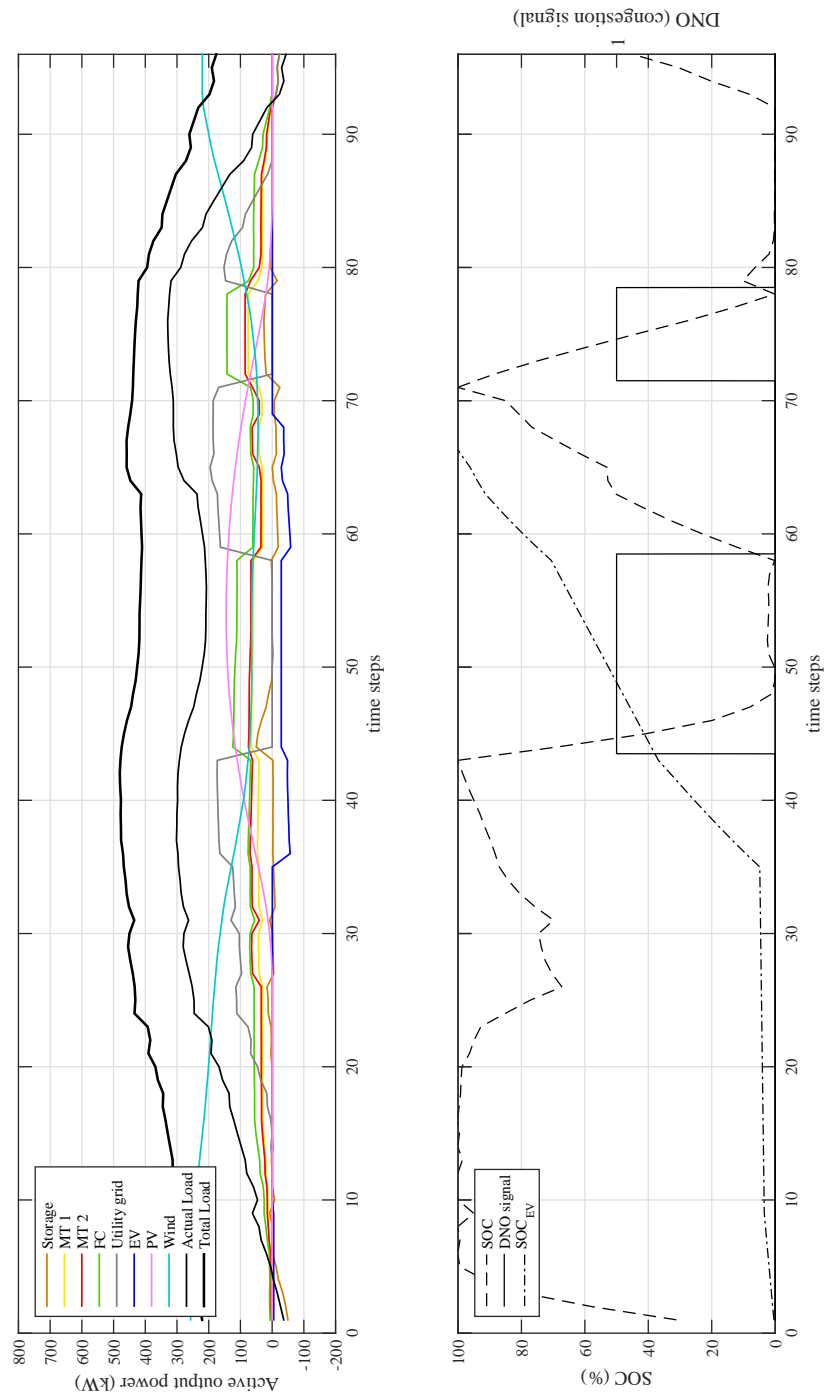is dependent on the voltage deviation.

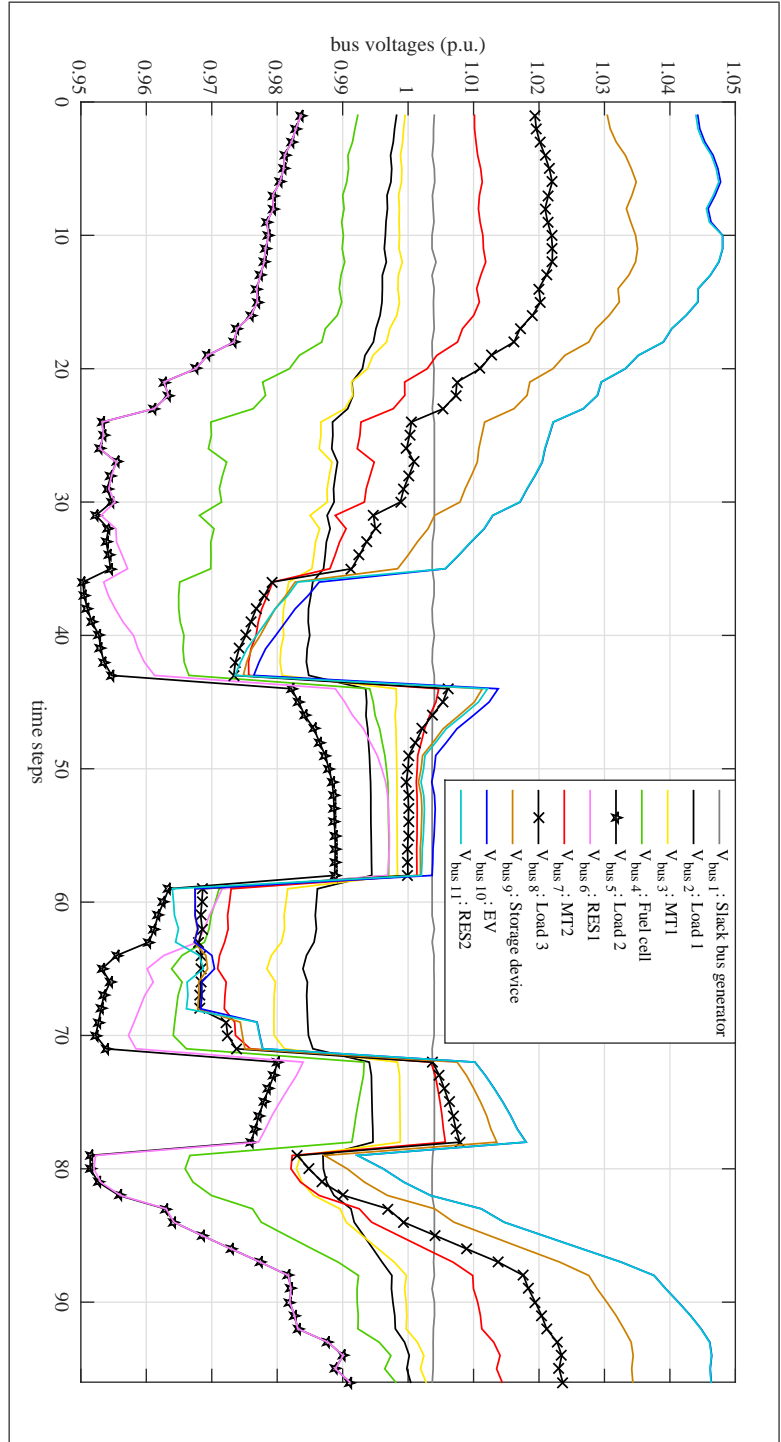**Figure 6.12:** Set points UC with voltage control

Figure 6.13: Bus voltages with voltage control

6.2.2 Case 2

In a second case study, a day-ahead microgrid was simulated with and without voltage control approach. Additionally, events of under and overvoltages will be discussed and how they are tackled by the voltage control approach. The profiles of the different microgrid loads, and the renewable energy production during the complete time horizon (24 hour, 96 time steps of 15 minutes) are depicted in Fig. 6.14. The different line parameters are presented in the 6.3 [47].

bus	length (m)	resistance (Ω/km)	inductance (mH/km)	R/X
$1 \to 2$	40	0.265	0.248	3.4
$2 \to 3$	40	0.265	0.248	3.4
$3 \to 4$	80	0.265	0.248	3.4
$4 \to 5$	40	0.265	0.248	3.4
$5 \to 6$	40	0.265	0.248	3.4
$6 \to 7$	100	0.410	0.243	5.37
$7 \to 8$	100	0.410	0.243	5.37
$8 \to 9$	100	0.410	0.243	5.37
$9 \to 10$	100	0.410	0.243	5.37
$10 \to 11$	100	0.410	0.243	5.37

Table 6.3: Line parameters

6.2.2.1   Scheduling layer

Based on the day-ahead energy market, the demand bids, and the availability of renewable energy sources, a 15 minute power generation schedule for the next 24 hours was calculated by the scheduling layer. The active power is scheduled among the different microgrid units while minimising the operating costs together with the produced CO_2 emissions. The reference set points are presented in Fig. 6.15. The total microgrid load (P_D^{total}) is presented by the thick black line. The actual load (P_D^a) (excluding the power produced by the renewable sources) is presented by the thin black line. Between 11:00 and 14:30 (time step 44-58), and between 18:00 and 19:30 (time step 72-78), a congestion signal is introduced by the DSO. Because of the lack of the slack bus generator, during this signal, the buying and selling price were neglected. During the virtual islanded operation mode, the fuel cell has the greatest contribution in the unit commitment. This can be explained by the fact that the fuel cell has the lowest fuel cost and lowest emission rate.

When the power produced by the wind turbine becomes high (time steps 1-15), the storage device will be charged. During periods of virtual islanded operation, the storage unit will be discharged, which reduces additional output power from the thermal generation units, and as a result reduces the total cost and emission of the microgrid operation. The EVs were plugged in between 09:00 and 17:00 (time step 36-68). At 17:00, the EVs are fully charged. During virtual islanded mode, the EVs are charged at their minimum rate in order reduce additional output power from the thermal generation units. During time steps 50-57, during high periods of high PV power and low microgrid demand, the EVs are charged at their maximum rate.
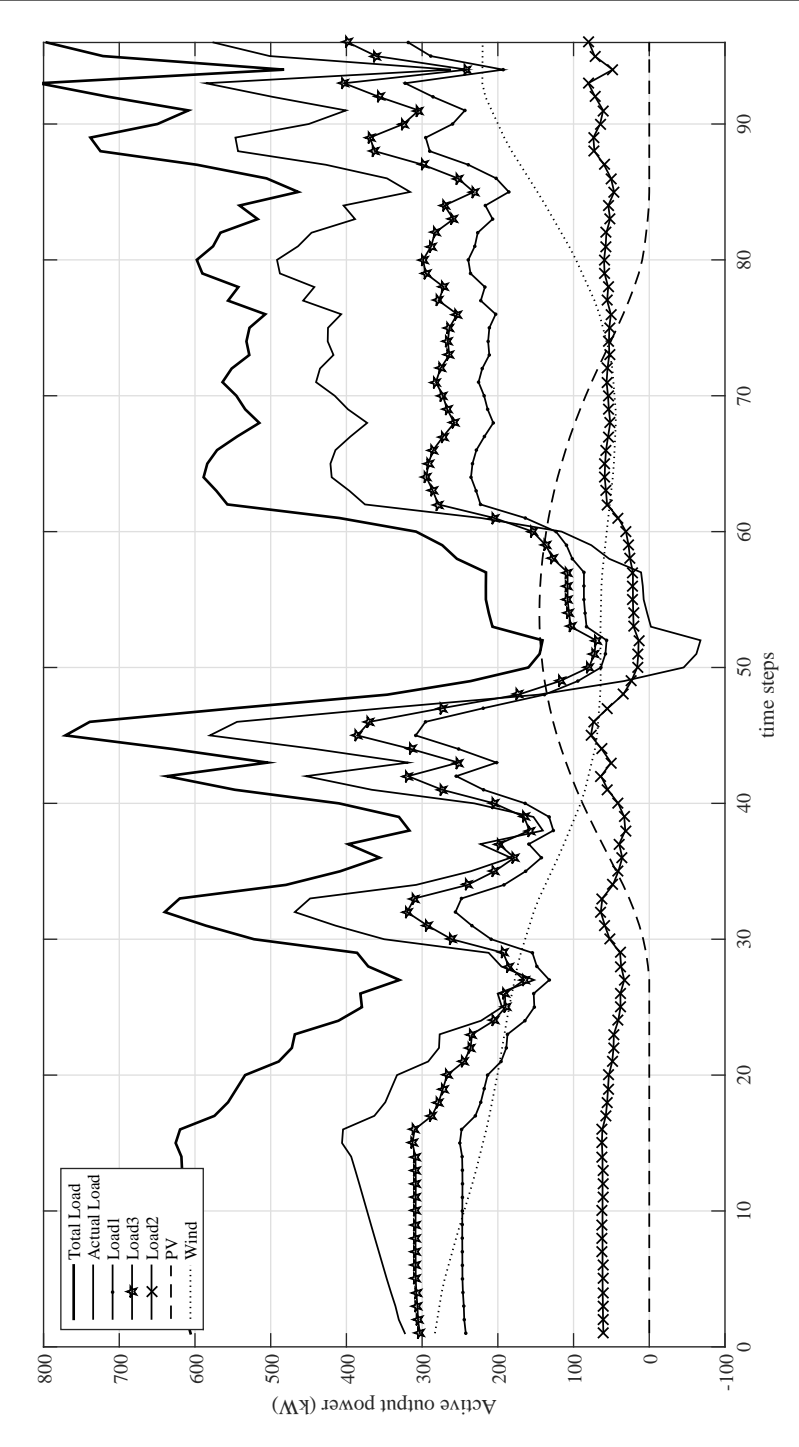
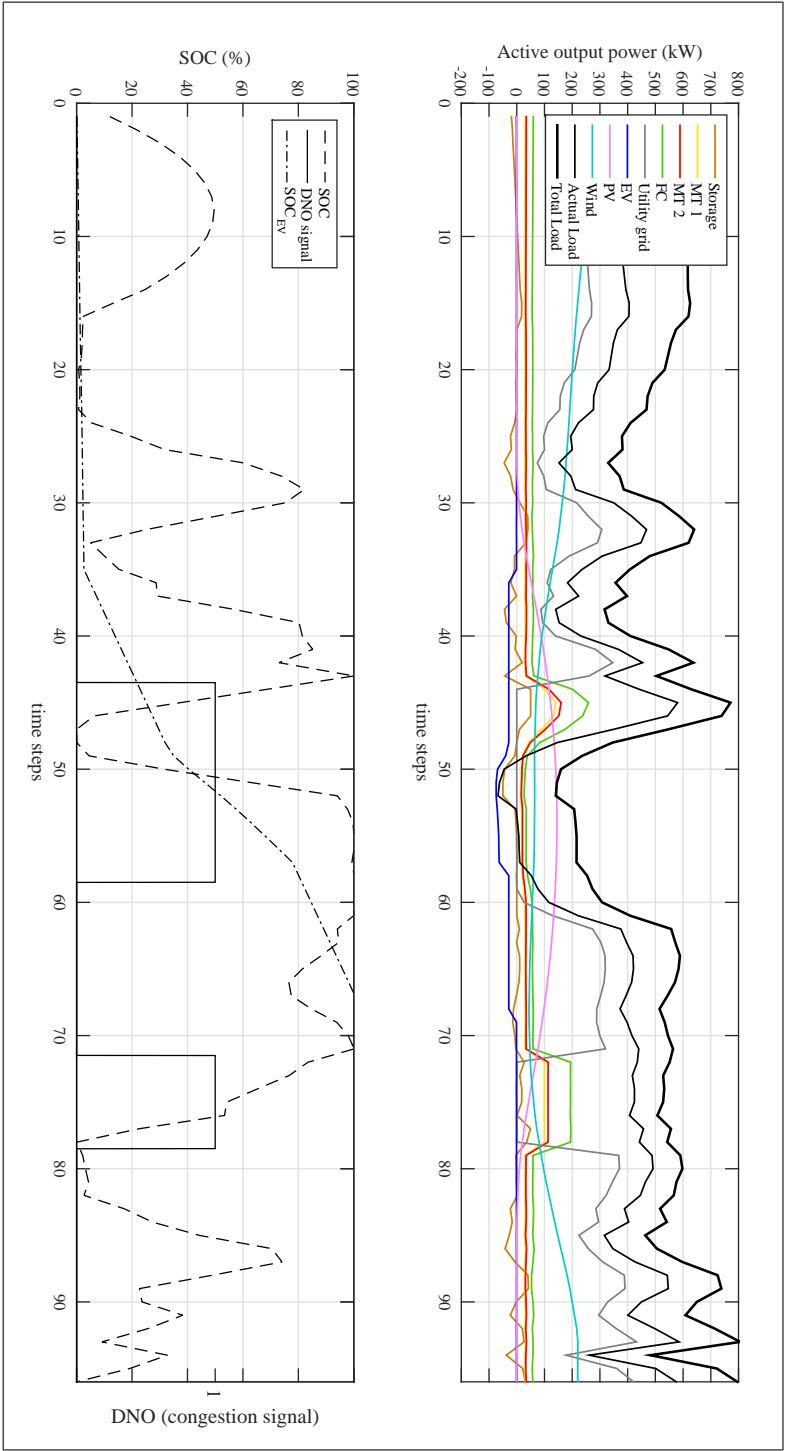**Figure 6.14:** Microgrid load profile and RES production

Figure 6.15: Set points UC without voltage control

6.2.2.2   Executive layer

Within the executive layer, an AC power flow calculation is performed with the power reference set points calculated by the scheduling layer. The bus voltages are presented in Fig. 6.16. During periods of high energy demand, the voltage drops below 5%. It is clear that during time steps 81-96 an undervoltage occur at bus 5 and bus 6, on which load 2 is connected. This can be explained by the fact that during this period (time step 96), the energy demand becomes excessively high and causes and undervoltage.

During periods of low microgrid demand (time steps 1-15 and 90-96) and while the power produced by the wind turbine becomes very high, an overvoltage occurs at bus 10 and bus 11 on which RES2 is connected.

We can conclude that power scheduling without considering the bus voltages can result in voltage violations. In the following section, the adjustment layer is presented, which is utilised to maintain the bus voltages and contains a security check with feedback control to the first layer.
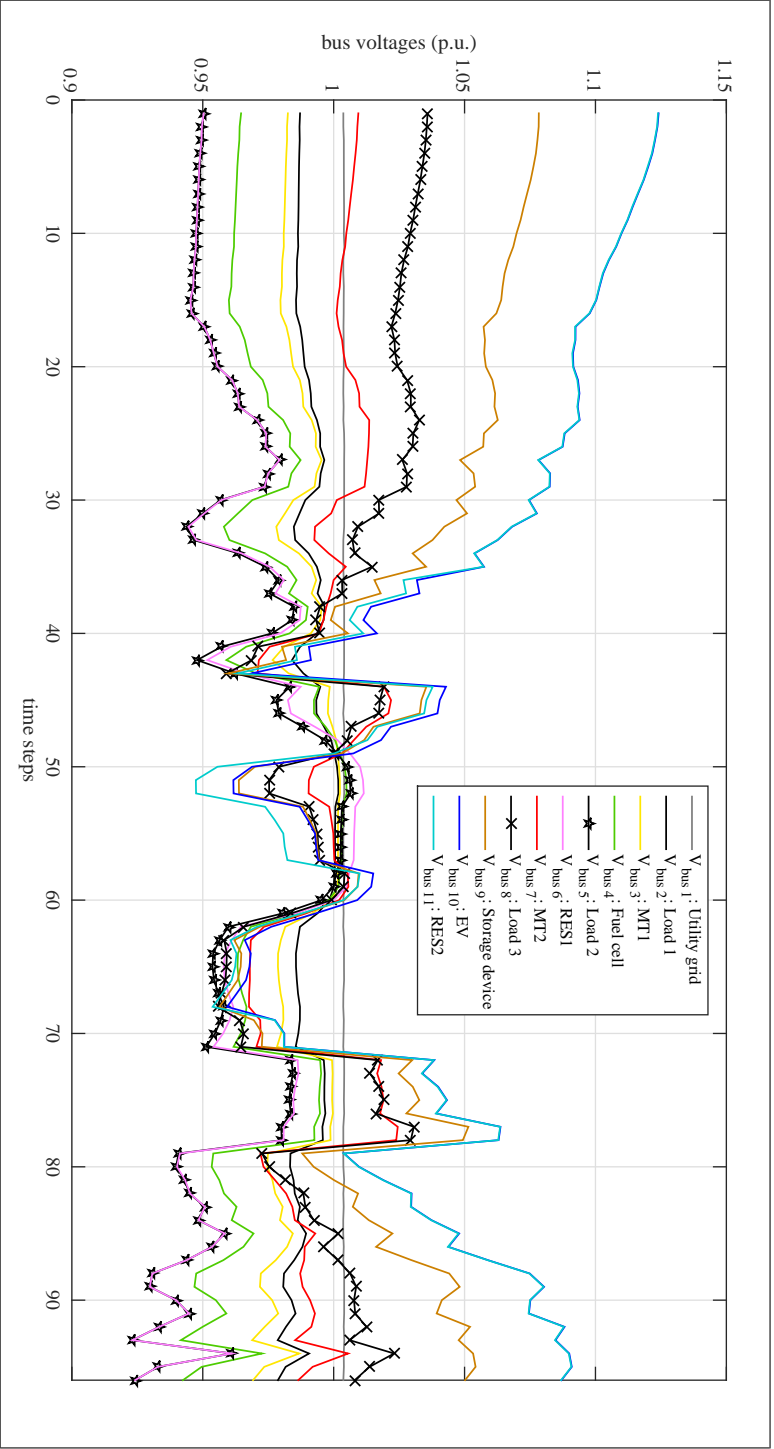
Figure 6.16: Busvoltages without voltage control

6.2.2.3 Adjustment layer

In order to clarify the operation of the voltage control strategy and it's dynamic gain, we will focus on the iterations within the hierarchical multilayer control approach each time for a certain time step a voltage deviation occurs.

The sequence of power references and the corresponding bus voltages are presented in presented in Fig. 6.15 and Fig. 6.16. Two events with a voltage deviation (greater that 5%) will be discussed in this case. One between time step 1-15 and one between time step 81-96. The first event of a voltage deviation (greater that 5%) occurs between time step 1 and 15 and a detailed plot of the power reference set points and the corresponding bus voltages during this period is presented in Fig. 6.17.
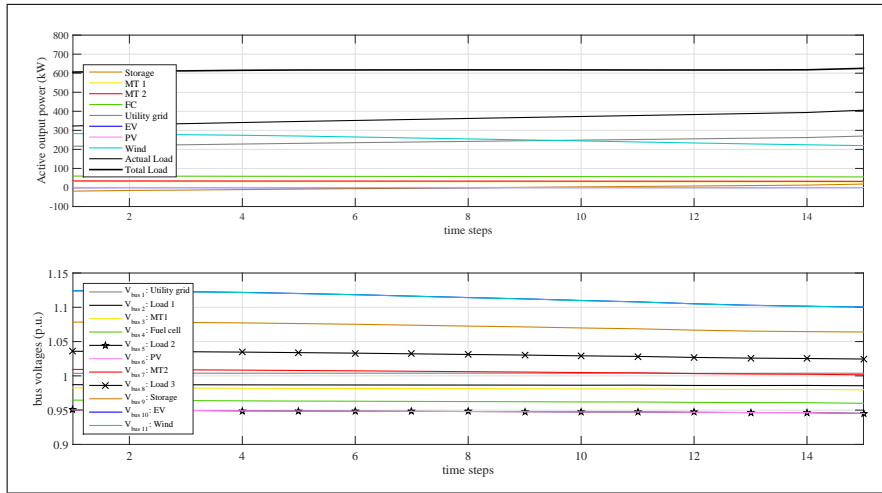
Figure 6.17: Set points and bus voltages between time steps 1-15

On time step 10, Load 1 consumes 246.89 kW, Load 2 consumes 308.61 and Load 3 consumes 61.72 kW. During this time step, RES2 (Wind) produces 244.48 kW. As a result, the voltage at bus 11 rises above 5% (which can be verified on Fig. 6.17) and as a result, the voltage control approach will be activated. The voltage control approach aims to reduce this deviation by providing a dynamic gain to the corresponding power generation units in order to adjust their boundaries, and as a result, their range in which they can be committed. In this particular case, the upper bound of RES2 will be decreased by the dynamic gain in order to decrease the reference set

points and to reduce the voltage deviation. This process continues until the microgrid bus voltages are within acceptable limits. The reference set points of RES2 throughout the iterations are presented in Fig 6.18.
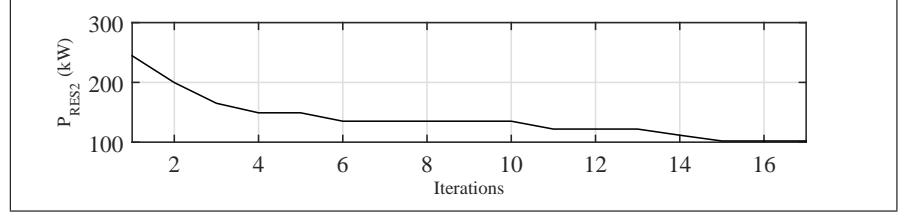
Figure 6.18: Set points and boundaries on time step 10

It is clear that the upper bound of RES2 is decreasing in order to decrease the reference set points and to reduce the voltage deviation at bus 11. The redistribution of the reference set points among the different microgrid units together with the bus voltages, between iteration 1 and 17, are presented in Fig. 6.19.

Figure 6.19: Set points and bus voltages on time step 10

Note that the reference set points of the other generation units are increasing in order to cover the reduced wind power and to maintain the power balance. After 17 iterations the overvoltage at bus 11 is reduced within the 5% tolerance band.

A second event of a voltage deviation (greater that 5%) occurs be-

tween time step 81 and 96. This can be explained by the fact that during this period, the energy demand becomes excessively high and causes and undervoltage in the network. A closer look of the power reference set points and the corresponding bus voltages during this period is presented in Fig. 6.20.

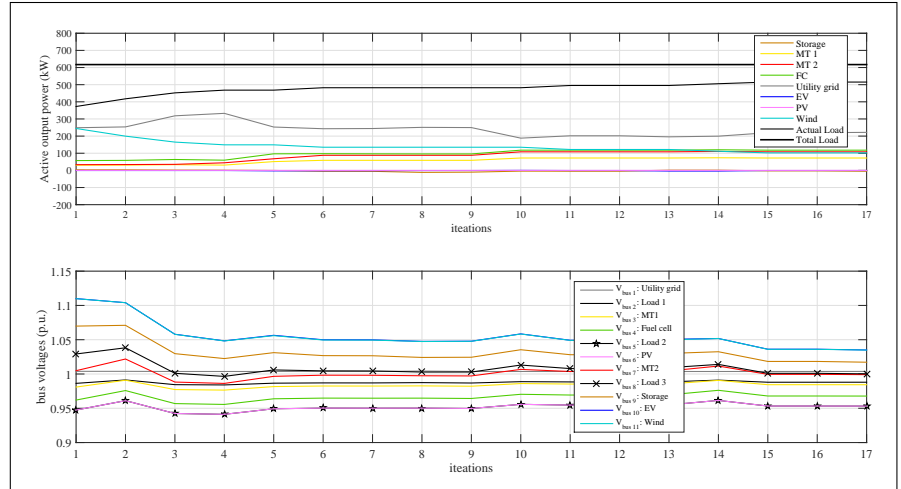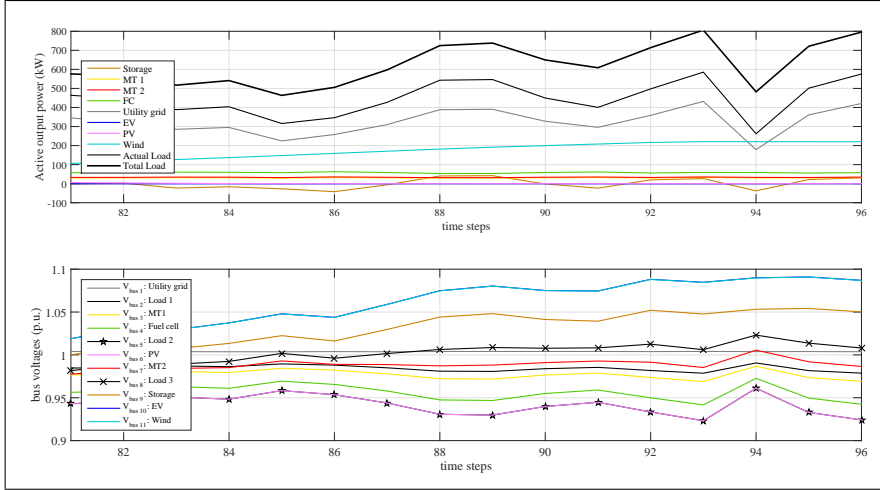**Figure 6.20:** Set points and bus voltages between time steps 81-96

On time step 96, Load 1 consumes 318.28 kW, Load 2 consumes 397.85 kW and Load 3 consumes 79.57 kW. During this time step, an undervoltage occurs at bus 5 and 6 due to the high power demand of Load 2 which can be verified on Fig. 6.20. During the same (17) iterations, the voltage control approach kicks in at this time step, and aims to reduce this deviation by providing a dynamic gain to the corresponding power generation units in order to adjust their boundaries, and as a result, their range in which they can be committed. The lower boundaries will be increased by the dynamic gain in order to increase the reference set points and to reduce the voltage deviation. The range and the reference set points of the microgrid units are presented in Fig 6.21.

The lower bounds of the microgrid units are increasing in order to increase the reference set points and to increase the voltage at bus 5. The lower boundary of the fuel cell has the steepest increase since this unit has the closest location to the voltage deviation (load 2). The increase of the lower bounds of micro turbine 1 and 2 are quite similar since their distance to bus 5 is equal. After 9 iterations the undervoltage at bus 5 and 6 (on time step 96) is reduced within the
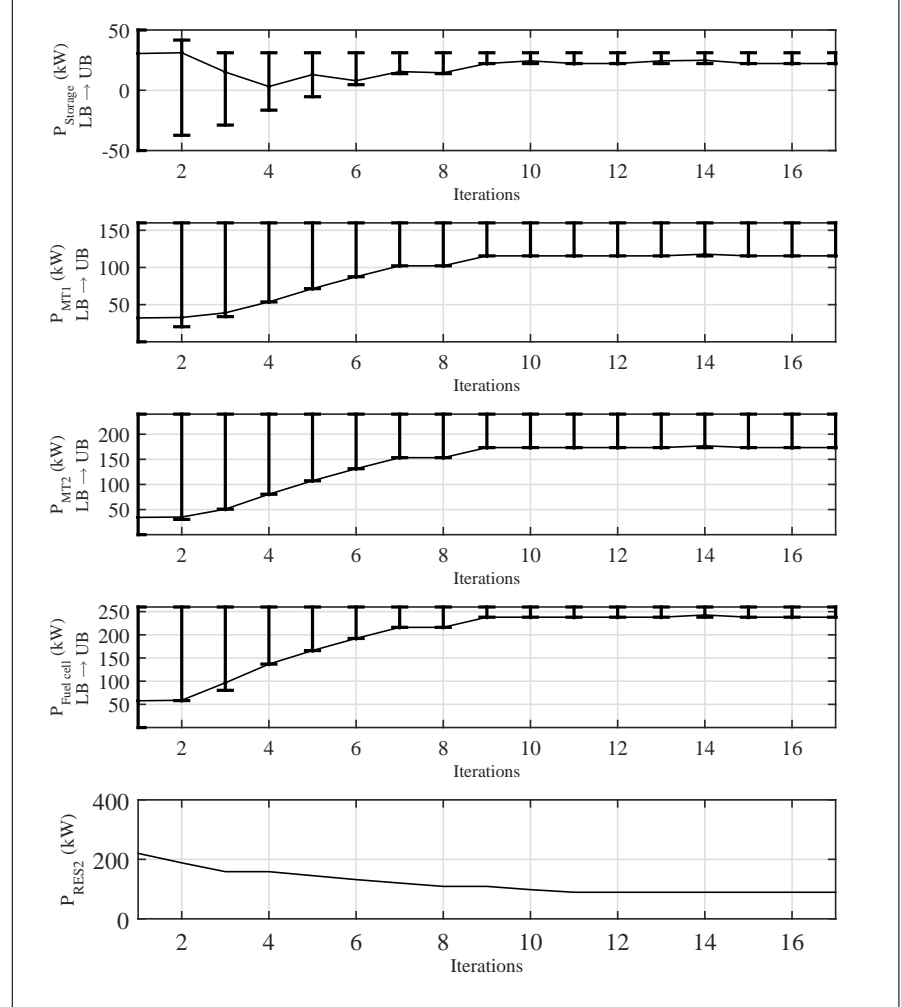
Figure 6.21: Set points and boundaries on time step 96

5% tolerance band. Note that the process continues for 17 iterations. This can be explained by the fact that the voltage control application eliminates the overvoltage at the same time step (96) which takes 17 iterations. The redistribution of the reference set points among the different microgrid units together with the bus voltages are presented in Fig. 6.22.

The converged sequence of power references and the corresponding bus voltages are presented in Fig. 6.23 and Fig. 6.24. During the complete time horizon, the voltages at every bus in the microgrid are
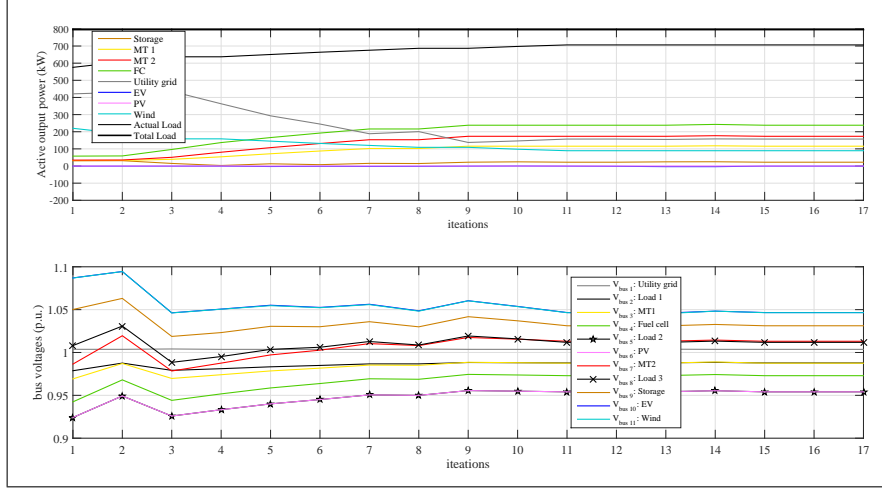
Figure 6.22: Set points and bus voltages on time step 96

reduced within the 5% tolerance band. The total cost is increased with 11.62% and the total CO_2 emission is increased with 12.13%. This can be explained by the fact that the power produced by RES2 was curtailed in order to reduce the overvoltages at bus 10 and bus 11. In order to compensate this reduction, the thermal generators were committed in a higher output range, and with a higher emission rate, and a surplus cost. The difference in total cost and total emission is high. This can be explained by the fact that the redistribution of the power reference set points among the different microgrid units is dependent on the voltage deviations, their location in the network, and by which unit they are caused. In this particular case, the voltage deviations were, i.a., caused by renewable sources which was producing power at zero running cost.
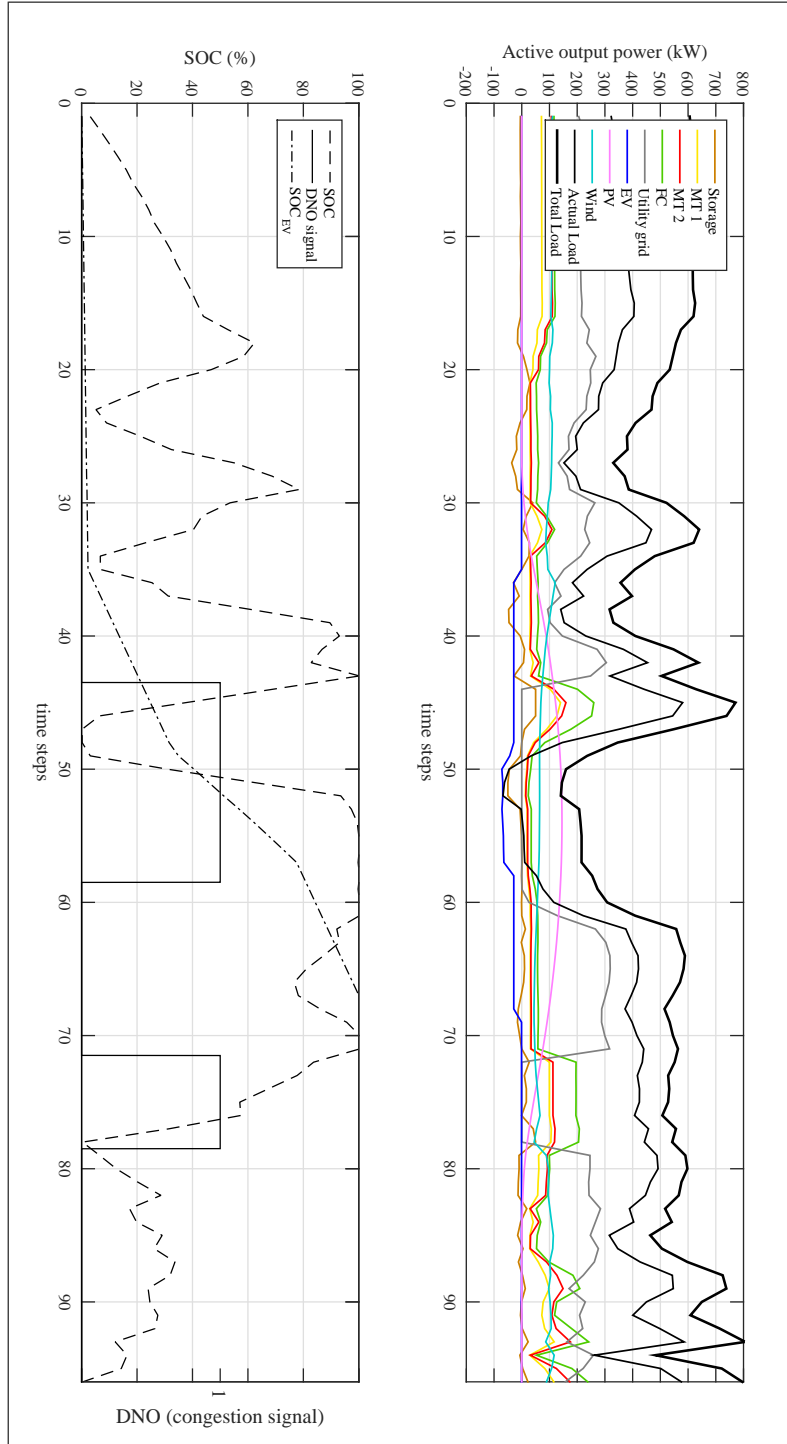
Figure 6.23: Set points UC with voltage control

Figure 6.24: Bus voltages with voltage control

6.3　Sensitivity

In order to control and manage the microgrid units in real-time while fully exploiting the benefit of long-term prediction, an offline optimisation approach was developed in this work in order to devise the online microgrid management. The energy management system solves the optimisation problem over the entire time horizon and provides optimal solutions by assuming that the futur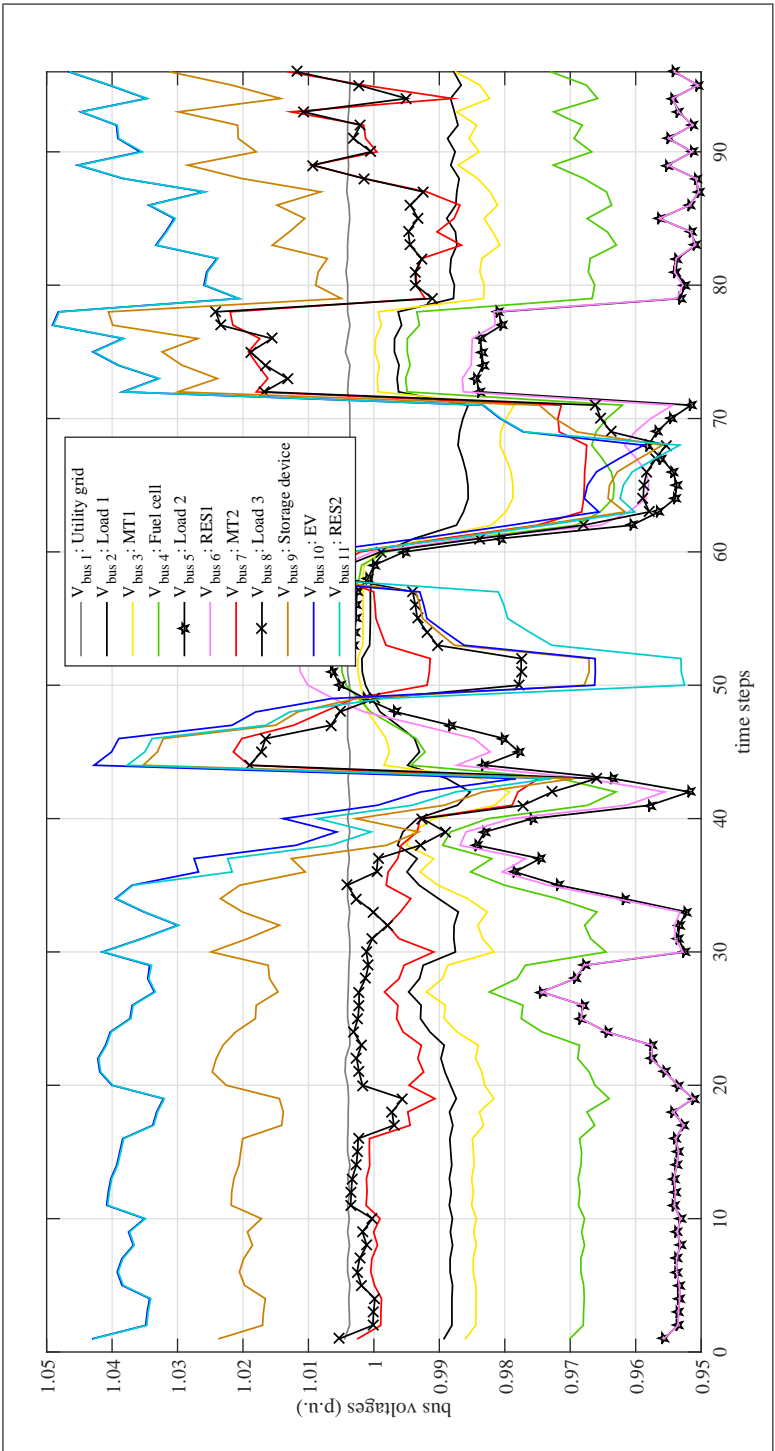e user and grid information are known in advance. However, because of the uncertainties in the demand and renewable energy forecast, further research could be done on forecast techniques and the influence of forecast errors on the offline and online management of microgrids.

Uncertainty management becomes an active research area in scheduling of microgrids. Techniques have been introduced by researchers for managing the uncertainties in microgrids. Stochastic and robust optimisation are among the noticeable techniques available in the literature for uncertainty management in scheduling of active distribution systems and microgrids. The optimisation problem can be formulated in a stochastic framework.

The prominent disadvantages associated with the stochastic optimisation-based uncertainty management of microgrids are listed below [111]:

- increase in problem size and computational requirements with increase in number of scenarios,

- dependence of accuracy on scenario generating technique,

- provision of probabilistic guarantee for feasibility of solution,

- and requirement of accurate information of uncertainty for generation of precise probability distribution functions (PDFs).

In contrast to stochastic optimisation, RO only requires moderate information of underlying uncertainties (uncertainty bounds), provides immunity against all possible realisations of uncertain data within the uncertainty bounds, and formulation of tractable models even for large systems. The major drawbacks associated with the stochastic optimisation and merits of RO can be summarized as follows:

- Stochastic optimisation only provides probabilistic guarantee to the feasibility of solution while, RO provides immunity against all possible realisations of the uncertain data within a deterministic uncertainty set;

- In stochastic optimisation large number of scenarios are required to ensure quality of the scheduling solution which results in growth of problem size and computational requirements, while RO puts the random problem parameters in a deterministic uncertainty set including the worst-case scenario and the robust model remains computationally tractable for all cases;

- In case of stochastic optimisation, accurate information of uncertainties is required to construct accurate PDFs, while RO describes uncertainties by sets, i.e., upper and lower bounds and need not assume probability distributions;

- The accuracy of solution is sensitive to the technique used for scenario generation in stochastic optimisation but RO only needs information about the upper and lower bounds.

The features of the deterministic tool developed in this work can be used for the development of a robust optimisation tool.
In this section extra simulations were added in order clarify how the uncertainty in the output of the model can be apportioned to different sources of uncertainty in its inputs. More specifically, a brief analysis was done in order to quantify the impact of forecast errors.
Simulations were done including deviations on the forecast of the renewable energy production and the total demand.

6.3.0.4 Overview of the results

Table 6.4 represents an overview of the different optimisation results:

	Total cost	Total emission
	reference	reference
Wind power forecast +25%	-5.64%	-5%
Wind power forecast -25%	-38.17%	+75.94%
PV power forecast +25%	-3.03%	-2.87%
PV power forecast -25%	+3.22%	+69.77%
Total energy demand forecast +25%	+29.15%	+33.78%
Total energy demand forecast -25%	-24.90%	-26.10%

Table 6.4: Overview of different forecast scenarios

A positive forecast error (+25%) of renewable energy leads to a decrease in costs and emissions. However, a negative deviation on the prediction of wind energy leads to a decrease in costs and increase in emissions. This can be explained by the fact that, less wind energy leads to a higher actual microgrid demand. This extra demand will be covered by the thermal generators which reduces the costs, but increases the emissions. A positive forecast error (+25%) of the microgrid demand leads to a decrease in costs and emissions and vice versa.

We can conclude that the system's sensitivity is dependent on the (re)distribution of the different reference set points of the microgrid units. However, further research should be done on forecast techniques and the influence of forecast errors on the offline and online management of microgrids.

7
Concluding remarks and future research directions

This chapter summarises the highlights of this work, focussing on the main innovative contributions of this PhD thesis. Finally, suggestions for future research directions subsequent to this work are pointed out.

7.1 Concluding remarks and overview of research contributions

Distributed energy resources play a major role in the path towards the future energy landscape. These technologies, which are currently in different stages of development, drive us to a more decentralised energy world. Fuel cells, wind turbines, photovoltaics, or more traditional energy sources such as diesel generators, are being deployed at a rapid pace. Deploying these sources in a widespread, efficient and cost-effective way requires advanced control strategies and can help the distribution grid in the progress towards a smarter grid. Without introduction of a coordinated approach, the continuous increase in the deployment of DER will reach a limit, threatening the power quality of the distribution grid.

The trend towards the enhancement of the environomical effectiveness and resilience of the main grid can be supported by microgrids.

By aggregating DER into a microgrid, several opportunities and benefits are created for both end-users and utilities. However, several issues associated with planning and management must be addressed before the full benefits of the microgrid can be achieved. The large number of economic and technical factors raised by both DER units and distribution network properties has an impact on the operation of the microgrid. An active management of DER is needed to achieve a least-cost solution while satisfying all technical requirements. In this context, the main contribution of this PhD thesis is the development of an efficient multilayer control approach that obtains a day-ahead unit commitment method to provide an economic and environmentally viable unit commitment that is feasible in terms of voltage violations. With the multilayer control approach, the future operational states of the controllable units within the microgrid are determined ahead of time. The proposed concept follows the idea of a day-ahead coordination including the unit commitment problem (scheduling layer), an offline power flow calculation (executive layer) and a security check with feedback control (adjustment layer). Since the complete multilayer control concept works on a day-ahead time scale, the model can be considered as an offline optimisation approach. The power reference set points provided by the multilayer control approach can, in turn, be used for an online microgrid implementation to achieve real-time system state updates.

In Chapter 2, the main shape and the necessary elements of the microgrid multilayer control approach are outlined to reveal the structure. Each layer is described an discussed briefly. This chapter is written to expose the structure of this PhD thesis. A more detailed presentation of the different layers is provided later in the thesis, chapter by chapter.

A survey of the different optimisation methods for power systems is presented in chapter 3. Several optimisation methods for power system planning are explained, making it easy to compare and point out the specific advantages and disadvantages. It is concluded that using the multi-objective genetic algorithm, the region near an optimal Pareto front can be determined relatively fast, but it can take many function evaluations to achieve convergence. Therefore, an additional (hybrid) technique is introduced that performs the genetic algorithm for a small number of generations to get near an optimum front. The solution returned from the genetic algorithm is used as an initial point for the hybrid goal attainment method. The hybrid

scheme starts at all the points on the Pareto front returned by the genetic algorithm. The new individuals returned by the hybrid scheme are combined with the existing population and a new, more accurate, Pareto front is obtained. This technique is used in order to solve the microgrid power system scheduling problem that is demonstrated in the next chapters.

In chapter 4, an analytical method based on a multi-objective hybrid genetic algorithm is proposed and demonstrated for a microgrid day-ahead unit commitment model. The model aims to schedule the power among the different microgrid units while minimising the operating costs together with the CO_2 emissions produced. The approach is demonstrated on a test case including a variety of DER units which are likely to be found in a microgrid. A storage device is added where the charge and discharge schedule is calculated according to both objectives. In addition, as a part of the demand side participation strategy, a charging schedule is determined for the electric vehicles. A 24-hour microgrid simulation has been performed with an interval or time span of 15 minutes where the objectives are considered simultaneously.

Chapter 5 emerges as an extension to chapter 4, with a deeper focus on the voltage control in microgrids. The main contribution of this chapter is the development of a voltage control approach, for low voltage microgrids, which maintains the bus voltages within pre-specified limits. Due to the introduction of this voltage control approach, active power reference set points can be provided (for real-time microgrid scheduling) not only according to the economical and the environmental objectives, but also taking into account the voltage level at every bus in the microgrid. This chapter ends with a demonstration and evaluation of the voltage control approach.

For the demonstration of the developed multilayer control strategy for microgrids, chapter 6 presents case studies involving the planning of a microgrid including a variety of DER units and loads which are likely to be found in a microgrid. The proposed microgrid includes renewable energy resources, a storage unit, micro turbines, a fuel cell and electric vehicles. The system should run as much as possible on its renewable technologies, and when more power is needed using the distributed generators or batteries. Finally, the system should provide perfect reliability that is, it should never fail to meet total customer demand. Based on the results, the multilayer control strat-

egy generates a set of optimal operating strategies that will minimise costs and emissions while satisfying all technical requirements.

In this PhD thesis, the day-ahead multilayer control concept is presented for microgrids, which is the main aim of this work. Since the complete multilayer control concept works on a day-ahead time scale, the model can be considered as an offline optimisation approach. The power reference set points provided by the multilayer control approach can, in turn, be used for an online microgrid implementation to achieve real-time system state updates.

7.2   Future research directions

The microgrid is a relatively new concept and has attracted attention in research and industry because of its advantages. It allows a coordinated integration of distributed generation, and especially renewable energy sources, in the power system. However, many issues have to be resolved before implementing this concept extensively. Subsequent to this work, some future directions which require further investigation are suggested below.

- The multilayer control approach, developed in this PhD thesis, works on a day-ahead time scale, and therefore, the model can be considered as an offline optimisation approach. The power reference set points provided by the multilayer control approach can, in turn, be used for an online microgrid implementation to achieve real-time system state updates.
  In order to achieve a full-scale development in practice, further research efforts could be done in the context of real-time management strategies for microgrids. A real-time management operates in an online setting, where the complete input is not known a priori. The real-time management finds its usefulness in addressing the lack of accurate mathematical models and the lack of future information for electricity demand and supply in this problem.

- In order to control and manage the microgrid units in real-time while fully exploiting the benefit of long-term prediction, an offline optimisation approach was developed in this PhD in order to devise the online microgrid management. The offline energy management system solves the optimisation problem over the entire time horizon and provides optimal solutions by assuming

that the future user and grid information are known in advance. However, because of the uncertainties in the demand and renewable energy forecast, it may be further research could be done on forecast techniques and the influence of forecast errors on the offline and online management of microgrids.

- The ultimate goal of RD&D efforts is to implement the proposed approaches in the power system. In order to examine real-time simulations and evaluate the experimental performance, field demonstrations as well as pilot projects need to be carried out.

- Microgrids can be considered as an aggregation of (controllable) loads and DER units including. By aggregating microgrids into a virtual power plant, further benefit can be taken from the microgrid concept. A virtual power plant is not geographically limited and can tackle large-scale grid issues by providing ancillary services to the grid operators. Hence, further research needs to be done to investigate their full-scale development.

- Finally, despite all the technical challenges, information and communication management is a major avenue for realising the benefits of microgrids. The related research is interdisciplinary in nature and calls for a close collaboration between the researchers in the power/energy system discipline and in the information/communication system discipline.

A
Appendix

A.1 Background on biological genetic systems

All living organisms are composed of cells, and each cell contains chromosomes (DNA strands) which can be considered as a blueprint for the organism. The collection of all chromosomes is called the genome of an organism. A chromosome can be divided into genes, each carrying information of a specific inherited trait. This structure is depicted in Fig. A.1.
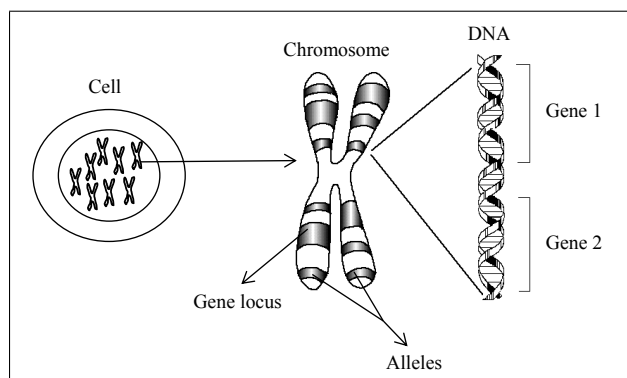
Figure A.1: Genetic algorithm: cell structure

Each gene can have two or more versions, and each version is called
an allele. The locus is the place in the chromosome where a particular
gene is situated.

The genotype is the genetic information about a characteristic of an
organism. Organisms in which the chromosomes occur in pairs of
two are called diploids. Organisms that only have one set of chro-
mosomes per cell are called haploids. Recombination (or crossover)
takes place when reproducing. For diploid organisms (like humans),
first a gene exchange between each pair of chromosomes takes place
which leads to a gamete, a haploid cell which is used exclusively for
reproduction. Subsequently, the gametes of the two parents merge
into a diploid cell. For haploid reproduction, genes are exchanged
between the single chromosomes from the parents. When copying
DNA, mutation can occur wherein nucleotides (the building blocks
of DNA) can be changed.

The fitness of an organism is often defined as the probability that an
organism will survive until it can reproduce. This concept is linked to
that of natural selection, organisms that are better adapted to their
environment are more likely to have descendants as compared to less
adapted organisms, so that the type of the fittest organism remains.
Building up a genetic algorithm starts from a gene which can be con-
sidered as a bit string with an arbitrary length. A chromosome can
be seen as a sequence of genes. A possible solution to a problem can
be described by genes without really being the answer to the prob-
lem. The smallest unit in chromosomes is called an allele represented
by a single symbol or binary bit. It is the value a gene takes for
a particular chromosome. Individuals in a group form a population
which can be considered as a subset of all the possible solutions to
a given problem. The population of genetic algorithms is analogous
to the population of human beings except that instead of human be-
ings, we have candidate solutions representing human beings. Both
the initial population and population size are major population fea-
tures in within the genetic algorithm. The population size is usually
determined by the nature of the problem and is initially generated
randomly. The fitness of each individual in the population is eval-
uated. Individuals with higher fitness produce more offspring than
those with lower fitness.

A.1.1 Context of the genetic algorithm

As explained before, the basic concept of the genetic algorithm was derived from evolutionary biology and survival of the fittest. When implementing the genetic algorithm, critical parameters have to be set, including population size, mutation probability and crossover probability, and their interrelations.

Within the context of genetic algorithms, chromosomes are abstract representations of possible solutions (candidate solutions), often coded in the form of a row of binary numbers (bit sequence or bit string). A candidate solution is also called an individual. All the individuals make up the population. The genes are loose bits, or short blocks of adjacent bits, which form a possible solution for a particular element. An allele in a bit string is 0 or 1. For larger alphabets multiple alleles are possible per locus. Figure A.2 gives a representation of the biological genetic system in the context of the genetic algorithm.
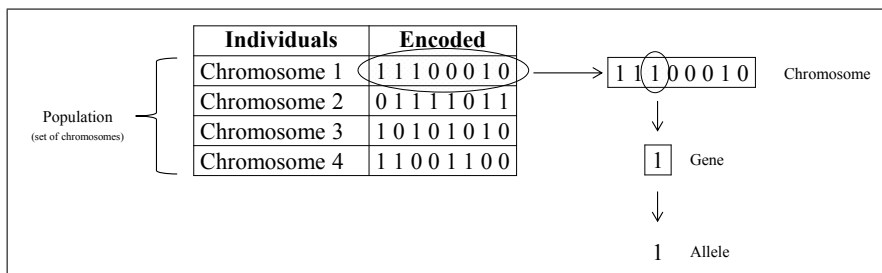
Figure A.2: Representation of chromosome, gene and allele

Genotype is the population in the computation space. In the computation space, the solutions are represented in a way that can be easily understood and manipulated using a computing system.

Phenotype is the population in the actual real world solution space, where solutions are represented in a way they are represented in real world situations. A phenotype gives an external description of the individual. The phenotype and genotype spaces are different.

Decoding is a process of transforming a solution from the genotype to the phenotype space, while encoding is a process of transforming from the phenotype to genotype space. Decoding should be fast as it is carried out repeatedly by the genetic algorithm during the fitness value calculation.

A fitness function can be defined as a function which takes the solution as input and produces the suitability of the solution as the
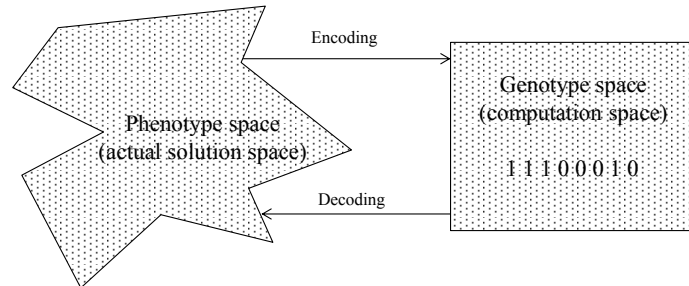
Figure A.3: Decoding and encoding

output. The genetic operators which alter the genetic composition of
the offspring will be explained in the next subsection.

A.1.2   Outline and operators of the genetic algorithm

Genetic algorithms are based on the process of natural selection which
means they take the fundamental properties of natural selection and
apply them to the problem to be solved. In Fig. A.4, the basic process
of the genetic algorithm is presented by a flow diagram which will be
explained with a step by step walk-through.

A.1.2.1   Initialisation

The process of the genetic algorithm starts with the initialisation
which creates an initial population. The population is initialised by
randomly generating a collection of DNA samples. The size of the
population depends on the size of the search space of the problem,
and the computational time it takes to evaluate each individual.

A.1.2.2   Evaluation

Secondly, the chromosomes will be evaluated. During this step, each
member of the population is evaluated and a "fitness" for that in-
dividual will be calculated. This is the most important part to the
algorithm. If this function is improper, the algorithm will not produce
proper results. The evaluation function should not return a Boolean
(true/false) value, it has to be a comparable result. When the indi-
viduals can be sorted from fittest to weakest, it is a viable evaluation
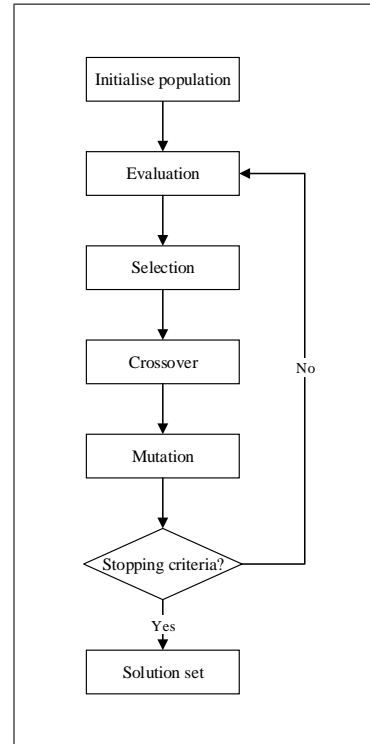
Figure A.4: Genetic algorithm process

function. For example, when evaluating distances between cities, the algorithm may return the total distance travelled as a fitness score.

A.1.2.3   Selection

The goal is to constantly improve the overall fitness of the population. The selection step discards the bad designs and keeps the best individuals in the population. Selection is where the parents for mating will be chosen and happens for each child in the new population. Different selection techniques exist that specify how the genetic algorithm chooses parents for the next generation.

A well-known selection technique is the roulette wheel selection were the probability of selection of a sector within a roulette wheel is proportional to the magnitude of the central angle of the sector. Within the context of the genetic algorithm, the whole population is partitioned on the roulette wheel and each part of sector represents an individual. The proportion of fitness of the individuals to the total

fitness values of the whole population decides the probability of se-
lection of that individual in the next generation. This consequently
decides the area occupied by that individual on the wheel [112]. The
roulette wheel selection includes the following steps:

1. Calculate the sum of the fitness values of each individual within
   the population.

2. Calculate the probability of selection (of each individual) by
   dividing the individual fitness of the chromosome by the sum
   of fitness values of whole population.

3. Divide the roulette wheel into parts (or sectors) according to
   the probabilities calculated in the step 2.

4. Spin the wheel n number of times. The sector on which the
   pointer points (when the roulette stops) corresponds to the in-
   dividual being selected.

The roulette wheel selection method selects the next solution chro-
mosome that will create a new generation and be genetic parents for
the next generations based on the value of fitness function. Due to
the possible presence of a dominant individual which may always win
the competition and is selected as a parent, this technique can have
the risk of premature convergence of the genetic algorithm to a local
optimum.

A second selection technique is the rank selection. Rank selection in
genetic algorithms was introduced by Baker to eliminate the disad-
vantages of proportionate selection techniques [112]. First, the indi-
viduals are sorted according to their fitness value. Second, the ranks
are assigned to these individuals (to every chromosome). The best
individual gets rank 'N' and the worst one gets rank '1'. The worst
will have fitness 1, second worst 2 etc. and the best will have fitness N
(number of chromosomes in population). After all, the chromosomes
have a chance to be selected. Because the difference between the best
chromosomes and the other ones is relatively small, this method can
lead to slower convergence.

Tournament selection is a variant of the rank-based selection method.
Due to ease of implementation and the efficiency, this technique is the
most popular selection technique of the genetic algorithm. In tour-
nament selection, individuals are chosen at random. This method
randomly selects a set of individuals from the entire population. The
selected individuals compete against each other. The individual with

the highest fitness value wins and will be selected for further processing of the genetic algorithm. The number of individuals taking part in every tournament is referred as tournament size. By means of an example, the process of the tournament selection technique is presented Fig. A.5.
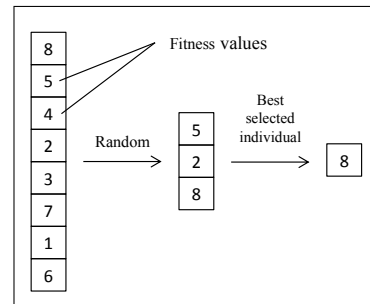
Figure A.5: Tournament selection process

The tournament size is set to three, which means three individuals compete against each other in one tournament. The larger the tournament size, the greater is the probability of loss of diversity [113]. There are two reasons for loss of diversity. Either the individual did not get the opportunity to be selected (because of random selection), or the individual did not get selected in the intermediate population because they lost some tournament.

Due to the lower time complexity (the total time required by the program to run to completion), low vulnerability to takeover by dominant individuals, and no requirement for fitness scaling or sorting, the tournament selection strategy is more efficient as compared to the techniques as described above. In this work, the tournament selection strategy was used where the tournament size was set to 2.

A.1.2.4   Crossover

Once individuals, also known as the parents, are selected, their DNA needs to be mixed and matched to produce a new population of children. This process is called crossover. During crossover, new individuals by combining aspects of our selected individuals will be created. By combining certain traits from two or more individuals, an even "fitter" offspring can be created which will inherit the best traits from each of the parents. Crossover options indicate how the genetic algorithm combines two individuals to form a crossover child for the

next generation.

Single point is a crossover technique which chooses a random integer n between 1 and the number of variables N_{var}. Subsequently, the vector entries numbered less than or equal to n will be selected from the first parent. The vector entries numbered greater than n will be selected from the second parent. Once the parts from each parent are selected, these entries will be connected (or coupled) to form a child vector. Consider two parents with a chromosome length of 8 and a random integer $n = 4$. Figure A.6 presents both children.
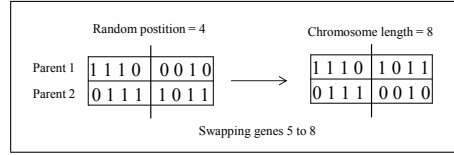
Figure A.6: Single point crossover

Two-point crossover is very similar to single point crossover. For two point crossover, two cut-points are randomly generated instead of one. The genes between the random position entries will be swapped in order to generate new offsprings. Using single point or two point crossover for optimisation problems with linear constraints can result in a population which will not satisfy the constraints since the potential exists for the generation of infeasible candidate solutions [70,114]. In this work, intermediate crossover is used to create children (offspring) by taking a weighted average of the parents. The weights can be specified by a single parameter (Ratio) which can be a scalar or a row vector of length N_{var}. This function creates the child from both parents using the following formula:

$$child = parent_1 + rand \cdot Ratio \cdot (parent_2 - parent_1) \qquad (A.1)$$

A.1.2.5 Mutation

Mutation allows the algorithm to introduce diversity into the population, expanding the opportunity to search unexplored areas in the search space for fitter solutions. Mutation is implemented by giving each element in the DNA array a probability of 2-5% of being randomly altered. The mutation procedure is called for every child.

Mutation options specify how the genetic algorithm makes small random changes in the individuals in the population to create mutation children. Well-known mutation methods are Gaussian and uniform.

Gaussian adds a random number, chosen from a Gaussian distribution, to each entry of the parent vector. Typically, the amount of mutation, which is proportional to the standard deviation of the distribution, decreases at each new generation.

Uniform mutation consist of a two-step process. First, the genetic algorithm selects a fraction of the vector entries of an individual for mutation, where each entry has a probability *Rate* of being mutated. Secondly, the genetic algorithm replaces each selected entry by a random number selected uniformly from the range for that entry.

Using the Gaussians or uniform mutation method, risks to produce infeasible individuals, and as a result, the population will not necessarily satisfy the constraints [70]. Therefore, the method used in this work is called adaptive mutation. This method randomly generates directions that are adaptive with respect to the last successful or unsuccessful generation. The mutation chooses a direction and step length that satisfies bounds and linear constraints.

A.1.2.6   Stopping criteria

After mutation, we have our next generation and we can start again from step 2 (Evaluation) until the termination condition will be reached. The genetic algorithm should be terminated when a solution is found which is proper enough and meets a predefined minimum criterion. Other reasons for terminating could be constraints such as time or cost.

Since the behaviour of the algorithm and the accuracy of the result is i.a. dependent on the solver options and settings, it is important to determine the parameters properly.

Bibliography

[1] U. E. P. Agency, "Global Greenhouse Gas Emissions Data." `http://www.epa.gov/climatechange/ghgemissions/global.html`. [Online; accessed 6 December 2016].

[2] R. Schaeffer, A. S. Szklo, A. F. P. de Lucena, B. S. M. C. Borba, L. P. P. Nogueira, F. P. Fleming, A. Troccoli, M. Harrison, and M. S. Boulahya, "Energy sector vulnerability to climate change: A review," *Energy*, vol. 38, no. 1, pp. 1 – 12, 2012.

[3] International Energy Agency, "Medium-Term Renewable Energy Market Report 2016." `https://www.iea.org/Textbase/npsum/MTrenew2016sum.pdf/`. [Online; accessed 6 December 2016].

[4] International Energy Agency, "Technology Roadmap: How2Guide for Smart Grids in Distribution Networks." `https://www.iea.org/publications/`, 2015. [Online; accessed 5 December 2016].

[5] J. Driesen and R. Belmans, "Distributed generation: challenges and possible solutions," in *IEEE Power Engineering Society General Meeting, Montreal, Canada*, pp. 8 pp.–, 2006.

[6] P. A. Daly and J. Morrison, "Understanding the potential benefits of distributed generation on power delivery systems," in *Rural Electric Power Conference*, pp. A2/1–A213, 2001.

[7] A. Ali A B M Shawkat, *Smart Grids : Opportunities, Developments, and Trends.* Springer London, 2013.

[8] T. L. Vandoorn and L. Vandevelde, "Contribution of microgrids to the development of the smart grid," in *Smart grids : clouds, communications, open source, and automation* (D. Bakken and K. Iniewski, eds.), Devices, Circuits, and Systems, pp. 191–211, CRC Press, 2014.

[9] W. Frye, "Transforming the electricity system to meet future demand and reduce greenhouse gas emissions," *Cisco Internet Business Solutions Group*, 2008.

[10] Q. Huang, S. Jing, J. Yi, and W. Zhen, *Innovative Testing and Measurement Solutions for Smart Grid.* John Wiley and Sons, 2015.

[11] E. Al-Shaer and M. A. Rahman, *Security and Resiliency Analytics for Smart Grids: Static and Dynamic Approaches.* Springer Publishing Company, Incorporated, 2016.

[12] E. Commission, "European smart grids technology platform: vision and strategy for Europe's electricity." `http://www.ec.europa.eu/`. [Online; accessed 5 December 2016].

[13] H. Gharavi and R. Ghafurian, "Special issue on smart grid: The electric energy system of the future," *Proceedings of the IEEE*, vol. 99, pp. 913–914, June 2011.

[14] E. Antonio, *The Next Generation of Economic Issues in Energy Policy in Europe.* Centre for Economic Policy Research, 2014.

[15] T. L. Vandoorn, B. Meersman, L. Degroote, B. Renders, and L. Vandevelde, "A control strategy for islanded microgrids with dc-link voltage control," *IEEE Transactions on Power Delivery*, vol. 26, pp. 703–713, April 2011.

[16] S. Chowdhury, *Microgrids and Active Distribution Networks.* Energy Engineering, Institution of Engineering and Technology, 2009.

[17] F. Katiraei, R. Iravani, N. Hatziargyriou, and A. Dimeas, "Microgrids management," *IEEE Power and Energy Magazine*, vol. 6, pp. 54–65, May 2008.

[18] N. Hatziargyriou, H. Asano, R. Iravani, and C. Marnay, "Microgrids," *IEEE Power and Energy Magazine*, vol. 5, pp. 78–94, July 2007.

[19] M. Soshinskaya, W. H. Crijns-Graus, J. M. Guerrero, and J. C. Vasquez, "Microgrids: Experiences, barriers and success factors," *Renewable and Sustainable Energy Reviews*, vol. 40, pp. 659 – 672, 2014.

[20] H. A. Gil and G. Joos, "Models for quantifying the economic benefits of distributed generation," *IEEE Transactions on Power Systems*, vol. 23, pp. 327–335, May 2008.

[21] G. Y. Morris, C. Abbey, S. Wong, and G. Joós, "Evaluation of the costs and benefits of microgrids with consideration of services beyond energy supply," in *IEEE Power and Energy Society General Meeting*, July 2012.

[22] P. M. Costa and M. A. Matos, "Assessing the contribution of microgrids to the reliability of distribution networks," *Electric Power Systems Research*, vol. 79, no. 2, pp. 382–389, 2009.

[23] H. Jiayi, J. Chuanwen, and X. Rong, "A review on distributed energy resources and microgrid," *Renewable and Sustainable Energy Reviews*, vol. 12, no. 9, pp. 2472 – 2483, 2008.

[24] P. Basak, A. K. Saha, S. Chowdhury, and S. P. Chowdhury, "Microgrid: Control techniques and modeling," in *2009 44th International Universities Power Engineering Conference (UPEC), Glasgow, United Kingdom*, Sept 2009.

[25] I. Krzysztof, *Smart Grid Infrastructure & Networking*. US McGraw-Hill Professional, 2012.

[26] R. H. Lasseter, A. A. Akhil, C. Marnay, J. Stephens, J. E. Dagle, R. T. Guttromson, A. S. Meliopoulous, R. J. Yinger, and J. H. Eto, "Integration of distributed energy resources: The certs microgrid concept," p. 32, 2003.

[27] E. Planas, A. G. de Muro, J. Andreu, I. Kortabarria, and I. M. de Alegría, "General aspects, hierarchical controls and droop methods in microgrids: A review," *Renewable and Sustainable Energy Reviews*, vol. 17, pp. 147–159, 2013.

[28] E. R. Díaz, X. Su, M. Savaghebi, J. C. Vasquez, M. Han, and J. M. Guerrero, "Intelligent dc microgrid living laboratories - a chinese-danish cooperation project," in *IEEE First International Conference on DC Microgrids (ICDCM), Atlanta, Georgia, USA*, pp. 365–370, June 2015.

[29] A. to the carbon economy. `www.ace-low-carbon-economy.eu`, 2016. [Online; accessed 2 December 2016].

[30] J. Timmerman, C. Deckmyn, L. Vandevelde, and G. Van Eetvelde, *Low carbon business park manual: a guide for developing and managing energy efficient and low carbon businesses and business parks.* Ghent University, 2014.

[31] K. T. Tan, P. L. So, Y. C. Chu, and M. Z. Q. Chen, "Coordinated control and energy management of distributed generation inverters in a microgrid," *IEEE Transactions on Power Delivery*, vol. 28, pp. 704–713, April 2013.

[32] A. Bidram, A. Davoudi, F. Lewis, and S. S. Ge, "Distributed adaptive voltage control of inverter-based microgrids," *IEEE Transactions on Energy Conversion*, vol. 29, pp. 862–872, Dec 2014.

[33] W. Su and J. Wang, "Energy management systems in microgrid operations," *The Electricity Journal*, vol. 25, no. 8, pp. 45–60, 2012.

[34] X. Li, G. Geng, and Q. Jiang, "A hierarchical energy management strategy for grid-connected microgrid," in *IEEE PES General Meeting, Washington DC, USA*, July 2014.

[35] Q. Jiang, M. Xue, and G. Geng, "Energy management of microgrid in grid-connected and stand-alone modes," *IEEE Transactions on Power Systems*, vol. 28, Aug 2013.

[36] S. J. Ahn, S. R. Nam, J. H. Choi, and S. I. Moon, "Power scheduling of distributed generators for economic and stable operation of a microgrid," *IEEE Transactions on Smart Grid*, vol. 4, pp. 398–405, March 2013.

[37] W. Shi, X. Xie, C. C. Chu, and R. Gadh, "Distributed optimal energy management in microgrids," *IEEE Transactions on Smart Grid*, vol. 6, pp. 1137–1146, May 2015.

[38] D. E. Olivares, C. A. Cañizares, and M. Kazerani, "A centralized optimal energy management system for microgrids," in *IEEE Power and Energy Society General Meeting, Detroit, Michigan, USA*, pp. 1–6, July 2011.

[39] A. L. Dimeas and N. D. Hatziargyriou, "Operation of a multiagent system for microgrid control," *IEEE Transactions on Power Systems*, vol. 20, pp. 1447–1455, Aug 2005.

[40] L. Meng, E. R. Sanseverino, A. Luna, T. Dragicevic, J. C. Vasquez, and J. M. Guerrero, "Microgrid supervisory controllers and energy management systems: A literature review," *Renewable and Sustainable Energy Reviews*, vol. 60, pp. 1263–1273, 2016.

[41] L. I. Minchala-Avila, L. E. Garza-Castañón, A. Vargas-Martínez, and Y. Zhang, "A review of optimal control techniques applied to the energy management and control of microgrids," *Procedia Computer Science*, vol. 52, pp. 780 – 787, 2015.

[42] L. Meng, E. R. Sanseverino, A. Luna, T. Dragicevic, J. C. Vasquez, and J. M. Guerrero, "Microgrid supervisory controllers and energy management systems: A literature review," *Renewable and Sustainable Energy Reviews*, vol. 60, pp. 1263 – 1273, 2016.

[43] T. L. Vandoorn, J. C. Vasquez, J. D. Kooning, J. M. Guerrero, and L. Vandevelde, "Microgrids: Hierarchical control and an overview of the control and reserve management strategies," *IEEE Industrial Electronics Magazine*, vol. 7, pp. 42–55, Dec 2013.

[44] T. Vandoorn, J. D. Kooning, B. Meersman, and L. Vandevelde, "Review of primary control strategies for islanded microgrids with power-electronic interfaces," *Renewable and Sustainable Energy Reviews*, vol. 19, pp. 613–628, 2013.

[45] X. Yu, X. Ni, and A. Huang, "Multiple objectives tertiary control strategy for solid state transformer interfaced dc microgrid," in *IEEE Energy Conversion Congress and Exposition (ECCE), Pittsburgh, USA*, pp. 4537–4544, Sep 2014.

[46] T. Maes, G. V. Eetvelde, E. D. Ras, C. Block, A. Pisman, B. Verhofstede, F. Vandendriessche, and L. Vandevelde, "Energy management on industrial parks in Flanders," *Renewable and Sustainable Energy Reviews*, vol. 15, no. 4, pp. 1988 – 2005, 2011.

[47] T. Vandoorn, *Voltage-based droop control of converter-interfaced distributed generation units in microgrids*. PhD thesis, Ghent University, 2013.

[48] C. Deckmyn, T. L. Vandoorn, M. Moradzadeh, and L. Vande-velde, "Multi-objective optimization for environomic scheduling in microgrids," in *IEEE PES General Meeting, Washington DC, USA*, July 2014.

[49] C. Deckmyn, J. Van de Vyver, T. L. Vandoorn, B. Meerman, J. Desmet, and L. Vandevelde, "A day-ahead unit commitment model for microgrids," *IET Generation, Transmission & Distribution*, Sep 2016.

[50] F. A. Mohamed and H. N. Koivo, "Multiobjective optimization using mesh adaptive direct search for power dispatch problem of microgrid," *International Journal of Electrical Power & Energy Systems*, vol. 42, no. 1, pp. 728 – 735, 2012.

[51] H. M. Khodr, J. C. Gomez, L. Barinique, J. H. Vivas, P. Paiva, J. M. Yusta, and A. J. Urdaneta, "A linear programming methodology for the optimization of electric power generation schemes," *IEEE Power Engineering Review*, vol. 22, pp. 58–58, July 2002.

[52] R. Jabr, A. Coonick, and B. Cory, "A homogeneous linear programming algorithm for the security constrained economic dispatch problem," *IEEE Transactions on Power Systems*, vol. 15, pp. 930–936, Aug 2000.

[53] K. Zehar and S. Sayah, "Optimal power flow with environmental constraint using a fast successive linear programming algorithm: Application to the algerian power system," *Energy Conversion and Management*, vol. 49, no. 11, pp. 3362 – 3366, 2008.

[54] L. Zarate, C. Castro, J. Ramos, and E. Ramos, "Fast computation of voltage stability security margins using nonlinear programming techniques," *IEEE Transactions on Power Systems*, vol. 21, pp. 19–27, Feb 2006.

[55] K. Lee, *Modern Heuristic Optimization Techniques With Applications To Power Systems*. John Wiley & Sons, 2005.

[56] "Nature-inspired optimization algorithms," in *Nature-Inspired Optimization Algorithms* (X.-S. Yang, ed.), Oxford: Elsevier, 2014.

[57] M. Tabatabaei, J. Hakanen, M. Hartikainen, K. Miettinen, and K. Sindhya, "A survey on handling computationally expensive multiobjective optimization problems using surrogates: non-nature inspired methods," *Structural and Multidisciplinary Optimization*, vol. 52, no. 1, 2015.

[58] W. Luo and Y. Li, "Benchmarking heuristic search and optimisation algorithms in matlab," in *22nd International Conference on Automation and Computing (ICAC)*, pp. 250–255, Sept 2016.

[59] R. Nayak and J. Sharma, "A hybrid neural network and simulated annealing approach to the unit commitment problem," *Computers & Electrical Engineering*, vol. 26, no. 6, pp. 461 – 477, 2000.

[60] A. Mantawy, Y. L. Abdel-Magid, and S. Z. Selim, "A new genetic-based tabu search algorithm for unit commitment problem," *Electric Power Systems Research*, vol. 49, no. 2, pp. 71 – 78, 1999.

[61] "A dynamic programming based fast computation hopfield neural network for unit commitment and economic dispatch," *Electric Power Systems Research*, vol. 77, no. 8, pp. 917 – 925, 2007.

[62] S. B. A. BUKHARI, A. AHMAD, S. A. RAZA, and M. N. SIDDIQUE, "A ring crossover genetic algorithm for the unit commitment problem," in *Turkish Journal of Electrical Engineering & Computer Science*, 2016.

[63] S. B. A. Bukhari, A. Ahmad, S. A. Raza, and A. U. M. Zaki, "Genetic algorithm based generator scheduling-a review," *World Applied Sciences Journal*, vol. 30, no. 12, pp. 1826–1833, 2014.

[64] L. Davis, ed. Van Nostrand Reinhold, 1991.

[65] M. Randall, "The future and applications of genetic algorithms," in *IEEE Computer Proceedings of the Electronic Directions to the Year 2000 Conference*, pp. 471–475, 1995.

[66] J. H. Holland, *Adaptation in Natural and Artificial Systems: An Introductory Analysis with Applications to Biology, Control and Artificial Intelligence.* Cambridge, MA, USA: MIT Press, 1992.

[67] D. E. Goldberg, *Genetic Algorithms in Search, Optimization and Machine Learning.* Boston, MA, USA: Addison-Wesley Longman Publishing Co., Inc., 1989.

[68] J. R. Koza, *Genetic Programming II: Automatic Discovery of Reusable Programs.* 1994.

[69] K. Deb and D. Kalyanmoy, *Multi-Objective Optimization Using Evolutionary Algorithms.* New York, NY, USA: John Wiley & Sons, Inc., 2001.

[70] MathWorks, "Matlab Genetic Algorithm." `http://www.mathworks.nl/discovery/genetic-algorithm.html`, 2016. [Online; accessed 30 November 2016].

[71] K. Deb, A. Pratap, S. Agarwal, and T. Meyarivan, "A fast and elitist multiobjective genetic algorithm: Nsga-ii," *IEEE Transactions on Evolutionary Computation*, vol. 6, pp. 182–197, Apr 2002.

[72] MathWorks, "Multiobjective genetic algorithm options," 2016.

[73] "International energy outlook 2016," tech. rep., United States Energy Information Administration (EIA), 2016.

[74] G. Pepermans, J. Driesen, D. Haeseldonckx, R. Belmans, and W. D'haeseleer, "Distributed generation: definition, benefits and issues," *Energy Policy*, vol. 33, no. 6, pp. 787 – 798, 2005.

[75] M. S. Shahriar, M. J. Rana, M. A. Asif, M. M. Hasan, and M. M. Hawlader, "Optimization of unit commitment problem for wind-thermal generation using fuzzy optimization technique," in *International Conference on Advances in Electrical Engineering (ICAEE), Bashundhara Dhaka, Bangladesh*, pp. 88–92, Dec 2015.

[76] A. Bhardwaj, V. K. Kamboj, V. K. Shukla, B. Singh, and P. Khurana, "Unit commitment in electrical power system-a literature review," in *IEEE International Power Engineering and Optimization Conference (PEDCO) Melaka, Malaysia*, pp. 275–280, June 2012.

[77] C.-A. Li, A. J. Svoboda, C.-L. Tseng, R. B. Johnson, and E. Hsu, "Hydro unit commitment in hydro-thermal optimization," *IEEE Transactions on Power Systems*, vol. 12, pp. 764–769, May 1997.

[78] B. Saravanan, S. Das, S. Sikri, and D. P. Kothari, "A solution to the unit commitment problem - a review," *Frontiers in Energy*, vol. 7, no. 2, pp. 223–2360, 2013.

[79] N. P. Padhy, "Unit commitment - a bibliographical survey," *IEEE Transactions on Power Systems*, vol. 19, pp. 1196–1205, May 2004.

[80] S. M. Ryan, R. J. B. Wets, D. L. Woodruff, C. Silva-Monroy, and J. P. Watson, "Toward scalable, parallel progressive hedging for stochastic unit commitment," in *IEEE Power Energy Society General Meeting, Vancouver, Canada*, July 2013.

[81] D. Bertsimas, E. Litvinov, X. A. Sun, J. Zhao, and T. Zheng, "Adaptive robust optimization for the security constrained unit commitment problem," *IEEE Transactions on Power Systems*, vol. 28, pp. 52–63, Feb 2013.

[82] Y. Wang, Q. Xia, and C. Kang, "Unit commitment with volatile node injections by using interval optimization," *IEEE Transactions on Power Systems*, vol. 26, pp. 1705–1713, Aug 2011.

[83] A. Tuohy, P. Meibom, E. Denny, and M. O'Malley, "Unit commitment for systems with significant wind penetration," *IEEE Transactions on Power Systems*, vol. 24, pp. 592–601, May 2009.

[84] H. Pandžić, Y. Dvorkin, Y. Wang, T. Qiu, and D. S. Kirschen, "Effect of time resolution on unit commitment decisions in systems with high wind penetration," in *IEEE PES General Meeting, Washington DC, USA*, July 2014.

[85] M. C. Caramanis and J. M. Foster, "Coupling of day ahead and real-time power markets for energy and reserves incorporating local distribution network costs and congestion," in *2010 48th Annual Allerton Conference on Communication, Control, and Computing (Allerton)*, pp. 42–49, Sept 2010.

[86] The USA Federal Energy Regulatory Commission, "Integration of Variable Energy Resources." `https://www.ferc.gov/whats-new/comm-meet/2012/062112/E-3.pdf`, 2012. [Online; accessed 4 January 2017].

[87] B. Taylor and C. Taylor, "Demand response: Managing electric power peak load shortages with market mechanisms," tech. rep., RAP Energy Solutions for a Changing World, 2015.

[88] "Benefits of demand response in electricity markets and recommendations for achieving them: A report to the united states congress pursuant to section 1252 of the energy policy act of 2005," tech. rep., Department of Energy Office of Electricity Delivery and Energy Reliability, 2006.

[89] X.-F. Wang, Y. Song, and M. Irving, *Modern Power Systems Analysis*. Springer US, 2008.

[90] L. Grigsby, *Power System Stability and Control, Third Edition*. The electric power engineering handbook, CRC Press, 2016.

[91] J. Zhu, *Optimization of power system operation (ieee press series on power engineering); 2nd ed.* Wiley-Blackwell, Feb 2015.

[92] Belpex, "The Belgian Power Exchange." `http://www.belpex.be/`, 2016. [Online; accessed 2 December 2016].

[93] Commissie voor de Regulering van de Elektriciteit en het Gas (CREG), "De werking van de Belgische groothandelsmarkt voor elektriciteit." `http://www.creg.info/pdf/Studies/F1050NL.pdf`, 2012. [Online; accessed 4 January 2017].

[94] B. Marti, "Emissions of power delivery systems," Master's thesis, Swiss Federal Institute of Technology (ETH) Zurich, 2005.

[95] W.-T. Huang, K.-C. Yao, and C.-C. Wu, "Using the direct search method for optimal dispatch of distributed generation in a medium-voltage microgrid," *Energies*, vol. 7, no. 12, pp. 8355–8373, 2014.

[96] "Effect of fuel cell units in economic and environmental dispatch of a microgrid with penetration of photovoltaic and micro turbine units," *International Journal of Hydrogen Energy*, pp. –, 2016.

[97] B. Zhao, Y. Shi, X. Dong, W. Luan, and J. Bornemann, "Short-term operation scheduling in renewable-powered microgrids: A duality-based approach," *IEEE Transactions on Sustainable Energy*, vol. 5, pp. 209–217, Jan 2014.

[98] F. A. Mohamed and H. N. Koivo, "Online management of microgrid with battery storage using multiobjective optimization," in *International Conference on Power Engineering, Energy and Electrical Drives, Setubal, Portugal*, pp. 231–236, April 2007.

[99] S. Youli, Z. Litifu, and K. Nagasaka, "Efficiency of micro grid with storage battery in reliability, economy and environment assessments," *Electrical Power and Energy Systems*, vol. 3, pp. 154–162, 2009.

[100] M. A. Jangjoo and A. R. Seifi, "Optimal voltage control and loss reduction in microgrid by active and reactive power generation," *Journal of Intelligent & Fuzzy Systems*, no. 4, pp. 1649–1658, 2014.

[101] H. Laaksonen, P. Saari, and R. Komulainen, "Voltage and frequency control of inverter based weak LV network microgrid, amsterdam, netherlands," in *International Conference on Future Power Systems*, pp. 6 pp.–6, Nov 2005.

[102] T. L. Vandoorn, B. Renders, L. Degroote, B. Meersman, and L. Vandevelde, "Active load control in islanded microgrids based on the grid voltage," *IEEE Transactions on Smart Grid*, vol. 2, pp. 139–151, March 2011.

[103] K. D. Brabandere, B. Bolsens, J. V. den Keybus, A. Woyte, J. Driesen, and R. Belmans, "A voltage and frequency droop control method for parallel inverters," *IEEE Transactions on Power Electronics*, vol. 22, pp. 1107–1115, July 2007.

[104] F. Saccomanno, *Electric Power Systems*. Wiley- Interscience IEEE Press, Piscataway, 2003.

[105] M. Brenna, E. D. Berardinis, L. D. Carpini, F. Foiadelli, P. Paulon, P. Petroni, G. Sapienza, G. Scrosati, and D. Zaninelli, "Automatic distributed voltage control algorithm in smart grids applications," *IEEE Transactions on Smart Grid*, vol. 4, no. 2, pp. 877–885, 2013.

[106] G. Massa, G. Gross, V. Galdi, and A. Piccolo, "Dispersed voltage control in microgrids," *IEEE Transactions on Power Systems*, vol. 31, Sept 2016.

[107] J. Goñi, M. Angel, G. Yang, and K. Søren Bækhøj, "Voltage regulation in LV grids by coordinated Volt-VAr control strategies," 2014.

[108] "Power system voltage stability assessment through artificial neural network," *Procedia Engineering*, vol. 30, pp. 53 – 60, 2012.

[109] SynerGrid, "Technische voorschriften elektriciteit c10/11," June 2012.

[110] C. Deckmyn, T. Vandoorn, J. V. de Vyver, J. Desmet, and L. Vandevelde, "A microgrid multilayer control concept for optimal power scheduling and voltage control," *IEEE Transactions on Smart Grid*, vol. PP, no. 99, pp. 1–1, 2017.

[111] A. Hussain, V.-H. Bui, and H.-M. Kim, "Robust optimization-based scheduling of multi-microgrids considering uncertainties," *Energies*, vol. 9, no. 4, 2016.

[112] A. Shukla, H. M. Pandey, and D. Mehrotra, "Comparative review of selection techniques in genetic algorithm," in *International Conference on Futuristic Trends on Computational Analysis and Knowledge Management (ABLAZE), New Delhi, India*, pp. 515–519, Feb 2015.

[113] "Performance evaluation of selection methods of genetic algorithm and network security concerns," *Procedia Computer Science*, vol. 78, pp. 13 – 18, 2016.

[114] D. Reid, "Genetic algorithms in constrained optimization," *Mathematical and Computer Modelling*, vol. 23, no. 5, pp. 87 – 111, 1996.

Publication list of C. Deckmyn

1. C. Deckmyn, T. Vandoorn, J. Van de Vyver, J. Desmet, and L. Vandevelde, "A microgrid multilayer control concept for optimal power scheduling and voltage control," in *IEEE Transactions on Smart Grid.* 2017, DOI: 10.1109/TSG.2017. 2658865

2. C. Deckmyn, J. Van de Vyver, T. Vandoorn, B. Meersman, J. Desmet, and L. Vandevelde, "Day-ahead unit commitment model for microgrids," in *IET Generation, Transmission & Distribution.* 2016, pp. 1–9. DOI: 10.1049/iet-gtd.2016.0222

3. C. Deckmyn, T. Vandoorn, B. Meersman, L. Gevaert, J. Desmet, and L. Vandevelde, "A coordinated voltage control strategy for on-load tap changing transformers with the utilisation of distributed generators," in *Proceedings of the IEEE International Energy Conference (Energycon 2016).* IEEE, 2016, pp. 1–6. [Online]. Available: http://dx.doi.org/10.1109/ENERGYCON.2016.7514093

4. L. Gevaert, T. Vandoorn, C. Deckmyn, J. Van de Vyver, and L. Vandevelde, "Oltc selection and switching reduction in multiple-feeder lv distribution networks," in *International Conference on Renewable Energy Research and Applications.* IEEE, 2015, pp. 562–566.

5. C. Deckmyn, T. Vandoorn, M. Moradzadeh, and L. Vandevelde, "Dynamic optimisation for environomic power dispatch in microgrids," in *Chemical Engineering Transactions*, P. Varbanov, J. Klemeš, P. Y. Liew, and J. Y. Yong, Eds., vol. 39. AIDIC Servizi, 2014, pp. 1765–1770. [Online]. Available: http://dx.doi.org/10.3303/CET1439295

6. C. Deckmyn, T. Vandoorn, M. Moradzadeh, and L. Vandevelde, "Multi-objective optimization for environomic scheduling in microgrids," in *IEEE Power and Energy Society General Meeting PESGM*.   IEEE, 2014, pp. 1–5.

7. J. Timmerman, C. Deckmyn, L. Vandevelde, and G. Van Eetvelde, *Low carbon business park manual: a guide for developing and managing energy efficient and low carbon businesses and business parks*.   Ghent University, 2014, vol. 1. [Online]. Available: http://www.ace-low-carbon-economy.eu/ files/Publicaties/manual/LowCarbonBPManualWEBHR.pdf

8. C. Deckmyn, T. Vandoorn, M. Moradzadeh, and L. Vandevelde, "Dynamic optimisation for power dispatch in microgrids," in *Proceedings of the IEEE Young Researchers Symposium 2014*. EESA, 2014, pp. 1–4.

9. J. Laveyne, C. Deckmyn, M. Moradzadeh, L. Vandevelde, and G. Van Eetvelde, "Development of a cloud-based renewable energy monitoring platform," in *IEEE PES Asia-Pacific Power and Energy Engineering Conference (APPEEC), Dublin, Ireland*. IEEE, 2013, p. 6.

10. C. Deckmyn, T. Vandoorn, L. Vandevelde, J. Desmet, G. Van Eetvelde, and J. Timmerman, "Energy management and dynamic optimisation of eco-industrial parks," in *2013 45th International Universities Power Engineering Conference (UPEC)*.

11. J. Timmerman, C. Deckmyn, L. Vandevelde, and G. Van Eetvelde, "Techno-economic energy models for low carbon business parks," in *Chemical Engineering Transactions*, P. Varbanov, J. Klemes, P. Seferlis, A. Papadopoulos, S. Voutetakis, and S. Pierucci, Eds., vol. 35.   AIDIC - The Italian Association of Chemical Engineering, 2013, pp. 571–576. [Online]. Available: http://dx.doi.org/10.3303/CET1335095